

Mathematical modelling of cytokine dynamics in arthritic disease

Michelle Baker

Thesis submitted to the University of Nottingham for the
degree of Doctor of Philosophy

July 2015

Abstract

Arthritic diseases, a group of degenerative joint diseases, cause pain, disability and the loss of independence. Research over the last 30 years has improved our understanding of these conditions. We now know that these conditions are pathological in nature, and are mediated by cytokines, cell signalling proteins. We still have much to learn about disease initiation, control and progression if we wish to develop reliable and effective disease-modifying treatments.

In this thesis we use mathematical modelling to extend our understanding of arthritic disease. We focus our attention on two arthritic diseases, rheumatoid arthritis (RA), predominantly initiated in the synovium of joints, and osteoarthritis (OA), predominantly initiated in the cartilage of joints.

We develop an ODE model of cytokine dynamics in the synovium and show that it contains some features associated with RA. We find that increases in cytokine production rates over time can lead to initiation of RA, including periods of relapsing-remitting disease. We find that dose timing and interval as well as dose size are all important to treatment outcome.

We develop two models of cytokine dynamics in cartilage and use these to analyse OA initiation and progression. The first model is an ODE model, expanding on the synovium model, and the second model is a spatial Cellular Potts model. We use these to consider pathways that could lead to the development of OA, and show that combined treatment strategies are more effective than single target therapies in treating OA. We also show that diffusion in cartilage plays an important role in OA.

We look briefly at the downstream signalling pathways of cytokines, which are also not fully understood. Here we focus on the binding of a family of transcription factors (STAT proteins) to DNA. We find that multiple high affinity binding sites are not a requirement for cooperative binding of STAT proteins.

Acknowledgements

I would like to express my sincere gratitude to my supervisors Professor Markus R Owen and Dr Bindi S Brook, for their constant support throughout the four years of this PhD. They have given me their valuable time whenever I have needed it, guided me through my studies and offered advice that I will take with me in my future career.

I would also like to thank Dr Ian Gaywood and Professor Uwe Vinkemeier, with whom I have been fortunate to collaborate with during my studies, for broadening my horizons. I would like to acknowledge the fantastic support staff in the School of Mathematical Sciences, who have all been so helpful with everything from travel arrangements to laptop problems.

Finally I would like to thank my dear husband David for his boundless belief in me and my son Oscar for being a wonderful distraction whenever I have felt overwhelmed.

Contents

1	Introduction	1
1.1	Motivation	1
1.2	Joint Biology	2
1.3	Cytokine Signalling	6
1.4	Rheumatoid Arthritis	9
1.5	Osteoarthritis	10
1.6	Previous modelling work	20
1.6.1	Articular Cartilage and Subchondral Bone	20
1.6.2	Arthritic Diseases	21
1.6.3	Inflammation	22
1.6.4	Cytokines	23
1.7	Thesis Outline	24
2	Pro- and anti-inflammatory cytokine model for rheumatoid arthritis	26
2.1	Introduction	26
2.2	An activator-inhibitor model for cytokine interactions	28
2.3	Model Analysis	32
2.3.1	Nullclines and Steady states	32
2.3.2	One Parameter Bifurcation Diagrams	35
2.3.3	Two Parameter Bifurcation Diagrams	43
2.4	Time-Dependent Parameter Variations	49
2.5	Treatment Strategies	53
2.6	Discussion	57
3	Mathematical modelling of cytokines, MMPs and ECM fragments in osteoarthritic cartilage	62

CONTENTS

3.1	Model Rationale	64
3.2	Model Equations	66
3.3	Steady States	67
3.4	Bifurcation Analysis	72
3.4.1	Changes in P_{bp}, P_{pp} and P_{fp}	78
3.4.2	Changes in A_{pp} and A_{fp}	83
3.4.3	Changes in M_{pp} and M_{bp}	84
3.4.4	Changes in A_{ph}, A_{fh} and M_{ph}	85
3.4.5	Changes in γ_p, γ_m and γ_f	87
3.4.6	Additional behaviour seen in the model	89
3.5	Two Parameter Variations	96
3.5.1	P_{pp} variations	97
3.5.2	P_{fp} variations	100
3.5.3	A_{pp} variations	101
3.5.4	A_{fp} variations	102
3.5.5	M_{pp} variations	102
3.5.6	γ_f variations	103
3.6	Mechanical Damage	104
3.7	Biological Applications	105
3.7.1	Time dependent changes in feedback parameters	106
3.7.2	Mechanical Damage	120
3.8	Treatment Strategies	122
3.8.1	Treatment for bistable cases	123
3.8.2	Treatment for tristable cases	129
3.8.3	Treatment for monostable cases	132
3.9	Discussion	133
4	Spatial modelling of joint degradation in OA	138
4.1	Introduction	138
4.2	Model specification	139
4.2.1	Modelling approach	141
4.2.2	Physical properties of the model	145
4.2.3	Biochemical properties	149
4.3	Model Parameters	151

CONTENTS

4.4	Transition from ODE to spatial model	154
4.4.1	Direct Comparison	154
4.4.2	Number of cells	156
4.4.3	Tissue boundaries	158
4.4.4	Tissue degradation and disease measures	161
4.5	Classification of behaviours in the spatial model	163
4.6	Impact of diffusion rate variation	172
4.7	Discussion	174
5	Binding interactions in cytokine mediated STAT signalling	177
5.1	Introduction	177
5.2	Experimental Work	179
5.3	Cooperative Binding Model	183
5.3.1	Model Rationale	183
5.3.2	Model Simulations	188
5.4	Competitive Binding Model	193
5.4.1	Model Rationale	193
5.4.2	Model Simulations	195
5.5	Discussion	215
6	Summary and Future Directions	218
	References	223
	Appendix A Hill Coefficients in the Pro- and anti-inflammatory cy- tokine model	240
	Appendix B STAT signalling model reactions	243
B.0.1	Cooperative Four Site Model	243
B.0.2	Competitive Three Site Model	245
B.0.3	Competitive Four Site Model	247

Chapter 1

Introduction

1.1 Motivation

The focus of this thesis is to study the dynamics of cytokines, particularly in arthritic disease. Cytokines are cell signalling molecules present in joint tissue, and have been implicated in initiation and progression of arthritic diseases such as rheumatoid arthritis (RA) and osteoarthritis (OA). We aim to model the key interactions that lead to arthritic disease and find suitable strategies for pharmacological interventions. In particular we focus on two types of arthritic joint disease, RA and OA. In the case of RA, drug therapies targeting key cytokines have been successful in treating, although not curing the condition. However, there are no similar therapies available for OA. The World Health Organisation estimates that there 9.6% of men and 18% of women over 60 have symptomatic OA [129]. Whilst literature suggests that up to 80% of those over 75 have radiographic evidence (where joint damage is seen on x-ray images) of OA, although they may be asymptomatic [7]. As life expectancy increases the burden of OA on both individuals and healthcare systems will likely increase.

Research into therapeutic interventions for OA has been largely unsuccessful.

Whilst experimental research has provided some promising potential targets for OA treatments, only a small number have made it to clinical trial stage, the results of which have been disappointing. This highlights the need for a better understanding of the key mediators in OA, and importantly, how these interact with each other. Mathematical modelling is a useful tool in human disease and is particularly useful in understanding the dynamics of interacting species. We first consider RA, where although disease modifying treatments exist, optimum treatment strategies are based mainly on clinician experience and the dynamics leading to disease remission in some individuals are still largely unknown. We hope to gain a better understanding of why remission is achievable only in some cases, and give insight into optimum dose sizing and timing. We will then move on to investigate OA, for which we know much less. Our aim in this thesis is to produce a feasible model of the dynamics of key mediators of OA which can then inform future experimental and clinical research into OA treatments. This may highlight possible targets that would otherwise have been dismissed or suggest that some current targets of research are unlikely to be successful.

1.2 Joint Biology

Joints are structures in the body where two or more bones meet. Articular (freely moving) joints, those affected by RA and OA are mainly weight-bearing joints whose function is to provide movement. Examples of these joints include the knee and hip joints. The joint is made up of three primary components, all relevant to OA. These are cartilage, bone and the synovium (Figure 1.1).

Articular cartilage lines the articular joints and has the dual function of providing a smooth surface for movement and absorbing stress [53]. These functions are essential for maintaining joint integrity, and cartilage damage can lead to long term mobility issues.

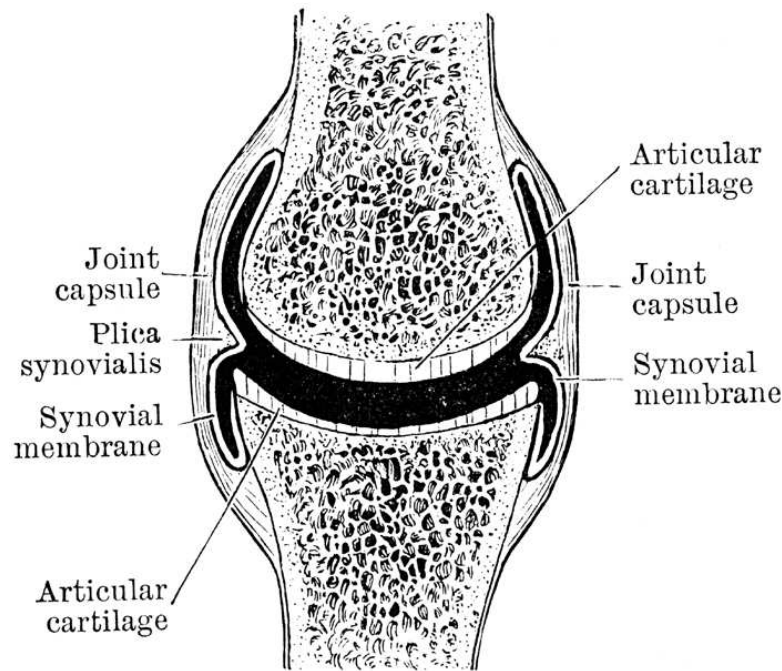


Figure 1.1: Diagram of an articular joint showing the bone, cartilage and joint capsule, taken from *Textbook of Anatomy* [30]

Cartilage tissue is avascular and aneural, comprised mainly of an extracellular matrix (ECM) of collagen and proteoglycans (Figure 1.2). The ECM is sparsely populated with chondrocytes, the only cell type. These are responsible for maintaining cartilage homeostasis by degradation, synthesis and remodelling of the ECM [86]. ECM synthesis and remodelling takes place on long time scales. ECM structure varies through the tissue and can be divided into four zones: superficial, intermediate, deep and calcified [7]. Collagen fibres, predominantly type II collagen, constitute up to 30% of the ECM [27]. The fibers form cross-links resulting in a mesh of collagen that imparts tensile strength to the ECM [117]. Proteoglycans, constituting up to 10% [27], are hydrophilic in nature and give elasticity to the ECM. The shape of cartilage is restored after deformation as water molecules are pulled back into the tissue by proteoglycans [3].

Chondrocytes derive from the mesenchymal stem cell line but specialisation makes them unique from all other cell types [97]. They are present in greatest numbers

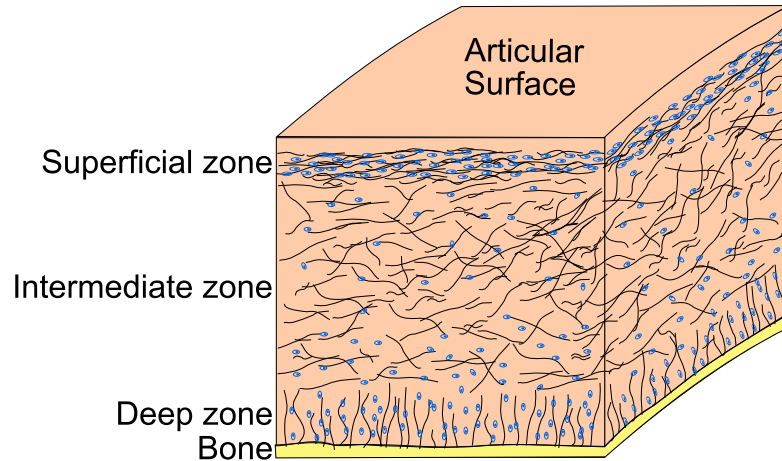


Figure 1.2: Schematic of cartilage tissue showing an ECM densely filled with collagen fibres and sparsely populated with chondrocytes (blue dots)

through childhood and adolescence then cell numbers start to decline when maturity is reached at around 30 years of age [3]. Since there is little proliferation after maturity chondrocytes have a long lifespan of decades. Chondrocytes enable the cartilage to cope with the everyday wear and tear of a mechanically loaded tissue. They respond both to mechanical changes in their environment and to chemical signals from the surrounding tissue, by remodelling the ECM [55]. They do this by producing a wide range of cytokines which have both autocrine (acting on the cell that produced them) and paracrine (acting on other cells) effects locally. Despite this chondrocytes are poor at repairing tissue from major injury or trauma since they are unable to adequately compensate tissue loss and replace the intricate network of cross-links in the cartilage. To help protect chondrocytes from the effect of excessive mechanical loading they are encapsulated within fluid-filled sacs called chondrons [109].

The synovium consists of the synovial membrane and the synovial fluid within the membrane. The synovial membrane is important to the correct functioning of articular joints and is implicated in the pathobiology of articular disease [50]. It provides a capsule for the synovial fluid, which cushions the joint against stress and provides a medium for chemical transport and immune cells; it provides a bar-

rier to control which molecules and cells are able to move through the joint space; and synoviocytes within the membrane play a crucial role in the biochemistry of the joint by synthesis of enzymes, growth factors and cytokines. Synoviocytes are the cells that make up the synovial membrane. Rather than there just being one cell type present, as in cartilage, synoviocytes come in two forms, types A and B. Type A cells are macrophages and as such are involved in the immune response of the synovial membrane [65]. They have a key role in synovial inflammation (synovitis), since as well as their phagocytic function they produce pro-inflammatory cytokines such as IL-1 [17]. Type B cells are fibroblasts whose main function is the secretion of components of synovial fluid [65]. They produce hyaluronic acid which is a major constituent of synovial fluid and the main source of lubrication, whose concentration is known to be depleted in arthritic joints [119]. Synovial fibroblasts have also been shown to produce matrix metalloproteinases (MMPs) which are tissue degrading enzymes, pro-inflammatory and anti-inflammatory cytokines when aggravated by microparticles [37], such as those present in synovitis.

Subchondral bone is the bone located immediately under the articular cartilage and provides a surface for the cartilage to anchor to. It undergoes continual repair and remodelling and releases growth factors and cytokines, some of which may move into the cartilage [86].

In addition to the cells already discussed, that are native to the tissues of the joint, some other cell types migrate to the tissue in the presence of inflammation and disease. T cells are a class of lymphocyte, a type of white blood cell, responsible for the cell mediated immune response which is part of the adaptive immune system [67]. T cells have been shown to be present in the synovial fluid of osteoarthritic joints, suggesting that at least part of the OA inflammatory response is T cell mediated [98]. T cell involvement has also been shown for related conditions such as rheumatoid arthritis [87] and juvenile idiopathic arthritis [33], however unlike OA these are both classed as autoimmune conditions (conditions where the

immune system attacks its own cells). B cells are part of the humoral immune system, another part of the adaptive immune response and their main function is to secrete antibodies [67]. These cells have been found to be activated in the synovium of osteoarthritic patients [111].

1.3 Cytokine Signalling

Cytokines are cell signalling proteins that act by binding to receptors on the cell surface. This initiates a chain of events that leads to transcription factors within the nucleus binding to promoter regions of DNA. This in turn leads to the gene expression, which involves the transcribing of the DNA and eventually the translation of this transcribed DNA (RNA) to proteins. The exact process of signal transduction varies between cell types and different cytokines and there is still much to be discovered about the control of these processes. However, there are two common pathways that are initiated by cytokine signalling and that are reasonably well understood. These are the Janus kinase / Signal Transducer and Activator of Transcription (JAK/STAT) and the Nuclear Factor - κ B (NF- κ B) signalling cascades.

The JAK/STAT kinase signalling cascade is one of the simplest pathways since STAT proteins are uniquely able to move from the cytokine receptor through the nucleus to bind to DNA as a transcription factor with no other molecules involved [31] (Figure 1.3). Upon activation of the receptor a JAK kinase protein phosphorylates the tyrosine residues (tyrosine containing monomers) on the receptor. This allows the receptor, in turn, to phosphorylate a STAT monomer [104]. Phosphorylated STAT monomers dimerise and enter the nucleus, where they bind to the DNA at high affinity sites, initiating gene transcription. This sequence of events leading to DNA binding is shown in Figure 1.3. There are 7 types of STAT and although they are similar, there are some physical and functional differences

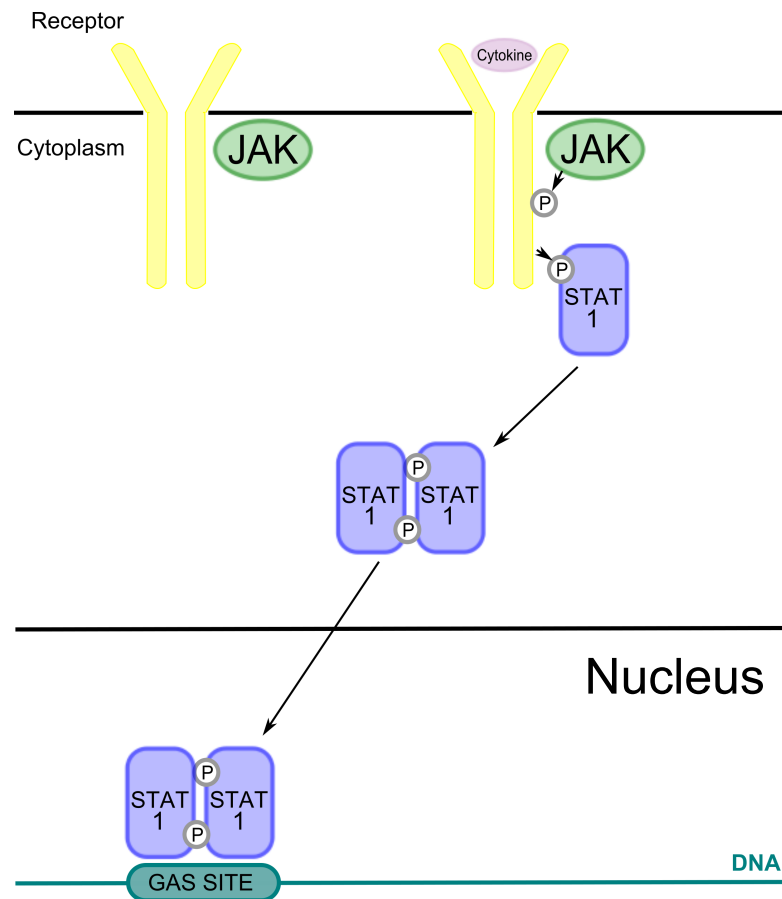


Figure 1.3: Schematic showing the JAK/STAT signalling pathway. Upon binding of a cytokine to the receptor, the STAT monomer is phosphorylated, which allows it to polymerise and move into the nucleus.

which allows for binding and activation of different gene sequences [63]. Binding of STAT proteins to DNA is not fully understood, with some members of the STAT family requiring polymerisation to remain bound to DNA and others able to bind as dimers. These issues are areas of ongoing research, see Chapter 5.

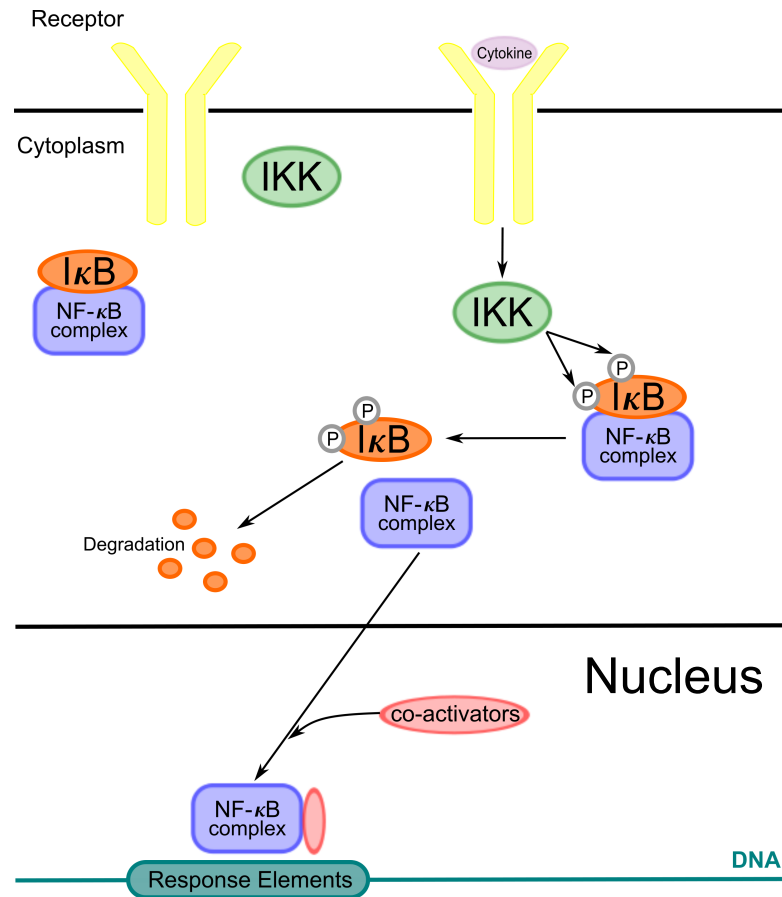


Figure 1.4: Schematic showing the NF- κ B signalling pathway. The binding of a cytokine to the receptor sets off a chain of events leading to the NF- κ B complex binding to DNA.

NF- κ B signalling is one of the best characterised signalling pathways. Its widespread involvement in inflammatory, immune, neurological and oncogenesis processes means it is implicated in a wide variety of diseases. NF- κ B consists of a family of eight closely related transcription factors [102]. When inactive they exist mainly in the cytoplasm bound to I κ B molecules. Upon activation of the relevant cytokine receptor I κ B molecules are phosphorylated by receptor-associated I κ B ki-

nases, which causes them to release the NF- κ B complex. This complex then moves into the nucleus where it binds to DNA, often in conjunction with co-activators (see Figure 1.4). NF- κ B is involved in many of the signalling cascades relevant to OA cartilage, including IL-1 and TNF- α signalling [13]. Its potential as a target for OA treatments has been researched but it is crucial for many normal biological functions so inhibition-type treatments are impractical [113].

1.4 Rheumatoid Arthritis

Rheumatoid Arthritis (RA) is an autoimmune disease predominantly affecting the joints. The condition causes chronic inflammation of the synovium due to raised cytokine levels, this leads to joint degradation and eventual destruction of the joint [26]. Symptoms of RA include pain, stiffness, immobility and inflammation. Additionally, individuals with RA may suffer from systemic symptoms such as fatigue and weight loss [61]. As a result of high circulating levels of pro-inflammatory cytokines, there is also a higher risk of developing cardiovascular diseases such as ischemic heart disease, as a result of systemic inflammation affecting coronary arteries [56]. RA patients are also at higher risk of developing some cancers and lung problems [18, 54, 92].

Causes of RA are still being investigated, however it has been established that in active RA the telomeres within some types of T cells are excessively shortened [24]. Telomeres are regions at the ends of chromosomes that are shortened over an individual's life span as part of the normal chromosome replication process, protecting genes within the chromosome from degradation [57]. Excessive or premature shortening of the telomeres can lead to defects and is associated with a range of diseases [23]. It is thought that in RA this shortening leads to a loss of T cell homeostasis and the loss of the ability to control pro-inflammatory cytokine production [72, 89]. Excessive cytokine production lies at the heart of

RA. The pro-inflammatory cytokines $\text{TNF-}\alpha$, IL-1 and IL-6 are found in raised levels in the synovium, having been released by B cells and T cells in the joint [90]. Anti-inflammatory cytokine levels, such as IL-10 and IL-4, are also raised in response but are unable to halt the pro-inflammatory cytokine production. For many individuals symptoms of RA are cyclic, and flare ups may be linked to high pro-inflammatory cytokine levels.

Treatments for RA include both pain relieving drugs and disease modifying drugs. In terms of pain relief, the range of options is the same as that for OA (see Section 1.5). Several types of disease modifying drugs are available for RA. The most widely prescribed drugs are anti-rheumatic drugs such as Methotrexate and Sulfasalazine, which are immunosuppressants. These drugs suppress the immune system, throughout the body, allowing them to be used for a range of immune and autoimmune conditions. This general action however, does mean that there can be serious side effects associated with their use [61]. For individuals where anti-rheumatic drugs are not effective biologic therapy may be used, such as anti-cytokine therapy. These drugs work by suppressing the action of one of the key cytokines active in RA. The first licensed and most widely used drugs are anti- $\text{TNF-}\alpha$ drugs such as Infliximab and Etanercept [43]. Other biologics include Tocilizumab, an IL-6 inhibitor and Rituzimab, a B cell inhibitor. All the biologic therapies are relatively new drugs, having been available for only the last 15 years, which means long term side effects are not yet fully explored. For this reason, as well as cost, biologic drugs are not currently used as a first-line treatment.

1.5 Osteoarthritis

Osteoarthritis (OA) is a disorder of the synovial joints characterised by a loss of cartilage, inflammation and changes to the subchondral bone [82]. Clinical symptoms of the disease include inflammation, pain, stiffness in affected joints,

and instability of the joints. The joints in an individual are not typically affected homogeneously, particularly if injury or repetitive strain has been a contributing factor [7]. Studies of the epidemiology of OA show it is more prevalent in aged individuals and more likely to affect women than men [32]. Other risk factors include obesity, genetic factors, particularly mutations of the Col2A gene, which affects collagen production, and a history of joint injury or excessive mechanical strain as seen in certain manual occupations as well as professional sportsmen [7].

OA is a disease of the whole joint and changes associated with disease onset and progression are seen in the cartilage, subchondral bone and synovium [46]. Changes in the cartilage are most pronounced and are thought to be most important in terms of progression and loss of joint function [16]. However the cause of disease onset is as yet unclear and may not be cartilage based. In some animal models subchondral bone changes have been shown to precede cartilage damage [74], whilst in other work increased numbers of pro-inflammatory cytokine receptors have been found in OA chondrocytes [15]. One popular viewpoint is that OA is not a disease with a single cause but rather a set of initial abnormalities that lead to a single progression pathway [45]. Another viewpoint is that OA is a repair mechanism for a variety of problems in the joint and with increasing age the repair mechanism itself develops faults leading to clinically diagnosed OA. More research is needed into the initiation and early stages of OA as it is likely that this is the point where treatment would be most effective as has been found in RA [96]. The biological changes in OA are described below and summarised in Table 1.1.

In osteoarthritic cartilage the normal homeostatic balance between ECM synthesis and degradation fails and both processes accelerate [115]. The changes that characterise early OA are different to those that characterise late OA. In early OA there is an increased rate of cell proliferation, stimulated by cytokines, and characteristic chondrocyte clustering is seen [50]. Synthesis of the ECM is increased, either as the result of higher levels of anabolic cytokines (cytokines mediating

ECM synthesis) or greater sensitivity to anabolic cytokines, both of which have been observed [15]. However, despite the increased synthesis the fibrils laid down are disorganised and lacking the cross linkage needed to give strength. Cartilage breakdown is also accelerated through raised pro-inflammatory cytokine levels, which results in additional MMPs [86]. The degradation of the ECM includes fibronectin breakdown and waste fibronectin fragments act as an irritant stimulating further pro-inflammatory cytokine response [85].

As OA progresses, raised levels of TNF- α lead to increased levels of chondrocyte apoptosis, although this has only a small effect on the cartilage [115]. In later OA however, there is a significant decrease in matrix synthesis and increased rates of degradation, some of which may be due to the reduction in chondrocytes. Inflammation is often present in late osteoarthritis and evidence suggests that as well as being an undesirable clinical symptom, inflammation leads to further breakdown of the cartilage and a loss of function, probably due to additional inflammatory cytokines [17]. Ultimately the ECM degradation processes begin to dominate the ECM synthesis and the cartilage is thinned and damaged. Without cartilage the bone endings rub together, causing pain, immobility and inappropriate mechanical loading. Another change in late OA is the development of osteophytes, bony spurs growing on the bone endings of OA joints, due to subchondral bone damage. These are formed at the growth plate between the cartilage and subchondral bone through ossification of cartilage and bone remodelling. It is likely that this process is mediated by anabolic cytokines since these are found in high levels in osteophytes in experimental models [14]. Often, osteophytes do not have any symptoms and may be an attempt to distribute loads more effectively, but they may cause pain and loss of mobility if they are in particularly sensitive areas, e.g. close to nerve endings [20].

As previously discussed matrix degradation is a major reason for progression of OA and is the main cause of joint instability and inflammation. It is now generally

accepted that cytokines play a major role in the pathways leading to excessive degradation as well as a role in the efforts to limit or repair the damage [116]. Type II collagen is broken down by MMP-1 (Collagenase-1), MMP-8 and MMP-13 and synthesis of these MMPs is increased in OA by raised levels of IL-1 and TNF- α [126]. IL-1 and TNF- α bind to different receptors on the cell but both initiate similar responses once bound which involves activation of several types of kinases, including NF- κ B kinase, leading to activation of transcription factors for the MMPs [126]. Offsetting some of this activity IL-1Ra will also bind to the IL-1 receptors but will not activate these pathways. Synthesis of proteoglycans, another major component of the ECM is also inhibited by a pro-inflammatory cytokine mediated pathway. Chondrocytes are induced to produce nitric oxide (NO) by IL-1 and studies have shown that NO inhibits the synthesis of proteoglycans within articular cartilage [121]. To a lesser degree TNF- α and IL-6 also reduce proteoglycan synthesis, although in the case of the latter only in the presence of soluble IL-6 receptor α .

OA bone shows increased remodelling near the joint which leads to greater density [75], which is associated with protection from osteoporosis. Mineralisation is not increased so overall the bone contains less minerals and is more brittle [75]. This means that bone is more susceptible to damage on loading and more likely to transfer inappropriate loads to the cartilage leading to damage. It has been suggested that the increased bone density can be an initiating factor in OA [75]. In early OA bone resorption by osteoclasts is increased and lesions appear in the bone. The number and size of these lesions increase as the disease progresses and can be used as a measure of disease severity, since they are easily viewed by MRI. In later OA additional bone is laid down by osteoblasts, and it has been suggested that this is an attempt at widening the joint surface to distribute the load [46]. Subchondral bone is known to express increased levels of growth factors including insulin-like growth factor I (IGF-1) and TGF- β . These growth factors

stimulate proliferation and differentiation of osteocytes as well as increased bone matrix synthesis [74]. It is likely that these factors also pass directly across the damaged growth plate in OA, to the cartilage, where they exert similar effects on the chondrocytes [46]. In late OA the synovium starts to show changes associated with chronic inflammation.

Treatment for OA is aimed at relieving symptoms such as pain, inflammation and stiffness rather than reducing or repairing the damage caused by OA. In part this may be due to the historical difficulties in differentiating OA from general joint pain at an early enough stage, meaning that patients present with considerable damage to both the cartilage and subchondral bone. However, another major reason for the lack of preventative treatments is the poor understanding of the mediators of matrix degradation.

A range of pain relief drugs are offered to individuals with OA, the most basic of which are simple systemic analgesics such as paracetamol for moderate pain or stronger opioids for more intense pain. More sophisticated treatments involve reducing the inflammation, which increases mobility and reduces pain, typically via Non Steroidal Anti Inflammatory Drugs (NSAIDs), such as ibuprofen or diclofenac [70]. Alternatively COX-2 inhibitors, such as celecoxib, may be used if NSAIDs are unsuitable [32]. In severe cases, steroid treatment may be used at the site of the inflammation in the form of corticosteroid injections [100].

As OA progresses conventional drugs may be inadequate to alleviate the symptoms sufficiently so in these cases surgery may be used. Surgical options include keyhole surgery to clean out the joint and reduce inflammation, partial removal of subchondral bone (in knee joints) and joint replacement surgery [84]. In extreme cases a procedure called arthrodesis may be offered, which involves fusing the joint into a permanent position to increase stability [84]. Options such as these highlight the need for research into effective treatment in early OA to slow

progression of the disease. Other complementary treatments for osteoarthritis may be recommended alongside those mentioned above. These include treatments to slow disease progression and increase mobility such as low impact exercise or physiotherapy [32]. Another treatment used is Transcutaneous Electrical Nerve Stimulation (TENS) therapy, which uses electrical impulses to block pain related nerve signals [100]. However, although widely used evidence for the effectiveness of this treatment is lacking [91].

Treatments being researched for OA tend to fall into three categories: drugs aimed at reducing the symptoms and progression of OA, tissue engineering to help repair damage to the joints and gene therapy. Cytokines are involved in both inflammation and matrix degradation in OA, meaning that they are relevant both to disease progression and the clinical symptoms of OA. This makes them a good target for possible treatment strategies. Many cytokines have been implicated in OA but those thought to be of particular relevance are the pro-inflammatory cytokines, IL-1 and TNF- α , and the anti-inflammatory cytokines, IL-4, IL-10 and IL-1Ra. All of these have been shown to be present at higher than normal levels in OA. Since so many growth factors, cytokines and hormones are involved in OA pathways there are many potential targets for treatment, however the complexity means that blocking one pathway will be unlikely to halt progression of the disease altogether. In addition to this, specificity and side effects make finding suitable treatments difficult. One treatment possibility is anti TNF- α treatment, which inhibits the action of TNF- α thereby reducing the matrix degradation and inflammation associated with OA. Anti TNF- α treatment was first developed for the treatment of rheumatoid arthritis, where inflammation plays a greater role. Experimental studies showed blocking the action of TNF- α reduced inflammation and clinical trials showed that this treatment was beneficial in RA sufferers [2]. TNF- α has been shown to be important in the inflammatory response and ECM degradation in OA so may prove to be a good therapeutic target. One anti TNF- α

drug is currently undergoing clinical trials as a treatment for OA, but no results have been reported [12]. Several other targets are in various stages of clinical trials. These include drugs to target Nerve Growth Factor in order to reduce pain; MMP inhibitors to reduce matrix degradation; and IL-1 inhibitors including IL-1Ra injections [12]. One of the IL-1 inhibitors recently tested for OA was Anakinra [25], this drug is clinically effective in the treatment of RA (although not recommended for treatment due to poor cost effectiveness) however clinical trials found it was not effective as a treatment for OA.

Gene therapy has two potential uses in OA, firstly if used early enough it may prevent the progression of the disease, secondly it may be used in the repair of damaged tissue [41]. The first of these cases includes injecting vectors carrying genes into the synovium or articular cartilage. This method has had some success in experimental models, particularly using genes coding for IL-1Ra, known to be effective at inhibiting the effects of IL-1 [41]. Several of these treatments have made it to the clinical trials stage, however these are still in the early stages so although safety has been established, effectiveness has still to be determined. The use of gene therapy to initiate cartilage repair in partial thickness lesions, as seen in OA, has also been successfully demonstrated in animal models, see Gelse et al. [47] and Goomer et al. [51].

In order for cytokine related drug treatments to be used in OA, we need a clear understanding of typical cytokine levels and a link between this and disease progression. Levels of cytokines are difficult to measure and vary greatly in OA between different individuals. This may be the result of different stages of disease progression, differing levels of inflammation or the complex interactions of different cytokines. There is also some evidence that genetic factors are important. However generally, there is a consensus that the levels of the major cytokines involved in OA are high compared with those of normal subjects [50, 116]. The classification of normal and osteoarthritic subjects is difficult due to the nature

of OA. There is no one marker that indicates the presence of OA and symptoms vary both between individuals and within different joints of a single individual. An additional complication is that OA is highly prevalent in the elderly, who are most at risk of the disease, so finding comparable healthy non arthritic subjects is difficult. It has been suggested that OA affects as many as 80% of those over 75 years of age [7]. Despite these difficulties some studies have found that cytokine levels are raised in OA, Moos et al. [94] found the levels of IL-1, TNF- α , IL-4, IL-6 and IL-10 were all raised compared to the level in normal cartilage tissue, which was negligible. In a study by Goekoop et al. [48] subjects were taken from volunteers of a cohort study of people born in the city of Leiden, The Netherlands, rather than being taken from patients presenting with a illness as is more usual. The subjects had blood samples taken at the age of 85, and a measure of *ex vivo* cytokine levels was taken. Five years later the subjects completed a medical questionnaire to determine the presence or absence of OA. Sixteen of the 82 subjects that were available for both parts of the study were considered to be free of OA (no OA in the hips, knees or hands) and the study reported lower levels of IL-1b, IL-6 and IL-1Ra. Levels of IL-10 and TNF- α were not significantly different. Levels of TNF- α are not elevated in many of the studies conducted, one reason for this may be that TNF- α is implicated only in the most severe, late stage OA [86], so raised levels would not be seen in most subjects with OA. Another reason may be that rather than the TNF- α levels becoming raised, the cells themselves may become more sensitive to this cytokine, this has been suggested by Arntz et al. [8].

We have a good understanding of the biochemical processes in the cartilage, and which processes are implicated in OA. However, there is no clear understanding of what the initiating events that cause OA are, or how the process may be halted. Additionally, research in this area is challenging for many reasons. Cytokines are short lived and act locally, hence making them difficult to detect in easily obtainable samples (e.g. blood serum, urine). Symptoms of OA in humans do

not generally occur until late in the disease process, making research into early OA limited. Finally, OA is a truly multi-scale disease with joint mechanics as well as biochemical processes both being important factors. This means that experimental cell based research cannot be easily extrapolated *in vivo*. Similarly, joint mechanics in animal models are significantly different to human. All these factors make this area an ideal candidate for mathematical modelling.

Tissue	Change	Mechanism	Stage of OA
Cartilage	Chondrocyte Proliferation	Stimulated by anabolic cytokines	Early
	Increased Proteoglycan Synthesis	Stimulated by anabolic cytokines	Early
	Increased Collagen Synthesis	Stimulated by anabolic cytokines	Early
	Increased MMPs	Stimulated by pro-inflammatory cytokines	Early; Late
	Increased ECM Turnover	Mediated by MMPs	Early; Late
	Chondrocyte Apoptosis	Stimulated by pro-inflammatory cytokines	Late
	Increased anti-inflammatory cytokine production	Stimulated by pro-inflammatory cytokines	Early; Late
	Inflammation	Stimulated by pro-inflammatory cytokines	Late
	Osteophyte Development	Subchondral bone damage	Late
	Increased fibronectin fragments	Waste product of ECM turnover	Early; Late
Subchondral Bone	Bone resorption	Osteoclast activity	Early
	Bone production	Osteoblast activity	Late
	Osteoblast proliferation and differentiation	Stimulated by anabolic cytokines	Late
Synovial Changes	Localised synovial inflammation	Fibronectin fragments and pro-inflammatory cytokines from cartilage	Subclinical and Early
	Generalised synovial inflammation	Inflammatory factors from cartilage and locally produced pro-inflammatory cytokines	Late

Table 1.1: Summary of the biological changes seen on osteoarthritis

1.6 Previous modelling work

1.6.1 Articular Cartilage and Subchondral Bone

The modelling of normal cartilage and bone has been relatively widely researched in order to give an insight into what happens when these normal processes start to malfunction. These models are often of the mechanics of the tissue rather than the biochemical properties which may provide insight into some of the stimulus or responses resulting from the biochemical changes during osteoarthritis. Several authors have developed models of chondrocytes surrounded by ECM and these may be particularly relevant as OA progresses and symptoms of OA such as apoptosis and depleted collagen and proteoglycan content become more profound. For example, Wu et al. [130] proposed a model of cartilage containing chondrocytes surrounded by ECM. These were considered to have different material properties as suggested by experimental results and showed how the tissue would deform in space and time under mechanical loading. The authors did not explore how this might change under degenerative conditions such as OA but did suggest that the model could be used to look at degeneration and remodelling.

A paper by Treweek [125] presented a continuum model of a single chondrocyte producing an extracellular matrix. This model differed from previous studies in two main aspects, firstly it looked at a single chondrocyte in isolation, rather than looking at cartilage as a tissue and secondly it considered two methods of movement of matrix components, diffusion and advection. Generally diffusion is considered to be the only significant method of movement. In this article the authors investigated the model in relation to the development of tissue engineered cartilage, however it may have some relevance to the attempts at cartilage repair during early OA, and the movement of cytokines through the ECM.

A model of fracture healing in bone by Bailón-Plaza et al. [9] may be relevant

to our work. This model simulates cell migration, proliferation, ECM remodelling and growth factor levels. The model used PDEs and ODEs to successfully demonstrate the regulatory mechanisms of the fracture healing process which requires migration and differentiation of mesenchymal stem cells followed by cartilage formation and ossification. The model neglects many of the growth factors and cells involved in the process and concentrates on only two growth factors and three cells types, which the authors considered to be most important, however the results are still comparable to experimental results. Whilst the tissue and processes here are different to osteoarthritis in articular cartilage (the involvement of the vasculature for example), the paper shows how models of the regulatory molecules and cells can be used to simulate structural changes in the tissue.

More recent modelling include attempts to model synthetic or repaired cartilage, such as a model by Lutianov et al, which used PDEs to model the cartilage response to cell regeneration therapy [83], or a model by Catt et al [22], simulating cartilage growth on a scaffold.

1.6.2 Arthritic Diseases

There is very little published work modelling arthritic conditions and those that are available generally consider the mechanical aspects for the conditions rather than the biochemistry mediating these events. In an early model of RA by Witten [128] the author presents a second order logistic growth model of articular erosion in RA. The model shows how the cartilage might erode over time based on reported erosion at presentation of an individual, however the model does not consider the processes behind the erosion and so is of little use in investigating how the disease progresses. Similarly, Pollatschek and Nadir [107] present a high level ODE model of the deterioration of certain components in OA, such as proteoglycan content, shock absorbance and microfractures. Whilst the model serves

to demonstrate that OA can be modelled mathematically, the components identified are the observable clinical symptoms of OA rather than underlying factors and processes such as cytokine mediation. Whilst models of OA and RA are not common, some of the typical processes of these diseases are more widely modelled, albeit for different applications. For example, angiogenesis present in RA has been modelled in relation to tumour growth (see [88], [106] and [69]), and bone remodelling as seen in osteophyte formation has also been modelled [123]. Inflammation is now thought to be involved in osteoarthritis as well as RA and models of inflammation are discussed below.

1.6.3 Inflammation

Models of inflammatory responses may be the most relevant models to look to when building models of cytokine interactions in osteoarthritis, since inflammation is increasingly seen as an important part of OA [17], and even some non-inflammatory events in OA are mediated by the same cytokines. Inflammation may be classified as either an acute or chronic response, both of which may be present in OA [19].

A model of acute systemic inflammation as a result of pathogen infection was presented by Kumar *et al.* [73]. The model identified five possible outcomes dependent on parameters: healthy response, non-infectious inflammation, infectious inflammation, recurrent inflammation and immuno-deficient response. It seems likely, given reported clinical symptoms that some of these responses would be present in OA, particularly healthy response and recurrent inflammation, although the stimulus of inflammatory response would not be pathogen related and the inflammation in OA is not systemic but is restricted to particular joints within an individual. A general model of inflammation was proposed by Herald [60], which showed conditions under which an inflammatory response would become chronic

in the absence of ongoing infection. The model showed that if the macrophages are particularly sensitive to pro-inflammatory cytokines, or if anti-inflammatory cytokine levels are low, then even small inflammatory responses to infection become chronic rather than being resolved.

1.6.4 Cytokines

There has been very little published work modelling cytokines either as part of a biological process or alone, however two key models may be relevant to OA modelling. One model uses a set of six continuous differential equations to describe the behaviour of IL-1 and IL-10 with TNF- α in monocytes as an external stimulus for IL-1 [118]. The model showed different types of behaviour dependent upon the parameter values including uncontrolled production of IL-1, stable equilibria and stable limit cycles. The authors were able to link the model results to observed behaviour in RA and Septic Shock, and it is likely that with some modification, some parts of this model could be incorporated into a model of synovitis in OA. This may be complicated however by the involvement of chondrocytes as well as macrophages.

A related model by Jit [68] looked in more depth at the pro-inflammatory TNF- α and in particular, modelled the effects of anti TNF- α drugs in the inflamed synovial joint. The study considered the issue of why anti TNF- α drugs worked well in the treatment of RA but were not effective in Systemic Inflammatory Response Syndrome (SIRS), another TNF- α mediated condition. From the model results the authors suggested that cytokine levels in RA were usually in equilibrium and anti TNF- α treatment forced a shift from a disease equilibrium to a healthy equilibrium. However, they suggested that SIRS was a non-equilibrium condition and as such was not able to be moved to a healthy equilibrium state, further they suggested that the drugs may interfere with the body's natural attempts at repair.

1.7 Thesis Outline

In the rest of this thesis we develop several models relevant to cytokine dynamics in arthritic disease. In Chapter 2 we develop a two-variable model of pro- and anti-inflammatory cytokine dynamics in the synovium. We use bifurcation analysis to explore the parameter space and find monostable, bistable and oscillatory behaviours. We consider how changes in cytokine production rates could lead to RA and demonstrate that this model displays features present in RA initiation and progression. We model anti-cytokine treatment and consider the importance of dose size, interval and timing to treatment outcome.

In Chapter 3 we extend the previous model to include MMPs and fibronectin fragments, making it relevant to cartilage cytokine dynamics. We use one- and two-parameter bifurcation analysis to explore the transitions between behaviour types. We replace constant parameters with time dependent functions to explore possible pathways to OA initiation. We consider the effectiveness of different treatment strategies, and combine treatments to find the best treatment outcome.

We consider the spatial aspects of cartilage cytokine dynamics in Chapter 4 by developing a model of OA cartilage using a Cellular Potts model. We consider two main tissue types, chondrocytes and ECM, surrounded by synovial fluid and bone. We investigate how the spatial separation of chondrocytes changes the dynamics that we see in Chapter 3. Diffusion coefficients are not readily available for cytokines, MMPs and Fn-fs in cartilage so we consider the effect that differing diffusion rates may have on the model.

In Chapter 5 we consider some of the downstream signalling dynamics that we have so far neglected, but which could affect cytokine signalling. In particular we focus on the JAK/STAT pathway and focus our analysis on the binding of STAT proteins to DNA. Given that STAT1 is known to require cooperative binding to remain bound to DNA, we investigate whether there is a requirement for multiple

high affinity binding sites. We also consider how STAT3, another member of the STAT family of proteins, interacts with STAT1 when competing for binding sites.

Finally in Chapter 6 we summarise the results we have found in this work and consider how this could be developed in future work.

Chapter 2

Pro- and anti-inflammatory cytokine model for rheumatoid arthritis

2.1 Introduction

Rheumatoid arthritis (RA) is a chronic inflammatory joint disease which affects around 1% of the adult population [128]. The condition is three times more likely to affect women (likely due to changes in hormone levels with age) than men and disease onset generally occurs over the age of 40, although it occurs much earlier in a small number of individuals [64].

The disease is characterised by chronic inflammation of the synovial lining of joints (synovitis) with consequent destruction of cartilage and bone [26]. Cells in inflammatory synovitis produce high levels of numerous cytokines which act locally to produce the characteristic joint pain, swelling and stiffness, and systemically to produce a range of effects including the production of acute phase proteins by the liver, part of the systemic immune response [64]. In addition to being easily measurable markers of inflammation, these proteins contribute to some of the long term systemic effects of RA including the two-fold increase in cardiovascular

mortality [34], as a result of exacerbated tissue injury during myocardial infarction [105]. It is thought that cytokine interactions play a crucial role in the development of RA and can modulate the severity and duration of the associated inflammation [52].

A range of cytokines have been identified in the synovium and each one has a unique but overlapping set of functions. They can be classified into pro-inflammatory and anti-inflammatory groups according to the primary function of the cytokine in the synovium. Two of the most important pro-inflammatory cytokines in rheumatoid arthritis are interleukin-1 (IL-1) and tumour necrosis factor- α (TNF- α) [26]. Examples of anti-inflammatory cytokines found in the synovium include IL-1 receptor antagonist (IL-1Ra) and Interleukin-10 (IL-10) [36]. Based on this we think it is useful to model this system using the classification of pro- and anti-inflammatory cytokine groups. To date, there has been no RA-specific modelling that considers the dynamics of both pro- and anti-inflammatory cytokines. By modelling these two groups we can look at the involvement of cytokines in RA onset and treatment, which has not been considered previously.

The redundancy and dual role of many cytokines suggests that a functional rather than chemical classification may prove particularly useful. We therefore aim to represent the complex cytokine network in the synovium by a simple two variable model. This will allow us to assess whether changes in the parameters governing these two groups and their interactions can lead to the features seen in RA. In addition to looking at the development and progression of RA we would like to consider the effect of anti-cytokine treatment of RA and consider which properties of treatment lead to a beneficial response.

In the following section we look at the model development and justify the terms within the model. We also non-dimensionalise the model and give a biological interpretation of each of the parameters. In Section 2.3 we analyse the model,

beginning with consideration of the nullclines and steady states of the system. We then look at bifurcations as we vary the pro-inflammatory cytokine production parameter, which allows us to classify the different types of behaviour in the system. Lastly we look at bifurcations in two parameter space and consider how these change for different values of the other parameters. In Section 2.4 we consider the possibility of time dependent changes in patient-specific parameters leading to the onset of RA. In Section 2.5 we consider the effect of treatment involving doses of anti-inflammatory cytokines. We look at different dose levels and regimes and how these affect the behaviour of the model. Finally in Section 2.6, we consider possible clinical implications of the model as well as its limitations.

2.2 An activator-inhibitor model for cytokine interactions

The synovium consists of a variety of cells including fibroblasts, macrophages and T cells and each individual cell has a different response pattern [4], as discussed Chapter 1. We neglect this variability in cell behaviour and the synovium is modelled as a spatially uniform collection of homogeneous, generic cells. We focus on the cells' production of pro-inflammatory and anti-inflammatory cytokine molecules and neglect other functions such as cytotoxic mechanisms or proliferation. The binding of pro-inflammatory cytokine molecules to membrane-bound receptors induces production of both pro-inflammatory and anti-inflammatory cytokines whilst the binding of anti-inflammatory molecules causes a downregulation in production of pro-inflammatory molecules. This has been demonstrated by Brennan et al. [21] who showed that $\text{TNF-}\alpha$ has both an autocrine and paracrine pro-inflammatory function, and upregulates itself as well as other pro-inflammatory cytokines (particularly IL-1). $\text{TNF-}\alpha$ is also known to upreg-

ulate the production of IL-10 which functions to downregulate both TNF- α and IL-1 [36].

We denote the concentration of pro-inflammatory cytokine molecules by p and the concentration of anti-inflammatory cytokine molecules by a . The degradation of a cytokine concentration is assumed to be linear, with rates d_p and d_a . The general form of the equations for the cytokine dynamics is then

$$\frac{dp}{dt} = -d_p p + \phi(p)\theta(a) \quad (2.2.1)$$

$$\frac{da}{dt} = -d_a a + \psi(p). \quad (2.2.2)$$

The product $\phi(p)\theta(a)$ models the combined effect of pro-inflammatory and anti-inflammatory stimuli on pro-inflammatory cytokine production, based on the assumption that anti-inflammatory molecules work by inhibiting the synthesis of pro-inflammatory cytokine molecules [103]. $\phi(p)$ and $\psi(p)$ are increasing saturating functions of p , so that they represent induced upregulation with some maximum production rate. Similarly, $\theta(a)$ represents the downregulation of p in response to an increase in a and with a decreasing effect from some maximum at $a = 0$. Examples of functions which have these properties are

$$\phi(p) = c_0 + c_1 \frac{p^{m_1}}{c_2^{m_1} + p^{m_1}} \quad (2.2.3)$$

$$\theta(a) = c_3 \frac{c_4^{m_2}}{c_4^{m_2} + a^{m_2}} \quad (2.2.4)$$

$$\psi(p) = c_5 \frac{p^{m_3}}{c_6^{m_3} + p^{m_3}}. \quad (2.2.5)$$

where $c_0, c_1, c_2, c_3, c_4, c_5$ and c_6 are non-negative constant parameters. Since pro-inflammatory production is stimulated by an external stimulus and is detected in low levels in normal blood [124], a background production term c_0 has been included in $\phi(p)$, anti-inflammatory production is stimulated only by pro-

inflammatory cytokine molecules so no background term is necessary. The coefficients m_1 , m_2 and m_3 will all be taken as 2 for the analysis of this system since values greater than 2 show qualitatively similar behaviour and a value of 1 reduces the range of behaviours, this is discussed further in Appendix A. Some sample forms for these feedback functions are shown in Figure 2.1.

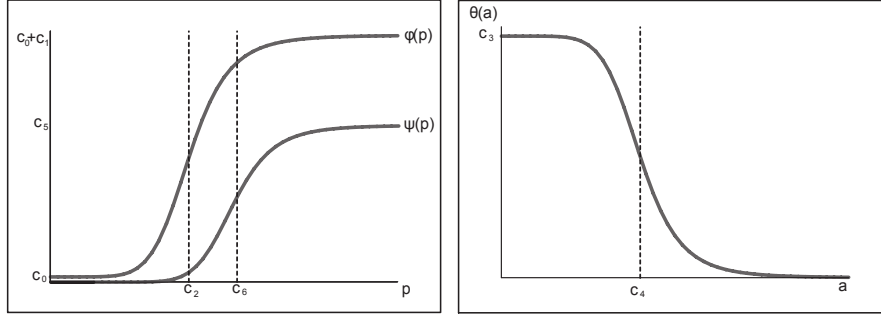


Figure 2.1: Examples of qualitative forms for the production feedback functions $\phi(p)$, $\theta(a)$ and $\psi(p)$ (Equations 2.2.3, 2.2.4, and 2.2.5).

The model equations are nondimensionalised using

$$p = p^* c_2, \quad a = a^* c_4 \quad \text{and} \quad t = t^* \frac{1}{d_a};$$

With the asterisks dropped for notational simplicity and setting $m_1 = m_2 = m_3 = 2$, equations (2.2.1) - (2.2.2), with the equations 2.2.3, 2.2.4, and 2.2.5, become

$$\frac{dp}{dt} = -\gamma_p p + \frac{1}{1+a^2} \left(P_{bp} + P_{pp} \frac{p^2}{1+p^2} \right) \quad (2.2.6)$$

$$\frac{da}{dt} = -a + A_{pp} \frac{p^2}{A_{ph}^2 + p^2}, \quad (2.2.7)$$

where

$$P_{bp} = \frac{c_0 c_3}{c_2 d_a}, \quad P_{pp} = \frac{c_1 c_3}{c_2 d_a}, \quad A_{ph} = \frac{c_6}{c_2}, \quad A_{pp} = \frac{c_5}{c_4 d_a} \quad \text{and} \quad \gamma_p = \frac{d_p}{d_a}.$$

P_{bp} is the dimensionless background production rate for pro-inflammatory cytokine so that when $a = p = 0$, pro-inflammatory production occurs at a rate P_{bp} . The parameter P_{pp} corresponds to the maximum rate of pro-inflammatory cytokine production over and above the basal rate. A_{ph} is the concentration of pro-inflammatory cytokine at which anti-inflammatory production is half maximal. A_{pp} corresponds to the maximum rate of production of anti-inflammatory cytokine. γ_p is the ratio of the pro-inflammatory and anti-inflammatory decay rates.

Throughout this work we explore the behaviour of the system by looking at different parameter values so it is useful to have some idea of the values that would be reasonable. We can gain some insight into this by examining the definitions of the parameters which are summarised for reference in Table 2.1.

Parameter	Interpretation
P_{bp}	Background pro-inflammatory production rate
P_{pp}	Magnitude of additional pro-inflammatory cytokine production
A_{ph}	Pro-inflammatory cytokine concentration at which anti-inflammatory production is half maximal
A_{pp}	Magnitude of anti-inflammatory cytokine production
γ_p	Relative rate of clearance of pro-inflammatory cytokine to anti-inflammatory cytokine

Table 2.1: Summary of the dimensionless parameters in the cytokine dynamics model (2.2.6)-(2.2.7)

If we assume that the cytokine degradation rates are similar then we would expect $\gamma_p = \frac{d_p}{d_a}$ to be close to 1. A_{ph} is the ratio of the EC_{50} of anti-inflammatory production to the EC_{50} of pro-inflammatory production, where EC_{50} is the concentration of the variable which induces a response halfway between the maximal and minimal response. Since both c_2 and c_6 are both thresholds for p and are

activated via the same receptors we would expect them have similar values, hence we expect A_{ph} to be of order 1.

We expect P_{pp} to be of the same order as the maximum anti-inflammatory cytokine production rate, A_{pp} . We consider a range of values for these parameters in the bifurcation analysis that follows in Sections 2.3.2 and 2.3.3. In order to have an effective response to infection and injury, the background level of cytokines must be much smaller than the event stimulated production, hence P_{bp} needs to be small, and should be much smaller than P_{pp} .

In the following sections we will consider how the nullclines of the system can intersect for different parameter values, determining the number of steady states in the system. We show how through bifurcation analysis how bistability and oscillatory behaviour can arise from this model and consider possible interpretations of this behaviour in a biological context.

2.3 Model Analysis

2.3.1 Nullclines and Steady states

To analyse the steady states of this system we will consider the forms of the nullclines, and consider only the positive quadrant. The nullclines of the system (2.2.6), (2.2.7) respectively, are as follows:

$$a = N_a(p) = \frac{A_{pp}p^2}{A_{ph} + p^2}$$

$$a = N_p(p) = \sqrt{f(p)}$$

where

$$f(p) = \frac{p^2(P_{bp} + P_{pp}) + P_{bp}}{\gamma_p p(1 + p^2)} - 1.$$

Figure 2.2 shows the ways that these nullclines may intersect and hence how the steady states may arise. The diagrams suggest there is always at least one steady state and for some parameter values three steady states exist: S_0 , S_1 and S_2 .

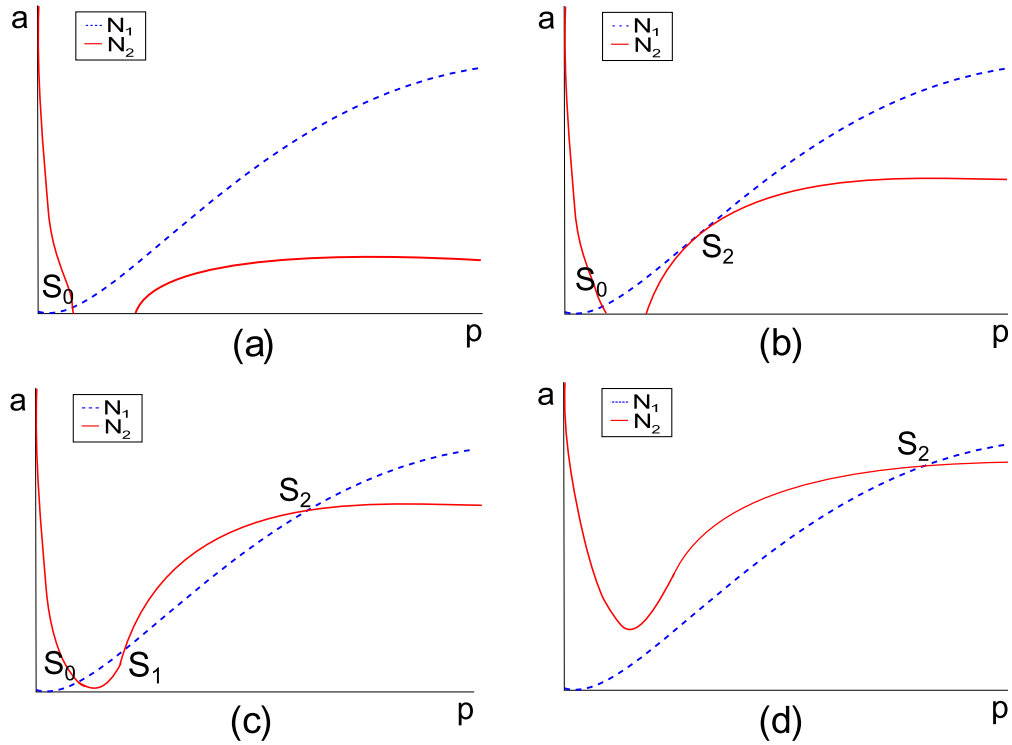


Figure 2.2: Schematic showing the nullclines of the system (2.2.6), (2.2.7) and the different ways they may intersect. The dashed line represents the a nullcline ($\frac{da}{dt} = 0$) and the solid line represents the p nullcline ($\frac{dp}{dt} = 0$).

We cannot find the steady states of this system analytically but by looking at the turning points of each nullcline we can identify how many possible steady states there may be. $N_a(p)$ is simply an increasing Hill function and always goes through the point $(p, a) = (0, 0)$. The number of turning points of $N_p(p)$ cannot be found analytically but since we need only consider real positive values of p and a , we can see that the number of turning points of $N_p(p)$ will be equal to the number of turning points in $f(p)$.

Differentiating $f(p)$ shows it has four possible turning points at,

$$p = \frac{\sqrt{2} \sqrt{(P_{bp} + P_{pp})((P_{pp} - 2P_{bp}) \pm \sqrt{P_{pp}^2 - 8P_{pp}P_{bp}})}}{2(P_{bp} + P_{pp})} \quad (2.3.1)$$

and

$$p = -\frac{\sqrt{2} \sqrt{(P_{bp} + P_{pp})((P_{pp} - 2P_{bp}) \pm \sqrt{P_{pp}^2 - 8P_{pp}P_{bp}})}}{2(P_{bp} + P_{pp})}. \quad (2.3.2)$$

p will always be either negative or complex in Equation 2.3.2, leaving only two relevant turning points. If $P_{pp} < 8P_{bp}$ then both these points will be complex. This means that $N_p(p)$ will be a monotonically decreasing function and can cross $N_a(p)$ only once, giving a single steady state. Otherwise, $f(p)$ and consequently $N_p(p)$ must decrease to zero and then increase again from zero so can cross $N_a(p)$ three times giving a maximum of three steady states. It is not possible to find the stability of the steady states analytically, but the Jacobian, A , shown below, does give us some information regarding the stability,

$$A = \begin{pmatrix} -\gamma + \frac{2P_{pp}}{(1+a^2)} \frac{p}{(1+p^2)^2} & \frac{-2a}{(1+a^2)^2} \left(P_{bp} + P_{pp} \frac{p^2}{1+p^2} \right) \\ 2A_{pp} \frac{A_{ph}^2 p}{(A_{ph}^2 + p^2)^2} & -1 \end{pmatrix} \quad (2.3.3)$$

Hence,

$$\text{Tr}A = \frac{2P_{pp}}{(1+a^2)} \frac{p}{(1+p^2)^2} - \gamma - 1 \quad (2.3.4)$$

$$\det A = \gamma - \frac{2P_{pp}}{(1+a^2)} \frac{p}{(1+p^2)^2} + 4A_{pp} \frac{a}{1+a^2} \left(P_{bp} + P_{pp} \frac{p^2}{1+p^2} \right) \left(\frac{A_{ph}^2 p}{(A_{ph}^2 + p^2)^2} \right) \quad (2.3.5)$$

We can see that when $p \ll 1$ and $a \ll 1$ then $\text{Tr}A \approx -\gamma - 1$ and $\det A \approx \gamma$,

so for a small p , S_0 will be stable. At some point, for steady states at larger values of p and a , the steady state loses stability. The $\lim_{p \rightarrow \infty} \text{Tr}A = -\gamma - 1$ and $\lim_{p \rightarrow \infty} \det A = \gamma$; so, S_2 is stable for large values of p . The exact thresholds for the loss of stability depend on the both the variable and parameter values and cannot be determined analytically; however, numerical simulation reveals that in the parameter ranges we are interested in, S_0 is always stable, S_1 is always unstable and S_2 can be either stable or unstable.

There is one case in which a steady state and stability can be determined analytically: when P_{bp} is zero. We can see from the nullclines that if P_{bp} is zero (i.e. there is no background pro-inflammatory cytokine production) then there is a steady state at $(p,a)=(0,0)$. Examining the trace and determinant in this case gives $\text{Tr}A = -\gamma - 1$, which will always be negative and $\det A = \gamma$, which will always be positive, meaning that the steady state must be stable.

The case of two state states only occurs at bifurcations. For this reason, throughout this chapter we will focus more on the one and three steady state cases.

2.3.2 One Parameter Bifurcation Diagrams

Of the five free parameters, the cytokine production rates (P_{pp} and A_{pp}) are rates that could change as part of the immune response and so, are likely to change over time in response to injury, aging, or therapeutic intervention. If we assume that the rate of clearance is determined by the size and structure of the cytokine and by the chemical environment within the host, it is reasonable to assume the decay rate parameter γ_p will remain constant in an individual (or vary over a much longer timescale than that over which cytokine interactions occur). Similarly, we assume that the background production rate and the anti-inflammatory production threshold parameter, P_{bp} and A_{ph} , are fixed within an individual. To demonstrate the types of behaviour that can arise from this model we consider

bifurcation diagrams of variations in P_{pp} for a range of different values of the other parameters. The types of behaviour displayed are summarised in Table 2.2 and discussed in detail below. All bifurcation plots and simulations in this chapter were produced in XPPAUT [39] and MatCont [35].

Case	Steady States	Limit Cycles
Ai	S_0 - Stable	—
Aii	S_2 - Stable	—
Aiii	S_0 - Stable; S_1 - Unstable; S_2 - Unstable	—
B	S_2 - Unstable	L_1 - Stable
Ci	S_0 - Stable; S_1 - Unstable; S_2 - Stable	—
Cii	S_0 - Stable; S_1 - Unstable; S_2 - Stable	L_2 - Unstable
Di	S_0 - Stable; S_1 - Unstable; S_2 - Unstable	L_1 - Stable
Dii	S_0 - Stable; S_1 - Unstable; S_2 - Unstable	L_1 - Stable; L_2 - Unstable

Table 2.2: Summary of the behaviour types in the cytokine dynamics model (2.2.6)-(2.2.7). S denotes steady states and L denotes limit cycles

Monostable and Bistable Behaviour

In a simple case, illustrated in Figure 2.3, two fold bifurcations give rise to monostable and bistable behaviour. For sufficiently small values of P_{pp} monostable behaviour is seen where trajectories undergo at most one peak in p before decaying to the steady state S_0 which has a low level of p (case Ai). The phase plane for this case is shown in Figure 2.3b, and the nullclines correspond to Figure 2.2a. This case could generally be considered as a healthy state since p is always low and there are no oscillations.

For intermediate values of P_{pp} , bistable behaviour is observed, with two stable steady states and a single unstable steady state (case Ci), shown in Figure 2.3c. In this case the stable manifold of S_1 divides phase space into two regions, the basins of attraction of the healthy state S_0 and the disease state S_2 . The values of P_{pp} and A_{pp} determine the size of the region contained within the stable manifold. Increasing A_{pp} decreases the size of the region whereas increasing P_{pp} increases the size of the region. This means that if anti-inflammatory production is increased then the set of disease states is smaller and if the pro-inflammatory production is increased the set of disease states is larger. One counter-intuitive observation to be made from Figure 2.3c is that any state within the disease region could be returned to the healthy state by a stimulus that increases the pro-inflammatory concentration sufficiently. This would cause a further increase in p triggering an anti-inflammatory response which would raise both a and p before returning both to lower levels at the healthy steady state. Similarly, but more intuitively, a sufficient increase in the anti-inflammatory concentration can always return the system to a state of health.

Finally, for sufficiently large P_{pp} there is another monostable case (case Aii), in which all trajectories in the phase plane undergo oscillations of decaying magnitude to S_2 (Figure 2.3d). In this case, the value of p is generally relatively high, indicative of a disease state. However, as A_{pp} is increased the value of p at S_2 decreases, and case Aii starts to behave like case Ai, making the distinction between health and disease less clear. Changes in A_{pp} are discussed further in Section 2.3.3.

Monostable and Bistable Behaviour with Oscillations

For larger values of A_{pp} (\sim 3-fold increase compared to Fig 2.3a) the model also displays oscillatory behaviour in addition to the behaviours described above (Figure 2.4). This more complex bifurcation diagram corresponds to two additional

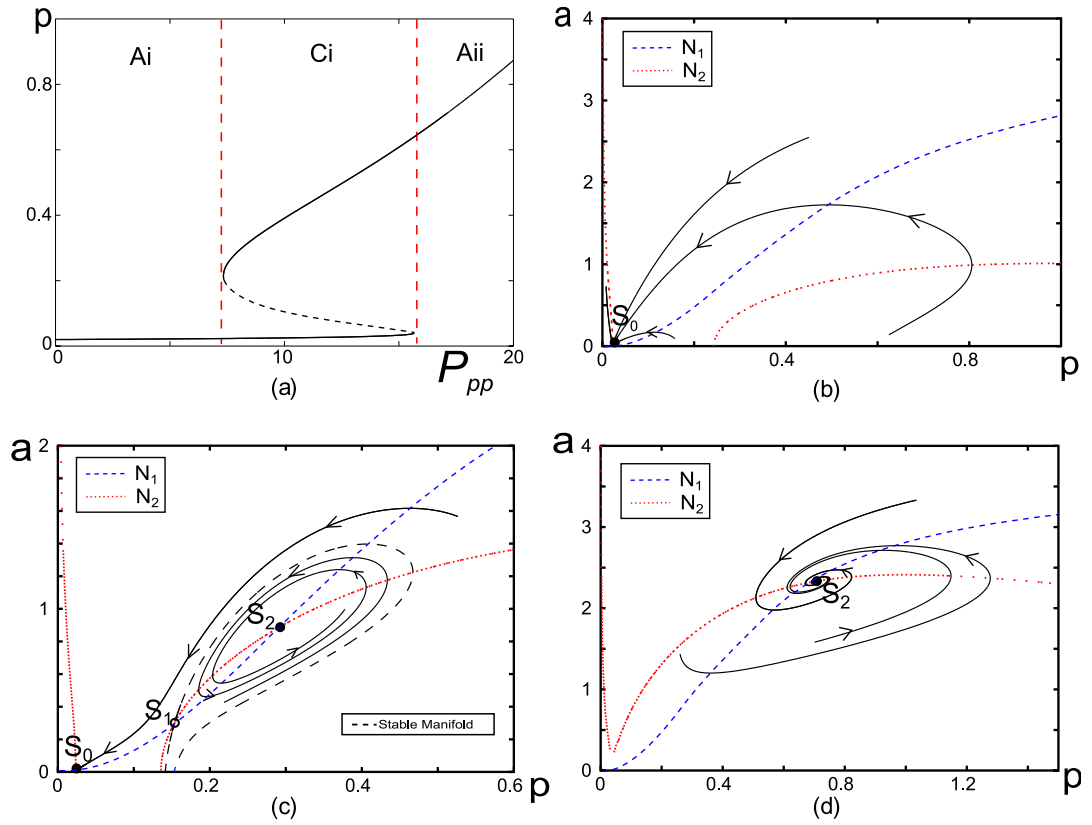


Figure 2.3: Monostable and Bistable behaviour in the model (2.2.6)-(2.2.7) for the interaction between pro and anti-inflammatory cytokines ($P_{bp} = 0.025$, $A_{ph} = 0.5$, $A_{pp} = 3.5$ and $\gamma_p = 1.25$). (a) Bifurcation plot of p against P_{pp} . The solid lines represent stable branches whilst the dashed lines represent unstable branches. The vertical red dashed lines signify the thresholds between different behaviour types. (b) Phase plane plot of Case Ai, a single healthy steady state ($P_{pp} = 5$). (c) Phase plane plot of Case Ci, two stable steady states (S_0 and S_2) and one unstable steady state (S_1) ($P_{pp} = 8$). (d) Phase plane plot of Case Aii, a single unhealthy steady state with ($P_{pp} = 17$).

types of phase-plane behaviour. The first type, case Di, has a single stable steady state (S_0), two unstable steady states (S_1 and S_2), and a stable limit cycle around S_2 (Figure 2.4b). In this situation the limit cycle represents inflammation in the system due to fluctuating high levels of p (perhaps reflecting relapsing-remitting disease, see [79]). This case is similar to Ci, with all states within the stable manifold of S_1 , evolving to the disease limit cycle and all states outside evolving to the healthy state.

The second new behaviour, case B, has only a single unstable steady state (S_2) surrounded by a stable limit cycle (Figure 2.4c). The limit cycle can be thought of as a disease state due both to high levels of p and the oscillatory behaviour. This is similar to case Aii, since all trajectories undergo decaying oscillations into the disease limit cycle.

The bifurcation plot in Figure 2.4a shows that as P_{pp} is increased it goes through a fold bifurcation, then a Hopf, followed by a second fold and finally a second Hopf. For larger values of A_{pp} (~ 6 -fold increase compared to Fig 2.3a) we encounter both the folds before the Hopf bifurcations (Figure 2.5a), which means that we lose Di behaviour. As A_{pp} is increased further (~ 10 -fold increase compared to Fig 2.3a) Ci behaviour is also lost (Figure 2.5b).

Monostable and Bistable Behaviour with Homoclinic Bifurcations

For a small range of parameters, there is a saddle node bifurcation that gives rise to a stable limit cycle, L_1 , surrounded by an unstable limit cycle, L_2 (Figure 2.6a). There is also a homoclinic bifurcation where the unstable limit cycle, L_2 , collides with the steady state S_1 , giving rise to additional behaviours. A monostable region exists with a stable steady state, S_0 , and two unstable steady states, S_1 and S_2 (case Aiii). This case behaves similarly to Ai, except that within the stable manifold trajectories will approach S_0 in an oscillatory manner (Figure 2.6b). For

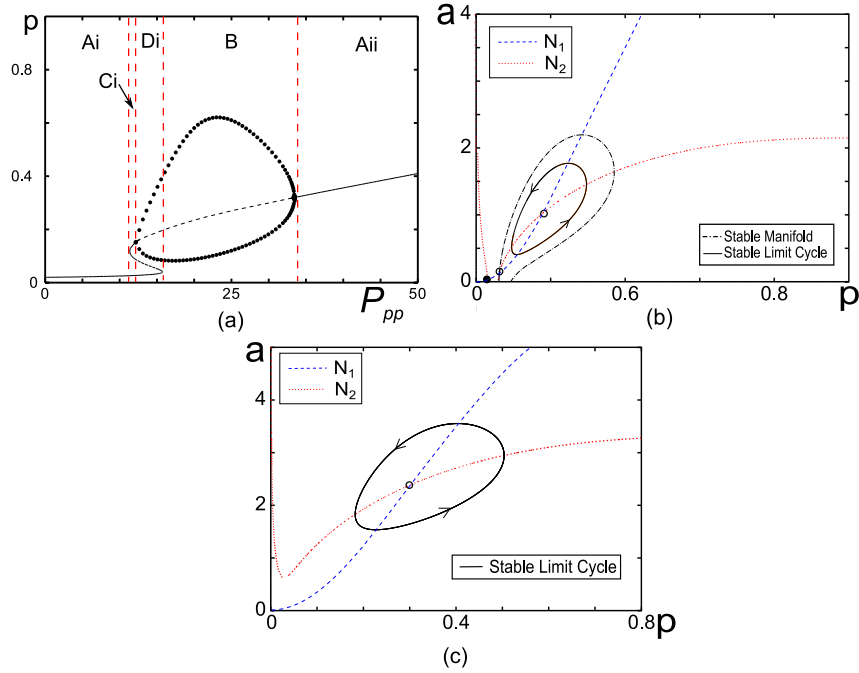


Figure 2.4: Monostable and Bistable behaviour with oscillations in the model (2.2.6)-(2.2.7) for the interaction between pro and anti-inflammatory cytokines ($P_{bp} = 0.025$, $A_{ph} = 0.5$, $A_{pp} = 9$ and $\gamma_p = 1.25$). (a) Bifurcation plot of p against P_{pp} . The solid lines represent stable branches whilst the dashed lines represent unstable branches. The vertical red dashed lines signify the thresholds between different behaviour types. (b) Phase plane plot of Case Di, one stable steady state (S_0) two unstable steady states and a stable limit cycle around S_2 ($P_{pp} = 15$). (c) Phase plane plot of Case B, one unstable steady state (S_2) surrounded by a globally stable limit cycle ($P_{pp} = 30$). Cases Ai, Ci and Aii are shown in Figure 2.3.

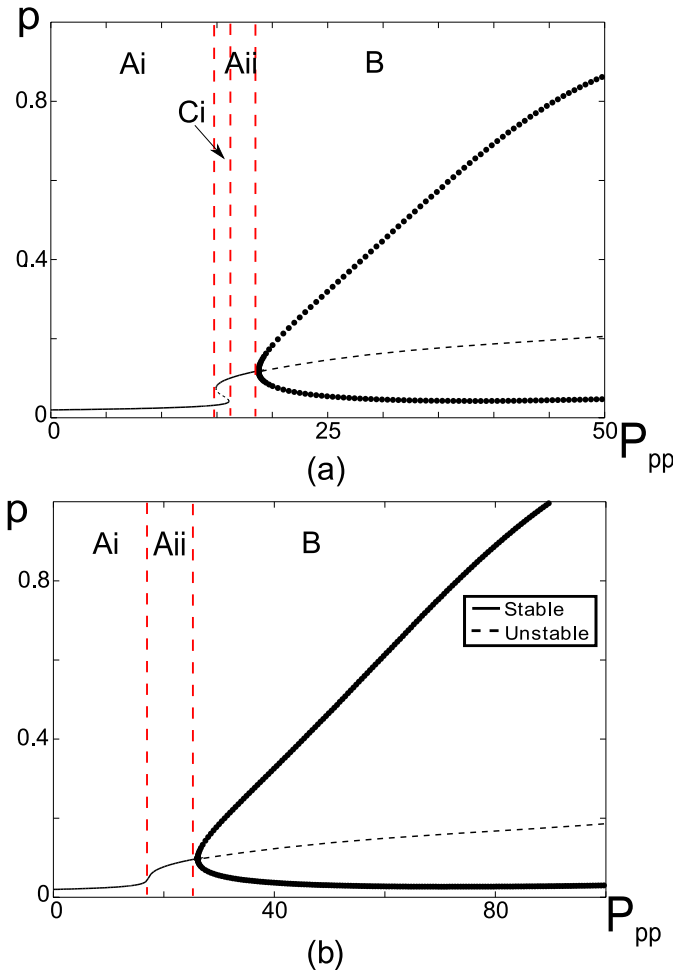


Figure 2.5: Bifurcation plots for different values of A_{pp} showing how cases Ci and Di are lost compared with Figure 2.4a ($P_{bp} = 0.025$, $A_{ph} = 0.5$ and $\gamma_p = 1.25$). The solid lines represent stable branches whilst the dashed lines represent unstable branches. The vertical red dashed lines signify the thresholds between different behaviour types. (a) $A_{pp} = 18$, first Hopf bifurcation moves to right of the second fold and case Di is lost (b) $A_{pp} = 30$, folds coalesce and all bistability is lost.

a very narrow parameter range the system is bistable (Figure 2.6c) with one stable steady state and one stable limit cycle, as well as two unstable steady states and an unstable limit cycle (case Dii). The stable limit cycle, L_1 , with high pro-inflammatory cytokine concentrations, represents a disease state and lies inside the unstable cycle, L_2 . L_2 defines the basin of attraction of the disease cycle and the most suitable treatment strategy depends on the current stage in the cycle. For example, if an individual has a high level of a and an intermediate level of p , then to bring about a state of health, an increase in anti-inflammatory cytokine would be more effective than a decrease in pro-inflammatory cytokine of similar magnitude.

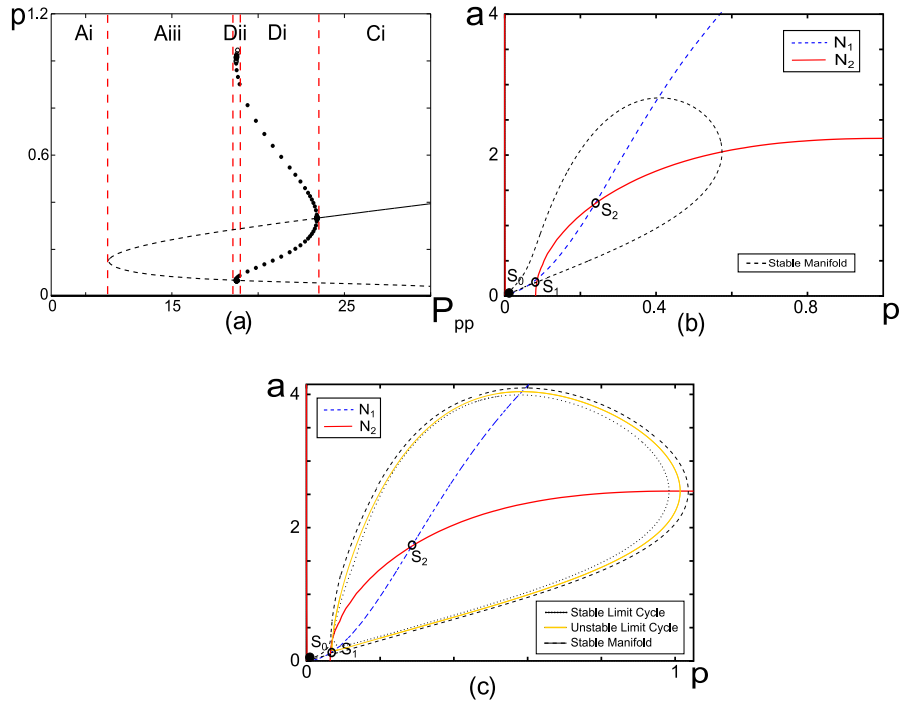


Figure 2.6: Monostable and Bistable behaviour with homoclinic bifurcations in the model (2.2.6)-(2.2.7) for the interaction between pro and anti-inflammatory cytokines, showing the new behaviours Aiii and Dii. (a) Bifurcation plot of P_{pp} against p . The solid lines represent stable branches whilst the dashed lines represent unstable branches. The vertical red dashed lines signify the thresholds between different behaviour types. (b) Phase plane plot of Case Aiii, a stable steady state (S_0) and two unstable steady states ($P_{pp} = 15$). (c) Phase plane plot of Case Dii, a stable steady state (S_0), two unstable steady states, a stable limit cycle and an unstable limit cycle ($P_{pp} = 18.73$). Cases Ai, Ci and Di are shown in Figure 2.4. ($P_{bp} = 0$, $A_{ph} = 0.5$, $A_{pp} = 7$ and $\gamma_p = 1.25$)

Bistable behaviour with a homoclinic bifurcation

One final type of behaviour (case Cii) can be seen for larger values of A_{ph} (Figure 2.7). Here, an unstable limit cycle exists with two stable steady states (S_0 and S_2) and one unstable steady state (S_1). The limit cycle is the boundary of the basin of attraction of S_2 . The unstable manifold of S_1 divides the remaining region into those states which evolve to health in an oscillatory fashion (those inside the unstable manifold) and those which have at most one extremum (those outside the unstable manifold). This state arises through a supercritical Hopf bifurcation, where the branch of limit cycles turn and become unstable almost immediately after the bifurcation.

So far we have considered only variations in the pro-inflammatory cytokine production rate, P_{pp} . It is likely that the anti-inflammatory cytokine production rate, A_{pp} , is also important in determining disease activity since anti-inflammatory cytokines will mitigate pro-inflammatory cytokine response. Hence, in the next section we will look at P_{pp} - A_{pp} parameter space for different values of the other three parameters.

2.3.3 Two Parameter Bifurcation Diagrams

It is useful to consider the two parameter bifurcation structure in P_{pp} - A_{pp} parameter space. Figure 2.8 shows bifurcation diagrams for several different values of P_{bp} . It illustrates the curves of Hopf and fold bifurcation points and the types of phase-plane behaviour that are observed in this space and demonstrates the effect that changes in P_{bp} have on the bifurcations. The figure also shows that where the Hopf and fold bifurcations meet we have Bogdanov-Takens points. A Bogdanov-Takens bifurcation is a bifurcation of codimension 2, i.e. it is only seen as we vary two parameters, and occurs where there is a pair of zero eigenvalues. From this point a homoclinic bifurcation emerges between the fold and Hopf bifurcations. In

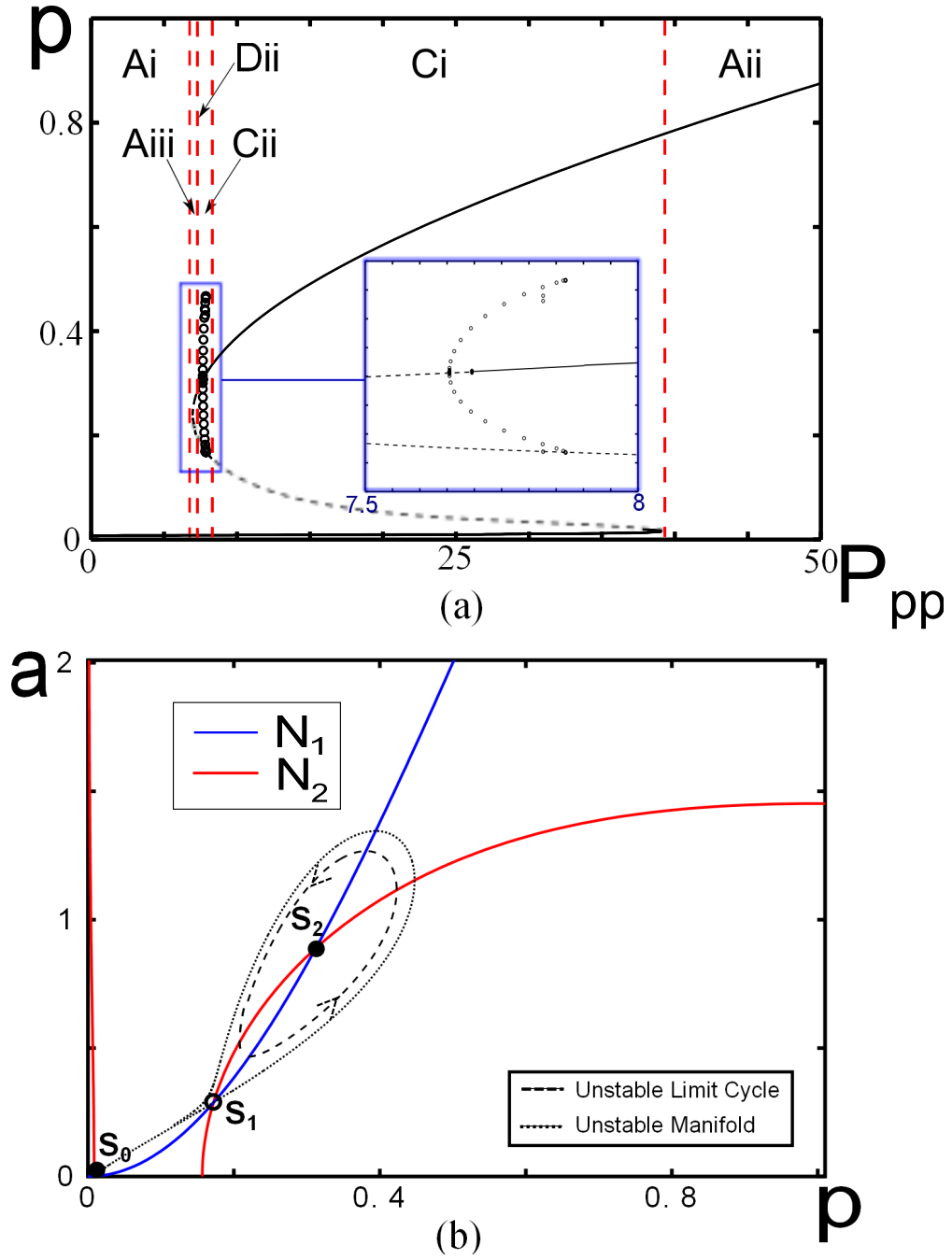


Figure 2.7: Bistable behaviour with a homoclinic bifurcation in the model (2.2.6)-(2.2.7) for the interaction between pro and anti-inflammatory cytokines. (a) Bifurcation plot showing P_{pp} plotted against p . The inset shows how Case Cii arises through a supercritical Hopf bifurcation where the branch of limit cycles turns and becomes unstable almost immediately after bifurcation. The solid lines represent stable branches whilst the dashed lines represent unstable branches. The vertical red dashed lines signify the thresholds between different behaviour types. (b) Phase plane plot showing case Cii, two stable steady states (S_0 and S_2), an unstable state (S_1) and an unstable limit cycle around S_2 ($P_{pp} = 7.75$). Cases Ai, Aii, Aiii and Ci are shown in Figures 2.4 and 2.6. ($P_{bp} = 0.01$, $A_{ph} = 1$, $A_{pp} = 10$ and $\gamma_p = 1.25$)

the diagrams in this section the Hopf bifurcations are denoted H_1 and H_2 , the fold bifurcations are denoted F_1 and F_2 and the Bogdanov-Takens points are labelled BT. The dotted line in Figure 2.8b corresponds to the one parameter bifurcation diagram shown in Figure 2.4. It is now clear why increasing A_{pp} results in the loss of Di and Ci, since the overlap of the regions enclosed by the Hopf and fold bifurcations is decreased and then the folds are destroyed at the cusp. It is important to make the distinction between a healthy state and a disease state since when A_{pp} is sufficiently small there is a range of P_{pp} over which two observable stable steady states can coexist. Where there are two stable steady states the relative levels of p allow one to be designated as disease and the other as health, since in any individual baseline levels of cytokines may vary. Where there is only one stable state, designation of health or disease is more difficult.

As P_{bp} is decreased, the fold and Hopf bifurcations connect at a Bogdanov-Takens point, one of the Hopf bifurcations is lost and a homoclinic bifurcation emerges. Additionally, the cusp where the fold bifurcations meet occurs at larger values of both P_{pp} and A_{pp} . The background production parameter P_{bp} does not significantly alter the position of the Hopf bifurcation H_1 . However, as P_{bp} is decreased H_2 moves closer to F_1 , with H_2 eventually being destroyed, leaving the system with only one Hopf bifurcation, H_1 , which is then supercritical as before and can cause the creation of a stable limit cycle.

Figure 2.8d shows the two parameter bifurcation diagram for $P_{bp} = 0$, where is no background production, and here the steady state structure of the system changes. When the system is at zero concentration no cytokine is produced and it remains at this state, thus the healthy state S_0 is fixed at $(p = 0, a = 0)$ and is stable. The system still has an unstable state S_1 and a state S_2 which can be stable or unstable. Since S_2 occurs at a relatively high value of p , if S_2 is stable it represents a disease state and may lie an unstable limit cycle. S_2 can also be unstable in which case the system can only be in the healthy cytokine-free state unless S_2 lies

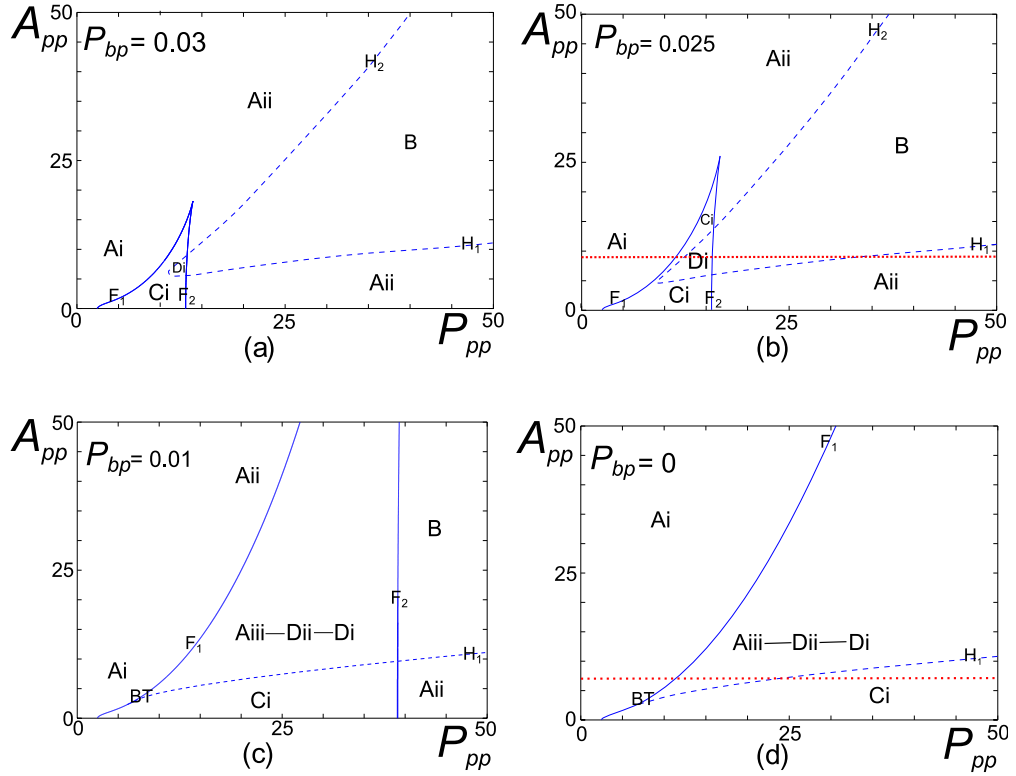


Figure 2.8: Parameter space plots in P_{pp} - A_{pp} ($A_{ph} = 0.5$ and $\gamma_p = 1.25$) showing the fold (F_1 and F_2) and Hopf (H_1 and H_2) bifurcations and types of phase space for decreasing values of P_{bp} . (a) Cases Ai, Aii, B, Ci and Di are shown. (b) Cases Ai, Aii, B, Ci and Di are shown. The red dashed line represents a slice through the parameter space at $A_{pp} = 9$, consistent with the bifurcation plot in Figure 2.4 ($P_{bp} = 0.025$). (c) Cases Ai, Aii, Aiii, B, Ci, Di and Dii are shown., (d) Cases Ai, Aii, Aiii, Ci, Di and Dii are shown. The red dashed line represents a slice through the parameter space at $A_{pp} = 7$, consistent with the bifurcation plot in Figure 2.6 ($P_{bp} = 0$).

within a stable limit cycle (with the system at either the healthy state or in a state of periodically varying cytokine concentrations). When this is compared with the behaviour when $P_{bp} > 0$ we see that cases Aii and B are no longer possible since there is always a stable healthy state.

Variations in A_{ph} and γ_p show similar effects to variations in P_{bp} . Figure 2.9 shows P_{pp} - A_{pp} parameter space for a range of values of A_{ph} . As A_{ph} increases, the cusp at which the fold bifurcations meet and are destroyed occurs for a higher value of the anti-inflammatory production parameter A_{pp} . The pro-inflammatory production parameter P_{pp} at the cusp varies little with A_{ph} . One consequence of this effect is that if the threshold A_{ph} is large then the range of states which can exhibit health and disease is increased. When A_{ph} is small, most conditions lead a single state with pro- and anti-inflammatory concentrations varying according to P_{pp} . Figure 2.10 shows a two parameter bifurcation diagram for a large value of A_{ph} but a smaller value of P_{bp} . Here, all the possible behaviours are observed through variations in P_{pp} and A_{pp} .

Figure 2.11 shows P_{pp} - A_{pp} parameter space diagrams for various values of γ_p and demonstrates that as γ_p decreases the fold and Hopf bifurcations move apart. This means that the parameter region over which there is bistability decreases and the majority of parameter space leads to a single generic stable steady state or a stable limit cycle. Biologically this implies that decreasing the clearance of pro-inflammatory cytokine from the system, leads to disease, and reduces the likelihood of curable disease. Conversely, increases to the rate of clearance could offer better treatment response rates.

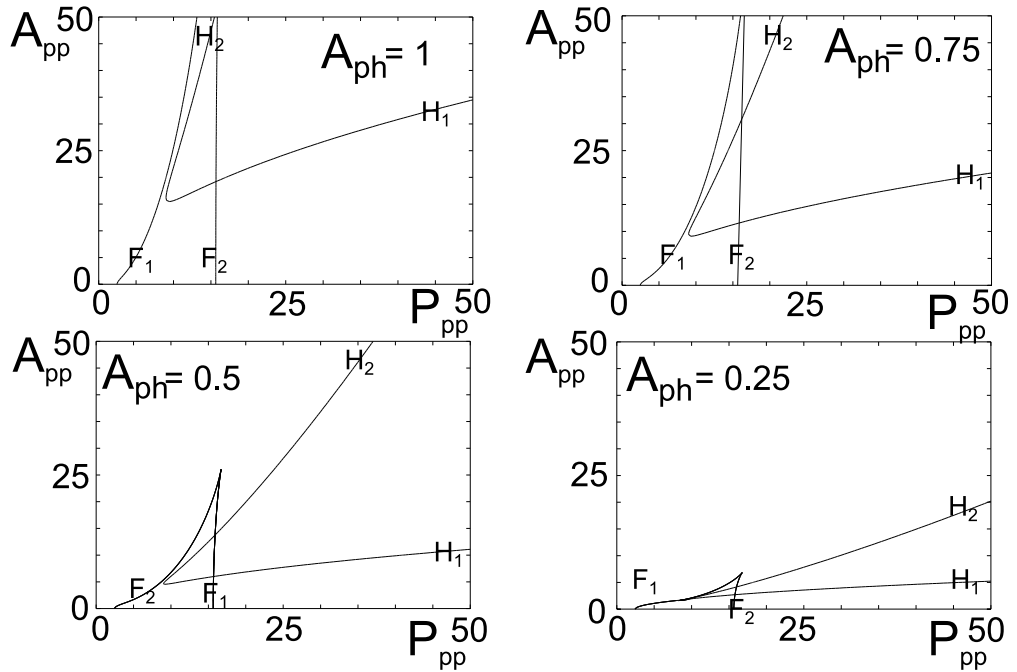


Figure 2.9: Figure showing the dependence on threshold parameter A_{ph} of the location of fold and Hopf bifurcations in P_{pp} - A_{pp} parameter space for parameter values ($P_{bp} = 0.025$, $\gamma_p = 1.25$).

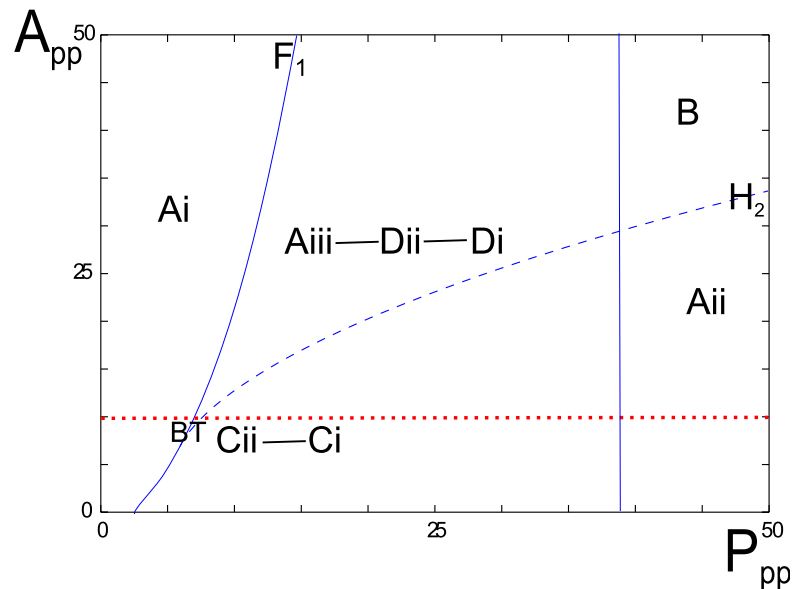


Figure 2.10: P_{pp} - A_{pp} parameter space showing all the behaviour types found in the model. The red dashed line represents a slice through the parameter space at $A_{pp} = 10$, corresponding to the bifurcation plot in Figure 2.7 ($P_{bp} = 0.01$, $A_{ph} = 1$ and $\gamma_p = 1.25$)

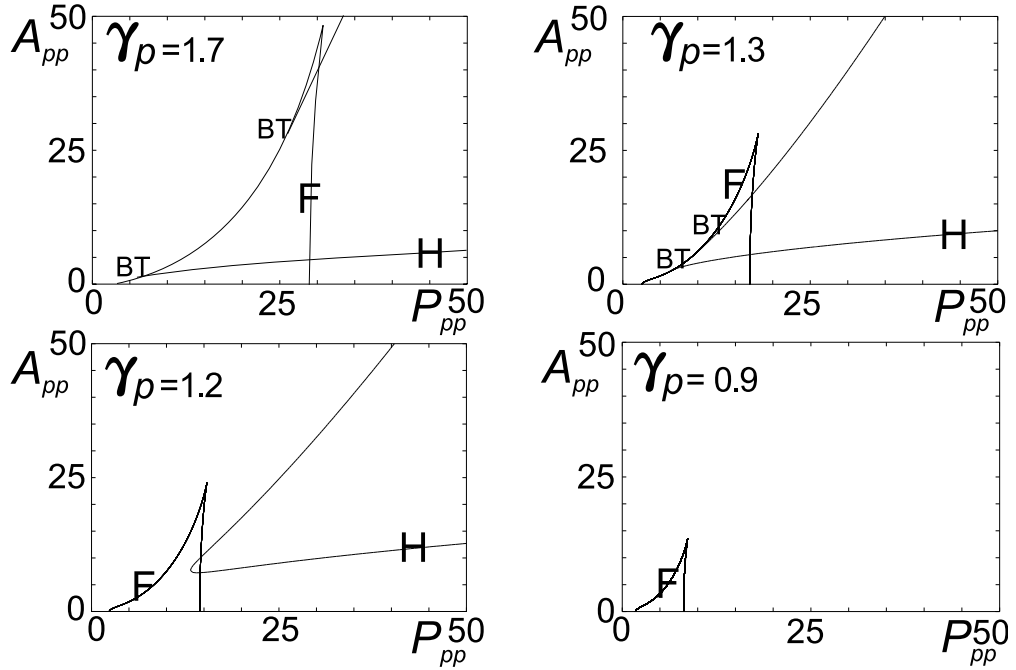


Figure 2.11: Diagrams showing the positions of the fold (F) and Hopf (H) bifurcations in P_{pp} - A_{pp} parameter space for decreasing values of γ_p and the parameters ($P_{bp} = 0.025$ and $A_{ph} = 0.5$).

2.4 Time-Dependent Parameter Variations

Some cases of rheumatoid arthritis have a characteristic mode of onset in which an initially healthy individual experiences flaring and remitting inflammation (palindromic RA) over a sustained length of time before eventually reaching a state of persistent synovitis. The model given by equations (2.2.6)-(2.2.7) is capable of reproducing some of the key features of this onset pattern by using a time-dependent pro-inflammatory production parameter P_{pp} . It is likely that such fluctuations in P_{pp} occur *in vivo* due either to a spontaneous rise in pro-inflammatory cytokine production in response to injury or infection or a gradual rise in production with increasing age [29, 114]. To illustrate the potential of this approach we can consider P_{pp} as an increasing, saturating function of time,

$$P_{pp}(t) = P_{pp}^{min} + \frac{(P_{pp}^{max} - P_{pp}^{min})t^2}{P_{pp}^{T^2} + t^2}$$

so that $P_{pp}(0) = P_{pp}^{min}$ with P_{pp} increasing with time and $\lim_{t \rightarrow \infty} P_{pp}(t) = P_{pp}^{max}$. The parameter P_{pp}^T is the time at which the $P_{pp}(t)$ is at half maximal. We take $P_{pp}^{min} = 1$, $P_{pp}^{max} = 50$ and $P_{pp}^T = 15$ with the remaining parameters given by $\{\gamma_p = 1.25, P_{bp} = 0.025, A_{ph} = 0.50\}$. Figure 2.12 shows how P_{pp} changes over time.

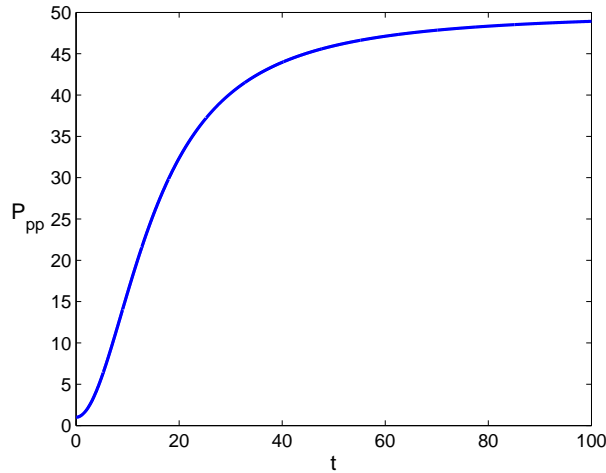


Figure 2.12: Plot of the time dependent pro-inflammatory cytokine production parameter P_{pp} against time.

We run simulations for a set of constant values of A_{pp} , equivalent to taking a horizontal section through the parameter plane in Figure 2.8(b). It is immediately obvious that A_{pp} will be critical in determining the evolution pattern. To show this effect the simulation is run for the values $A_{pp} = \{2, 7, 15\}$ and the concentration evolution in each case is shown in Figure 2.13.

These results show that in each case, when P_{pp} is sufficiently large, the system is forced to the disease state, S_2 , but significant differences in the form of the cytokine response are observed. For low A_{pp} , as P_{pp} increases with time, the state is forced to stable disease without any oscillations. For larger A_{pp} , as P_{pp} increases the state is still forced into stable disease but has an intermediate period of oscillations. The length of time over which the system is in an oscillatory state increases with A_{pp} and for a large A_{pp} the system is forced into sustained

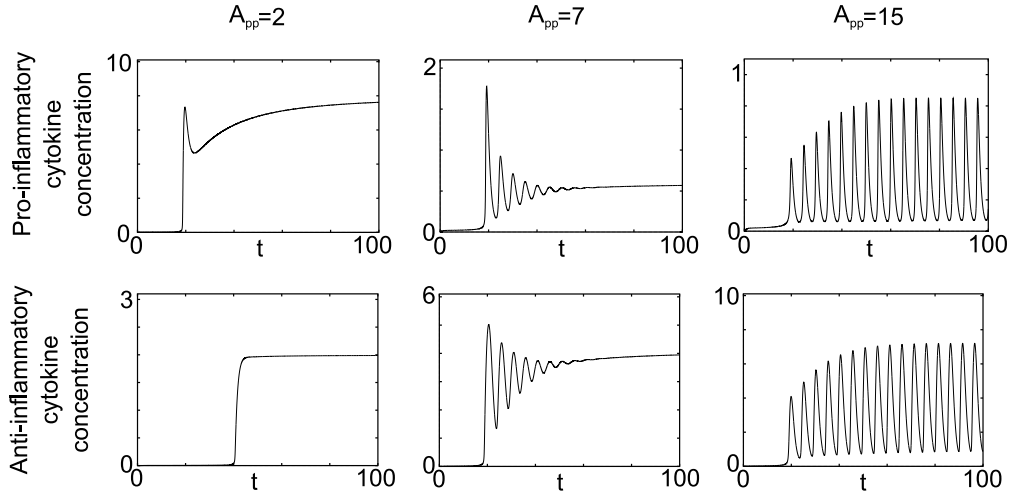


Figure 2.13: Plots of pro-inflammatory and anti-inflammatory cytokine concentrations for $A_{pp} = 2, 7$ and 15 . ($P_{bp} = 0.025$, $A_{ph} = 0.5$, $\gamma_p = 1.25$). In each case, the system moves to a disease state over time as P_{pp} increases. As A_{pp} gets larger, the time the system is in an oscillatory state increases until, for some value of A_{pp} , the system moves onto a stable limit cycle. The parameter P_{pp} increases over time and this is equivalent to taking a horizontal slice through the bifurcation diagram in Figure 2.8(b).

oscillations. The highest values of A_{pp} result in a disease state with lowest pro-inflammatory concentration and highest anti-inflammatory concentration. These concentration patterns emphasise the differences which can be attributed to an individual's ability to produce anti-inflammatory cytokine. Those individuals with a faster rate of anti-inflammatory cytokine production (large A_{pp}) may be more likely to see the remitting and relapsing pattern of disease onset.

The function used here for P_{pp} is representative of an age related increase in P_{pp} over time. Responses due to infection may lead to an initial spike in pro-inflammatory production rate (P_{pp}) followed by the gradual decline of the rate to a new base line rate (Figure 2.14). In this case the system may settle either to a state of health or disease, determined by the value of P_{pp} after infection. For appropriate parameter values there can be a period of oscillations, which may be representative of the mechanism by which some individuals go on to develop sustained RA after a period of palindromic RA, whilst others move into remission.

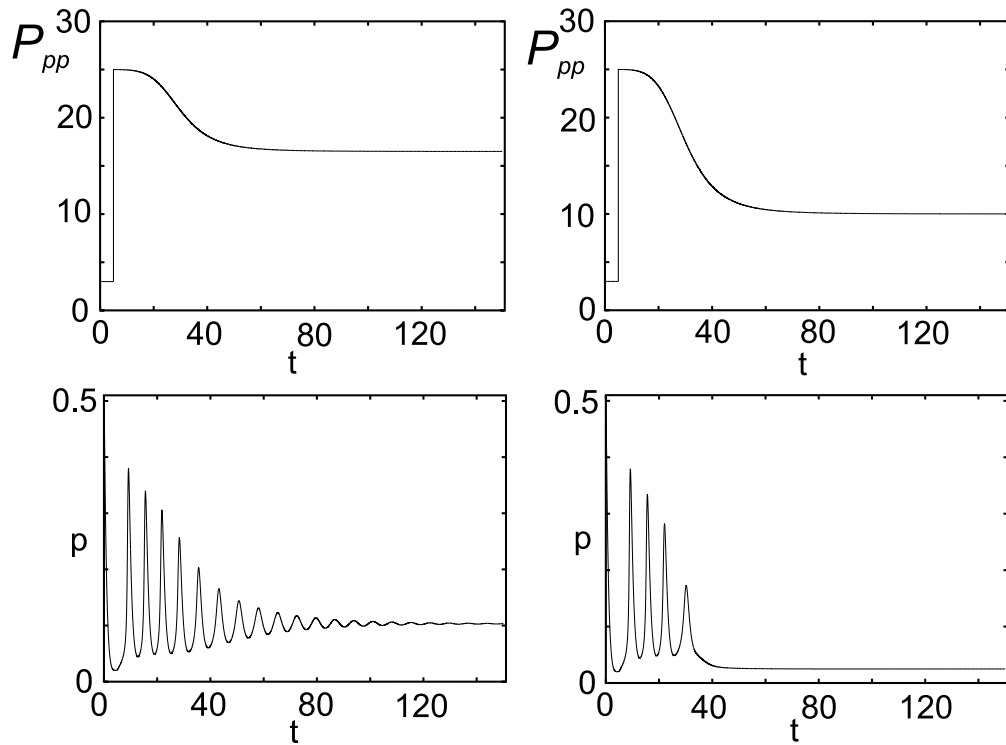


Figure 2.14: Plots of P_{pp} and pro-inflammatory cytokine concentrations against time. The two plots in the upper panel show two forms of the P_{pp} function, in both cases P_{pp} starts at 3 and spikes to 25 after $t=5$. They then settle to a new value of P_{pp} , 16.5 in the first column and 10 in the second. The plots in the lower panel show how the concentration of pro-inflammatory cytokine varies over the same time period. Both plots show decaying oscillations to a steady state, in the first column the steady state is a disease state and in the second it is healthy.

2.5 Treatment Strategies

Some individuals with RA are treated with doses of pro-inflammatory cytokine inhibitors, known as anti-cytokine therapy, either in the form of pro-inflammatory cytokine receptor antagonists or antibodies targeting pro-inflammatory cytokines [49]. Doses are given either by subcutaneous injection or intravenous infusion at intervals ranging from weekly to four-weekly. Short term effects of the reduction of pro-inflammatory cytokine activity include reduction in joint swelling, pain and stiffness and improvement in general well-being [80]. Long term effects include reduction in the rate and severity of joint damage [44]. For simplicity, we assume that each dose of pro-inflammatory cytokine inhibitors causes a proportional decrease in pro-inflammatory cytokine level. We then use an instantaneous decrease in pro-inflammatory cytokine concentration (p) in the model to mimic these cytokine treatments. Some effects similar to those reported during cytokine treatment, such as a temporary reduction in disease activity or remission, are exhibited by the model.

To see the importance of dose size and interval, parameters for which the system displays type Ci behaviour (see Section 3.2.1) are taken so that the system can show both healthy and disease stable steady states. We start the system at a stable disease state (S_2) and reduce the value of p by a fixed amount at a specific time point. An increase in dose magnitude is modelled by a larger reduction in the level of p . If the system is at the disease state and a single dose of anti-cytokine treatment is given then the response of the system depends entirely on the size of that dose.

A reduction in pro-inflammatory concentration which is not sufficient to shift the system to a state outside the basin of attraction of S_2 can cause a temporary fall in pro-inflammatory concentration followed by an overshoot and decaying oscillations back to the disease state (Figure 2.15). A larger dose can be sufficient to trigger a

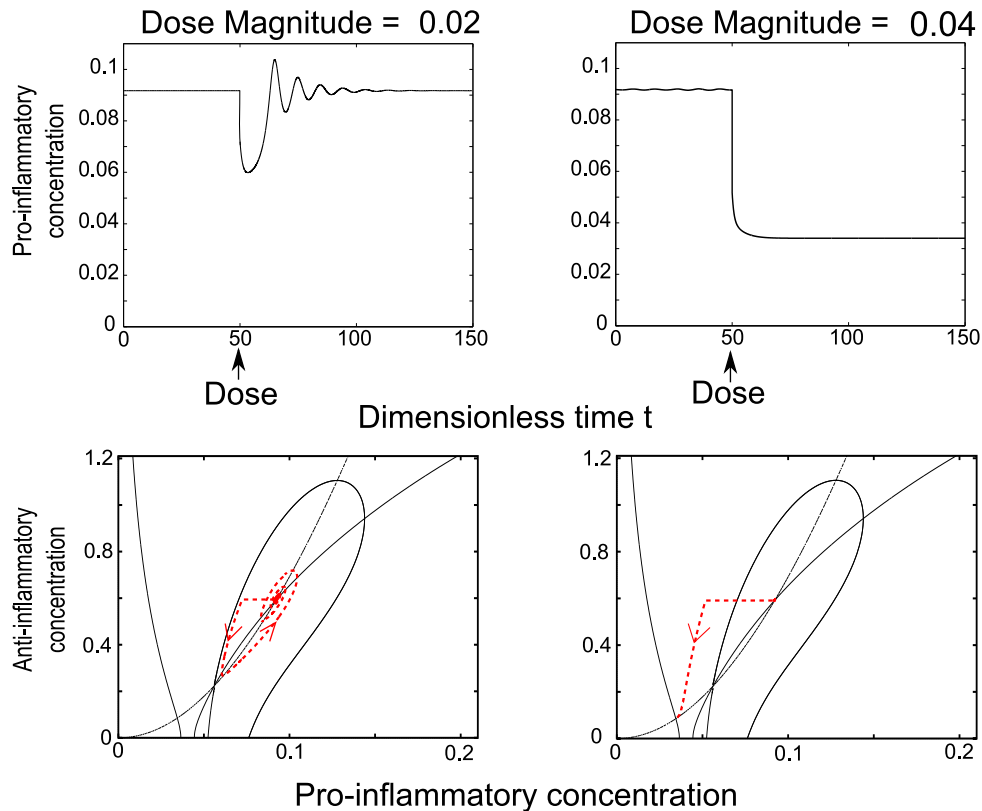


Figure 2.15: Pro-inflammatory and anti-inflammatory cytokine concentration response to a single infusion of anti-inflammatory cytokine at time $t = 50$ (dose of magnitude 0.02 in the first column and 0.04 in the second). The first row shows the time course for the change in Pro-inflammatory cytokine concentration, whilst the second row shows the phase plane for the parameters used. The red curves on the phase plane track the time evolution of p as seen on the time course. The time courses of anti-inflammatory cytokine concentration are not shown for brevity, but profiles look similar to pro-inflammatory cytokine concentration. The parameters used are $\{P_{bp} = 0.025, P_{pp} = 15.5, A_{ph} = 0.5, A_{pp} = 18$ and $\gamma_p = 1.25\}$.

monotonic decrease in p until the system settles at the healthy state. This is not a feature that is normally seen in clinical practice which may suggest that either the dose levels used do not move the system outside of the basin of attraction of S_2 , or that disease relapses by a change in the parameters, moving the system from a healthy steady state or that the patient is not curable.

The pattern of treatment is also pivotal to the results obtained. By administering multiple treatments it may be possible to achieve results which are not seen for a single dose, although the timing can be crucial. Using the same parameter values as in Figure 2.15, taking a dose of magnitude 0.02 (which as a single dose did not return the system to S_0) and giving two doses at different intervals, shows that the response depends in a non-trivial way on timing (Figure 2.16).

A dose interval of 10 units drives the system to the stable healthy state, whilst a 15 unit interval sees a return to stable disease after an initial response. Remarkably, a longer interval can be beneficial; for a 17 unit interval a healthy state is achieved. This dependence on timing arises because in the 15 time unit dosing interval protocol, the second dose is applied when the pro-inflammatory and anti-inflammatory concentration have risen significantly from their first minimum, meaning that the second dose is insufficient to force the trajectory out of the stable manifold (Figure 2.16). In the first and third case, the second dose is administered at a point where the pro-inflammatory concentration is low and so the dose pushes the trajectory out of the basin of attraction of the disease state. The trajectory must be sufficiently close to the basin boundary (the manifold) at the time the second dose is given.

So far, each of the doses provided has been able to shift the system to the healthy state. Some doses, however, are not large enough to achieve this, regardless of the number of doses unless the pattern of dose administration is changed. Using the same parameters as before with a dose half the size of the previous dose size

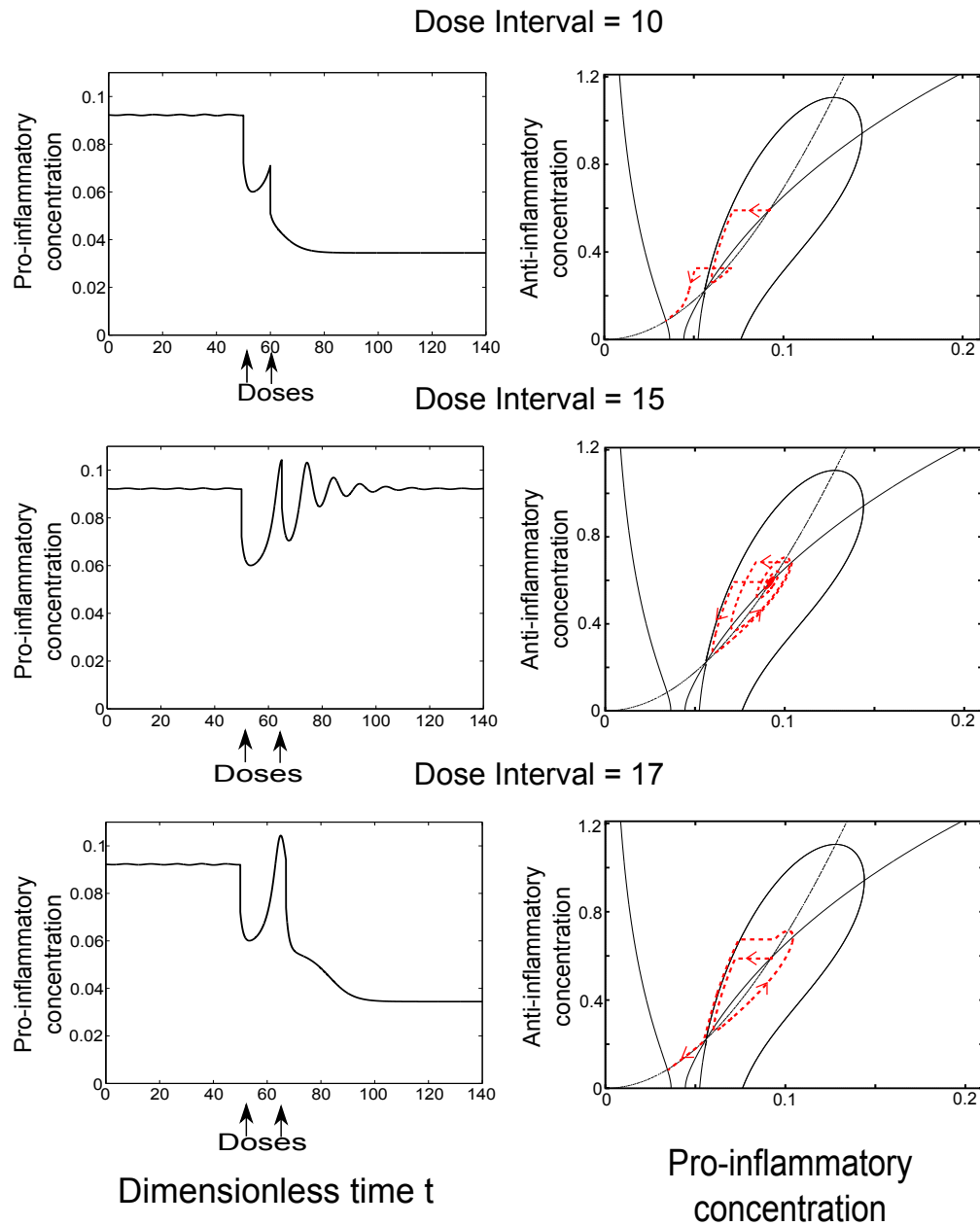


Figure 2.16: Time dependence of pro-inflammatory and anti-inflammatory cytokine concentration for different time separation between doses. All doses have a magnitude of 0.02 and the parameters values are $\{P_{bp} = 0.025, P_{pp} = 15.5, A_{ph} = 0.5, A_{pp} = 18 \text{ and } \gamma_p = 1.25\}$. The first column shows the time courses of pro-inflammatory concentration for two doses given 10, 15 and 17 time units apart. The time courses of anti-inflammatory cytokine concentration are not shown for brevity, but profiles look similar to pro-inflammatory cytokine concentration. The second column shows phase plane diagrams of the simulations, with the red curves showing the time evolution of p .

(0.01) and applying it at time intervals of 5 units over a sustained period of time, we obtain the pro-inflammatory concentration profile shown in Figure 2.17a. This treatment pattern brings about a temporary reduction in the concentration of pro-inflammatory cytokine although there are oscillations in the level. When the treatment ceases, the pro-inflammatory cytokine concentration returns to the pre-treatment level. Only by reducing the time interval can this change be sustained after treatment has ceased (Figure 2.17b). The reduction in time interval means that the next dose is given before the system has moved fully back to disease, hence increasing the effective dose.

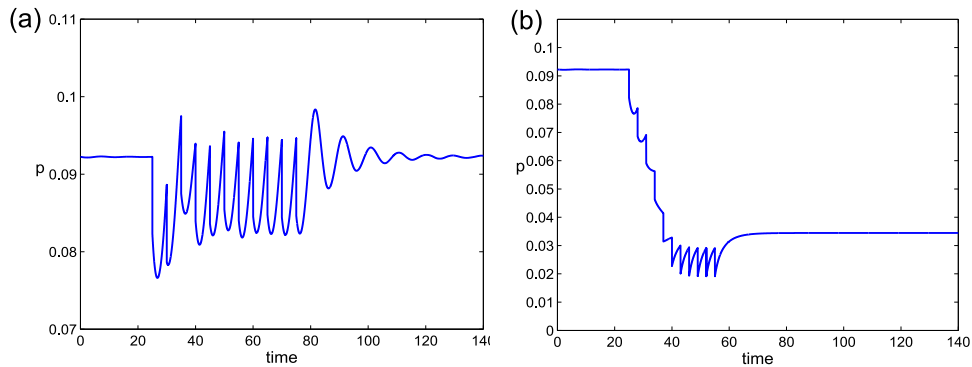


Figure 2.17: Pro-inflammatory cytokine profiles for the system with doses of anti-inflammatory cytokine of magnitude 0.01 at (a) 5 unit intervals between $t = 25$ and $t = 75$ and (b) 3 unit intervals between $t = 25$ and $t = 75$ and parameters $\{P_{bp} = 0.025, P_{pp} = 15.5, A_{ph} = 0.5, A_{pp} = 18$ and $\gamma_p = 1.25\}$. There is a trade off between dose size and interval. The dose interval needs to be reduced to give a sustained response for smaller dose sizes.

2.6 Discussion

Cytokines are important mediators in RA. The success of clinical treatments based on altering the synovial cytokine profile suggests that the composition and interactions of the cytokine network are key factors in at least the regulation, if not the onset, of rheumatoid arthritis [44]. The model developed here is a two variable activator-inhibitor system that simulates the dynamics of two classes of cytokines,

pro-inflammatory and anti-inflammatory. Five key dimensionless parameters have been identified. We have shown that the model can have either one steady state (S_0 or S_2) or three steady states (S_0 , S_1 and S_2). This leads to a range of phase plane behaviours.

The model shows four types of monostable phase plane behaviour (Ai, Aii, Aiii and B). These behaviours may be interpreted as a healthy response (Ai and Aiii) due to a low level of p , a disease response due to a high level of p (B) or an unclear response of health/disease due to an intermediate range of p . In addition to monostable behaviour, the model also shows four types of bistable phase plane behaviour (Ci, Cii, Di and Dii). These have a stable healthy steady state and a stable disease state which is either a fixed point or a limit cycle. One point to note is that if an individual has a high level of pro-inflammatory production, so that a monostable disease state prevails, increasing the magnitude of anti-inflammatory production, A_{pp} , does not return the system to distinct health, but does reduce the level of p at the fixed point (see Figure 2.8b). In clinical practice, only cytokine concentrations are changed rather than production rates, so increasing the magnitude of anti inflammatory cytokine production would relate only to intrinsic changes in parameters at present. However, this may be relevant for development of gene therapy approaches.

Figure 2.13 shows that as the pro-inflammatory production parameter (P_{pp}) increases over time the system moves from the healthy steady state to a disease state. Here, the anti-inflammatory production parameter, A_{pp} , determines the pattern of disease onset. As A_{pp} increases, the approach to the disease state changes from a straightforward switch to an oscillatory approach. The size of A_{pp} determines the time taken for the oscillations to settle until, for some larger A_{pp} , we have sustained oscillations. These counter-intuitive features highlight the need for a well-defined measure of the link between the cytokine profile and synovial inflammation in the model, since lower cytokine levels may still result in a longer

period of persistent disease. Figure 2.14 shows that temporary spikes in the pro-inflammatory production parameter, which may represent a response to infection, can also initiate disease onset. In this case, disease onset is determined by the level of pro-inflammatory cytokine production after the initial spike as well as the underlying individual's parameters.

Cytokine treatment simulations show the relevance of dose size to the efficacy of a particular treatment. Two doses were applied when the system was at rest at the disease state (Figure 2.15). We demonstrated that the larger dose could move the system to a state of health, whilst the smaller dose was insufficient. Repeated smaller doses could be used to move the system to health, but the dose interval used here is crucial. The key factor in determining the dose interval is the point in the oscillatory cycle at which the second or subsequent dose is administered (Figure 2.16). Intuitively, the best time to apply the second dose is when the pro-inflammatory concentration is at its lowest so that the cumulative effect is as large as possible. Mathematically, the best time to apply it is when the horizontal separation in the (p, a) phase plane between the bounding curve of the basin of attraction of S_2 and the concentration trajectory is a minimum, since this gives the best chance of leaving the basin of attraction of the disease state. These conditions are not necessarily equivalent. If the side effects of a high dose of a drug are unacceptable then we have shown that it may be possible to apply a course of smaller doses at targeted times to return the system to health. Clearly, it may be possible to manipulate the treatment regime to include the smallest possible dose over the fewest possible applications. The model has the surprising property that an increase in the pro-inflammatory cytokine level can also bring about remission, this has not been tested clinically but has interesting implications for novel treatment strategies.

In parameter regimes where only the disease state exists, no treatment of the types described here, no matter how large the dose, could ever achieve remission (i.e.

a sustained state of health). Manipulation of the system parameters is the only way this could be achieved. However, a dose of anti-cytokine therapy would move an individual to a lower pro-inflammatory cytokine level temporarily followed by a gradual return to the disease state. This is still a desirable outcome in clinical practice and justifies the use of anti-cytokine therapy, particularly when given as a series of regular treatments, even where remission is impossible.

We believe that a healthy individual at low risk of developing RA will have parameters corresponding to a phase plane with a single, globally stable, steady state. Individuals with very early RA or at risk of developing RA will have parameters defining a system with three steady states. These individuals may go on to occupy a steady disease state from which it is possible to return to a healthy state by appropriate manipulation of pro- and anti-inflammatory cytokine levels. Correspondingly, clinicians refer to a window of opportunity in treating early RA during which remission is more likely than in later disease [99], implying time dependence of the underlying parameters. In clinical practice, the closure of this window of opportunity marks the transition from early to established disease. In this model, it may mark the transition from a system with three steady states to one with a single, steady, inescapable disease state characterised by high pro-inflammatory cytokine levels, which occurs as P_{pp} changes. In established RA, remission rates with anti-cytokine therapy are only around 20% [60], suggesting that the either majority of patients with established RA are in this state or they are not being treated optimally.

This model has produced many of the features observed in real cytokine systems, but if the characteristics of this model are to be interpreted in a clinical context, then it is necessary to link concentration of cytokines to a measurable disease indicator. Ideally, we would like to link the model results to clinical data of cytokine levels over time in individuals with early and late RA. Practical considerations, including the short half life of cytokines and the difficulty of extracting synovial

fluid from the joint, mean this type of data is difficult to obtain in humans. It may be possible to collect similar data from animal models or alternatively we may be able to use other types of clinical data. The inflammatory marker C-Reactive Protein (CRP) is routinely used by clinicians as a measure of disease activity in RA [101]. However, variation between individuals is large and the link between cytokine level and CRP level or inflammation is as yet unclear. That said, in the majority of cases we identify from our model, the interpretation is very clear. We either have low levels of p indicating health or high levels of p indicating disease. It is only when the levels are intermediate that we are unable to define a clear threshold between health and disease. Whilst there is no precise link between model variables and specific disease markers, the interactions in the model are well-established and the predictions are robust to variations in parameter values and functional forms. It would ultimately be desirable to have a model which includes a number of specific cytokines and measurable disease markers to allow a clear link between model behaviour and disease activity. This would give a better idea of how cytokine levels influence disease manifestations and would provide a clearer definition of health and disease.

The dynamics of pro- and anti-inflammatory cytokines are likely to be relevant in a wider context than RA in the synovium. As discussed in Chapter 1, Osteoarthritis involves the same cytokines, and hence similar dynamics are likely to exist. It is likely that the RA model presented here could form a basis for examining the cytokine dynamics within OA tissue and we will consider this further in Chapter 3. Additionally, other conditions, such as diabetes, sepsis, Alzheimer's disease and lupus, are also known to have cytokine involvement and due to the generality of this model it may be applicable in these wider contexts.

Chapter 3

Mathematical modelling of cytokines, MMPs and ECM fragments in osteoarthritic cartilage

The focus of the model developed in the previous chapter was to understand the pro-inflammatory and anti-inflammatory cytokine interactions in the synovium. The network of cytokine interactions in the joint is more complex than in the synovium. In the cartilage, since the main role of the cytokines is to control ECM remodelling, it makes sense to extend the model to include the dynamics of MMPs, the enzymes that break down ECM fibres, and degraded fibronectin fragments (Fn-fs), a waste product which can stimulate cytokine production. A predominant feature of OA is excessive breakdown of the ECM. Higher than normal levels of Fn-fs have been found in osteoarthritic individuals and are thought to contribute to the acceleration of the disease [86]. The model we have developed is based on the simplified cytokine network schematised in Figure 3.1.

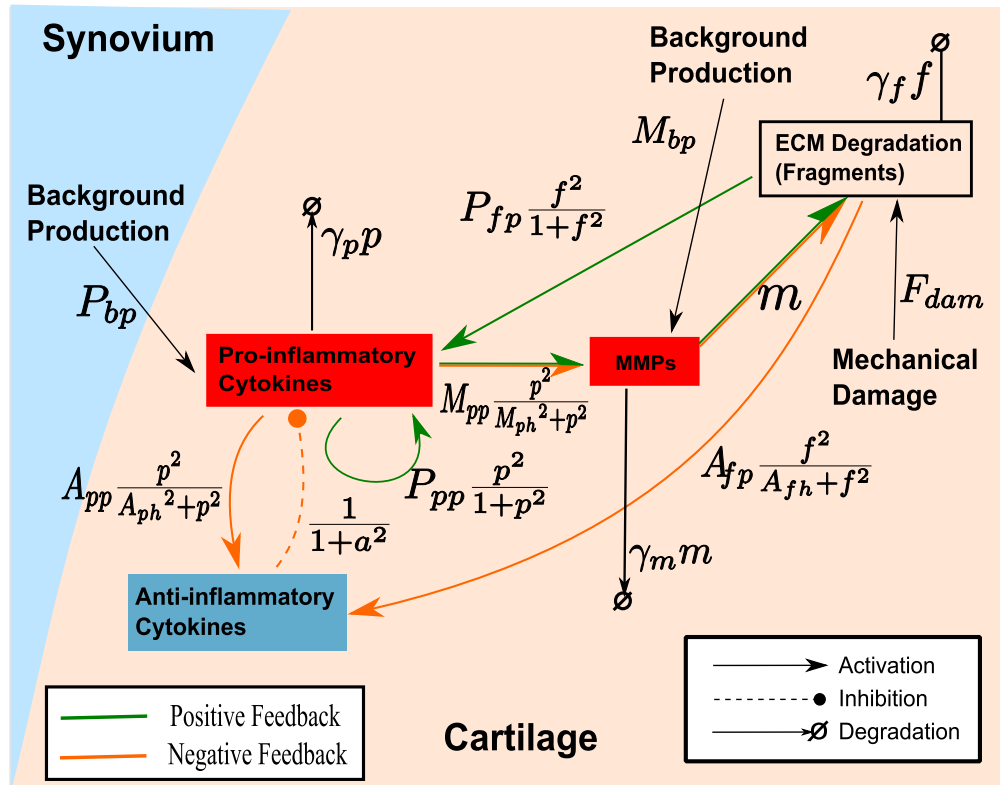


Figure 3.1: A simplified network of cytokine interactions within articular cartilage. Cytokines are classed as pro-inflammatory or anti-inflammatory. MMPs have a direct role in the breakdown of the ECM leading to increased Fn-fs. Fibronectin fragments are irritants to the cartilage and lead to increased cytokine production as part of the inflammatory response.

3.1 Model Rationale

In this paper we develop a four-variable model of cytokine interactions in the cartilage, as seen in OA. Our model variables are pro-inflammatory cytokines (p), anti-inflammatory cytokines (a), MMPs (m) and Fn-fs (f). In order to keep the model tractable, cytokines have been put into two functional groups, pro-inflammatory and anti-inflammatory. This is the same grouping as we used in the cytokine-only model of the synovium (Chapter 2). Pro-inflammatory cytokines are normally present at low levels in the cartilage as they play a role in mediating the normal turnover of the ECM [108], which involves remodelling the cartilage ECM at a very slow rate to maintain tissue integrity. Production of pro-inflammatory cytokine is up-regulated in response to trauma or infection, as part of the inflammatory response and repair mechanism. This response is usually kept in homeostatic balance by anti-inflammatory cytokines, which act both to inhibit the synthesis of pro-inflammatory cytokines and also to block pro-inflammatory cytokine receptors [103]. To model these processes we assume that production of pro-inflammatory cytokines, p , is dependent on itself, anti-inflammatory cytokines, a , and Fn-fs, f ,

$$\frac{dp}{dt} = \left(p_{bp} + p_{pp} \frac{p^2}{p_{ph}^2 + p^2} + p_{fp} \frac{f^2}{p_{fh}^2 + f^2} \right) \left(\frac{p_{ah}^2}{p_{ah}^2 + a^2} \right) - d_p p. \quad (3.1.1)$$

We make the source term saturating since we assume there will be a maximal production rate in the cell and therefore model functions of p , a and f as Hill functions. We also assume that pro-inflammatory cytokines will degrade naturally at rate d_p . We have chosen all the Hill coefficients to be 2. We choose to make the stimulatory terms additive as we expect these two pathways to be independent since they are biochemically distinct and activate different cell receptors. This means that even if there is no cartilage degradation there may still

be a large cytokine response due to an increase in p . This may be the case, for example, if there is an inflammatory episode where there is no physical damage to the cartilage. Since anti-inflammatory cytokines reduce production and effectiveness of pro-inflammatory cytokines regardless of the source we apply the anti-inflammatory inhibition term to all the source terms.

The dynamics of the anti-inflammatory cytokines, a , includes source terms representing the up-regulation of a , by both pro-inflammatory cytokines and Fn-fs, and a natural degradation term,

$$\frac{da}{dt} = a_{pp} \frac{p^2}{a_{ph}^2 + p^2} + a_{fp} \frac{f^2}{a_{fh}^2 + f^2} - d_a a. \quad (3.1.2)$$

The source terms are saturating Hill functions of p and f .

MMPs mediate ECM degradation and the synthesis of MMPs is stimulated by pro-inflammatory cytokines [126]. MMPs are also found at low levels in normal cartilage so we assume some basal production. The dynamics of MMPs (m) are therefore modelled as having source terms that account for basal production and up-regulation by pro-inflammatory cytokines and a natural degradation term,

$$\frac{dm}{dt} = m_{bp} + m_{pp} \frac{p^2}{m_{ph}^2 + p^2} - d_m m. \quad (3.1.3)$$

Fn-fs, produced as a result of ECM degradation, need to be explicitly included in the model since they are involved in the stimulation of cytokine production, see Figure 3.1. Since the ECM is degraded by MMPs the source term is a function of m . Additionally, breakdown of the ECM may be caused by mechanical damage, represented by the term f_{dam} . We also include natural degradation, giving

$$\frac{df}{dt} = f_{mp}m + f_{dam} - d_f f. \quad (3.1.4)$$

3.2 Model Equations

We non-dimensionalise the model using the scalings:

$$p = p_{ph}\tilde{p} \quad a = p_{ah}\tilde{a} \quad m = \frac{p_{fh}d_a\tilde{m}}{f_{mp}} \quad f = p_{fh}\tilde{f} \quad t = \frac{\tilde{t}}{d_a}$$

where the tilde denotes dimensionless quantities. Dropping the tildes for convenience, gives the dimensionless model:

$$\frac{dp}{dt} = \left(P_{bp} + P_{pp} \frac{p^2}{1+p^2} + P_{fp} \frac{f^2}{1+f^2} \right) \left(\frac{1}{1+a^2} \right) - \gamma_p p \quad (3.2.1)$$

$$\frac{da}{dt} = A_{pp} \frac{p^2}{A_{ph}^2 + p^2} + A_{fp} \frac{f^2}{A_{fh}^2 + f^2} - a \quad (3.2.2)$$

$$\frac{dm}{dt} = M_{bp} + M_{pp} \frac{p^2}{M_{ph}^2 + p^2} - \gamma_m m \quad (3.2.3)$$

$$\frac{df}{dt} = m + F_{dam} - \gamma_f f \quad (3.2.4)$$

where,

$$\begin{aligned}
 P_{bp} &= \frac{p_{bp}}{p_{ph}d_a}, & P_{pp} &= \frac{p_{pp}}{p_{ph}d_a}, & P_{fp} &= \frac{p_{fp}}{p_{ph}d_a}, & A_{pp} &= \frac{a_{pp}}{p_{ah}d_a}, \\
 A_{ph} &= \frac{a_{ph}}{p_{ph}}, & A_{fp} &= \frac{a_{fp}}{a_{ph}d_a}, & A_{fh} &= \frac{a_{fh}}{p_{fh}}, & M_{bp} &= \frac{m_{bp}m_{pp}}{p_{fh}d_a^2}, \\
 M_{pp} &= \frac{m_{pp}f_{mp}}{p_{fh}d_a^2}, & M_{ph} &= \frac{m_{ph}}{p_{ph}}, & F_{dam} &= \frac{f_{dam}}{p_{fh}d_a}, & \gamma_p &= \frac{d_p}{d_a}, \\
 \gamma_m &= \frac{d_m}{d_a}, & \gamma_f &= \frac{d_f}{d_a}.
 \end{aligned}$$

The meaning of each of these new parameters is summarised in Table 3.1.

Table 3.1: The parameters in the system (3.2.1) - (3.2.4) and their interpretation

Parameter	Description
P_{bp}	Background pro-inflammatory production
P_{pp}	Pro-inflammatory cytokine driven pro-inflammatory cytokine production
P_{fp}	Fibronectin fragment driven pro-inflammatory cytokine production
A_{pp}	Pro-inflammatory cytokine driven anti-inflammatory cytokine production
A_{ph}	Pro-inflammatory cytokine concentration at which pro-inflammatory cytokine driven anti-inflammatory cytokine production is half maximal
A_{fp}	Fibronectin fragment driven anti-inflammatory cytokine production
A_{fh}	Fibronectin fragment concentration at which Fn-fs driven anti-inflammatory cytokine production is half maximal
M_{bp}	Background MMP production
M_{pp}	Pro-inflammatory cytokine driven MMP production
M_{ph}	Pro-inflammatory cytokine concentration at which MMP production is half maximal
F_{dam}	Mechanical damage parameter
γ_p	Relative rate of clearance of pro-inflammatory cytokine to anti-inflammatory cytokine
γ_m	Relative rate of clearance of MMP to anti-inflammatory cytokine
γ_f	Relative rate of clearance of Fn-fs to anti-inflammatory cytokine

3.3 Steady States

Insight into the nature of the steady states of this system can be gained from the nullclines, hypersurfaces given by,

$$\dot{p} = 0 \iff a = N_p(p, f) = \sqrt{\mathbf{g}(p, f)}, \quad (3.3.1)$$

where

$$\mathbf{g}(p, f) = \frac{1}{\gamma_p p} \left(P_{bp} + P_{pp} \frac{p^2}{1+p^2} + P_{fp} \frac{f^2}{1+f^2} \right) - 1,$$

and

$$\dot{a} = 0 \iff a = N_a(p, f) = A_{pp} \frac{p^2}{A_{ph}^2 + p^2} + A_{fp} \frac{f^2}{A_{fh}^2 + f^2}, \quad (3.3.2)$$

$$\dot{m} = 0 \iff m = N_m(p) = \frac{M_{bp}}{\gamma_m} + \frac{M_{pp}}{\gamma_m} \frac{p^2}{M_{ph}^2 + p^2}, \quad (3.3.3)$$

$$\dot{f} = 0 \iff f = N_f(m) = \frac{m + F_{dam}}{\gamma_f}. \quad (3.3.4)$$

The steady states of the model are the points where all the nullclines intersect. We can locate these points by solving equations (3.3.1)-(3.3.4) simultaneously, however this is analytically intractable. We can, however, substitute $m = N_m$ and $f = N_f(N_m(p))$ into N_p and N_a , reducing the problem to two simultaneous equations,

$$a = N_p(p, N_f(N_m(p))), a = N_a(p, N_f(N_m(p))),$$

leading to,

$$a = \sqrt{\mathbf{h}(p)}, \quad (3.3.5)$$

where

$$h(p) = \frac{1}{\gamma_p p} \left(P_{bp} + P_{pp} \frac{p^2}{1+p^2} + P_{fp} \frac{\left(F_{dam} \gamma_m + M_{bp} + M_{pp} \frac{p^2}{M_{ph}^2 + p^2} \right)^2}{(\gamma_f \gamma_m)^2 + \left(F_{dam} \gamma_m + M_{bp} + M_{pp} \frac{p^2}{M_{ph}^2 + p^2} \right)^2} \right) - 1,$$

and

$$a = A_{pp} \frac{p^2}{A_{ph}^2 + p^2} + A_{fp} \frac{\left(F_{dam} \gamma_m + M_{bp} + M_{pp} \frac{p^2}{M_{ph}^2 + p^2} \right)^2}{(\gamma_f \gamma_m)^2 A_{fh}^2 + \left(F_{dam} \gamma_m + M_{bp} + M_{pp} \frac{p^2}{M_{ph}^2 + p^2} \right)^2}. \quad (3.3.6)$$

The intersections of these two curves, equations (3.3.5) and (3.3.6), give the steady states. Although analytical solutions are not tractable, the forms of the curves tell us the possible number of steady states.

Equation (3.3.6) consists of two terms, the first is a Hill function of p and the second is a Hill function of p embedded within another Hill function. This allows (3.3.6) to take two forms, either a sigmoidal shape, if A_{ph} and A_{fh} are close in value (Figure 3.2a), or a double sigmoidal shape if A_{ph} and A_{fh} are sufficiently different (Figure 3.2b).

Equation (3.3.5) involves the square root of the function $h(p)$, and therefore only exists when $h(p) \geq 0$. As $p \rightarrow 0$, $h(p) \rightarrow \infty$. As $p \rightarrow \infty$, $h(p) \rightarrow -1$ and $h(p)$ is continuous. Hence, (3.3.5) always meets the p -axis for a large enough value of p . If we consider $h(p)$ as,

$$h(p) = \frac{k(p)}{\gamma_p p} - 1,$$

the function $k(p)$, similar to eq. (3.3.6), can have either a sigmoidal or double

sigmoidal shape. The double sigmoidal shape is possible when the terms involving P_{pp} and P_{fp} are sufficiently different. This leads to several possible shapes for the function $h(p)$ and likewise $a = \sqrt{h(p)}$. These are shown in Figures 3.2c-f.

The forms of equations (3.3.5) and (3.3.6) mean that they will always intersect at least once, so the system will always have at least one steady state. It is clearly possible for these curves to also intersect three times. We could conceivably have up to nine intersections, but we have found a maximum of five (see Section 3.4.6) with the Hill coefficients of 2. Two or four steady states will only occur when the curves meet tangentially. Since this only occurs at bifurcations we will focus on cases with one, three or five steady states. In each case when the levels of p are low we assume this would indicate a healthy steady state. We chose the value of all the Hill coefficients in the model to be 2, which determines the shapes of the nullclines. With a coefficient of 1 we would restrict the number of steady states possible. Equation (3.3.6) increases monotonically and equation (3.3.5) decreases monotonically, giving only one possible steady state. For Hill coefficients greater than 2 or mixed coefficients, the nullclines take the same form as with coefficients of 2, although the parameter values differ and the steeper gradients allow for the possibility of additional steady states. For example we have been able to find up to seven steady states with mixed Hill coefficients of 2 and 4. These additional states occur in only small regions of parameter space. For this reason we consider only the case where the Hill coefficients are 2, and consider the implications of higher coefficients in the Discussion, as in our previous work, [10].

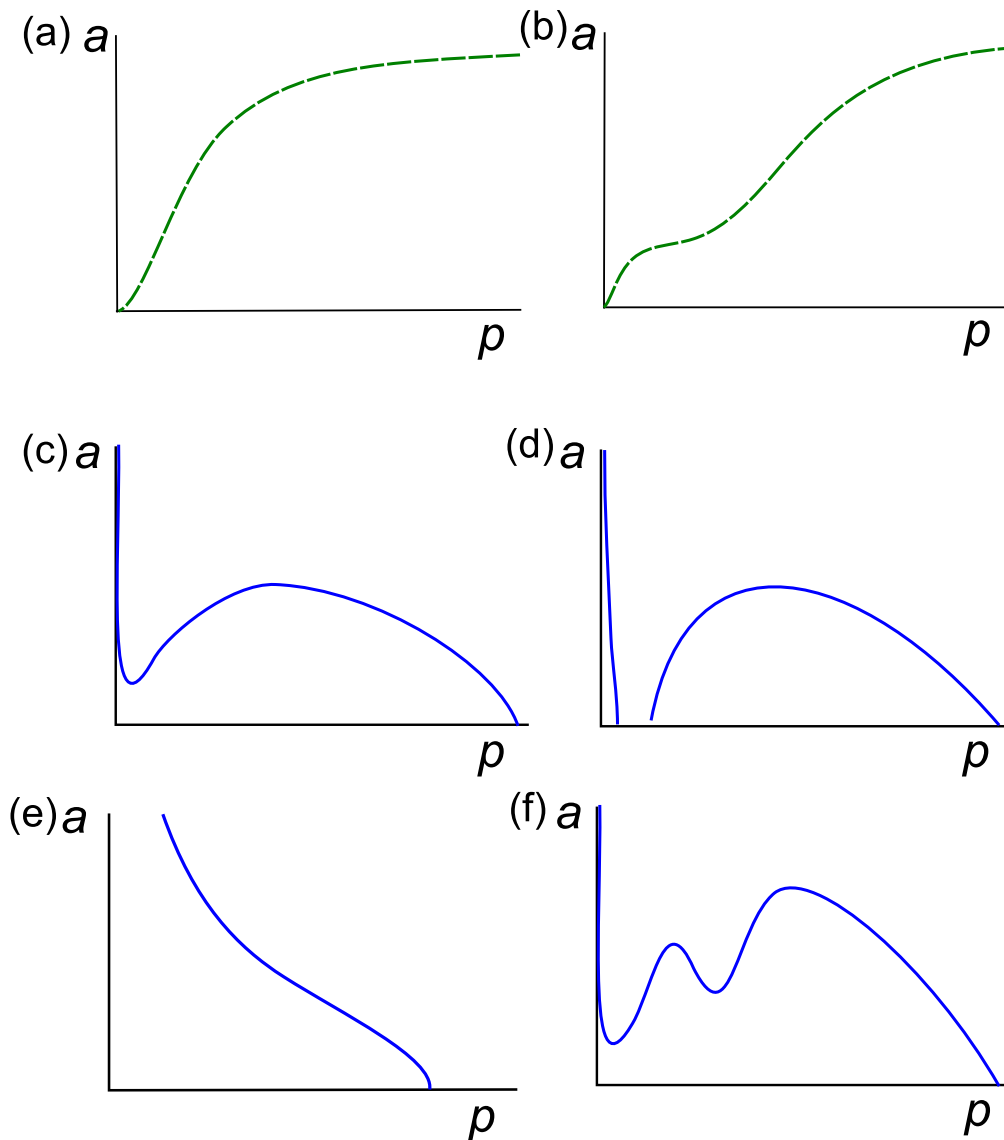


Figure 3.2: Diagrams of the shapes that the p and a nullclines may take, with $m = N_m(p)$ and $f = N_f(N_m(p))$. The steady states of the system occur where these equations intersect. The a nullcline is either sigmoidal (a) or double sigmoidal (b) in shape. The p nullcline can take up to several forms that may meet the x-axis zero (c) and (f), one (e) or two (d) times.

3.4 Bifurcation Analysis

This model has a large number of parameters and it is not feasible to explore the entire parameter space so we will limit our analysis of model behaviour to a reference parameter set and look at one- and two-parameter variations around that point, through bifurcation analysis. Additionally we will look at significant variations to that reference parameter set where the behaviour is of particular interest either mathematically or biologically.

Due to the difficulties of obtaining measurements of cytokine rates and levels both *in vivo* and *in vitro*, there is little reliable and reproducible data concerning the parameters in the model. We therefore start with a simple set of parameters, summarised in Table 3.2, avoiding unlikely scenarios. All the sensitivity parameters (A_{ph} , A_{fh} and M_{ph}) are set to 1 so that they are of the same magnitude as the thresholds of the other functions in the model. Similarly, the degradation rates (γ_p , γ_m and γ_f) are set to 1 to match the degradation rate of a . We set the mechanical damage parameter initially to 0. We set all the cytokine and MMP production parameters (P_{pp} , P_{fp} , A_{pp} , A_{fp} and M_{pp}) to 10, making them equal avoids unnecessary bias in the networks, and this magnitude allows the nullclines to intersect. We wish the background production parameters (P_{bp} and M_{bp}) to be much smaller so we set these to 0.01. We believe we have a clear understanding of the dynamics of the model as demonstrated below. Thus despite incomplete knowledge about the parameters, we think that variations reasonably close to this reference parameter set show the range of behaviours that the model can display.

With these parameters there are three steady states: S_0 , S_1 and S_2 (variable values and eigenvalues shown in Table 3.3). The system is bistable with S_0 likely to indicate health due to low levels of p and f , which are very close to basal production levels, and a limit cycle around S_2 likely to indicate disease due to high and fluctuating levels of p and f .

Parameter	Value
P_{bp}	0.01
P_{pp}	10
P_{fp}	10
A_{pp}	10
A_{ph}	1
A_{fp}	10
A_{fh}	1
M_{bp}	0.01
M_{pp}	10
M_{ph}	1
F_{dam}	0
γ_p	1
γ_m	1
γ_f	1

Table 3.2: Reference parameter set

	S_0	S_1	S_2
p	0.013	0.054	0.260
a	0.003	0.044	3.57
m	0.012	0.039	0.645
f	0.012	0.039	0.645
Eig(1)	-0.497	0.454	$0.015 + 0.780i$
Eig(2)	-1.00	-0.995	$0.015 - 0.780i$
Eig(3)	$-1.12 + 0.327i$	$-1.20 + 0.728i$	$-1.85 + 1.30i$
Eig(4)	$-1.12 + 0.327i$	$-1.20 - 0.728i$	$-1.85 - 1.30i$
Stability	Stable	Unstable	Unstable (with stable limit cycle)

Table 3.3: Details of the steady states of the reference parameter set used for bifurcation analysis of the dimensionless model (Eqn. 3.2.1-3.2.4). The position of the steady states, eigenvalues and stability of steady state are shown.

A sensitivity analysis of small parameter changes around the reference parameter set gives some insight into the behaviour of the system. Figure 3.3 shows sensitivity of the parameters to a $\pm 10\%$ change as measured by three features: the concentration of p at the steady state, the amplitude and the period of any limit cycles. We use a one-at-a-time sensitivity analysis to measure the sensitivity gain for each feature according to the sensitivity function,

$$S_k^\phi = \frac{\delta\phi/\phi}{\delta k/k}, \quad (3.4.1)$$

where ϕ is the feature being measured and k is the parameter being changed. Parameters related to anti-inflammatory cytokine production and clearance rate parameters are consistently the most sensitive when the system is at the disease state. This suggests that if we alter these parameters from the reference parameter set we may have significantly different bifurcation behaviour. We will consider this later in the next section. When the system is at the healthy state it is additionally sensitive to changes in P_{bp} and γ_p .

For this parameter set, due to γ_f being 1 and F_{dam} being zero, m and f are equal at the steady states. Figure 3.4a shows simulated solution trajectories for various sets of initial conditions for the reference parameter set as a three dimensional projection in (p, a, m) space.

The figure shows that the basin of attraction of the disease state is very large compared to that of the healthy state and that decaying oscillations into the disease state have a large amplitude. This may translate clinically to slow onset of OA with periods of flare up followed by asymptomatic periods. However, we need to view the basin of attraction in terms of realistic perturbations from the steady state. Figure 3.4b shows perturbations within a small range of the healthy steady

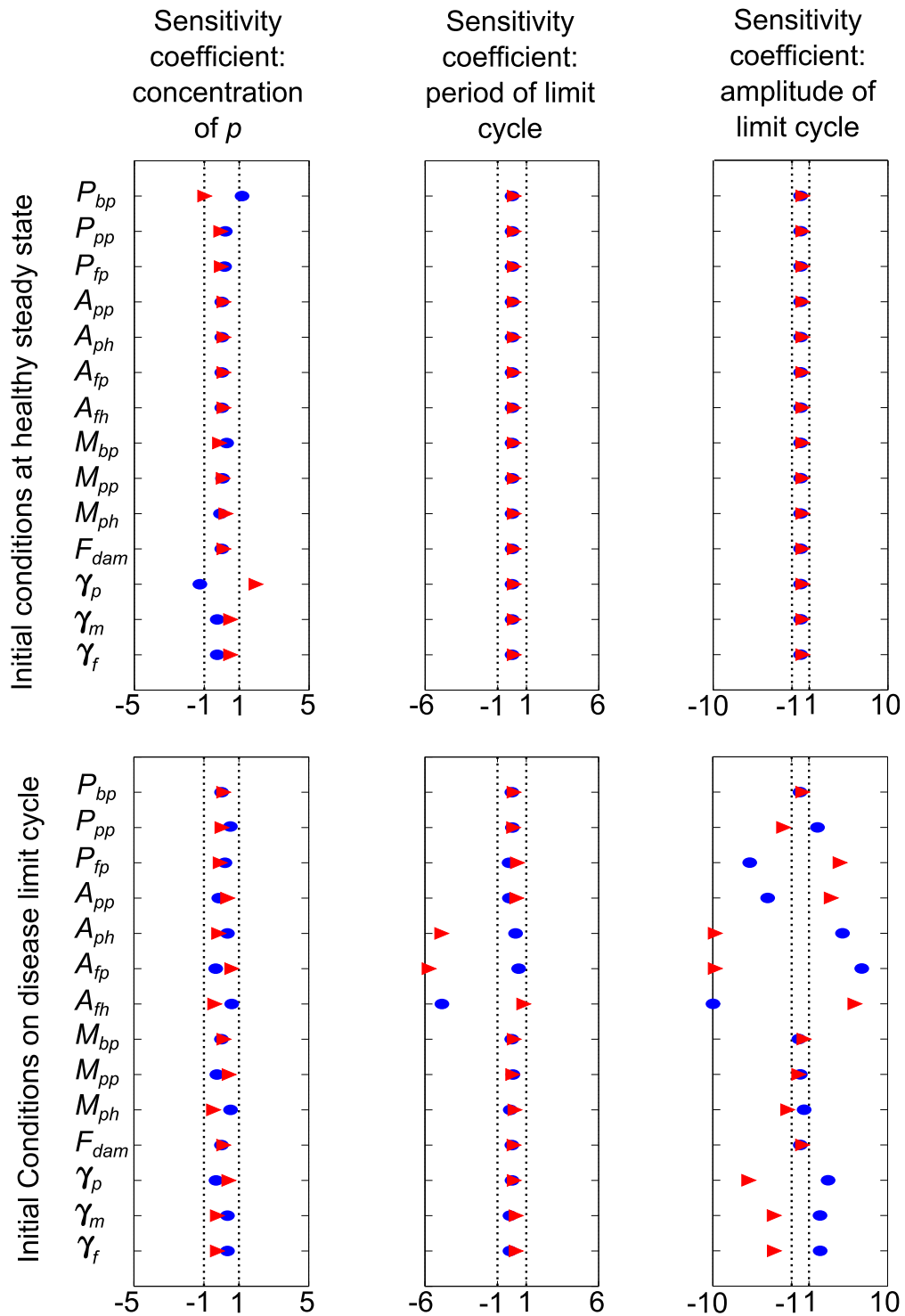


Figure 3.3: Diagrams of the sensitivity of the parameters as measured by the values of p at the steady state, the period and amplitude of limit cycles. The x-axis shows the relative sensitivity coefficient as the parameters are varied by 10% (blue circles) or -10% (red triangles). A value of 1 on the x-axis is representative of a 10% change in the feature given a 10% change in the parameter. The diagrams show that the parameters related to anti-inflammatory cytokine production are particularly sensitive to small changes.

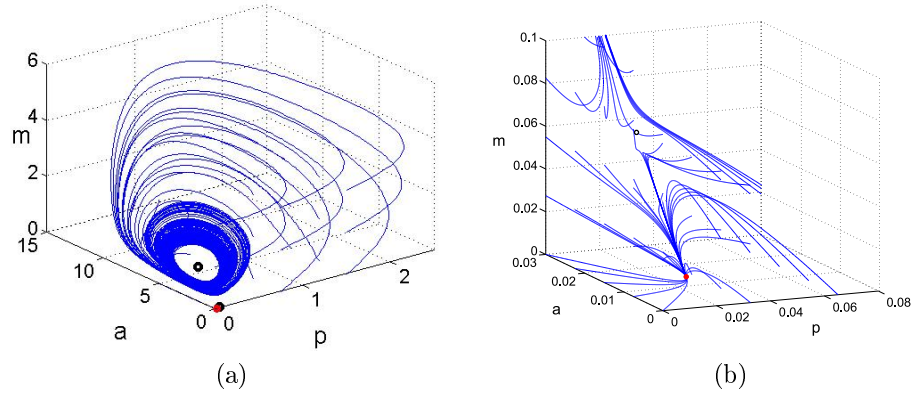


Figure 3.4: Projection of the phase space for the reference parameter set, specified above, showing trajectories, for the cartilage model, for various regularly spaced initial conditions in (p, a, m) space. (a) shows all three steady states whilst (b) focuses on the behaviour around the healthy steady state. The black circles show the position of unstable fixed points and the red dot shows the stable fixed point. The trajectories either move to the stable fixed point or the stable limit cycle which surrounds an unstable fixed point. The unstable steady state influences the path taken by trajectories.

state. We can see from this that increases in the anti-inflammatory cytokine level do not move the system to disease and, for this parameter set, up to a six fold increase in either pro-inflammatory cytokine, MMP or Fn-fs is required. We can also see that the unstable steady state influences the path taken by trajectories. In some cases, this may lead to large fluctuations, which we will discuss later.

Throughout this analysis we will be drawing comparisons with the cytokine-only model from the previous chapter. We have redone bifurcation plots from the previous chapter using the parameters we have chosen for this reference parameter set, Figure 3.5. Using parameter values $P_{bp}=0.01$, $P_{pp}=10$, $A_{pp}=10$, $A_{ph}=1$, $\gamma_p=1$ to match the reference parameter set from this model, we have produced single parameter bifurcation diagrams for each of the parameters. We use this for comparison with the fuller model later in this section.

The bifurcation analysis of the full cartilage model reveals a wide range of behaviours as we vary the parameters away from the reference parameter set, these

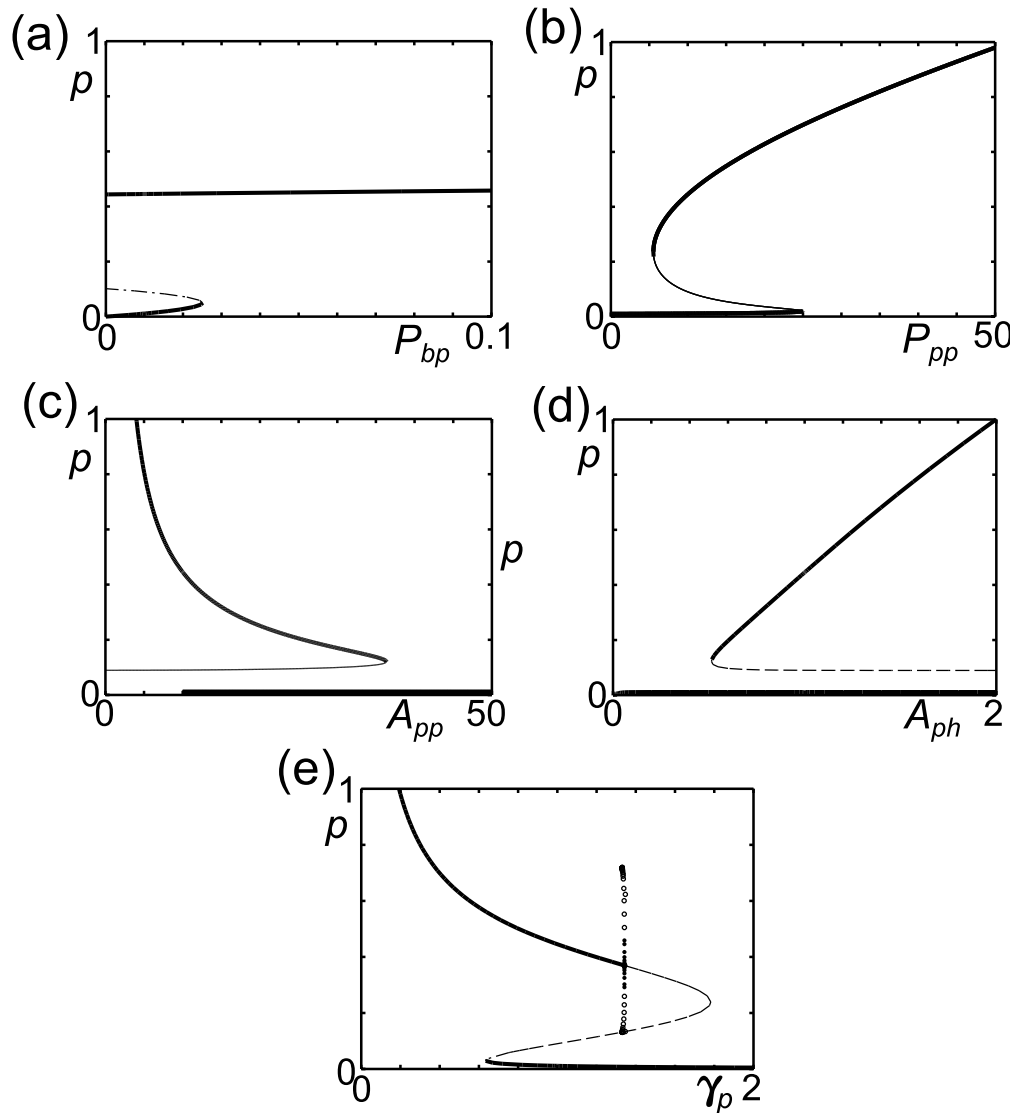


Figure 3.5: Bifurcation plots of the cytokine-only model using the reference parameter values used in this chapter showing the transitions from monostable to bistable. Comparison with the cartilage model in this chapter gives insight into the effect of the ECM fragment driven feedback.

Name	No. of Steady States	Stability of Steady States	Limit Cycles	Type
Ai	1	S_0^S	-	Monostable Health
Aii	1	S_0^S	-	Monostable Disease
Aiii	1	S_0^U	L_1^S	Monostable
Bi	3	S_0^S, S_1^U, S_2^U	-	Monostable Health
Bii	3	S_0^U, S_1^U, S_2^S	-	Monostable Disease
Biii	3	S_0^S, S_1^U, S_2^S	-	Bistable
Ci	3	S_0^S, S_1^U, S_2^U	L_1^S	Bistable
Cii	3	S_0^U, S_1^U, S_2^S	L_1^S	Bistable
Ciii	3	S_0^S, S_1^U, S_2^S	L_1^S	Bistable
Civ	3	S_0^S, S_1^U, S_2^S	L_1^U, L_2^S	Bistable
Cv	3	S_0^U, S_1^U, S_2^U	L_1^S	Monostable Disease
Di	3	S_0^S, S_1^U, S_2^S	L_1^U, L_2^S	Bistable
Dii	3	S_0^S, S_1^U, S_2^U	L_1^S, L_2^U	Bistable
Diii	3	S_0^U, S_1^U, S_2^S	L_1^U, L_2^S	Bistable
Ei	5	$S_0^S, S_1^U, S_2^S,$ S_3^U, S_4^S	-	Tristable
Eii	5	$S_0^S, S_1^U, S_2^U,$ S_3^U, S_4^S	-	Bistable
Fi	5	$S_0^S, S_1^U, S_2^U,$ S_3^U, S_4^S	L_1^S	Tristable
Fii	5	$S_0^S, S_1^U, S_2^S,$ S_3^U, S_4^S	L_1^U	Tristable

Table 3.4: Summary of the behaviours that arise for different values of the parameters in system (3.2.1 - 3.2.4). The abbreviation S means Stable and U means Unstable, indicating the stability of the steady state or limit cycle.

are summarised in Table 3.4. In the rest of this section we will look at single parameter variations away from the reference parameter set for each parameter. This may give insight into OA initiation and allow suitable treatment strategies to be considered.

3.4.1 Changes in P_{bp}, P_{pp} and P_{fp}

The parameters P_{bp} , P_{pp} and P_{fp} govern the production of pro-inflammatory cytokines. These cytokines are raised in OA and this has been implicated in disease

progression [59]. The mechanism by which these raised levels occur is unclear but could be the result of higher than normal production rates of pro-inflammatory cytokines.

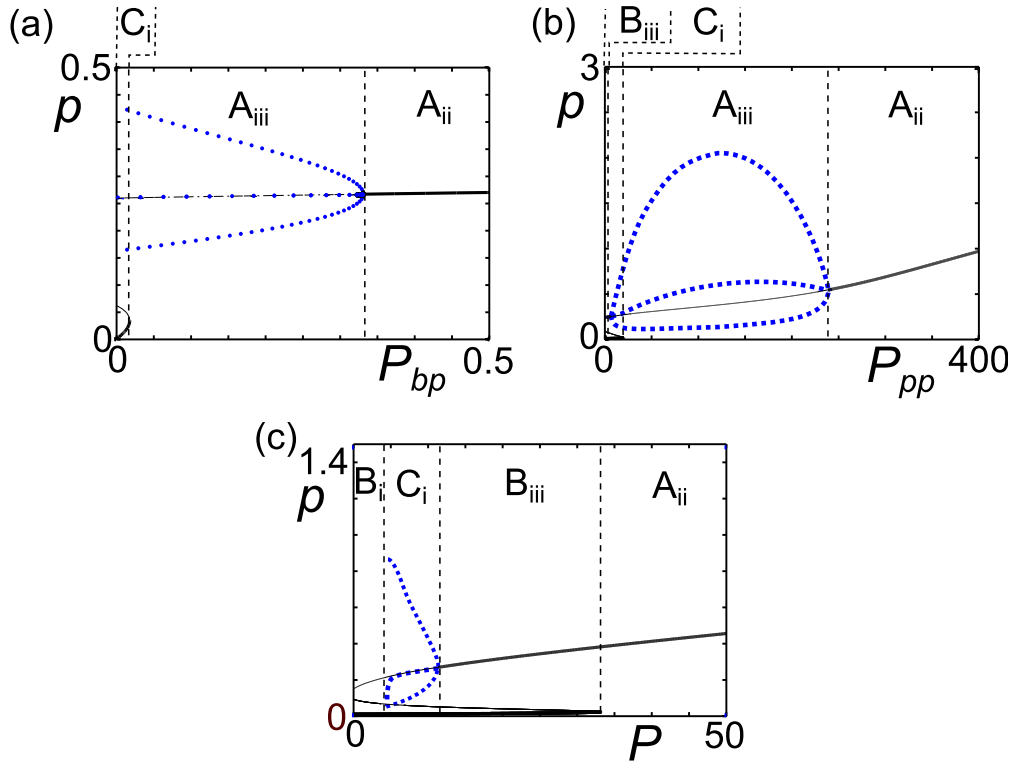


Figure 3.6: Bifurcation plots of the pro-inflammatory cytokine level (p) against the pro-inflammatory cytokine production parameters (a) P_{bp} , (b) P_{pp} and (c) P_{fp} . The dashed lines denote the transition between different behaviours, which are labelled.

In this four-variable model if any of these three parameters are sufficiently high bistability is lost through a fold bifurcation and there is a single steady state (Fig 3.6). For intermediate P_{bp} and P_{pp} values loss of bistability is followed by a single stable limit cycle (Figs 3.6a and b) representing an oscillatory state. Then at higher levels of these parameters this is lost, via a Hopf bifurcation, leaving a single stable steady state. For increases in P_{fp} , the Hopf bifurcation is encountered before the fold bifurcation, giving rise to two stable steady states for some values of P_{fp} . For low values of P_{fp} , we can have a single stable steady state representing health. As the limit cycle collides with S_1 at a homoclinic bifurcation it leaves

only one stable and two unstable steady states. Examination of the phase space suggests that, as for the reference parameter set, the basin of attraction of the disease state is large in the bistable region and remains large even as we move towards the homoclinic (Figure 3.7). Indeed, in the monostable health region, trajectories undergo large fluctuations in p before settling to the healthy state (Figure 3.8). One interpretation of these large basins of attraction is that major deviations from the state of health due to trauma or infection are likely to move an individual to a state of disease, since the large basins for disease persist over the range of small parameter variations, which we might expect to see in different individuals. Even in monostable health large deviations from the healthy state could cause cartilage damage. This behaviour may be point to the reasons for OA being so prevalent since the system trajectories deviate from the healthy steady state for wide ranges of parameters and initial conditions.

From our reference parameter set, variations in either of the other two pro-inflammatory cytokine production parameters (P_{bp} , P_{pp}) cannot lead to monostable health, although altering P_{pp} can change the stable disease state from a limit cycle to a fixed point. We do not know whether a fixed disease state or a oscillatory disease state is more damaging to the cartilage. An oscillatory state may be considered to be less damaging since it results in periods of low damage and possible repair. However, due to the poor repair capacity of cartilage it is also possible that a stable steady disease state might be preferable to a limit cycle disease state, since the large amplitude fluctuations may result in more cartilage damage at high points on the cycle and little repair at low points. The average value of the limit cycle (the blue dashed line on Figure 3.6) may indicate how damaging the limit cycle is compared to steady states.

Comparison of Figure 3.6a and b with Figure 3.5a and b (the cytokine-only model) shows similar behaviour. One important difference is that both P_{bp} and P_{pp} in Figure 3.6 show oscillatory behaviour whereas the disease states are fixed points

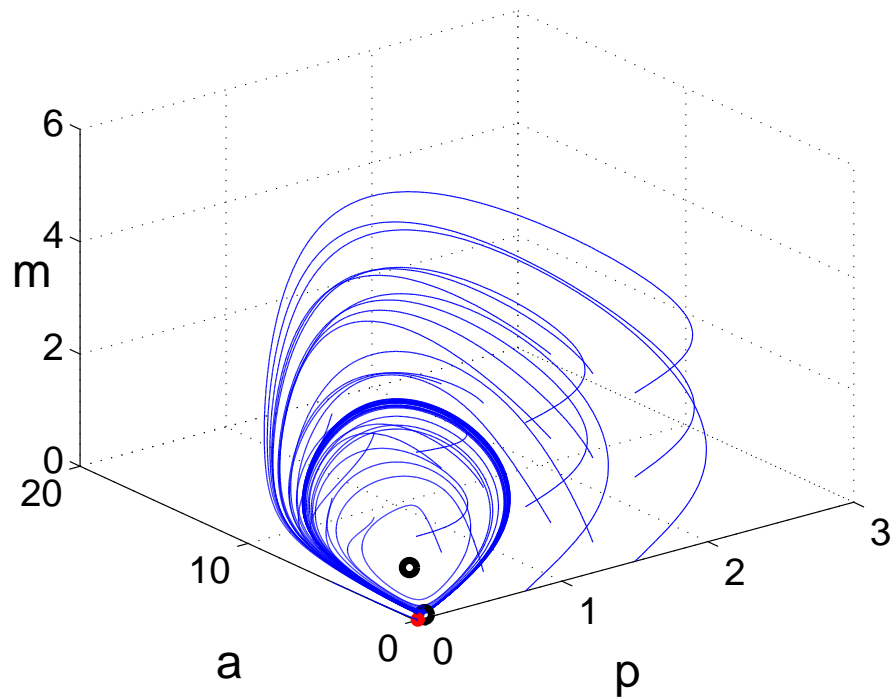


Figure 3.7: Projection of the phase space for the reference parameter set except $P_{fp} = 5$, showing trajectories for various regularly spaced initial conditions in $p - a - m$ space. These parameters are close to a homoclinic orbit and the plot shows that even here the basin of attraction of disease is large, compared to that of the healthy steady state. The red dot denotes a stable fixed point and the black circle denote unstable fixed points.

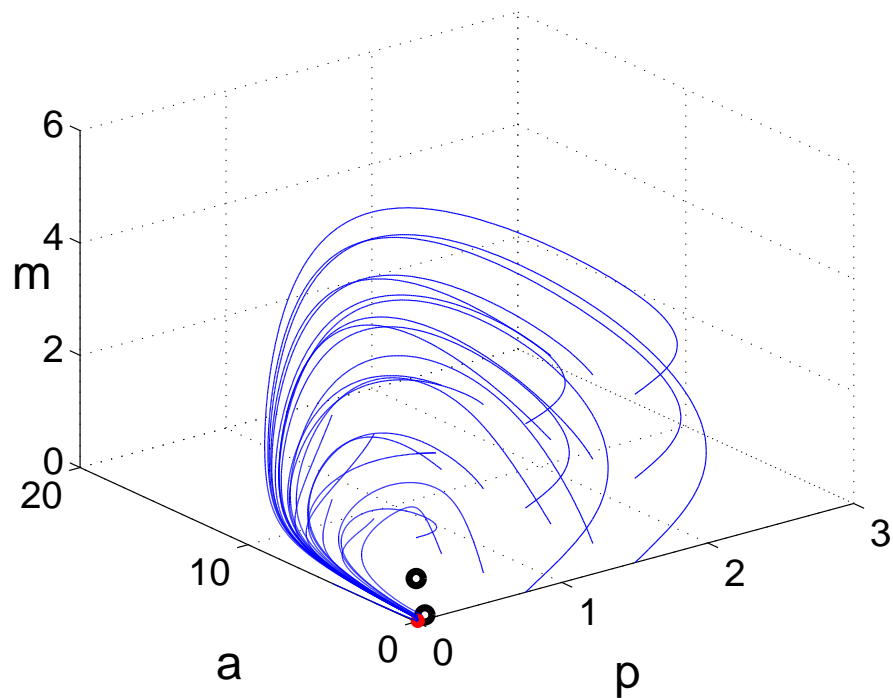


Figure 3.8: Projection of the phase space for the reference parameter set with P_{fp} changed to 3, showing trajectories for various regularly spaced initial conditions in $p - a - m$ space. There is only one stable steady state which is healthy but the fluctuations into the state are large. The red dot denotes a stable fixed point and the black circle denote unstable fixed points.

in the cytokine-only model. If a fixed disease state is clinically preferable to an oscillatory one the model suggests that inhibition of fragment-driven feedback may be a justifiable treatment aim. This may be achieved by greater clearance of fibronectin fragments or lower MMP production, both of which have been explored clinically, although without clear results. We consider these treatment options in Section 3.8.

3.4.2 Changes in A_{pp} and A_{fp}

Anti-inflammatory cytokines reduce the production and activation of pro-inflammatory cytokines and hence we expect that higher values of A_{pp} and A_{fp} , the anti-inflammatory cytokine production parameters, would lead to health. Figure 3.9 shows that this is indeed the case with high levels of either parameter resulting in the loss of the disease state. For A_{pp} the disease state is lost through a fold bifurcation. Whereas for A_{fp} , the disease state becomes unstable at a much lower level and the disease limit cycle is lost through a homoclinic orbit. Decreasing A_{pp} from its reference value leads to an increase in the amplitude of the limit cycle of the disease state (Fig 3.9a), which seems likely to have a detrimental affect. A lower level of A_{fp} results in the disease limit cycle being replaced with a disease steady state (Fig 3.9b). However, the average of the limit cycle decreases when A_{fp} increased so this will depend on the relationship between cytokine level and cartilage destruction. These bifurcation plots suggest that increases to anti-inflammatory cytokine production levels could be beneficial and lead to reduced or even halted cartilage degradation. As discussed previously, a shift from a disease limit cycle to the disease steady state could be beneficial. Hence decreases to anti-inflammatory production, whilst not moving the system to health, may also be beneficial.

Comparing this behaviour with the cytokine-only model (Fig 3.5c), the bistable region occurs over a much wider range for this cartilage model. In some cases this

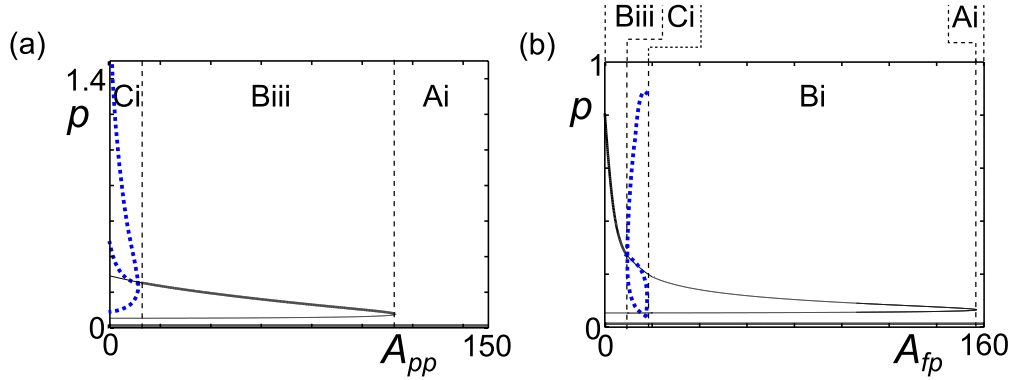


Figure 3.9: Bifurcation plots of the pro-inflammatory cytokine level (p) against anti-inflammatory cytokine production parameters (a) A_{pp} and (b) A_{fp} . The dashed lines denote the transition between different behaviours, which are labelled.

could mean that inhibition of fragment-driven feedback could move the system from disease to health.

3.4.3 Changes in M_{pp} and M_{bp}

The parameters M_{bp} and M_{pp} determine the maximum rates of MMP production. Since MMP levels are known to be raised in OA these parameters are of great interest. Figure 3.10 shows that, for variations in these parameters about the reference parameter set, there are no regions of monostable health. At high levels of MMP production, with either high M_{bp} or M_{pp} , there is a region of monostable disease with a stable steady state. In both cases, at production levels below the reference parameter set, a fold bifurcation leads to bistability with the introduction of stable and unstable steady states, providing the possibility of moving to a healthy state. For M_{pp} , Figure 3.10b, within the bistable region there is a region of oscillatory disease due to two Hopf points.

For this parameter set, for an individual in an oscillatory disease state, an increase in M_{pp} production pushes the system to a steady disease state in p which is lower than the average of the limit cycle in the oscillatory states. However, if the level is too high, although the disease state may result in slower cartilage destruction, we

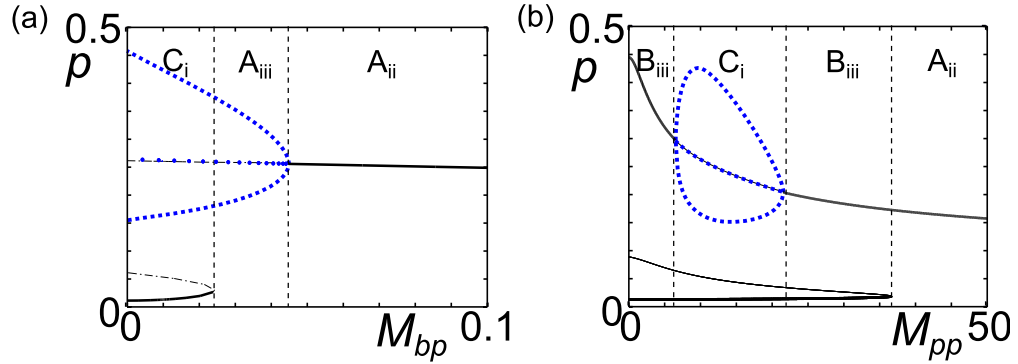


Figure 3.10: Bifurcation plots of the pro-inflammatory cytokine level (p) against the MMP production parameters M_{bp} and M_{pp} . The dashed lines denote the transition between different behaviours, which are labelled.

lose the possibility of moving to a healthy steady state. However, the level of f is lower at smaller values of M_{pp} so the lower levels of p do not necessarily imply less cartilage degradation. This counter-intuitive result arises as a result of a balance in the positive and negative feedback pathways. M_{pp} is part of both pathways and for the reference parameter set the negative feedback is dominant.

3.4.4 Changes in A_{ph} , A_{fh} and M_{ph}

The parameters A_{ph} and A_{fh} are the concentrations of p and f at which the anti-inflammatory cytokine production terms are half maximal. As such they represent the sensitivity of the anti-inflammatory cytokine response to pro-inflammatory and Fn-fs stimulation.

When either A_{ph} or A_{fh} is small, the anti-inflammatory cytokine response is maximal at low inputs, and we only have a low single steady state, indicative of health (Figure 3.11). At higher values of either A_{ph} or A_{fh} , larger concentrations of p or f are required for anti-inflammatory cytokine production, and there is a fold bifurcation. For A_{ph} this leads to bistability whereas for A_{fh} the region immediately after the fold bifurcation is still monostable since both additional states are unstable. This is due to the branch of a Hopf bifurcation at a higher value of A_{fh}

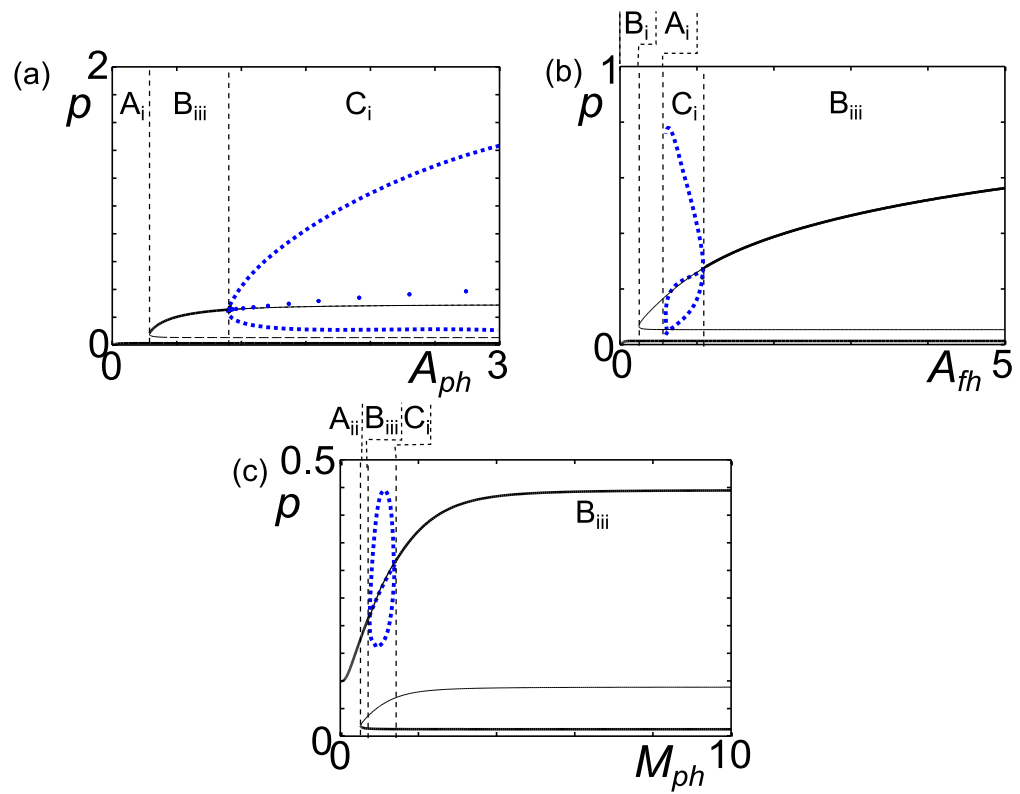


Figure 3.11: Bifurcation plots for the pro-inflammatory cytokine level (p) against the parameters A_{ph} , A_{fh} and M_{ph} . The dashed lines denote the transition between different behaviours, which are labelled.

colliding with the unstable branch. A Hopf bifurcation at higher values of A_{ph} leads to an oscillatory disease state.

The bifurcation plot of A_{ph} is similar to that in the cytokine-only model (Fig 3.5d) for low levels of A_{ph} . Here however, there is oscillatory disease in addition to a fixed disease state.

M_{ph} governs the sensitivity of MMP production in response to activation by pro-inflammatory cytokine. When M_{ph} is small there is a single stable steady state with a high value of p indicative of disease (Figure 3.11). For higher values of M_{ph} we move to bistability through a fold bifurcation. The disease state is also oscillatory for some values of M_{ph} due to two Hopf bifurcations.

3.4.5 Changes in γ_p , γ_m and γ_f

Figure 3.12a shows that when the clearance of pro-inflammatory cytokines, γ_p , is low the steady state is at a high level of p indicating disease. When γ_p is high there is a stable steady state, at low p , indicating health for these parameters. This implies that inactivation or rapid clearance of pro-inflammatory cytokines could be effective in halting the disease course of OA, and clinical trials investigating this approach have had some measure of success. The bifurcation plot here is relatively similar to the γ_p bifurcations on the cytokine only model (Fig 3.5e).

For the reference parameter set the bifurcation plots of γ_m (Fig 3.12b) and γ_f (Fig 3.12c) are qualitatively similar with monostable disease for low levels of γ_f and γ_m and bistability for higher levels. The bistable region is divided into a region with an oscillatory disease state and a region with a fixed disease state. γ_f is the degradation rate of fibronectin fragments and principally represents removal from the ECM via diffusion or advection. Diffusion rates are likely to be decreased by the changes in the joint that are seen in OA, e.g. increased water content and immobility, hence worsening OA progression. However, ECM fragment clearance can

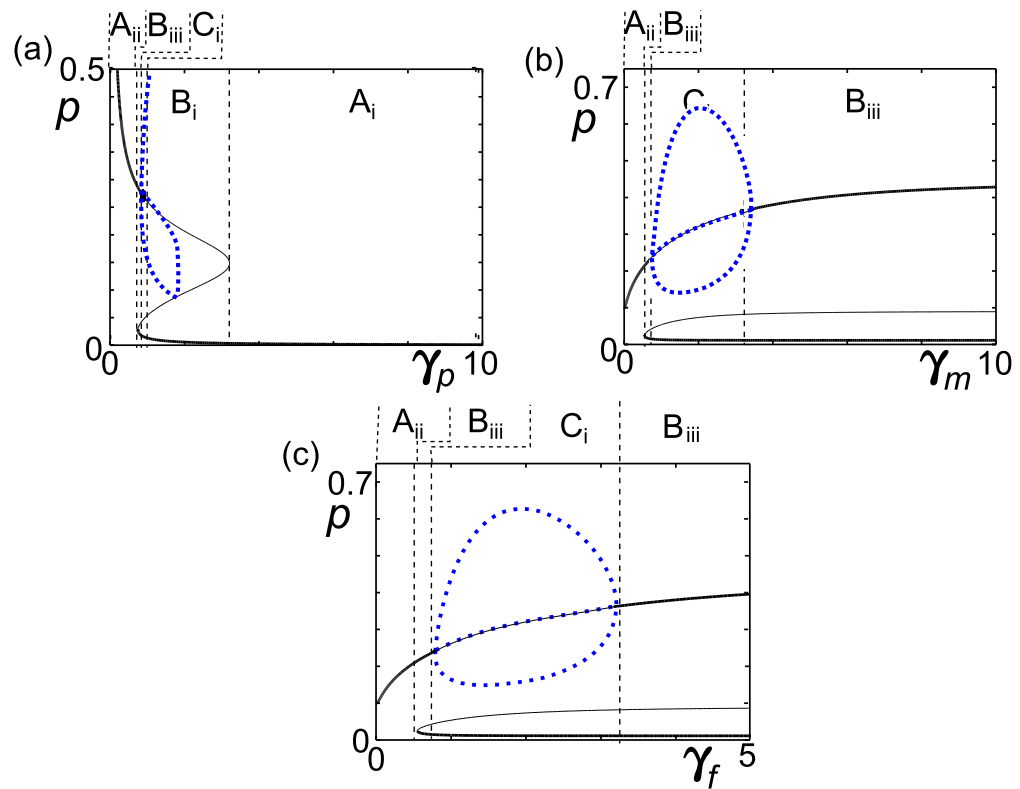


Figure 3.12: Bifurcation plots of the pro-inflammatory cytokine level (p) against the natural degradation parameters γ_p , γ_m and γ_f . The dashed lines denote the transition between different behaviours, which are labelled.

be increased by mechanical loading such as exercise. If the move from monostable disease to bistability exists *in vivo* it suggests that increasing ECM fragment clearance could be beneficial, possibly improving the outcome of treatment to reduce cytokine levels if the two treatments were used together, increasing the parameter at the same time as reducing variable levels.

3.4.6 Additional behaviour seen in the model

So far we have looked only at variations in a single parameter from the reference parameter set, which is a relatively restricted region. Explorations of other parameter sets reveal other features and bifurcation behaviour that we do not encounter with the reference set. These include regions with five steady states, tristability and isolas. We will now look at some of these in more detail and discuss the possible biological applications. Due to the large number of parameters involved we will focus particularly on those that we believe are most likely significant in the development and progression of OA. Background levels of cytokines and MMPs are unlikely to vary much as a result of disease, and although there may be significant variation between individuals we neglect changes in P_{bp} and M_{bp} in this analysis. Similarly, degradation rates of cytokines and enzymes are unlikely to vary significantly so variation in γ_p and γ_m can be ignored. In contrast γ_f may be affected by joint and behavioural changes as discussed above. A_{ph} , A_{fh} and M_{ph} are half maximal rate parameters and are likely to be determined by the chemistry of the molecules involved in the production of the cytokines and enzymes, hence are unlikely to change much either over time or in response to disease. F_{dam} is the mechanical damage parameter and we will look at the effects of mechanical damage later in this chapter. For the time being we shall set it to zero. This means that we are left with 6 parameters that we would like to focus the analysis on: P_{pp} , P_{fp} , A_{pp} , A_{fp} , M_{pp} and γ_f .

Tristable parameter values

As discussed in Section 3.3 the system can have one, three or five steady states. Single parameter variations from the reference set did not show any five-state behaviour, however this can arise from variations in two parameters. Figure 3.13 shows that the five states emerge as a result of fold bifurcations as A_{fp} and A_{ph} are varied. In the bottom left corner of the diagram, where the Hopf and fold bifurcation meet there is a Bogdanov-Takens bifurcation point. From this point the homoclinic bifurcation emerges between the fold and Hopf bifurcations.

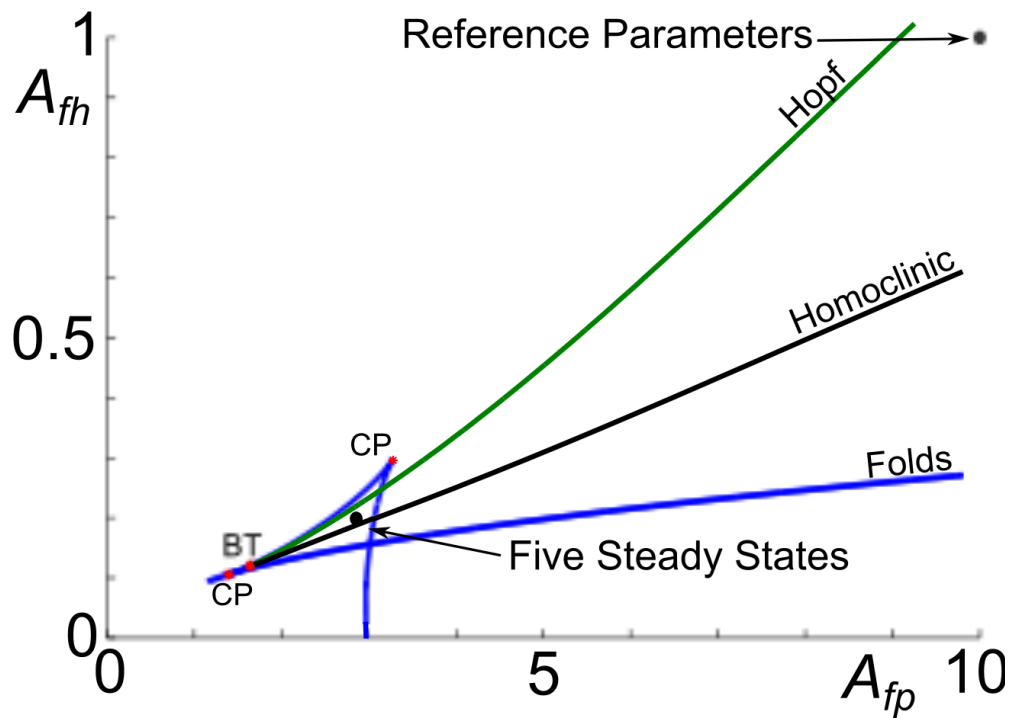


Figure 3.13: Bifurcation plot of A_{fh} against A_{fp} , for the reference parameter set. The diagram shows that if we reduce the value of both A_{fp} and A_{fh} from the values of the reference set there is a region where there are five steady states as a result of fold bifurcations (shown in blue). A homoclinic bifurcation is shown in black, which arises as a result of a Bogdanov-Takens bifurcation (labelled BT). Cusp points of the fold bifurcations are labelled CP. The Hopf bifurcation is shown in green.

At $A_{fp} = 3.2$ and $A_{fh} = 0.2$ there are five steady states (Figure 3.14) with two stable steady states and a stable limit cycle. As a result of the smaller value of

A_{fp} , the maximum rate of anti-inflammatory cytokine feedback is lower than that of the reference parameter set. However a smaller A_{fh} means the fragment-driven anti-inflammatory cytokine production rate may be stronger when levels of f are low. Tristability may be important for OA treatment, if realised biologically, since a move from one disease state to a less destructive one could slow the disease course where movement to the healthy state is not possible. This is discussed in Section 3.8. The phase space projection (Figure 3.14) for this alternative parameter set shows that like the reference parameter set, the basin of attraction of the healthy state is small, but the basin of attraction for the lower disease limit cycle is larger.

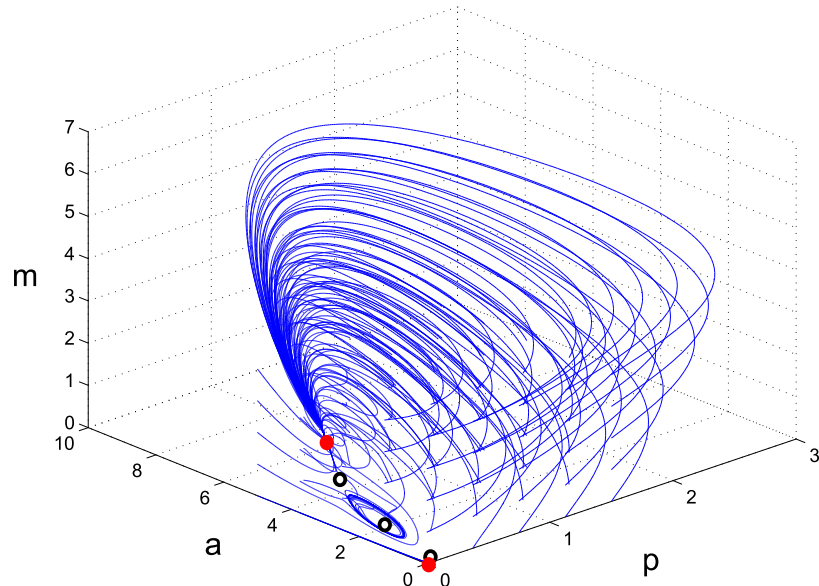


Figure 3.14: Projection of the phase space for a parameter set displaying tristability. The lower healthy stable state has a small basin of attraction whereas the disease steady state and disease limit cycle both have large basins of attraction. The red dots denote stable steady states, whilst the black circles denote unstable steady states. A stable limit cycle surrounds one of the unstable steady states. The reference parameters have been used except $A_{fp}=3.2$ and $A_{fh}=0.2$.

Figure 3.15 shows bifurcation plots for single parameters variations of P_{pp} , P_{fp} , A_{pp} , A_{fp} , M_{pp} and γ_f for this new parameter set. Comparing the plots in Figure

3.15 to those of the reference parameter set, for P_{bp} we see a reduced range of oscillatory behaviour and monostable disease occurs at lower values of P_{bp} . The bifurcation plot of P_{pp} , Fig 3.15b, shows that a region of monostable health emerges when A_{fp} and A_{fh} are lower, compared to the reference parameter set. As with P_{bp} the range over which oscillatory disease occurs is much reduced. P_{fp} variation (Fig 3.15) changes little from the bifurcations in the reference parameter set.

Bistability persists at high values of M_{bp} when A_{fp} and A_{fh} are lower (Fig 3.15d), however the levels of p in both states are high and are likely to indicate differing intensities of disease rather than health and disease. The plot for M_{pp} (Fig 3.15e) looks considerably different to that of the reference parameter set, as additional fold bifurcations in the upper branch cause the branch to fold back on itself. Additionally the limit cycle branches from the two Hopf points now collide with unstable branches at homoclinic bifurcation points rather than connecting. This has a significant effect as there is now a region of monostable health between the two regions rather than bistability. γ_F , (Figure 3.15f), like M_{bp} , has a new region of monostable health between two disease states.

Excitability

For some parameter sets (e.g. the reference parameter set with γ_p increased to 2) the model displays excitable behaviour. This behaviour is most pronounced where there is a single healthy steady state with unstable disease states. Here perturbations from the steady state result in long trajectories around the unstable states.

Figure 3.16 shows an example of this. Here, after a perturbation from the steady state of $p = 0.1$, the system moves directly back to the steady state, but a larger perturbation from the steady state ($p = 0.4$) has a long trajectory around both the unstable states. Perturbations close to the unstable state spiral outwards before

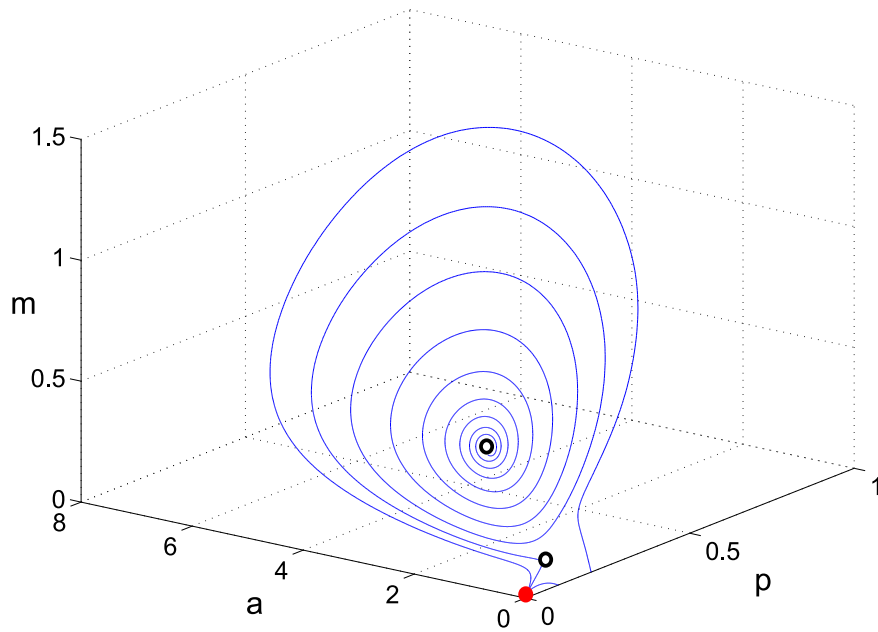


Figure 3.16: Plot of the (p, a, m) phase space showing excitable behaviour in the system. The red dot denotes the stable steady state which is healthy, whilst the black circles denote unstable steady states. Trajectories arising sufficiently close to the healthy state, quickly move into it. However, trajectories originating elsewhere have much longer paths including oscillations. [$P_{bp}=0.01$, $P_{pp}=10$, $P_{fp}=10$, $A_{pp}=10$, $A_{ph}=1$, $A_{fp}=10$, $A_{fh}=1$, $M_{bp}=0.01$, $M_{pp}=1$, $M_{ph}=1$, $F_{dam}=0$, $\gamma_p=2$, $\gamma_m=1$ and $\gamma_f=1$]

moving back to health.

Biologically, this excitable behaviour may mean that a healthy individual who sustains trauma to the cartilage may have a long recovery period and display OA-like symptoms as the cytokine levels return to normal.

Mushrooms and Isolals

If we move far away from the parameter sets we have considered so far, we find further new bifurcation behaviours. Figure 3.17 shows a parameter set which displays mushroom bifurcations, which are composed of four fold bifurcations.

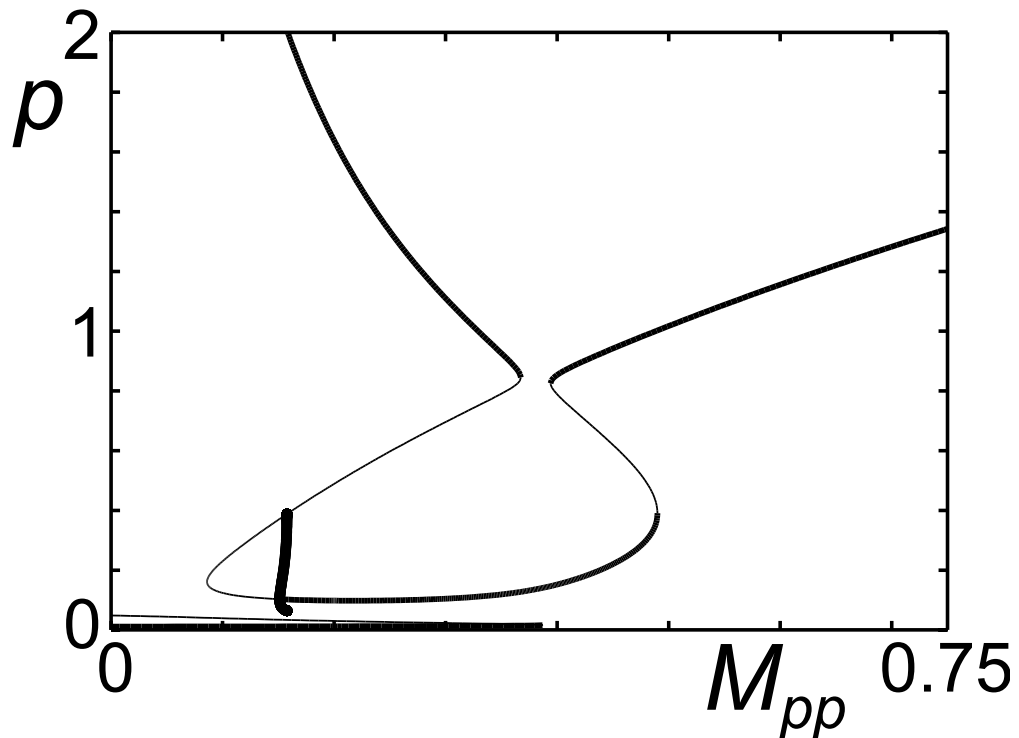


Figure 3.17: Bifurcation plots of p against M_{pp} showing fold bifurcations forming a mushroom. [$P_{bp}=0.01$, $P_{pp}=24$, $P_{fp}=25$, $A_{pp}=1.7$, $A_{ph}=0.1$, $A_{fp}=1.7$, $A_{fh}=0.1$, $M_{bp}=0.01$, $M_{ph}=0.1$, $F_{dam}=0$, $\gamma_p=1.25$, $\gamma_m=1.25$ and $\gamma_f=1.25$]

As we increase P_{pp} , two of the folds move together and the upper branch pinches off leaving an isola (Figure 3.18). Isolals are closed loops of equilibrium points and in this case contain both fold and Hopf bifurcations. This behaviour appears

to be displayed over a small range of parameters, which may not be biologically relevant.

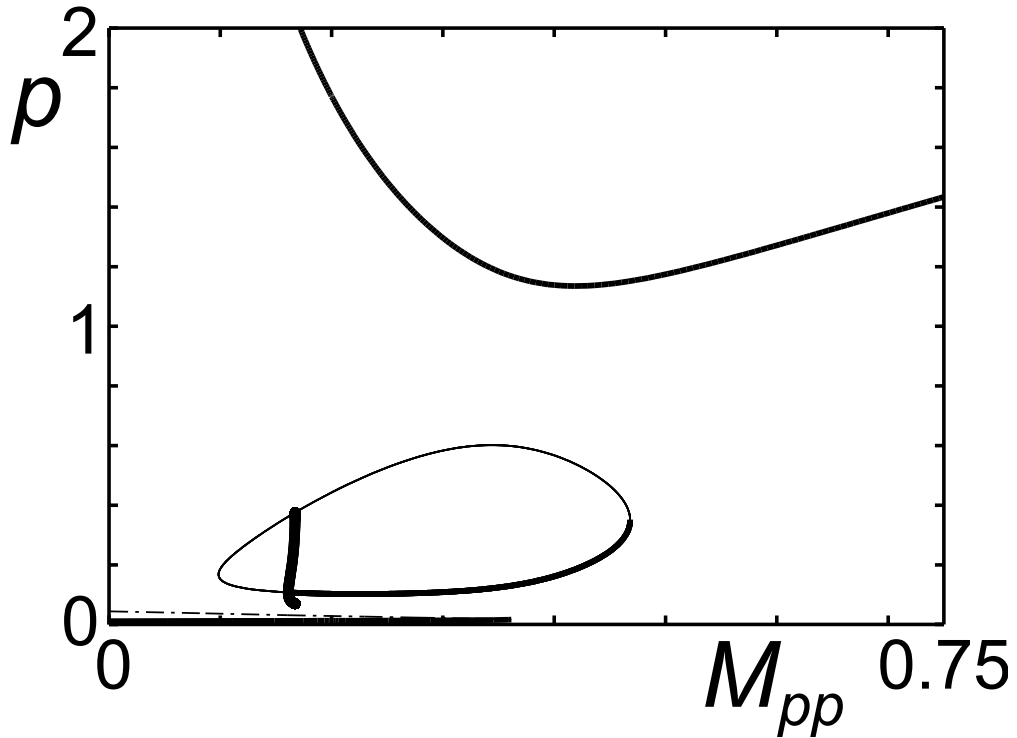


Figure 3.18: Bifurcation plots of p against M_{pp} showing a fold bifurcations forming an isola. [$P_{bp}=0.01$, $P_{pp}=25$, $P_{fp}=25$, $A_{pp}=1.7$, $A_{ph}=0.1$, $A_{fp}=1.7$, $A_{fh}=0.1$, $M_{bp}=0.01$, $M_{ph}=0.1$, $F_{dam}=0$, $\gamma_p=1.25$, $\gamma_m=1.25$ and $\gamma_f=1.25$]

However, if this behaviour does exist then it has interesting and counter-intuitive implications for the disease course. For instance in Figure 3.17 we can see that someone in a disease state at a low level of M_{pp} may be forced to a lower disease state if M_{pp} increases during the progression of their disease, for example by having M_{pp} between the upper two folds.

3.5 Two Parameter Variations

The previous section demonstrated how the behaviour of the model changes as we vary one parameter at a time. It also showed that these behaviours are sensitive to changes in the other parameter values and that varying two parameters could lead

to additional steady states. To further explore the parameter space and better understand how the different behaviours are connected we will now expand the bifurcation analysis in two parameters, to a wider group of parameters. Here we focus on the six parameters that we consider to be the most relevant to disease progression and most likely to change over the disease course: P_{pp} , P_{fp} , A_{pp} , A_{fp} , M_{pp} and γ_f .

3.5.1 P_{pp} variations

Two parameter bifurcation diagrams are shown in Figure 3.19 with the parameters P_{fp} , A_{pp} , A_{fp} , M_{pp} and γ_f plotted against P_{pp} .

In the one parameter analysis P_{fp} had a value of 10 and as P_{pp} was increased the system moved through four fold bifurcations moving from bistability at low P_{pp} to monostable disease. At a higher level of P_{fp} (Figure 3.19a) the bistable region is lost and we have monostable disease at a lower value of P_{pp} , as might be expected since P_{pp} and P_{fp} both increase pro-inflammatory cytokine production. Both the Hopf bifurcation and the homoclinic bifurcation are generated from a Bogdanov-Takens point at a low value of both P_{pp} and P_{fp} . These change the nature of monostable disease from fixed to oscillatory. A Bogdanov-Takens bifurcation is a bifurcation of codimension 2, i.e. it is only seen as we vary two parameters, and occurs where there is a pair of zero eigenvalues. At this point the fold and Hopf bifurcations collide. At parameter values close to this point the limit cycle connects with one of the two steady states, resulting in the loss of the limit cycle to a homoclinic orbit [66]. Often in the vicinity we also have a Generalised Hopf (GH) point (or Bautin bifurcation) where the Hopf switches from subcritical to supercritical. In this case the GH point is at a high level of P_{pp} , and results in a tiny region of bistability with a stable fixed point surrounded by both an unstable and stable limit cycle. Since this region is so small and also relies on huge differences

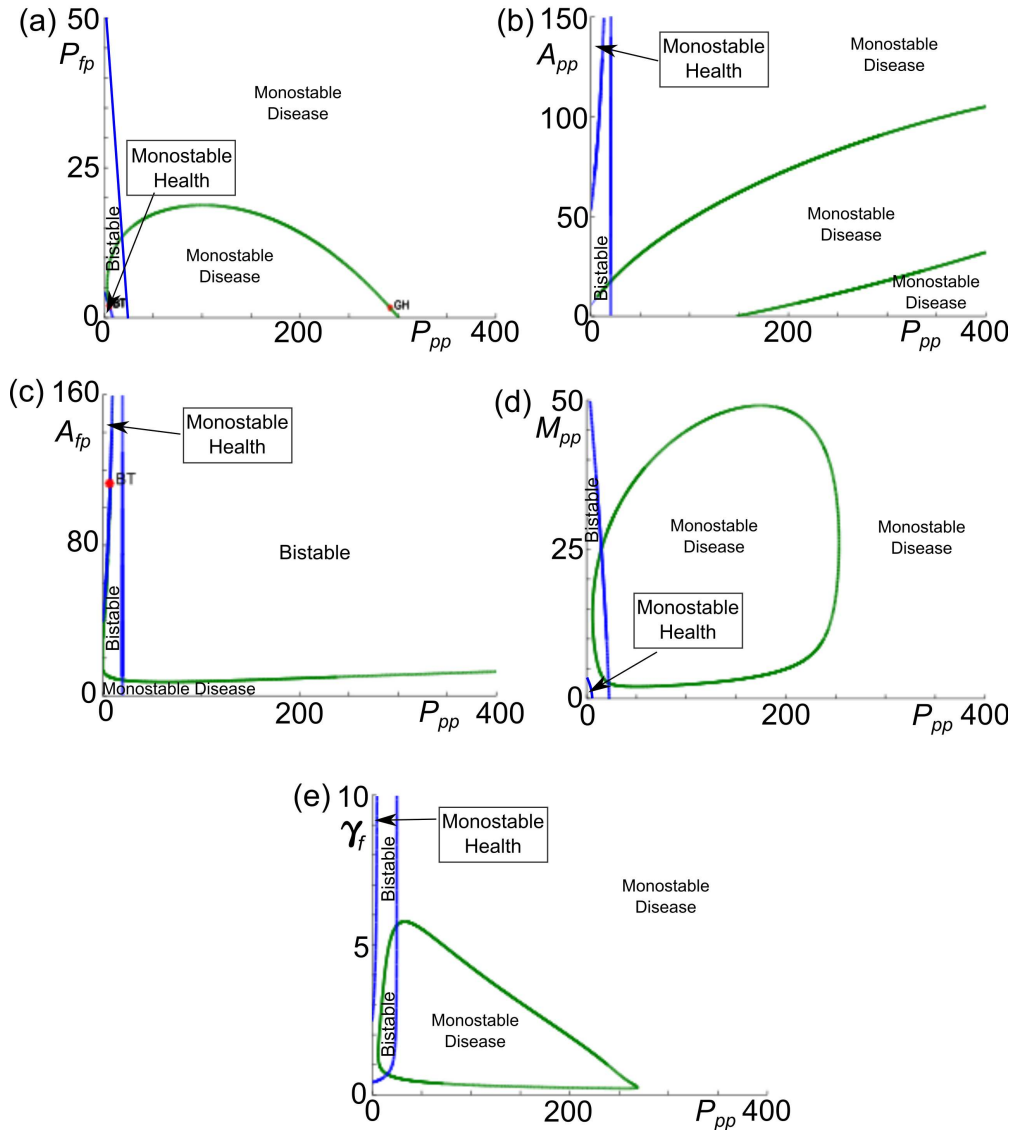


Figure 3.19: Two parameter bifurcation diagrams showing P_{pp} against P_{fp} , A_{pp} , A_{fp} , M_{pp} and γ_f . Fold bifurcations are shown as blue lines, Hopf bifurcations as green lines and homoclinic bifurcations are shown in black. Areas of monostable health, bistability and monostable disease are indicated. The reference parameter set is used.

in magnitude between P_{fp} and P_{pp} , it is unlikely to have biological significance.

A_{pp} is fixed at 10 in the previous P_{pp} bifurcation analysis. At much higher levels of A_{pp} we have a region of monostable health emerging for low values of P_{pp} as a result of a fold bifurcation. When A_{pp} is large enough we also lose the oscillatory disease behaviour which is replaced with monostable disease.

In contrast with A_{pp} the bifurcation diagram of A_{fp} against P_{pp} shows a large region of bistability and only a small region of monostable disease (Figure 3.19c). This may suggest that any changes to A_{pp} are more likely to be damaging than changes to A_{fp} since they are more likely to move an individual to monostable disease. As A_{fp} increases a small region of monostable health emerges at small values of P_{pp} .

When M_{pp} is very small two fold bifurcations move the system from monostable health, through bistability to monostable disease as P_{pp} increases (Figure 3.19d). For larger values of M_{pp} the region of health is lost and we have bistability and monostable disease. The bifurcation plot is dominated by a Hopf bifurcation which encloses a region where the disease state is oscillatory.

The two parameter bifurcation plot for γ_f against P_{pp} is relatively similar to that of M_{pp} . Here, however the region of health for a low P_{pp} occurs when γ_f is relatively large. Again, the closed Hopf bifurcation encloses the oscillatory region.

Generally, as Figure 3.19 shows, the behaviour of the system mostly displays behaviour associated with monostable disease. When P_{pp} is low we generally have bistability, with disease occurring at higher levels of P_{pp} . This behaviour may indicate that this parameter is important in OA initiation and progression. The behaviour suggests that increases in this parameter either through genetic, biochemical or physical processes, regardless of the parameters of the rest of the system, is likely lead to disease.

3.5.2 P_{fp} variations

Figure 3.20 shows the changes in the behaviour of the system as we vary P_{fp} alongside each of the other parameters (excepting P_{pp} which was discussed above). Generally, regardless of the value of the other parameter varied, if P_{fp} is made large enough the system moves to monostable disease. Compared to the P_{pp} parameter variations above, the regions of monostable health and bistability are much larger when we vary P_{fp} with other parameters. This suggests that the system is better able to withstand variation in P_{fp} than P_{pp} before the system is pushed to monostable disease, where treatment options are likely to be more limited.

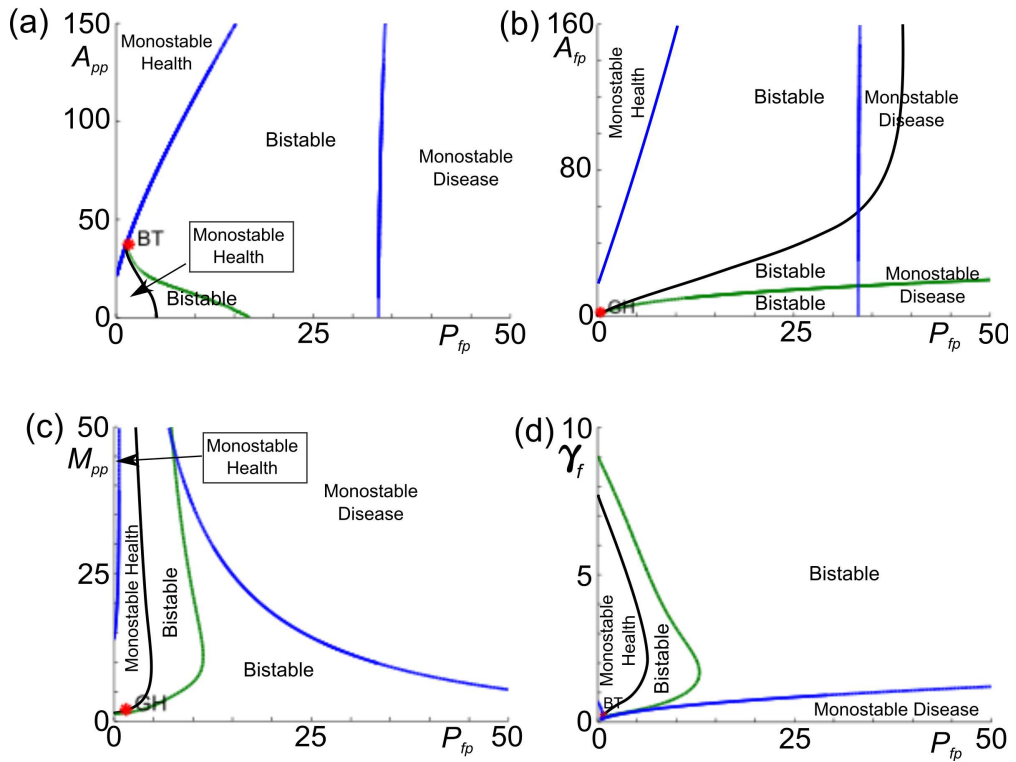


Figure 3.20: Two parameter bifurcation diagrams showing P_{fp} against A_{pp} , A_{fp} , M_{pp} and γ_f . Fold bifurcations are shown as blue lines, Hopf bifurcations as green lines and homoclinic bifurcations are shown in black. Areas of monostable health, bistability and monostable disease are indicated. The reference parameter set is used.

3.5.3 A_{pp} variations

Changes in the system behaviours as we vary A_{pp} with the other parameters are shown in Figure 3.21. In terms of the general behaviour as we change A_{pp} with the parameters A_{fp} , M_{pp} and γ_f we have only bistable and monostable healthy behaviour. However, in the case of P_{pp} and P_{fp} (Figs 3.19b and 3.20a) there is monostable disease at low levels of A_{pp} as the pro-inflammatory cytokines overwhelm the anti-inflammatory cytokine response.

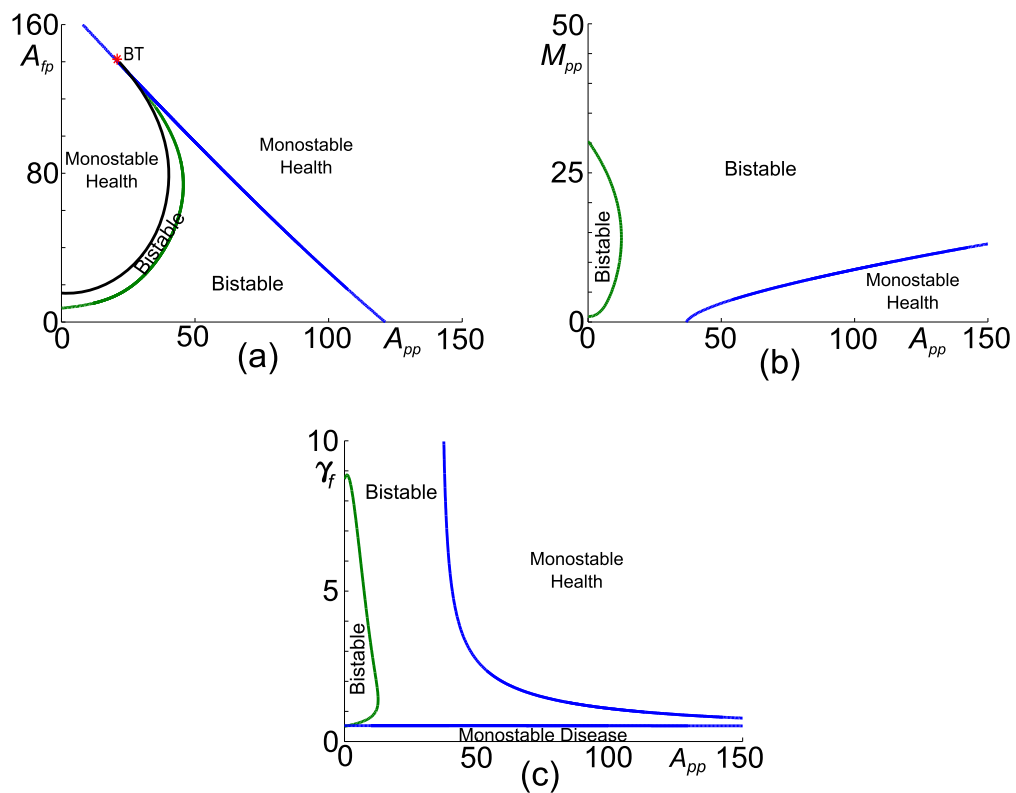


Figure 3.21: Two parameter bifurcation diagrams showing A_{pp} against A_{fp} , M_{pp} and γ_f . Fold bifurcations are shown as blue lines and Hopf bifurcations as green lines. Areas of monostable health, bistability and monostable disease are indicated. The reference parameter set is used.

3.5.4 A_{fp} variations

Figure 3.22 shows the bifurcation behaviour as we vary M_{pp} and γ_f with A_{fp} . In both diagrams there is a region of bistability for low A_{fp} moving to monostable health as A_{fp} increases. For a high value of M_{pp} there is a region of monostable disease regardless of the values of A_{fp} . Similarly, we have a region of monostable disease for low γ_f .

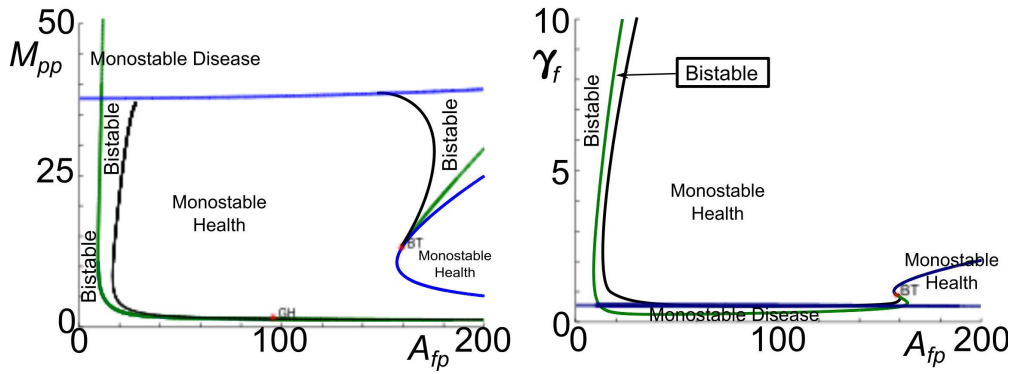


Figure 3.22: Two parameter bifurcation diagrams showing A_{fp} against M_{pp} and γ_f . Fold bifurcations are shown as blue lines, Hopf bifurcations as green lines and homoclinic bifurcations are shown in black. Areas of monostable health, bistability and monostable disease are indicated. The reference parameter set is used.

Generally, higher values of A_{fp} lead to health as we would expect, both in these plots and in the previous sections. However there is an exception to this for certain values of M_{pp} , where increasing A_{fp} moves the system from health to bistability.

3.5.5 M_{pp} variations

The bifurcation diagram of γ_f against M_{pp} is shown in Figure 3.23. The majority of the plot is bistable with a small area of monostable disease at small values of γ_f . There are no regions of monostable health for this parameter set, however, the variations of M_{pp} with other parameters (Figures 3.19d, 3.20c, 3.21b and 3.22a) do display monostable health.

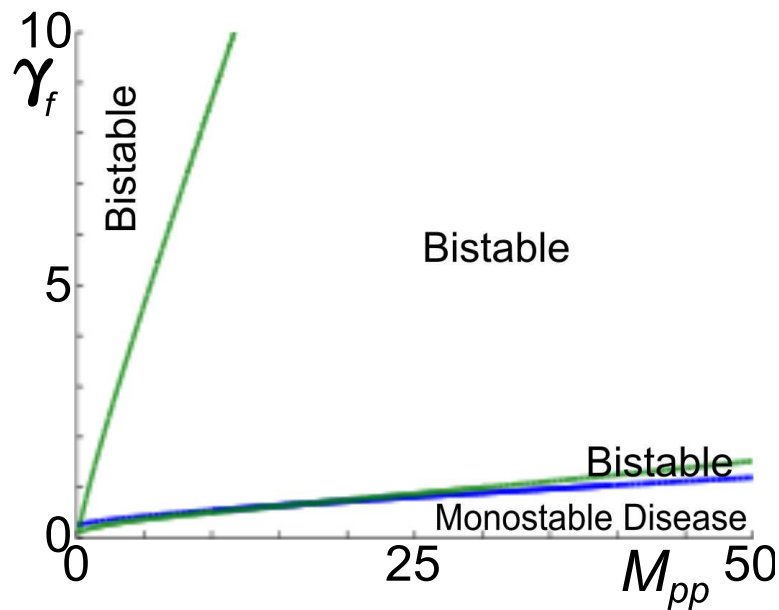


Figure 3.23: Two parameter bifurcation diagram showing M_{pp} against γ_f . Fold bifurcation is shown as a blue line and Hopf bifurcations as green lines. Areas of bistability and monostable disease are indicated. The reference parameter set is used.

Generally speaking, in the two parameter variations we have analysed, increases in M_{pp} are detrimental to individuals, moving the system from health to bistability or from bistability to disease. However, the single parameter bifurcations showed this was not always the case for other parameters sets. Since M_{pp} forms part of both negative and positive feedback loops within the model, the effect of increases is dependent upon which type of feedback is dominating the system.

3.5.6 γ_f variations

Two parameter variations in γ_f have been presented in the previous five sections. As in the case of M_{pp} , increases in γ_f can have both positive and negative effects in terms of moving the system from disease to health or vice versa.

3.6 Mechanical Damage

In our model we represent mechanical damage to the cartilage by an increase in F_{dam} , the rate at which fibronectin fragments are produced. Mechanical damage is considered to be a major risk factor in OA and the first stage of repair after mechanical damage to the cartilage is necrosis of the damaged tissue which leads to increased concentrations of fibronectin fragments. Thus, changes in the model behaviour as F_{dam} increases could be indicative of the changes in OA. Figure 3.24a shows the bifurcation diagram for small changes in F_{dam} , with the reference parameter set used for the other parameters. Since F_{dam} was zero in the reference parameter set, there is bistability at $F_{dam} = 0$ as before. As F_{dam} increases a fold bifurcation removes the lower two states leaving only monostable disease. As F_{dam} increases further a pitchfork bifurcation removes the upper state leaving only monostable disease.

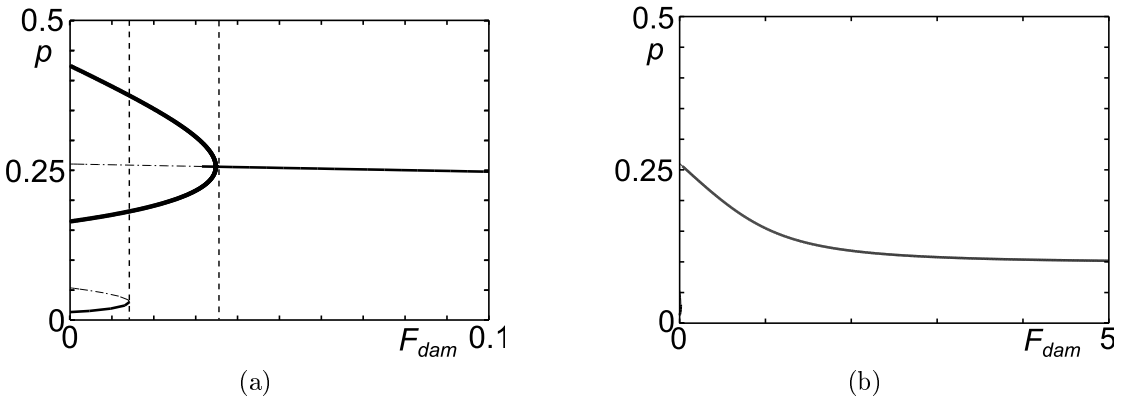


Figure 3.24: Bifurcation plots of the parameter F_{dam} against p . The changes in behaviour are indicated by dashed lines. a) shows small changes in F_{dam} close to zero where there is bistability. b) shows changes in F_{dam} extending further from zero. Here the level of p at the disease state decreases. The reference parameter set is used

For this parameter set even small levels of damage lead to sustained disease, however, when we look at F_{dam} on a larger scale (Fig 3.24b) we see that if we increase this parameter further the level of p at the disease state reduces. This feature is counter intuitive and may be due to the simplifying assumptions within the model, since large amounts of mechanical damage would most likely cause changes in joint

loading also.

3.7 Biological Applications

In the previous sections we have considered how the behaviour of the system depends on the parameter values. In clinical settings, we would generally be more interested in how the key variables change over time, stimulated by either changes in variable levels or parameter values. In this section we will examine time course simulations and consider such biological applications.

The reference parameter set discussed previously shows bistability. An individual at the healthy steady state will move to the disease state if an appropriate stimulus is applied (Figure 3.25). In this case an increase in the pro-inflammatory cytokine level to 0.05 at time 20 is not sufficient to move the system to disease, whilst a stimulus of 0.06, does move the system into the basin of attraction of the disease state.

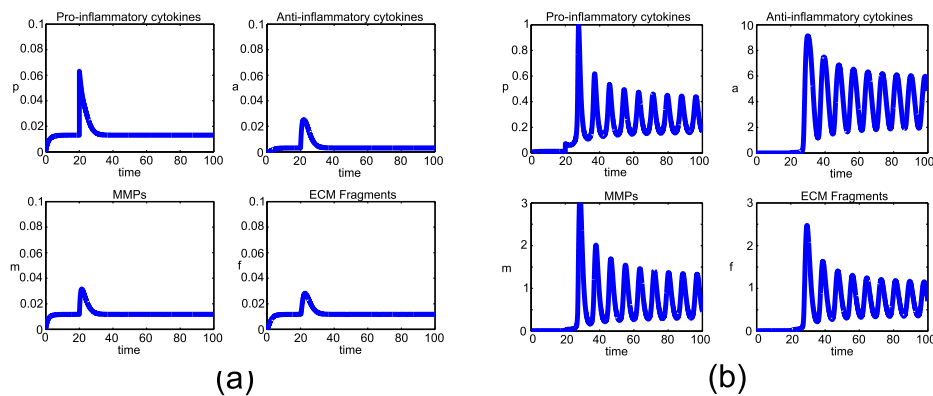


Figure 3.25: Time course plot of cartilage model with a pro-inflammatory stimulus at $t = 20$. (a) the pro-inflammatory level is increased to 0.05 and the system recovers after a short time. (b) the pro-inflammatory level is increased to 0.06 leading to disease. The parameters used are that of the reference parameter set.

In addition to bistability, for other parameter values, there are also regions of monostable health. As discussed earlier, the model displays regions of excitable

behaviour which means that not all regions of monostable health behave in the same way. Figure 3.26 shows two sets of time courses for parameters with only one stable steady state. In the first there are no other steady states and after a trauma the system, modelled as an instantaneous increase in all four variables, quickly moves back to the healthy state. In the second, there are two unstable steady states and the system oscillates around these for a short period before returning to health. In this case, the level of Fn-fs is raised, suggesting that the cartilage is being damaged as the system oscillates before health is restored.

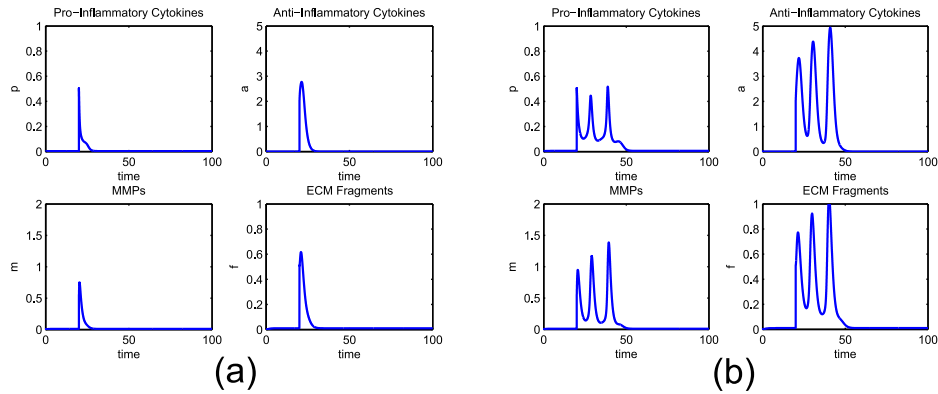


Figure 3.26: Time course plot of system with a stimulus [$p = 0.5$, $a = 2$, $m = 0.5$, $f = 0.5$] at $t = 20$. In figure (a) the parameter γ_p is 3 indicating monostable health with only one stable steady state. In figure (b) the parameter γ_p is 2 indicating monostable health with one stable and two unstable steady states. ($P_{bp} = 0.01$, $P_{pp} = 10$, $P_{fp} = 10$, $A_{pp} = 10$, $A_{ph} = 1$, $A_{fp} = 10$, $A_{fh} = 1$, $M_{bp} = 0.01$, $M_{pp} = 10$, $M_{ph} = 1$, $F_{dam} = 0$, $\gamma_m = 1$ and $\gamma_m = 1$)

3.7.1 Time dependent changes in feedback parameters

The previous sections have shown that a wide range of behaviours can be observed in this system. We will now show that changes in the system parameters over time could be biologically significant and lead to the development of OA. In the cytokine-only model (Chapter 2) we proposed that changes in key parameters over time could lead to the onset of RA. In this model we similarly suggest that changes in parameters could lead to OA in the cartilage. In RA it is thought

that the parameter changes are the result of premature aging in T cells [72, 89], whereas in OA much less is known about the reason for OA onset. It is likely that the onset of OA varies between individuals, and possible reasons include changes to chondrocytes, changes in chondrocyte numbers, and mechanical factors.

The network diagram (Figure 3.1) shows that there are four feedback pathways in this system and we will investigate whether changes in any or all of these can lead to disease.

Positive cytokine-driven feedback

The cytokine-driven positive feedback loop highlighted in Figure 3.27 has only one parameter, P_{pp} .

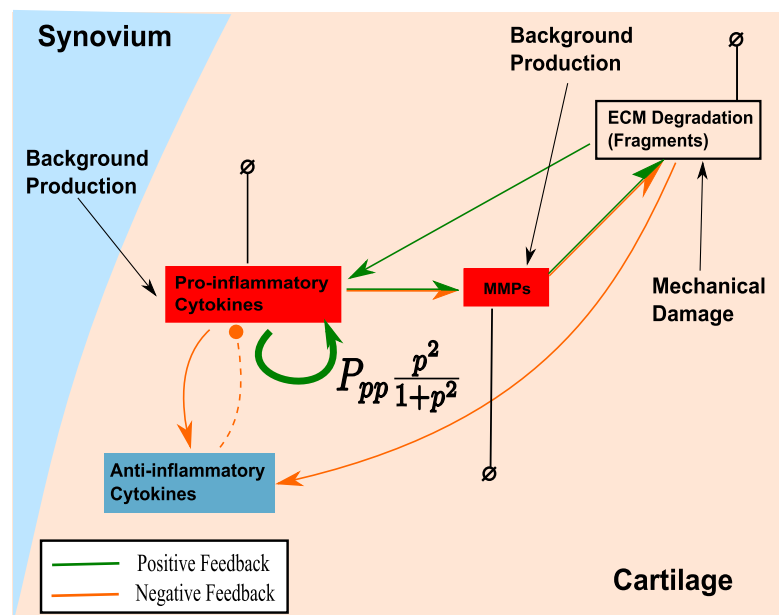


Figure 3.27: Cytokine network diagram showing the positive cytokine driven feedback loop which has only one parameter.

Bifurcation analysis suggested that high values of P_{pp} correspond to a disease state (Section 3.4.1). In the previous chapter we showed that increases in the equivalent parameter (P_{pp}) over time may lead to RA in the synovium. In this model increasing P_{pp} over time also leads to disease. We can simulate an increase

in the pro-inflammatory-driven pro-inflammatory cytokine production rate over time by making P_{pp} a function dependent on time, similar to the time varying function in the two variable model. In this model we use the function,

$$P_{pp} = P_{pp}^{min} + \frac{(P_{pp}^{max} - P_{pp}^{min})t^2}{P_{pp}^T + t^2}, \quad (3.7.1)$$

and set the parameters as $P_{pp}^{min} = 1$, $P_{pp}^{max} = 26$, and $P_{pp}^T = 20$. Figure 3.28 shows the system initially has a healthy steady state, but as the value of P_{pp} increases the system moves to an oscillatory disease state. This move corresponds to a fold bifurcation as we increase P_{pp} , see Figure 3.6. Since we set the maximum value of P_{pp} to 26 we do not encounter the Hopf bifurcation as P_{pp} changes. However, if we allowed P_{pp} to increase past the Hopf bifurcation the system would move from oscillatory disease to a stable steady disease state. Oscillatory behaviour of OA is difficult to confirm clinically due to the lack of biomarkers for OA, however some patients report intermittent pain or stiffness on early OA [58, 120]. Currently diagnosis of OA relies on pain, as reported by patients, and radiographic evidence, both of which are often not formally investigated until later in the disease course.

Positive fragment-driven feedback

The second positive feedback loop in the model is driven by MMP and ECM fragment interactions and involves the parameters P_{fp} , M_{pp} and M_{ph} (Figure 3.29). The latter two are also involved in negative feedback so we will consider these separately further on, leaving only P_{fp} . We simulate a time dependent increase in P_{fp} by,

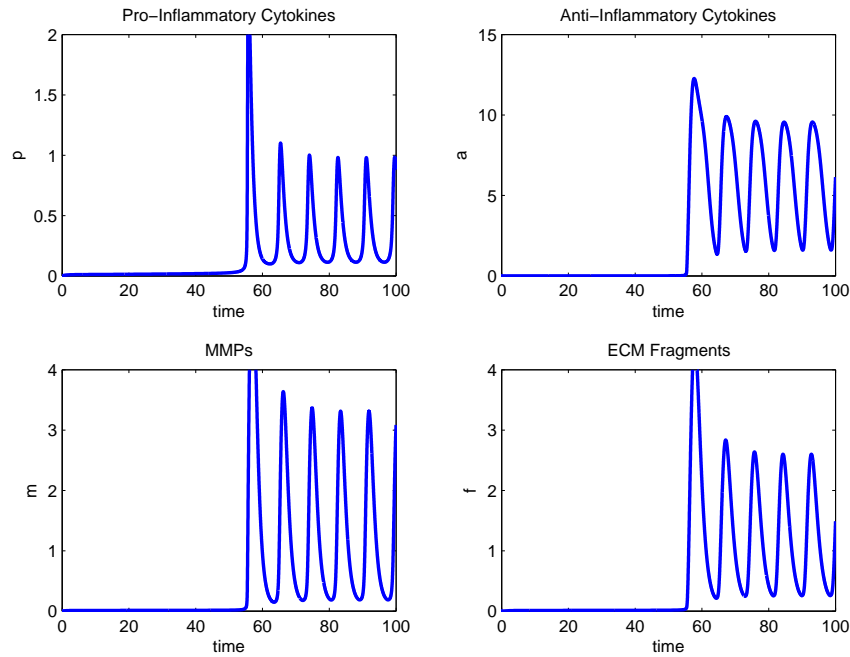


Figure 3.28: System variables plotted against time as the parameter P_{pp} increases in a time dependent fashion. The system moves to a disease state as P_{pp} moves through a fold bifurcation. The other parameters are the reference parameter set.

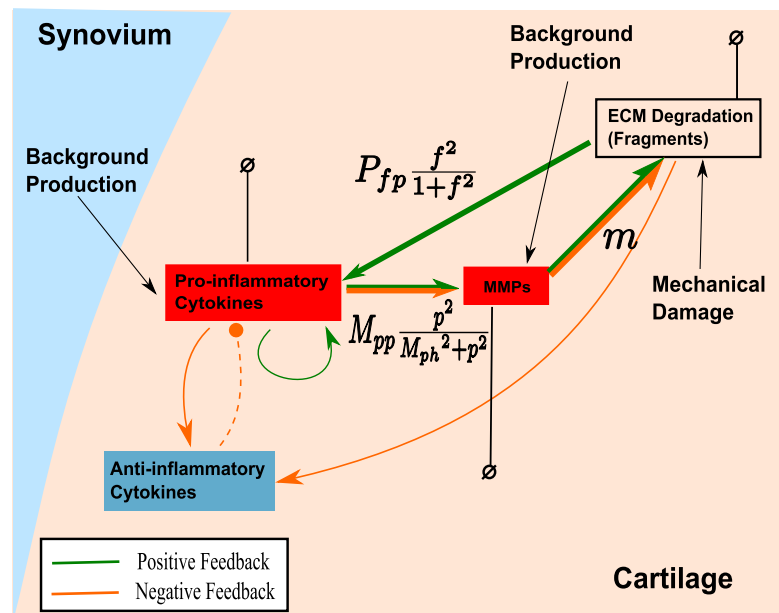


Figure 3.29: Cytokine network diagram from Fig 3.1, highlighting, the positive ECM fragment driven feedback loop which has only three parameters: P_{fp} , M_{pp} and M_{ph} .

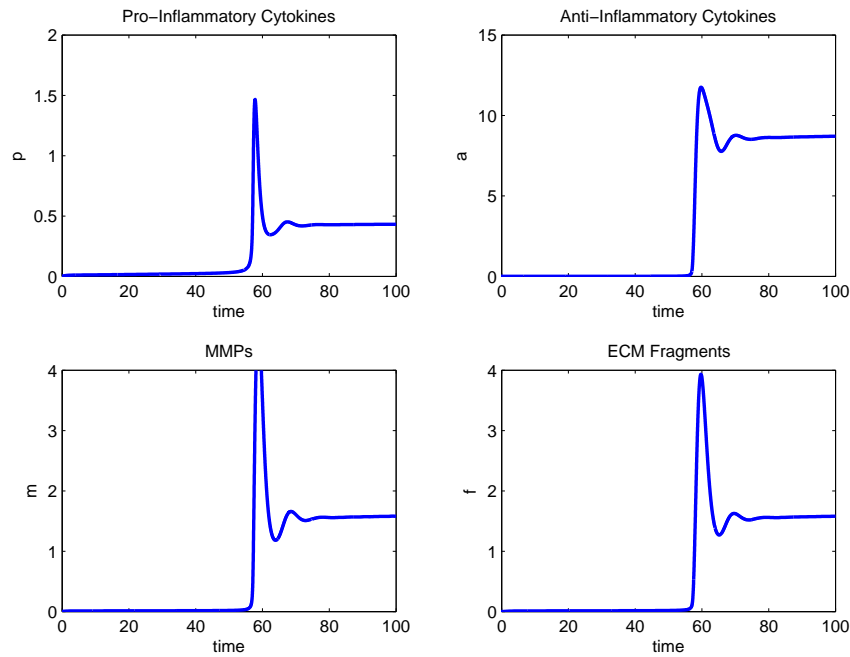


Figure 3.30: System variables plotted against time as the parameter P_{fp} increases in a time dependent fashion. The system moves to a disease state as P_{fp} moves through a fold bifurcation. The other parameters are the reference parameter set.

$$P_{fp} = P_{fp}^{min} + \frac{(P_{fp}^{max} - P_{fp}^{min})t^2}{P_{fp}^T{}^2 + t^2}, \quad (3.7.2)$$

where $P_{fp}^{min} = 1$, $P_{fp}^{max} = 45$, and $P_{fp}^T = 20$.

As in the case of P_{pp} , changes in P_{fp} move the system to a disease state (Figure 3.30) as time progresses, and this again corresponds to moving through a fold bifurcation. The disease state in this case is not oscillatory. These different disease states and routes to progression may account for the variability seen in clinical presentation and disease progression of OA.

Negative cytokine-driven feedback

The negative cytokine driven feedback is controlled by two parameters A_{pp} and A_{ph} (Figure 3.31), the first governing the maximum rate of production and the second controlling the sensitivity of the production rate to changes in p .

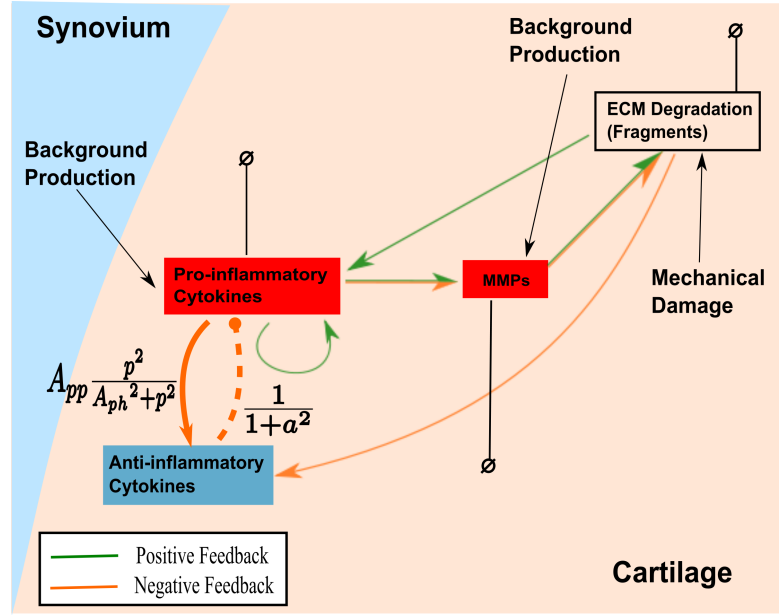


Figure 3.31: Cytokine network diagram highlighting the negative cytokine driven feedback loop which has two parameters: A_{pp} and A_{ph} .

The bifurcation analysis suggested that decreases in the parameter A_{pp} could lead to disease since this would interfere with the systems ability to down-regulate pro-inflammatory cytokines. We make A_{pp} dependent on time with the function,

$$A_{pp} = A_{pp}^{min} + \frac{(A_{pp}^{max} - A_{pp}^{min})}{A_{pp}^T t^2 + t^2}, \quad (3.7.3)$$

where $A_{pp}^{min} = 1$, $A_{pp}^{max} = 5$, and $A_{pp}^T = 20$, which decreases monotonically.

When we simulate the system with this time dependent anti-inflammatory production rate we remain in a state of health, confirming that decreases in A_{pp} alone

would not lead to OA as seen in the bifurcation analysis (Fig 3.9a). However, if we add a trauma to the simulation, modelled as an instantaneous increase in pro-inflammatory cytokine concentration as before, the system now moves to a state of disease due to bistability in the system (Figure 3.32). The move to disease is dependent on both the timing and the severity of the trauma.

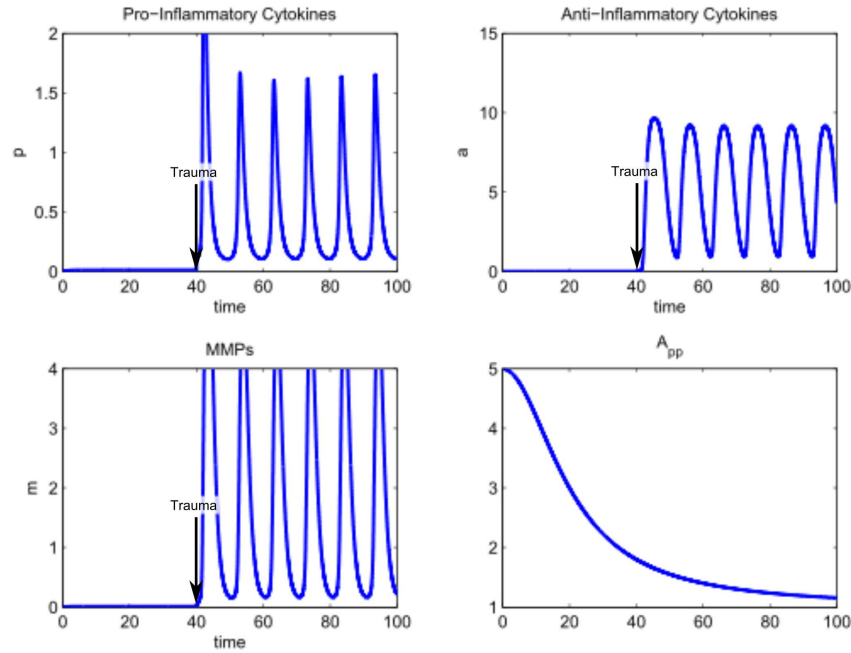


Figure 3.32: Time series plot of three system variables (p , a and m) against time as the parameter A_{pp} decreases in a time dependent fashion (A_{pp} profile shown in the lower right plot). A trauma is simulated at time = 40, modelled as an instantaneous increase in the p by 0.1. The system moves to a oscillatory disease state. The other parameters are the reference parameters.

Mathematically the trauma needs to take place once we have passed into the bistable region and be large enough to push the system outside of the basin of attraction of the healthy stable steady state. Intuitively, it seems to make sense that a decrease in anti-inflammatory cytokine alone would not lead to disease since the function of anti-inflammatory cytokines is to react to the presence of a pro-inflammatory response.

The second parameter in this feedback loop, A_{ph} controls the sensitivity of the

feedback to changes in the level of pro-inflammatory cytokine. If this is not sensitive enough then an inadequate anti-inflammatory cytokine response may lead to OA. We simulate a time dependent increase in A_{ph} using,

$$A_{ph} = A_{ph}^{min} + \frac{(A_{ph}^{max} - A_{ph}^{min})t^2}{A_{ph}^{T^2} + t^2}, \quad (3.7.4)$$

where $A_{ph}^{min} = 0.001$, $A_{ph}^{max} = 2$, and $A_{ph}^T = 20$.

As in the A_{pp} case, increasing the parameter alone is not sufficient to drive the system to disease. However with an additional trauma the system moves to disease as before (Figure 3.33).

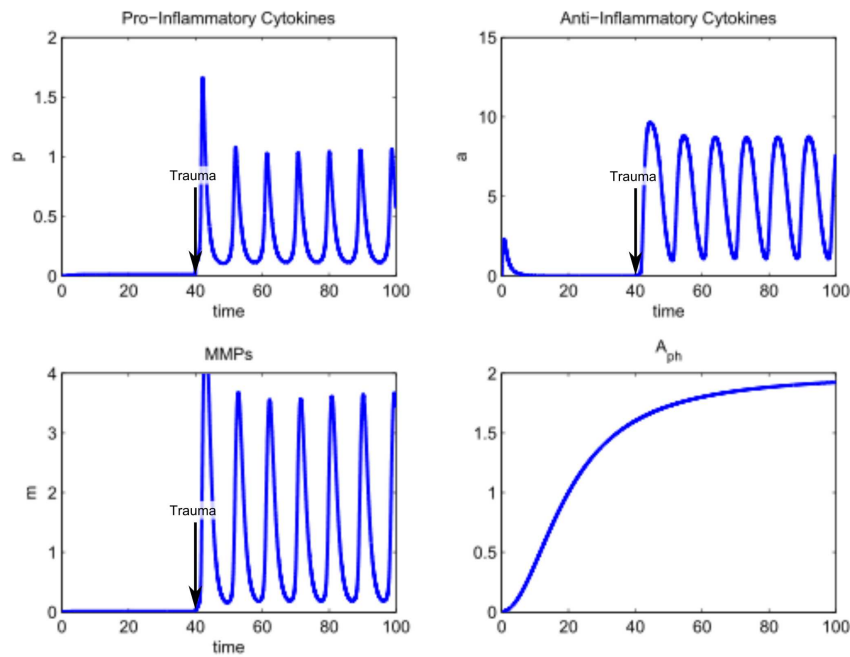


Figure 3.33: System variables plotted against time as the parameter A_{ph} increases in a time dependent fashion. A trauma is simulated at time = 40, modelled as an instantaneous increase in p by 0.1. The system moves to an oscillatory disease state. The other parameters are the reference parameters.

Negative fragment-driven feedback

The second negative feedback loop in this model is via MMP and Fn-fs production and contains the parameters A_{fp} , A_{fh} , M_{pp} and M_{ph} (Figure 3.34).

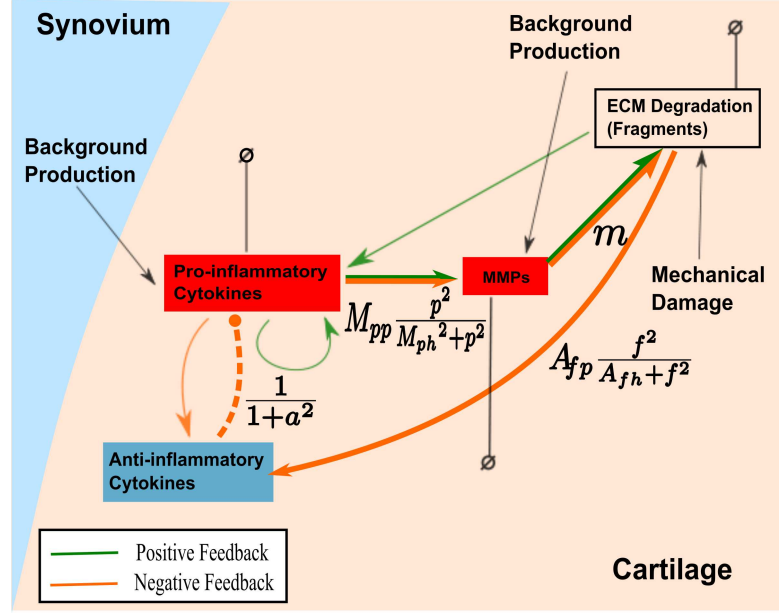


Figure 3.34: Cytokine network diagram highlighting the negative fragment driven feedback loop which has four parameters: A_{fp} , A_{fh} , M_{pp} and M_{ph} .

We will consider the latter two in the next section since these also have a role a positive feedback loop. We use the functions,

$$A_{fp} = A_{fp}^{min} + \frac{(A_{fp}^{max} - A_{fp}^{min})}{A_{fp}^T + t^2}, \quad (3.7.5)$$

and

$$A_{fh} = A_{fh}^{min} + \frac{(A_{fh}^{max} - A_{fh}^{min})t^2}{A_{fh}^T + t^2}, \quad (3.7.6)$$

where $A_{fp}^{min} = 1$, $A_{fp}^{max} = 5$, $A_{fh}^{min} = 0.001$, $A_{fh}^{max} = 2$, and $A_{fp}^T = A_{fh}^T = 20$.

As in the case of A_{pp} and A_{ph} , time dependent increases to A_{fp} and A_{fh} alone do not move the system to disease. Instead as before an additional stimulus is required. This time, however, as expected from the bifurcation plots in Figure 3.35, the disease state is fixed rather than oscillatory.

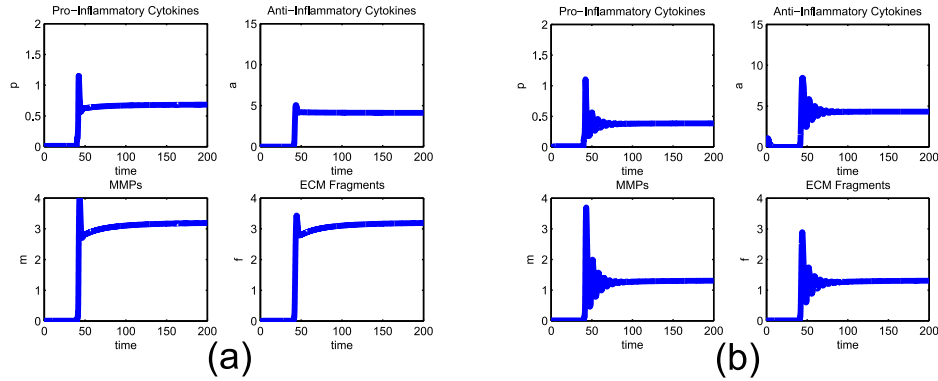


Figure 3.35: System variables against time as the parameters (a) A_{fp} and (b) A_{fh} increase in a time dependent fashion, given by equations 3.7.5 and 3.7.6. A trauma is simulated at $t = 40$, modelled as an instantaneous increase in the p by 0.1 in both cases. The systems move to a stable disease steady state. The other parameters are from the reference parameter set.

MMP-driven feedback

The MMP production rate parameters M_{pp} and M_{ph} , are involved in both positive and negative feedback (Figure 3.36).

Hence, the effect of time dependent changes in these parameters may be dependent on the relative strengths of the positive and negative feedback loops. In the parameter set we have been using in this section the feedback is relatively balanced and we expect increases in M_{pp} and decreases in M_{ph} to lead to disease. Using the functions,

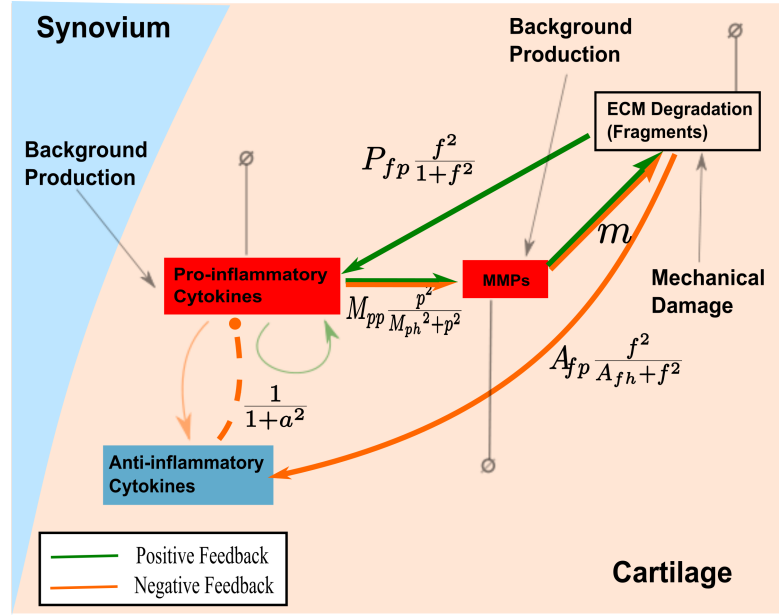


Figure 3.36: Cytokine network diagram highlighting the negative and positive feedback loops involving M_{pp} and M_{ph} .

$$M_{pp} = M_{pp}^{min} + \frac{(M_{pp}^{max} - M_{pp}^{min})t^2}{M_{pp}^T + t^2} \quad (3.7.7)$$

$$M_{ph} = M_{ph}^{min} + \frac{(M_{ph}^{max} - M_{ph}^{min})}{M_{ph}^T + t^2}, \quad (3.7.8)$$

where $M_{pp}^{min} = 0$, $M_{pp}^{max} = 5$, $M_{ph}^{min} = 0.001$, $M_{ph}^{max} = 0.5$, and $M_{pp}^T = M_{ph}^T = 20$,

we can show that this is indeed the case. Figures 3.37 and 3.38 show simulations using each of these functions and in both cases a disease state is reached.

In the case of M_{ph} the disease state has a comparatively low level of p , but higher levels of a , m and f . We can see from Figure 3.10 why this is the case since, by the time we move past the fold the disease state is relatively low. If we introduce a trauma, as we have done previously we force the system to move to the disease state much sooner (Figure 3.39).

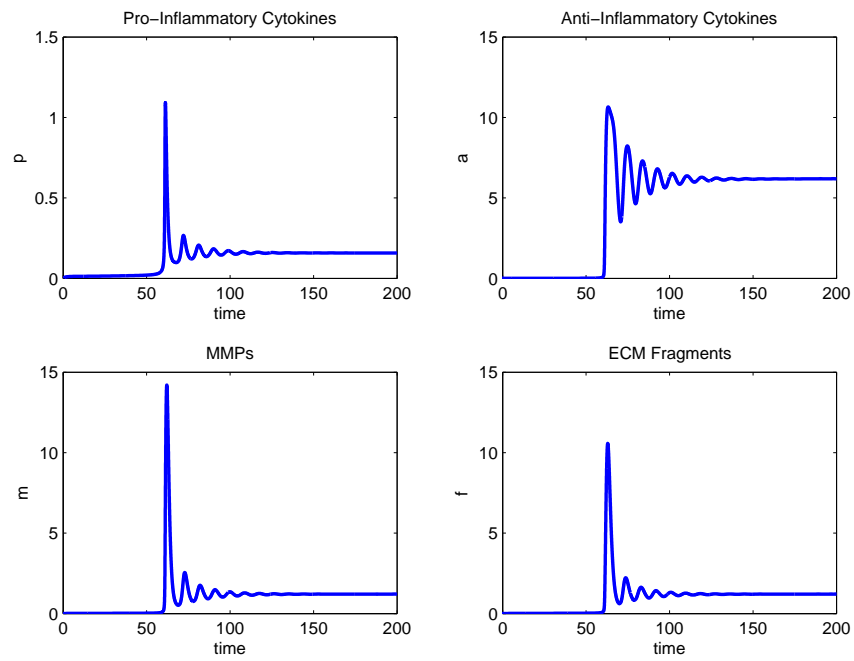


Figure 3.37: System variables plotted against time as the parameter M_{pp} increases in a time dependent fashion. The system moves to a disease state as M_{pp} moves through a fold bifurcation. The other parameters are from the reference parameter set.

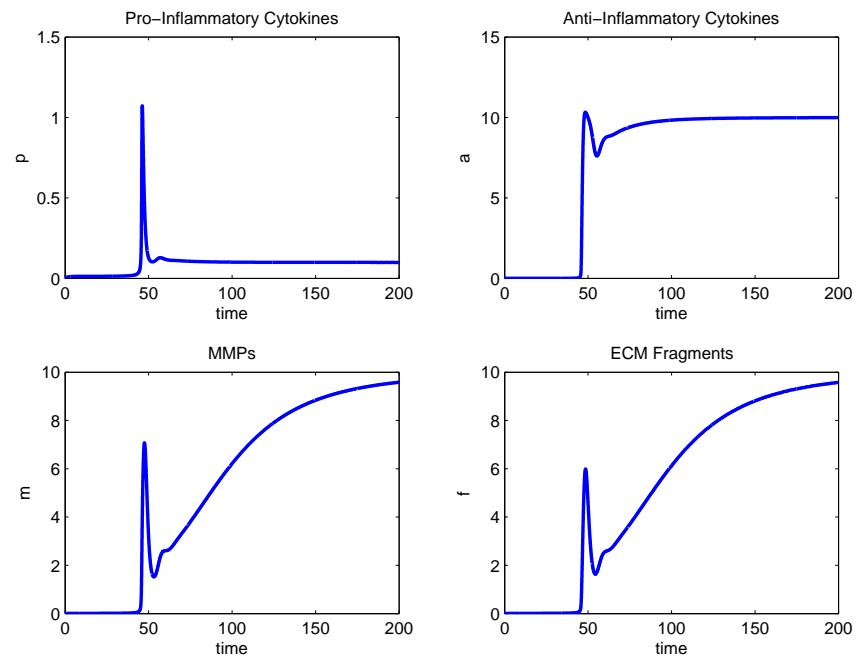


Figure 3.38: System variables plotted against time as the parameter M_{ph} decreases in a time dependent fashion. The system moves to a disease state as M_{ph} moves through a fold bifurcation. (The parameters are taken from the reference parameter set.)

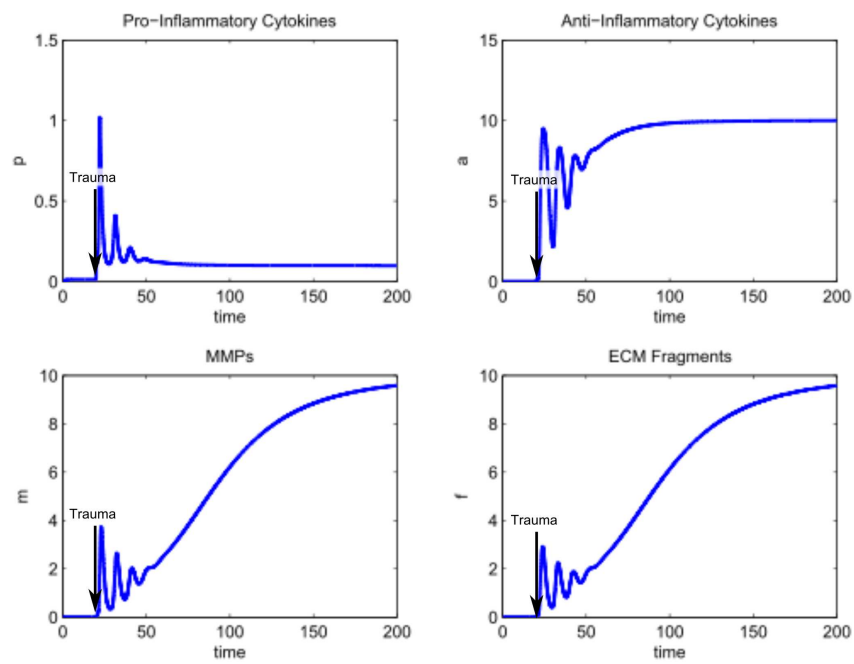


Figure 3.39: System variables plotted against time as the parameter M_{ph} decreases in a time dependent fashion. A trauma is added at $t = 20$ resulting in a move to the disease state. The other parameters are taken from the reference parameter set.

3.7.2 Mechanical Damage

Mechanical damage is a large risk factor in OA but the response to mechanical damage may differ between individuals. We consider two different scenarios involving mechanical damage, firstly where the damage causes a previously healthy individual, with parameters indicating monostable health, to move to a disease state and secondly where an individual susceptible to developing OA, with parameters indicating bistability, is pushed into active disease due to damage. In the first case a change to the parameter values would be required, whereas the second requires only a variable change.

In the first case, as in the previous section we increase the level of the parameter F_{dam} over time which may be representative of an individual who incurs a persistent level of damage over time for example through occupational stresses, gradual weight gain or high impact exercise. We model this increase as a function of time as before with,

$$F_{dam} = F_{dam}^{min} + \frac{(F_{dam}^{max} - F_{dam}^{min})t^2}{F_{dam}^{T^2} + t^2}, \quad (3.7.9)$$

where $F_{dam}^{min} = 0$, $F_{dam}^{max} = 0.5$, and $F_{dam}^T = 20$.

In this case the system moves to disease as time increases (Figure 3.40) and the system moves through a fold bifurcation.

In the second case we assume that individuals with high pro-inflammatory cytokine production rates are likely to be more susceptible to the development of OA and look at the effect of mechanical damage to these individuals. We take two parameter sets, the first, termed Lower Risk, has low pro-inflammatory cytokine production rates ($P_{pp} = 5$). The second, termed Higher Risk, has higher pro-inflammatory cytokine production rates ($P_{pp} = P_{fp} = 24$); all other param-

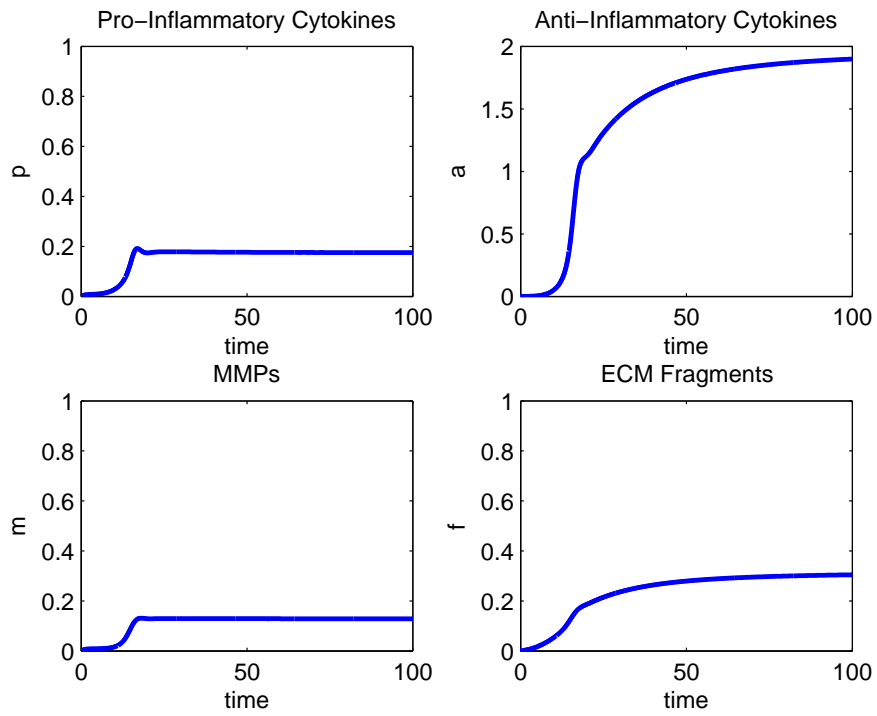


Figure 3.40: Plot of the system variables against time as the parameter F_{dam} increases in a time dependent fashion, according to equation 3.7.9. The system moves to a disease state as the value of p at the steady state increases. ($P_{bp} = 0.01$, $P_{pp} = 5$, $P_{fp} = 10$, $A_{pp} = 5$, $A_{ph} = 0.5$, $A_{fp} = 5$, $A_{fh} = 0.5$, $M_{bp} = 0.01$, $M_{pp} = 0.2$, $M_{ph} = 0.1$, $\gamma_p = 1.25$, $\gamma_m = 1.25$ and $\gamma_m = 2$)

eters are the same. For all the simulations we have used the initial conditions: $p = 0, a = 0, m = 0, f = 0$, which are close to a healthy steady state in both groups when $F_{dam} = 0$.

We simulate a short pulse of mechanical damage by an increase in F_{dam} , to 1, for $30 \leq t \leq 31$, this emulating a short time period of high damage, representing an injury, followed by a return to zero. Figure 3.41 shows that lower risk individuals maintain a healthy steady state with the anti-inflammatory feedback mechanism keeping the pro-inflammatory production low whereas in higher risk individuals the system moves to a disease state (Figure 3.41).

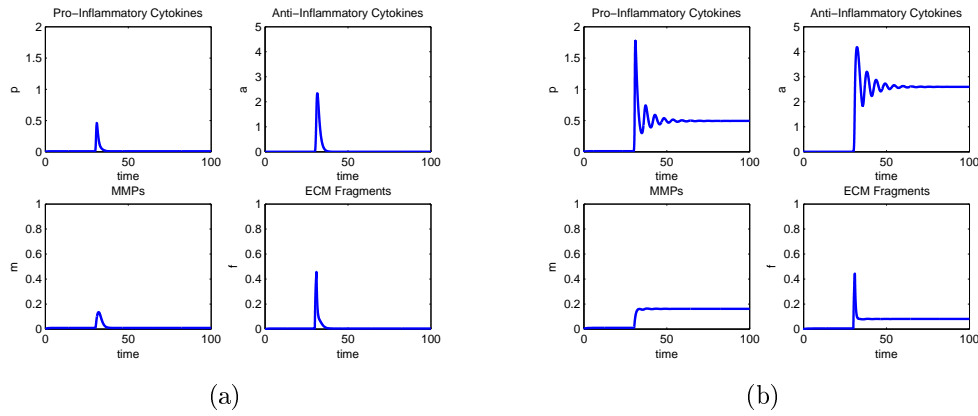


Figure 3.41: Time courses for two groups Lower Risk ($P_{pp} = 5$) and Higher Risk ($P_{pp} = 24$) with different pro-inflammatory production rates and a pulse of mechanical damage applied at time 30 ($F_{dam} = 1$). ($P_{bp} = 0.01$, $A_{pp} = 5$, $A_{ph} = 0.5$, $A_{fp} = 5$, $A_{fh} = 0.5$, $M_{bp} = 0.01$, $M_{pp} = 0.2$, $M_{ph} = 0.1$, $\gamma_p = 1.25$, $\gamma_m = 1.25$, $\gamma_f = 1.25$).

3.8 Treatment Strategies

Clinical trials of disease modifying drugs for OA so far have not shown a slowing down of disease progression, as measured by pain, inflammation and joint space, or have had unexpected complications. Several treatment options have reached clinical trials for OA and here we consider two of the main types that have been considered; anti-cytokine drugs and MMP inhibitors. Anti-cytokine therapy, licensed

for use in RA, inhibits either the production or functioning of pro-inflammatory cytokines, usually $\text{TNF-}\alpha$. We model this treatment option as an instantaneous reduction in the level of model variable p to a minimum of zero. Additionally we consider an anti-cytokine therapy which increases the level of anti-inflammatory cytokine. This type of treatment is licensed for RA but trials for OA have been unsuccessful [25]. We model this treatment type as an instantaneous increase in the level of the model variable a . We model MMP inhibitors as a reduction in the level of m in the system. In addition to these three types of therapies we also consider the possibility of Fn-fs as a target for OA treatment and model this as a reduction in the level of f . Here we consider how monostable disease, bistable and tristable behaviours may respond to treatments.

3.8.1 Treatment for bistable cases

In the bistable case (as in the reference parameter set we consider here) it is theoretically possible for an individual in the disease state to be moved to a state of health, and this should be the aim for disease modifying treatment, to achieve the best clinical outcome.

In this model, for the reference parameter set, we tried single doses of anti-cytokine therapy, MMP inhibition or Fn-fs inhibition modelled as instantaneous reductions in p , m or f respectively. In each case we modelled the largest possible dose by reducing the level to zero, but none of these treatments moved the system to health (Figure 3.42), since the system was not moved outside the basin of attraction of disease.

This result is in line with data from clinical trials, of anti-cytokine and MMP inhibition treatments, that have shown no long term benefit in single dose therapy [110]. However, we have found that a combined treatment strategy can bring the system to a state of health. Over several simulations we reduced the magnitude

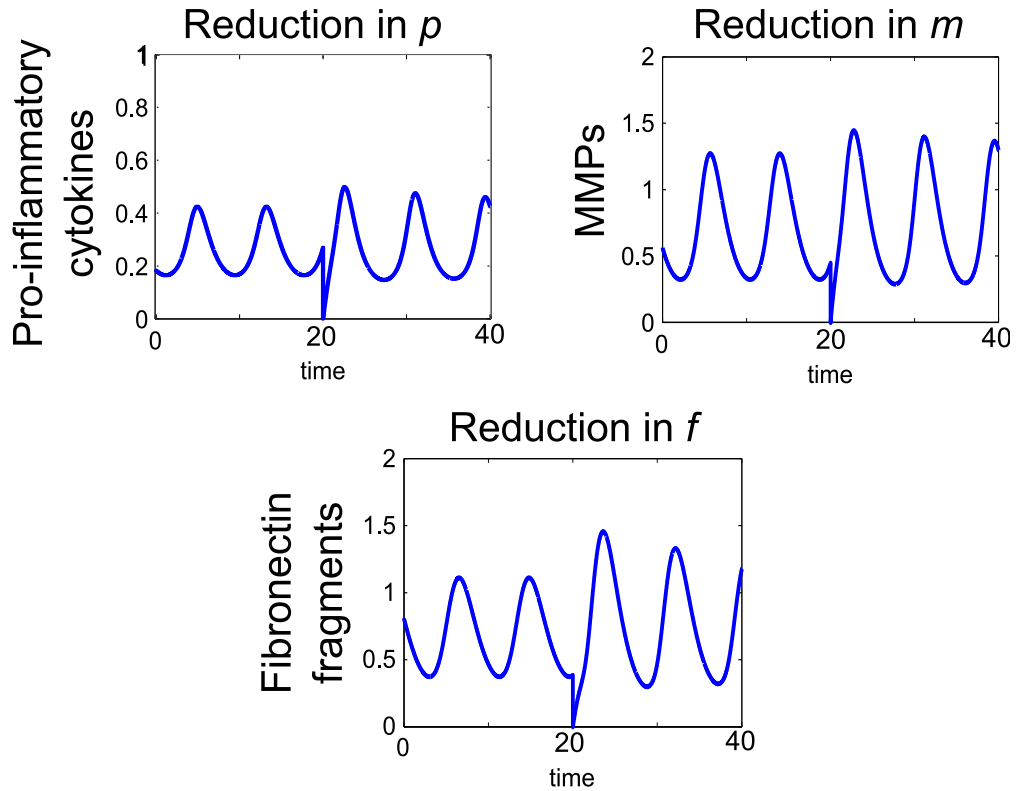


Figure 3.42: Time course simulations of single treatments where the system displays bistable behaviour. At $t = 0$ the system is at the disease limit cycle. A single dose of anti-cytokine (reduction in p), MMP inhibition (reduction in m) or Fn-fs inhibition (reduction in f) treatment was simulated at $t = 20$. The dose size given in each case was the maximum possible (i.e. an instantaneous decrease to zero of each of the variables). None of these treatments are sufficient to move the system to health. The reference parameter set was used for these simulations.

of the doses used, until we found the smallest dose of each treatment that would bring the system to health when combined, this is time-dependent. Figure 3.43 shows the system moving from disease to health with a combined dose of all three treatments, with the smallest dose of each treatment. In this case the magnitudes of the variable reductions are $0.2(p)$, $0.5(m)$ and $0.4(f)$.

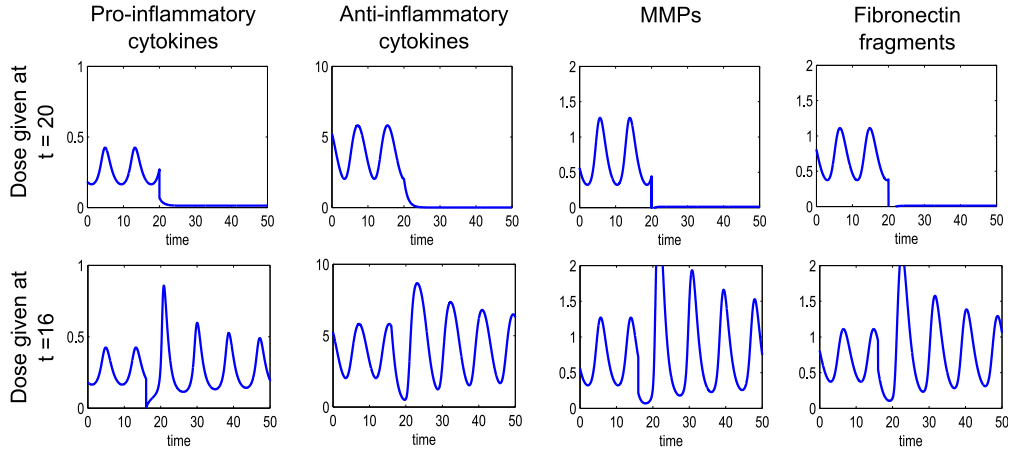


Figure 3.43: Time course simulations of combined treatments where we have bistable behaviour in the system. At $t = 0$ the system is at the disease limit cycle. A single combined dose of anti-cytokine, MMP inhibition and Fn-fs inhibition treatment was simulated at $t = 20$ and $t = 16$. The dose size is the minimum dose size (see text) that moves the system to health ($0.2(p)$, $0.5(m)$ and $0.4(f)$). The reference parameter set was used for these simulations. The diagrams show that dose timing as well as dose size is important

The timing of the dose is of crucial importance, particularly for this parameter set since the disease state is oscillatory. If a dose is given at the wrong point in the disease cycle then it may not be large enough to move out of the basin of attraction of the disease state and may result in a period of increased amplitude oscillations as it moves back to the disease state (Figure 3.43). This type of behaviour could have large implications both for clinical trial results and treatment regimens for drugs taken to market.

We find that multiple doses of treatment given over time can also reduce the system to health and allow smaller individual doses to be given. Figure 3.44 shows a series of six doses, given ten time units apart, which moves the system to

health; the magnitude of each dose is $0.1(p)$, $0.2(m)$ and $0.1(f)$. Compared to the single dose strategy this represents a large reduction in dosage at any particular time. This may be beneficial if there are side effects associated with the drugs, although overall, the dosage would be higher in this case. As with the single dose, the timing and size of the dose is important as well as the total number of doses.

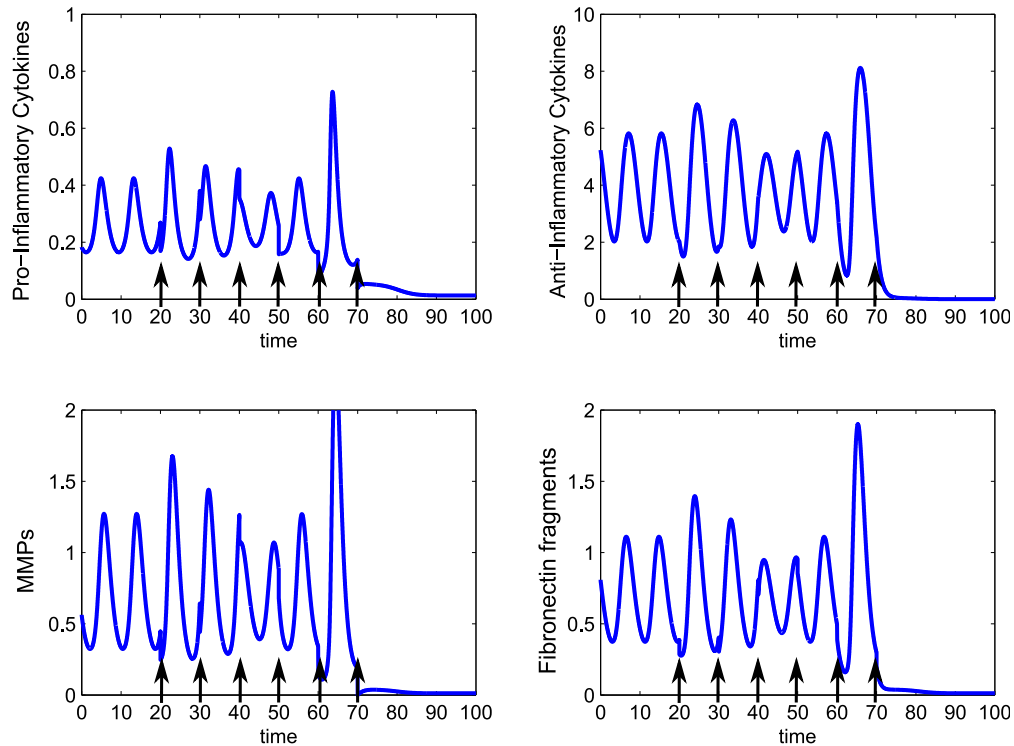


Figure 3.44: Time course simulations of multiple combined treatments where we have bistable behaviour in the system. At $t = 0$ the system is at the disease limit cycle. Six combined doses of anti-cytokine, MMP inhibition and fibronectin fragment inhibition treatment are simulated starting at $t = 20$, with a dose interval of ten time units. This allows the magnitude of the dose to be reduced from the single dose therapy. The dose magnitude for each of the six doses is $0.1(p)$, $0.2(m)$ and $0.1(f)$. The reference parameter set was used for these simulations.

Anti-inflammatory cytokines are not currently used in anti-cytokine therapy as they have shown poor responses in clinical trials. We found that a single dose of anti-inflammatory cytokines was able to bring the system to a healthy state from the disease state. Figure 3.45 shows a dose of 40 units given at time $t = 20$, which moves the system to health, when given at $t = 20$. This dose is the lowest that will bring the system to health. However, this dose is an order of magnitude

greater than the anti-inflammatory cytokine level at the disease state, so may not be clinically feasible.

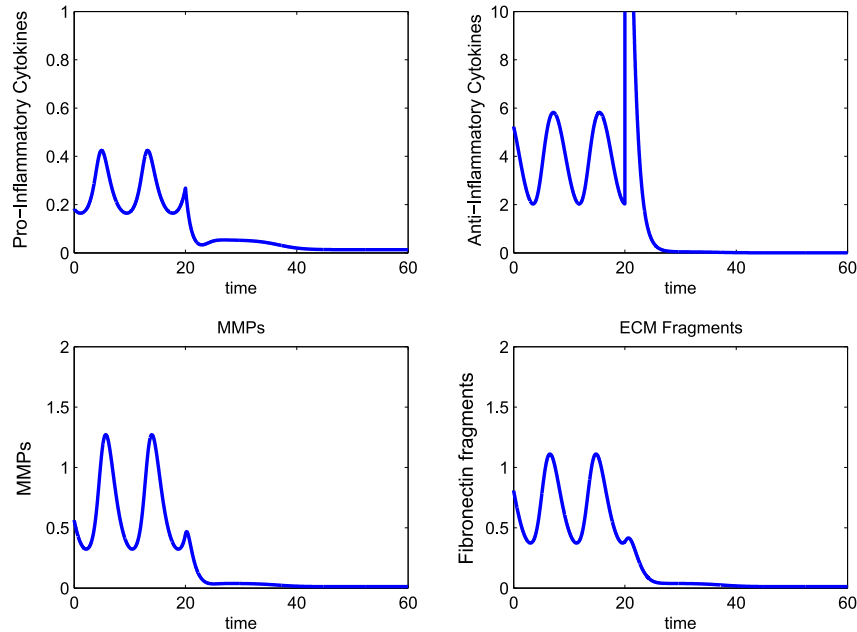


Figure 3.45: Time course simulations of single doses of anti-inflammatory cytokines where we have bistable behaviour in the system. At $t = 0$ the system is at the disease limit cycle. A dose of 40 units of a is given at $t = 20$ bringing the system to health. The reference parameter set (Table 3.2) was used for these simulations.

Since the disease state in this case is oscillatory, timing of doses can have an effect on the magnitude of the dose needed. For example, in this case by changing the timing of the dose to $t = 26$ we can reduce the dose required to 21 units, almost half that needed at $t = 20$. The timing of the dose however is not trivial and the optimal dose timing is not at the highest point of p of the limit cycle as might be expected, but at the point where the system is closest to the basin of attraction of the healthy state. This point may vary between individuals so individually tailored treatment plans may be necessary for most effective treatment.

We investigated application of multiple doses of anti-inflammatory cytokines in order to further reduce the dose size necessary. By giving 3 doses at intervals of

14 time units starting at $t = 20$ we were able to bring the system to health with a dose size of 20, reduced from 40 in the single dose case at this time (Figure 3.46). Again timing of the initial dose, the interval and number of intervals are of crucial importance.

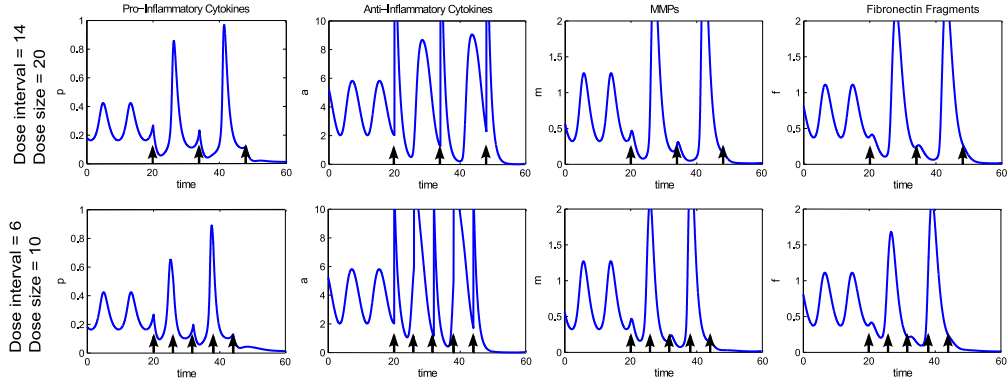


Figure 3.46: Time course simulations of multiple doses of anti-inflammatory cytokines where we have bistable behaviour in the system. At $t = 0$ the system is at the disease limit cycle. In the top row three doses of 20 units of a are given as indicated by the black arrows. In the bottom row five doses of 10 units of a are given as indicated by black arrows. Multiple doses reduces the size of dose need to move the system to health but timing of the initial dose, dose interval and dose size are all crucial in determining treatment outcome. The reference parameter set (Table 3.2) was used for these simulations.

Finally for the bistable case we have considered how an increased rate of Fn-fs clearance could affect treatment options. Research has shown that clearance of macromolecules such as Fn-fs is increased in the cartilage with cyclic loading [42], so an increase in γ_f alongside reductions in p or m , may be representative of a course of exercise or physiotherapy in combination with disease-modifying drugs. Increasing the value of γ_f has a similar effect to Fn-fs inhibition and simulations show that if this is raised we no longer need to alter the amount of f to bring the system to health (Fig 3.47). This may mean that combined anti-cytokine and MMP inhibition therapy, alongside physical therapy, could be a viable treatment option.

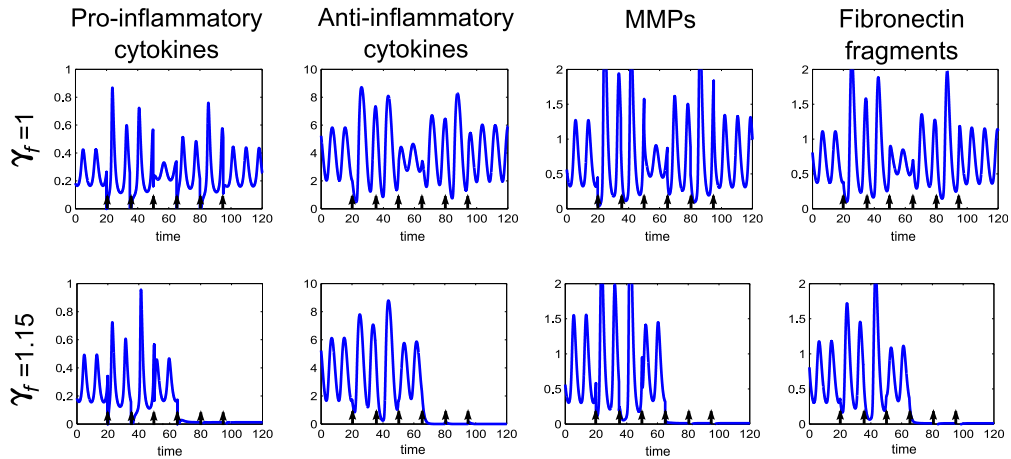


Figure 3.47: Time course simulations of multiple combined treatments where the system displays bistable behaviour. The first row shows the system with the reference parameter set, whilst the second row shows the same parameters except that γ_f is increased by 15%. At $t = 0$ the system is at the disease limit cycle. Six combined doses of only anti-cytokine and MMP inhibition treatment are simulated starting at $t = 20$, with a dose interval of ten time units. The dose magnitude for each of the six doses is $0.4(p)$ and $0.4(m)$.

3.8.2 Treatment for tristable cases

Where we have tristable behaviour we generally have two disease states and one healthy state. Simulations of treatment options for this type of behaviour show that if the system is at either one of the disease states it will act as in the bistable case and can be moved to the healthy state, with a sufficient number of doses of combined treatments. Additionally, if the system is at the higher disease state it can be moved to the lower disease state with fewer doses of treatment than are required to move the system to health. Figure 3.48 shows multiple doses of combined treatments of anti-cytokine, MMP inhibition and Fn-fs clearance therapies. Where two doses are given the system returns to the original disease state. When four doses are given the system moves to a lower disease state, which in this case is a limit cycle. Six doses are sufficient to move the system to a state of health. Figure 3.49, shows a similar pattern of behaviour for anti-inflammatory cytokine therapy. For this parameter set much lower doses of a bring about health compared to the bistable case.

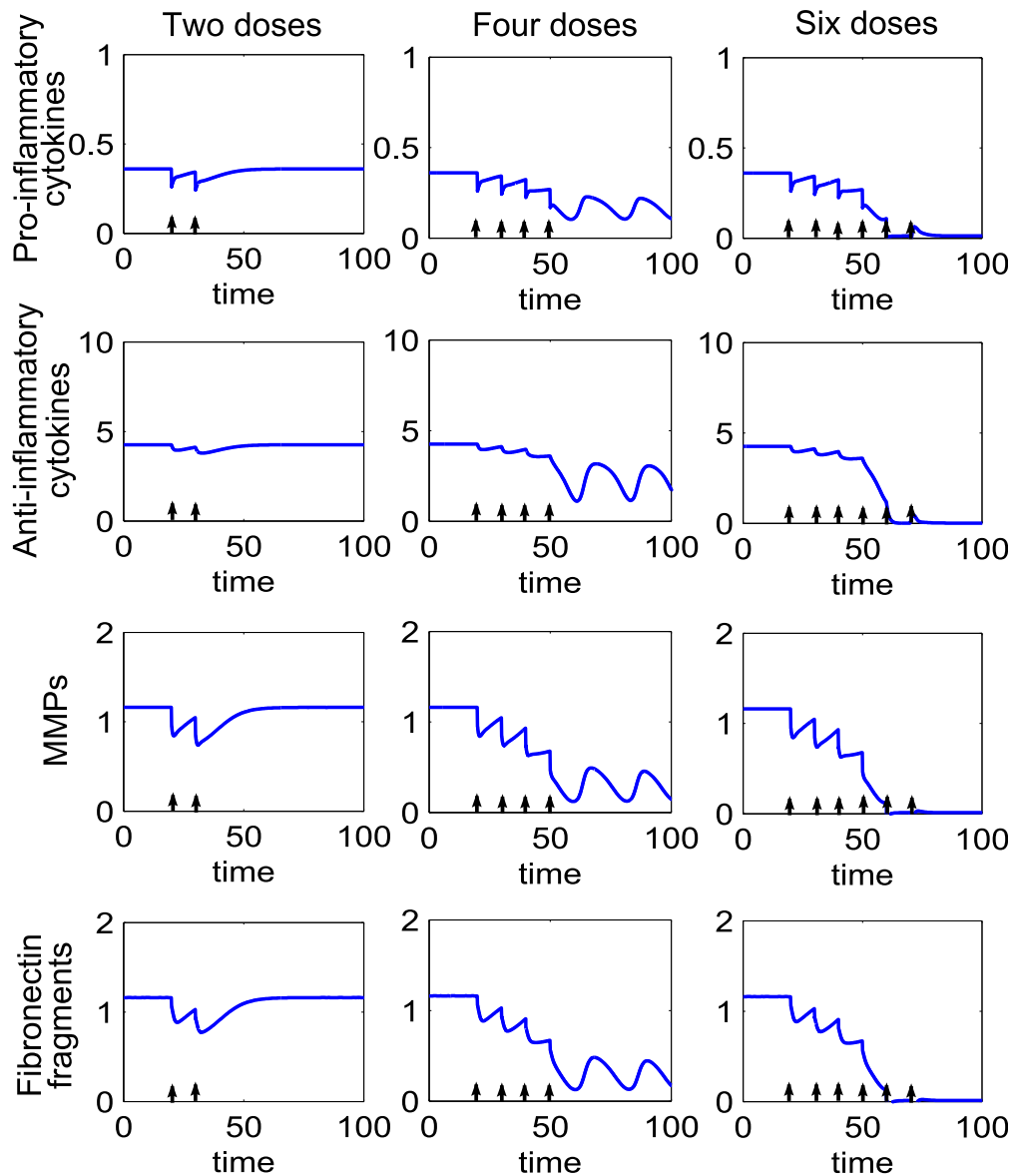


Figure 3.48: Time course simulations of multiple combined treatments where the system displays tristable behaviour. The first column shows two doses of treatment, the second column four doses and the third column six doses. The doses of anti-cytokine, MMP inhibition and fibronectin fragment inhibition treatment are simulated starting at $t = 20$, with a dose interval of ten time units. The dose magnitude for each of the doses is the same as in the bistable case. The number of doses determines which state the system is moved to.

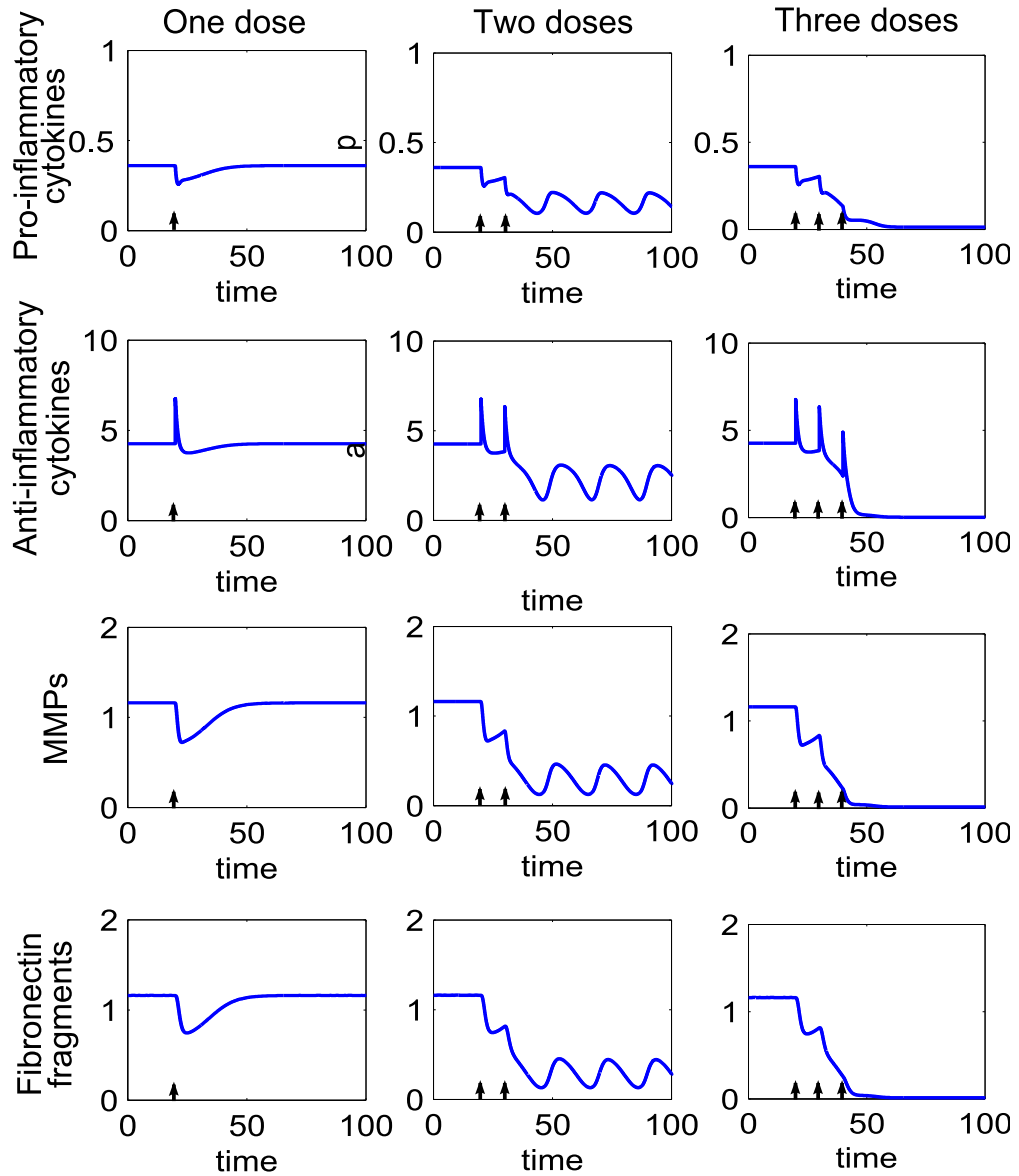


Figure 3.49: Time course simulations of multiple doses of anti-inflammatory cytokine where we have tristable behaviour in the system. The first column shows one dose of treatment, the second column two doses and the third column three doses. The doses of anti-inflammatory cytokine have a magnitude of 2.5 and are simulated starting at $t = 20$, with a dose interval of ten time units. The number of doses determines which state the system is moved to.

3.8.3 Treatment for monostable cases

In cases of monostable disease a move to a healthy state is not possible without parameter changes. However, disease control may still be possible with ongoing doses of disease modifying drugs (Figure 3.50) which can reduce the cytokine and fibronectin levels to those comparable with a healthy state. In this case the dose size required is much higher than that needed in the bistable case, to bring the system to low cytokine levels.

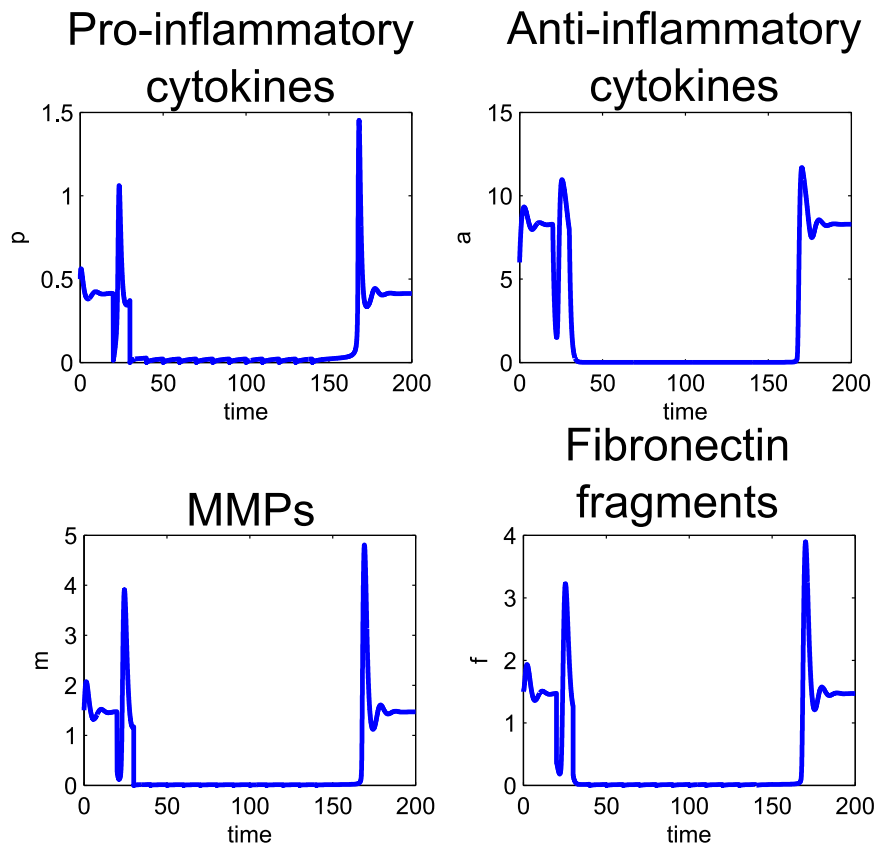


Figure 3.50: Time course for the system showing monostable disease. Multiple combined treatments are given ten time units apart starting at time 20. The dose size for the treatments are $0.4(p)$, $1.2(m)$ and $1.1(f)$ representing a 98%(p), 82%(m) and 75%(f) reduction from the disease state. These lower the system variables to a healthy level but cessation of treatment would cause the system to move back to the disease state. Parameters used are the reference parameter set as described in Section 3.4, except for $P_{fp}=40$.

There is a trade off between dose size and dose interval, with smaller intervals allowing a decrease in the size of the dose. However, in clinical practice there

would be both medical and practical considerations in reducing dose interval.

Repeated doses of anti-inflammatory cytokine can also reduce the cytokine and fibronectin levels. However, the dose size needs to be very high. For this parameter set a dose size of 500 units, 62 times greater than the disease state is required. The system is also very sensitive to dose size with some smaller dose sizes increasing the levels of p . The large dose size and sensitivity to change may make this type of treatment difficult to implement in a clinical setting.

3.9 Discussion

Cytokines, MMPs and fibronectin fragments are key mediators in destructive OA mechanisms. Effective disease modifying therapies are much needed for OA [110, 28], and these pathways appear to offer good targets. However, the lack of success in clinical trials suggests that we may not fully understand the dynamic interactions of these pathways. The aim of this modelling was to gain a better understanding of the nature of these dynamics. We have grouped cytokines by function, either pro-inflammatory or anti-inflammatory, in addition to MMPs and Fn-fs. This allowed us to simplify the problem to four variables and study the feedback loops in the system.

The bifurcation analysis revealed a range of different behaviour types. In general terms we can class the behaviour as monostable health, monostable disease, bistable or tristable. These groups respond very differently to treatment. In the cytokine-only model, Chapter 2, the regions of monostable health were relatively large and we suggested that many individuals would, therefore, not be susceptible to RA. However in this model, in all the parameter space we considered, monostable health only accounted for very small regions in comparison with the other behaviours. This may imply that most healthy individuals actually fall into the

bistable or tristable regions, and that given the necessary stimulus could be moved to a disease state. This idea corresponds with the etiology of OA, given the large percentage of affected individuals including asymptomatic individuals.

Both oscillatory and fixed disease states are present in the model. Some patients report intermittent periods of pain in early OA. This pattern of behaviour in RA has been linked to cyclic levels of cytokines, and the same may be true for OA, although data is not yet available for OA. It may be possible, with disease modifying drugs, to move a patient from an oscillatory disease state to a fixed disease state, such as in the tristable case illustrated in Figure 3.49 . In this model, we do not examine which type of disease behaviour is most destructive long term, but it may be possible to explore this with a spatial model of OA cartilage. It has been proposed that OA is a not a condition that has a single cause, but a group of many diseases with a common pathway of progression. The bifurcation analysis in Section 3.4 is consistent with this idea. Single parameter variation in all of the fourteen model parameters were considered for a reference parameter set and in each case led to regions of monostable and bistable behaviour. This would suggest that variations in any of these parameters outside of a normal range may lead to abnormal cartilage behaviour, moving an individual to a bistable region where they are more susceptible to OA or moving them from a bistable region to a monostable disease region, likely to indicate established disease. Additionally, analysis of the mechanical damage parameter showed that even small increases in this parameter can lead to monostable disease, consistent with the view that mechanical damage is the largest risk factor for OA.

The system shows a wide range of mathematically interesting behaviours, including five steady states which appear to be closely tied to Bogdonov-Takens bifurcations, mushrooms and isolas, and regions of excitability. It is also possible that there are additional behaviours that we have not found since we were unable to fully explore the parameter space.

The two parameter bifurcation analysis suggests that although the behaviour of the system is complex, the overall behaviour as some parameters vary is relatively simple. Increases in P_{fp} and P_{pp} and decreases in A_{pp} and A_{fp} lead to monostable disease, whereas the changes in M_{pp} and γ_f are not so easy to classify. This may mean that cytokine production levels may make the best molecular targets for therapy approaches as they are most likely to have consistent results in different individuals.

We have shown in Section 3.4 that changes in many of the system parameters over time can lead to raised levels of p which we believe to be indicative of OA. Increasing evidence suggests that aging chondrocytes undergo telomere shortening, which could lead to changes in production rates over time [81]. The pattern of disease onset is variable in the model and this may correlate with significant variation in clinical presentation of OA. However, this is difficult to prove without a better disease measure for OA, such as a biomarker, and also without a clear link between the disease measures used and the model variables. Similarly, whilst we describe a reduced level of p as a return to health, it is more likely that this simply reflects a reduction or halting of cartilage degradation, which may not result in an improvement in pain or symptoms for the individual, since the structural damage leading to pain persists. We have shown that increases in parameter values over time can lead to OA onset and generally lead to monostable disease after a period of time. To have the greatest chance of treating OA effectively treatment during the bistable phase would be preferable. For this it is likely that early diagnosis of OA would be needed in conjunction with disease modifying treatments.

We have shown that the system is sensitive to mechanical damage. Increases in this parameter can move the system from health to disease, either as a result of moving to another steady state in the case of bistability or as a result of increasing the value of p at a previously healthy steady state. These findings are consistent with that fact that mechanical damage is a large risk factor for initiation and

progression of OA. The absence of any reparative influences in this model however, may make the effect of mechanical damage more dominant than it is in reality.

We have considered four different treatment strategies: anti cytokine therapy, anti-inflammatory cytokines, MMP inhibitors and Fn-fs inhibitors. We found a combined treatment strategy could be effective at treating bistable, tristable and monostable disease. Dose size and timing were important to treatment outcome and it may be possible to optimise these using control theory. We found that the only effective monotherapy was to use anti-inflammatory cytokines, although this treatment often required very high dose sizes and treatment outcome was highly sensitive to dose timing and interval. These issues may make clinical treatment with anti-inflammatory cytokines, such as IL-1Ra, unfeasible and may explain the failure of IL-1Ra drugs trials [25], despite promising experimental results. For the other three treatment options any one of these alone was ineffective, and combined treatments were necessary (Section 3.8). We can see from the phase diagram (Figure 3.4) why this is the case. The basin of attraction of the healthy state is small and local to the state itself, for the reference parameter set. Any move from the disease state in only one direction would remain in the basin of attraction of the disease state. In all the parameter sets that we considered the basin of attraction of the healthy state was small. If this is seen biologically, results from our model suggest that combined treatments offer a much better possibility of success than single treatments, even where the single treatment showed no benefit alone (Figures 3.42 and 3.43). We saw that in the case of tristability we had an option of treatment to move the system from a higher disease state to that of a lower one. However it is unlikely that in the foreseeable future that we would be able to identify individuals with such multiple disease states or personalise the treatment plan to such a degree.

We explored the possibility that an increase in the Fn-fs clearance parameter, γ_f , could have a positive effect on cartilage health. An increase in γ_f (Figure

3.12) could move the system from monostable disease to bistability. Whilst this alone would not move an individual to health, since they would still be on the disease branch, this change could be combined with disease modifying drugs which might either improve treatment outcome or reduce the amount of drugs required. Research has shown that cyclic loading can increase the movement of molecules such as Fn-fs in the joint, which would result in an increased rate of clearance from the joint, so it seems likely that some form of low impact cyclic loading could increase this parameter. This form of therapy has already been established to have positive effect on OA patients [40, 38, 112] although the biophysical mechanisms of the improvements are not well understood.

In this chapter we have explored the behaviour of cytokine interactions in the joint and identified potential areas of future research into OA treatment strategies. Limitations of the model include the lack of a link to clinical disease measures, which include joint space narrowing and radiographic evidence of cartilage deterioration.. In future, as better measures of OA disease activity are developed, such as OA biomarkers (easily measurable indicators of disease severity) we may be able to draw more detailed conclusions about OA disease dynamics. We have not explored spatial and mechanical aspects of the disease, which play a large role in OA progression, and have been explored mathematically by others. We believe that future work in this area needs to combine all these aspects of OA and joint mechanics, as it is becoming increasingly clear from biological research that the interactions between the physical and biochemical factors in OA are significant.

In the next chapter we extend this model to a spatial version. This gives a new results variable, cartilage degradation, and allows us to consider the effects of cell sparsity and local tissue changes.

Chapter 4

Spatial modelling of joint degradation in OA

4.1 Introduction

In the previous chapter we considered an ODE model of the cytokine biochemistry of cartilage. We found asymptotic solutions associated with health and disease, and suggested possible treatment strategies based on these states. A major assumption of our ODE model is that of spatial homogeneity. This assumption is unlikely to hold in the cartilage, since the cartilage is a spatially structured tissue. Cartilage tissue, as shown in Figure 4.1, contains chondrocytes fixed in a collagen and proteoglycan matrix. The chondrocytes are spaced irregularly through the tissue with a higher density at the synovial interface. Chondrocytes are effectively immobile, trapped within a dense network of fibres [95], meaning that cytokines, MMPs and matrix components which are all secreted from the cell surface, rely on diffusion and advection to disperse through the tissue, leading to further inhomogeneity. Additionally, as the ECM degrades it does so non-uniformly [71].

In this chapter, we will assess whether the findings from the ODE model still

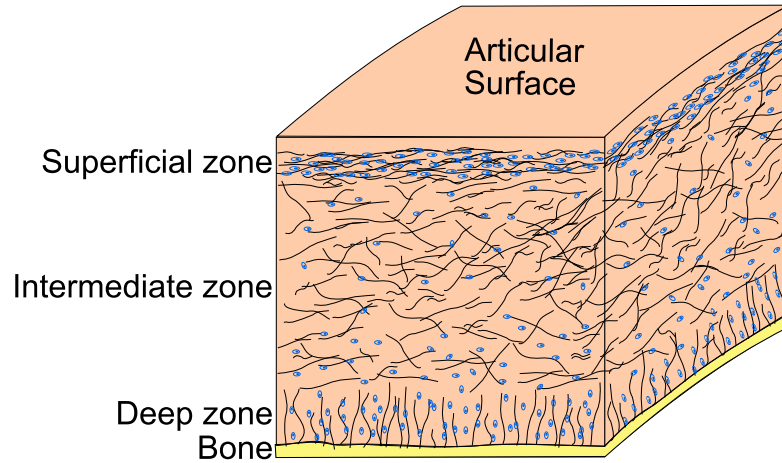


Figure 4.1: Diagram of cartilage tissue showing chondrocytes (represented by blue dots) enclosed in a mesh of collagenous ECM.

hold in a more realistic spatial model. We will consider the importance of spatial structure and diffusion to both the disease processes and possible treatment strategies.

4.2 Model specification

We model the biochemical network of cytokines, MMPs and fibronectin fragments in the cartilage and its effect on the tissue as depicted in Figure 4.2.

We require the model we develop to be cell based in order to simulate randomly-placed chondrocytes enclosed in an ECM, for this reason we choose not to use a PDE-only model and instead develop a hybrid model, with continuous variables, such as cytokine concentrations, represented by PDE's and the discrete elements of this model, such as chondrocytes, represented by a cellular approach. The CompuCell3D modelling environment [122] is a hybrid system which combines PDE and Cellular Potts models, making it ideal for combining cell and tissue dynamics we require. CompuCell3D uses an algorithm based on the Cellular Potts algorithm (also known as the Glazier-Graner-Hogeweg (GGH) algorithm) to simulate cells on

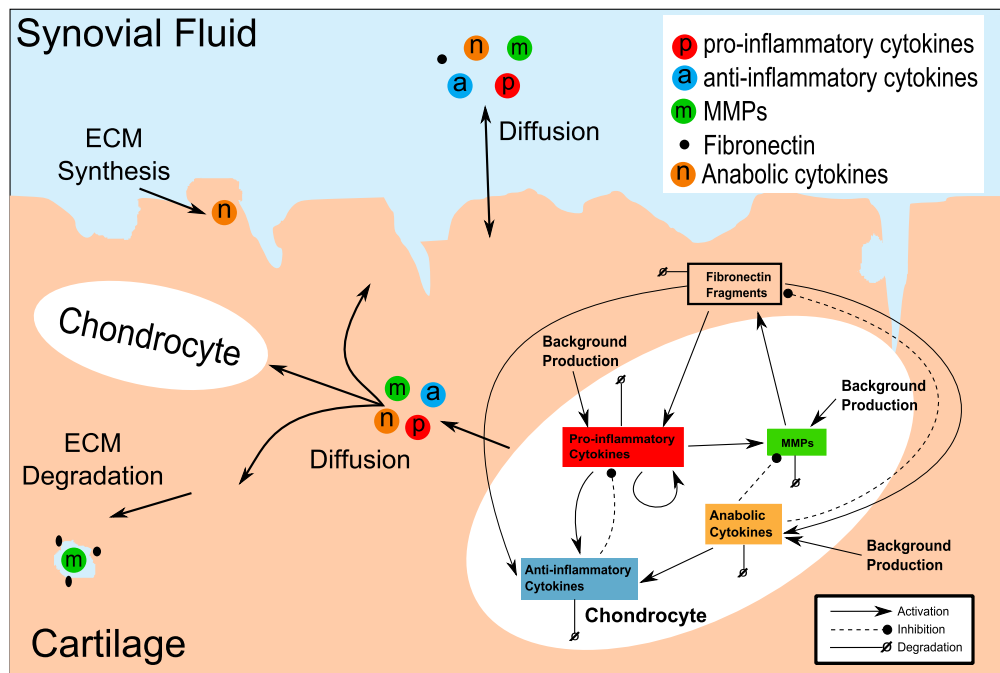


Figure 4.2: Schematic showing the tissue and cell signalling included in the model. The cell dynamics that were present in the ODE modelling take place within chondrocytes, with the exception of Fn-fs release, which takes place in the ECM. All biochemicals are secreted and move freely by diffusion through the domain, MMPs and anabolic cytokines act directly on the ECM.

a lattice. This allows us to simulate irregularly placed chondrocytes which secrete biochemical molecules. CompuCell3D is an open source modelling environment written in a combination of XML, Python and C++. Users can build simulations using a combination of pre-defined plugins, modules that calculate the effective energy in the model edited via XML scripts, and user-defined steppables, that perform cell based operations and are written in Python.

We model the system in two spatial dimensions for simplicity, but could extend to a three dimensional model within the modelling framework later if necessary. We consider three different tissue types as well as synovial fluid. These are ECM, chondrocytes and bone. For simplicity, we assume bone is an inert tissue providing a surface for the ECM to adhere to. We include five biochemical variables in the model, pro-inflammatory, anti-inflammatory and anabolic cytokines, fibronectin fragments and MMPs. Anabolic cytokines are a class of cytokines that stimulate the production of collagen to remodel the ECM. Since we include the ECM volume in this model, and since pro-inflammatory cytokines have a background production term, without the inclusion of anabolic cytokines we could not represent healthy ECM remodelling. Instead the ECM would always degrade. Anabolic cytokines are present to balance the background ECM degradation, simulating normal remodelling of the tissue. Initial conditions for the model consist of the spatial configuration of the tissue and initial concentrations of the biochemical variables. We also impose boundary conditions. Figure 4.3 shows an example of the initial configuration of the tissue we have used in the simulations. The chondrocytes are randomly spaced throughout the ECM, and make up 5% of the tissue.

4.2.1 Modelling approach

The GGH algorithm associates an effective energy to the system configuration, and accepts changes to that configuration with a probability that is an increasing

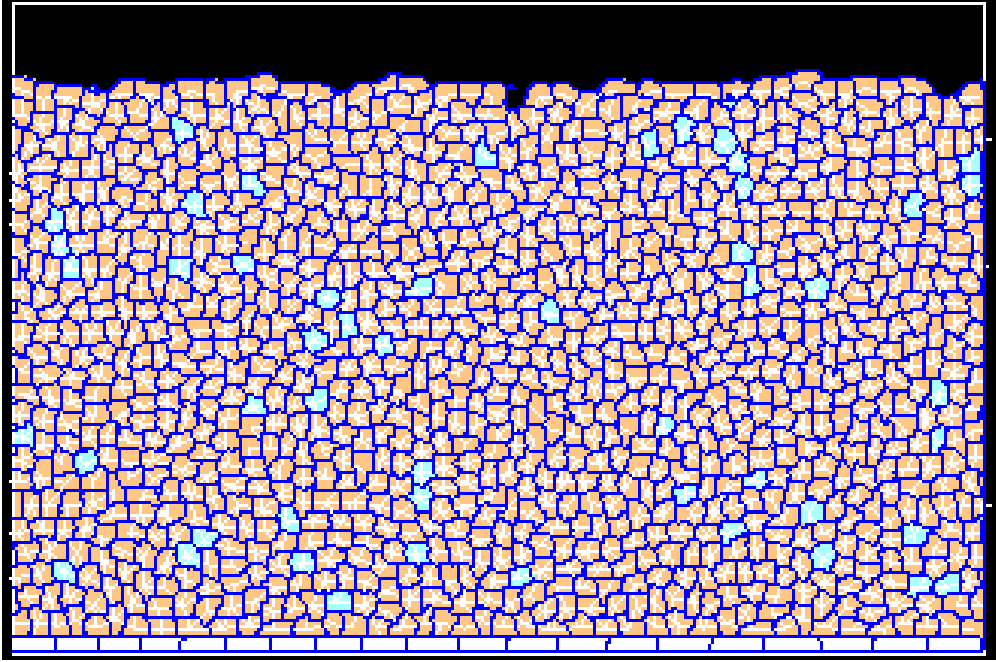


Figure 4.3: Example initial spatial configuration of tissue in model. ECM is shown in orange, and sparsely populated with chondrocytes (blue). A layer of bone (white) lines the bottom edge of the ECM and synovial fluid fills the top of the domain (black).

function of the associated effective energy reduction. Cell behaviours such as growth, cell-cell contact, mitosis and chemotactic responses are represented by energy terms, which may represent real energies or be metaphoric. The effective energy (H_{GGH}) of the cell is the sum of these terms. The effective energy term must include volume (or area in 2D models), surface area and boundary adhesion terms. In addition, in our model we also include a focal point plasticity term, giving,

$$H_{GGH} = H_{vol} + H_{surf} + H_{adhesion} + H_{focal}. \quad (4.2.1)$$

We shall discuss the calculation of these terms further below.

The system consists of a collection of lattice sites within a square grid. We divide

the grid into a series of *cells* each of which is a smaller collection of the lattice sites, each of which has a unique index (Figure 4.4). These *cells*, termed generalised cells, are distinct from biological cells and may consist of a single biological cell, a cluster of biological cells, or other tissue constituents, e.g. ECM. To differentiate generalised *cells* from biological cells we will italicise. In our model, we use a *cell* to represent a section of ECM, chondrocyte or a bone cell. Initially we set all these *cells* to be of similar volume since we expect chondrocytes and bone cells to be similar and the size of the ECM *cells* is arbitrary.

We simulate changes to the cells using a stochastic simulation mechanism through a series of Monte Carlo Steps and index copy attempts. The index copy is the basic building block. This has the effect of moving *cells*, changing cell size or changing their shape. We select a pixel at \vec{i} (target pixel) and a neighbouring pixel \vec{i}' (source pixel) randomly. If the two are in the same *cell* we do nothing. If they are different *cell* (i.e. we have selected a pixel on the *cell* border) we calculate the change in effective energy (ΔH_{GGH}) associated with copying selected pixel to the target pixel and accept the copy attempt with the probability,

$$P(\sigma(\vec{i} \rightarrow \vec{i}')) = \begin{cases} \exp(-\Delta H_{GGH}/T_m) & \text{if } \Delta H_{GGH} > 0 \\ 1 & \text{if } \Delta H_{GGH} \leq 0 \end{cases}, \quad (4.2.2)$$

where σ is the cell and T_m is the effective cell motility (the amplitude of cell membrane fluctuations).

Each Monte Carlo step (MCS) consists of a number of index copy attempts equal to the number of pixels in the simulation. Effective energy is calculated at each MCS. Monte Carlo steps move the simulation forward in time and between each MCS we perform additional operations such as diffusion and secretion. These affect the levels of the chemical field variables in the model but do not directly

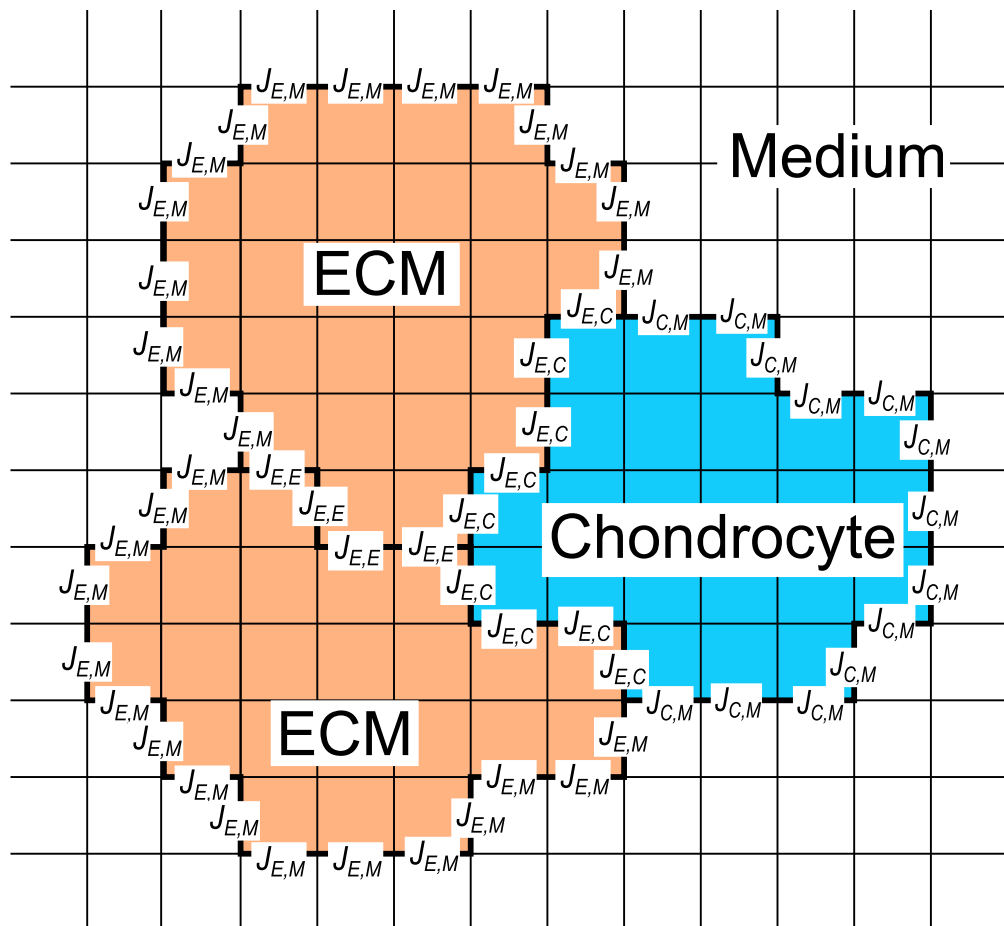


Figure 4.4: Schematic showing the lattice sites for three *cells* with two different cell types. The strength of the interactions between cells J depends on the difference in effective energy between the cells. Each pixel copy attempt will try and copy the cell type from one pixel to another, and the success of this will depend on the value of J .

change the effective energy of cells.

The main simulation process is shown in Figure 4.5, adapted from the Compu-cell3D documentation.

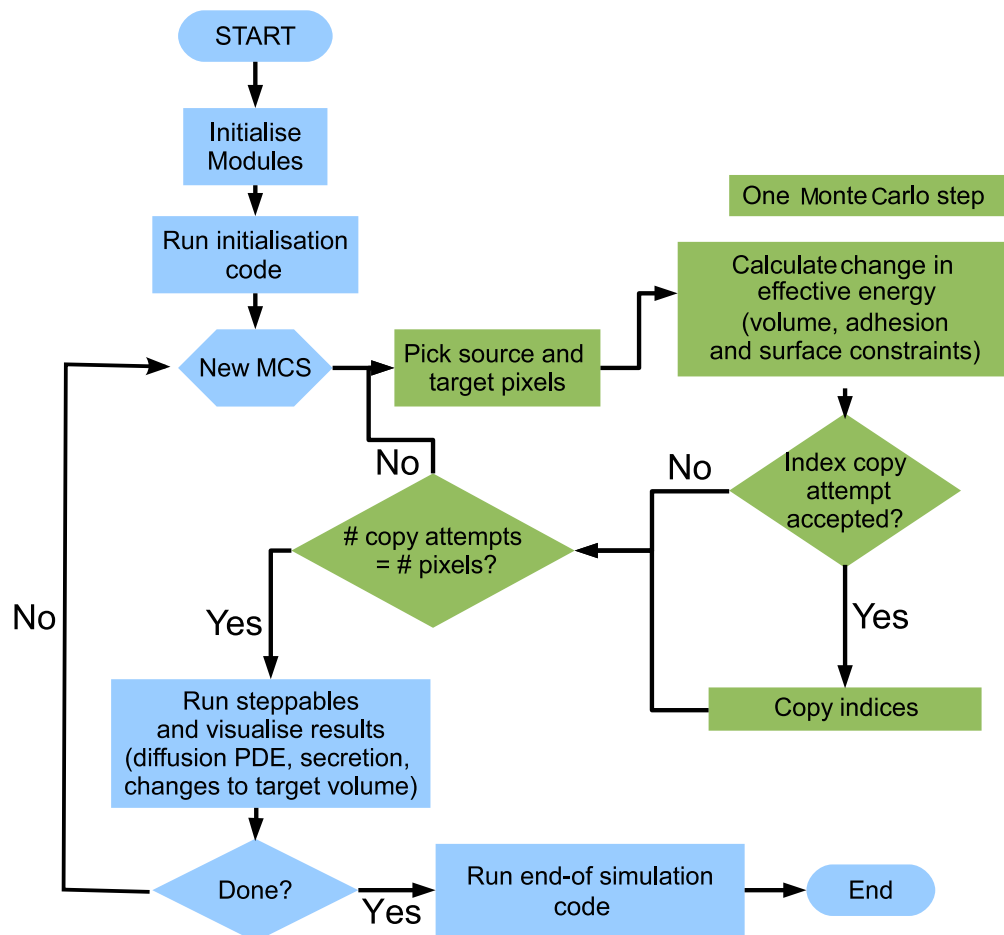


Figure 4.5: Flowchart showing the simulation process for the cartilage model in CompuCell3D. Each simulation is a series of Monte Carlo steps (MCS) consisting of many index copy attempts.

4.2.2 Physical properties of the model

Volume

The volume constraint along with the boundary adhesion constraint is a mandatory term in the GGH algorithm and these two terms combined give the basic GGH effective energy equations. In this model, since we are working in 2D the

volume constraints are actually area constraints. We use the volume constraint to simulate degradation of the collagen fibres within the cartilage. The volume constraint contribution to equation 4.2.1 is,

$$H_{vol} = \sum_{\sigma} \lambda_{vol}(\sigma)(v(\sigma) - V_t(\sigma))^2, \quad (4.2.3)$$

where σ is the cell, $\lambda_{vol}(\sigma)$ is the inverse compressibility of the cell, V_t is the target area and v is the actual area. Area is measured in units of pixels². Since site copies are more likely to be accepted if they decrease their effective energy this form of volume constraint will tend to drive the *cell* volumes towards their target volumes.

We set synovial fluid as the default tissue type (described as medium in Compu-cell3D) and hence it does not require a target volume as it simply fills in the space left by other cells to stop empty space appearing. We fix the volume and shape of bone cells, so we only consider changes to ECM and chondrocyte volumes in the model. ECM is degraded by MMPs and is synthesised by anabolic cytokines. Hence, we change the target volume of the ECM *cells* dynamically as a function of the MMP and anabolic cytokine concentrations according to the term,

$$\Delta V_t = f_{fp}(n_c - p_c), \quad (4.2.4)$$

where n_c and p_c are the concentrations of anabolic and pro-inflammatory cytokines respectively and f_{fp} is a non-negative parameter.

The target volume of the chondrocytes is generally fixed. However if these cells come in contact with synovial fluid their target volume is reduced to zero so that

the cell is degraded, and shrinks until it is removed when its actual volume reaches zero, which may be a short time later. This constraint stops individual chondrocytes existing in synovial fluid once the surrounding tissue has been degraded, since this is not seen *in vivo*.

Adhesion

Cellular adhesion refers to the way in which *cells* stick to each other to form a tissue. In this model the majority of the *cells* are ECM rather than true biological cells. Therefore, the adhesion properties of the model can be considered to be a proxy for the strength of the ECM. CompuCell3D defines adhesion as,

$$E_{adhesion} = \sum_{i,j} J(\tau_{\sigma(i)}, \tau_{\sigma(j)})(1 - \delta_{\sigma(i),\sigma(j)}),$$

where i and j are neighbouring lattice sites, J is the contact energy, τ denotes the cell type and σ denotes the cell ID. The first term sums the adhesion energies between different sites whilst the second term ensures that pairs of neighbours that belong to the same cell are discounted. The values of the contact energy between different cell types are model parameters and the values we have used are listed in Table 4.1. The units are dimensionless with the default value of ten indicating moderate adhesion and lower values indicating stronger adhesion since lower effective energies are favoured by the algorithm. We define neighbours in the model as any *cells* which directly touch the *cell*.

Since the cells of the ECM tissue are representing an interconnected mesh, as well as boundary adhesion we also include focal point plasticity in the model. This CompuCell3D plugin allows connections between the centers of mass of the cells. We specify a maximum distance constraint between the centre of mass of a *cell*

and the centre of mass of its neighbour and specify how many neighbours each *cell* will have. The determination of which cells are neighbours is determined by CompuCell3D based on these parameters and may change as the cells move/degrade. The energy contribution of the focal point plasticity term is given by,

$$E = \sum_{i,j-cellneighbours} \lambda_{ij}(I_{ij} - L_{ij})^2, \quad (4.2.5)$$

where λ is a measure of the plasticity, specified as a model parameter; I_{ij} is the distance between the cells i and j ; L_{ij} is the target distance between cells i and j and is another model parameter and the max distance, which is the point at which a link breaks. We also specify the likelihood of a new link being made in any particular pixel copy attempt. In this model we keep this likelihood low since we are modelling mature cartilage whose ability to form new collagen crosslinks is poor. The parameters we have used in the model are listed in Table 4.1.

Diffusion

We model diffusion of pro- and anti-inflammatory cytokines, MMPs and Fn-fs through both the ECM and synovial fluid. We have not found any experimental work giving the diffusion coefficients of these parameters in cartilage. However, we can estimate the diffusion coefficients of these proteins by considering their size. Leddy and Guilak [76] provides diffusion coefficients of various sizes of dextran molecules in cartilage. The values given are compatible with the value we calculate using the Einstein formula for diffusion. Hence we choose a diffusion coefficient for all tissue types of $2 \mu m^2 s^{-1}$ which is compatible both with the dextran experiments and the Einstein formula. However, we believe that the effective diffusion coefficient for these proteins could be much lower than that of dextran since

these cytokines, MMPs and fibronectin fragments will all be actively binding and unbinding to cell surface receptors on chondrocytes and possibly interacting with collagen. For this reason we also consider a slower rate of diffusion, $0.002\mu\text{m}^2\text{s}^{-1}$.

For the slower diffusion simulations we use non-steady state diffusion,

$$\frac{\partial c}{\partial t} = D\nabla^2 c - kc + \text{secretion}, \quad (4.2.6)$$

where D is the diffusion constant and k is the decay constant. We solve this at each MCS using the Forward Euler method. For faster diffusion this method is unsuitable, since numerical instabilities necessitate very small time steps, making simulations over longer timescales unfeasible. Hence, for faster diffusion we use a steady state approximation. We discuss this diffusion approximation further in Section 4.6. The secretion term for both types of diffusion is calculated separately and discussed in section 4.2.3. We use periodic boundary conditions in the x-direction and no flux boundary conditions in the y-direction for the diffusion.

4.2.3 Biochemical properties

Secretion

We model secretion of pro-inflammatory, anti-inflammatory and anabolic cytokines and MMPs from chondrocyte cells. Additionally we model release of fibronectin fragments from ECM *cells* as their volume reduces. Pro-inflammatory, anti-inflammatory and anabolic cytokines and MMPs are secreted according to the state at the beginning of each Monte Carlo step and the level secreted is a function of the state of the *cell* secreting. Pro-inflammatory cytokines are secreted according to the function,

$$p_{secreted} = \left(p_{bp} + p_{pp} \frac{p_c^2}{p_{ph}^2 + p_c^2} + p_{fp} \frac{f_c^2}{p_{fh}^2 + f_c^2} \right) \frac{p_{ah}^2}{p_{ah}^2 + a_c^2}. \quad (4.2.7)$$

where p_c and f_c are the concentrations of pro-inflammatory cytokine and fibronectin at the centre of the *cell*. The secretion term reflects up-regulation of pro-inflammatory cytokines, by themselves and fibronectin fragments, and the down-regulation of pro-inflammatory cytokine production by anti-inflammatory cytokines. Anti-inflammatory cytokines are secreted according to the term,

$$a_{secreted} = a_{pp} \frac{p_c^2}{a_{ph}^2 + p_c^2} + a_{fp} \frac{f_c^2}{a_{fh}^2 + f_c^2} + a_{np} \frac{n_c^2}{p_{nh}^2 + n_c^2}. \quad (4.2.8)$$

Here the level of anti-inflammatory cytokine secreted is up-regulated in the presence of pro-inflammatory cytokines, anabolic cytokines and ECM fragments.

MMPs are up-regulated by pro-inflammatory cytokines and down-regulated by anabolic cytokines, according to the term,

$$m_{secreted} = \left(m_{bp} + m_{pp} \frac{p_c^2}{m_{ph}^2 + p_c^2} \right) \frac{m_{np}^2}{m_{np}^2 + m_{nh} n^2}. \quad (4.2.9)$$

Anabolic cytokines are involved in the normal homeostasis of the ECM tissue, hence have a background production rate. They are also upregulated in response to fibronectin fragments in the joint according to the term,

$$n_{secreted} = \left(n_{bp} + n_{fp} \frac{f_c^2}{n_{fh}^2 + f_c^2} \right). \quad (4.2.10)$$

All of the chemicals secreted by chondrocytes in this model are secreted on the boundary of the cell, they then diffuse away from the cell according to the diffusion PDE.

During each MCS when the cell volume is amended in response to MMP levels we also make a corresponding secretion of Fn-fs. The amount of fibronectin fragments released is calculated as:

$$f_{secreted} = \begin{cases} -f_{fp}\Delta v & \text{if } \Delta v < 0 \\ 0 & \text{if } \Delta v \geq 0 \end{cases} \quad (4.2.11)$$

where Δv is the change in target volume of the *cell*.

4.3 Model Parameters

Table 4.1: Summary of base parameter values in model. Dimensionless unless otherwise stated.

Parameter	Value
Temperature	20
Neighbour Order	2
λ Surface ECM	2
λ Surface Chondrocytes	2
Target Surface ECM	2 pixels
Target Surface Chondrocytes	25 pixels
<i>Contact Adhesion Energy</i>	
Medium-Medium	10
Medium-ECM	10
Continued on next page	

Table 4.1 – continued from previous page

Parameter	Value
Medium-Chondrocyte	16
Medium-Bone	10
ECM-ECM	4
ECM-Chondrocyte	6
ECM-Bone	6
Chondrocyte-Chondrocyte	10
Chondrocyte-Bone	16
Bone-Bone	10
<i>Focal Point Plasticity</i>	
λ ECM-ECM	10
Activation Energy ECM-ECM	-100
Target Distance ECM-ECM	7 pixels
Max Distance ECM-ECM	10 pixels
Max no. of junction ECM-ECM	5
λ ECM-Chondrocyte	10
Activation Energy ECM-Chondrocyte	-100
Target Distance ECM-Chondrocyte	7 pixels
Max Distance ECM-Chondrocyte	10 pixels
Max no. of junction ECM-Chondrocyte	5
λ ECM-Bone	10
Activation Energy ECM-Bone	-100
Target Distance ECM-Bone	7 pixels
Max Distance ECM-Bone	10 pixels
Slow Diffusion Coefficient	1.8 pixels ² MCS ⁻¹ (0.002 μ^2s^{-1})
Fast Diffusion Coefficient	1800 pixels ² MCS ⁻¹ (2.0 μ^2s^{-1})
Continued on next page	

Table 4.1 – continued from previous page

Parameter	Value
Decay Coefficient	$0.17 \text{ MCS}^{-1} (0.69 \text{ hr}^{-1})$
ECM λ area	2 pixels ²
ECM target area	55 pixels ²
Chondrocyte λ area	2 pixels ²
Chondrocyte target area	55 pixels ²
p_{bp}	0.0017
p_{pp}	1.7
p_{ph}	1
p_{fp}	1.7
p_{fh}	1
p_{ah}	1
a_{pp}	1.7
a_{ph}	1
a_{fp}	1.7
a_{fh}	1
a_{np}	1
a_{nh}	1
m_{bp}	0.00017
m_{pp}	1
m_{ph}	1
m_{nh}	1
n_{bp}	0.0001
n_{fp}	0.001
n_{fh}	1
f_{fp}	0.17

4.4 Transition from ODE to spatial model

4.4.1 Direct Comparison

To explore the relationship of this model to the ODE model we start by simplifying the spatial model to minimise the differences between the two models. We replace the synovial fluid, ECM and bone tissue in the model with chondrocytes to create a uniform domain, which also necessitates allowing fibronectin to be released from chondrocytes rather than ECM. We also change the parameters n_{bp} and n_{fp} to zero, to remove anabolic cytokine production. We change the boundary conditions to be periodic in both the x- and y-axis. We then run a series of simulations of the model varying the parameter p_{pp} each time. We use non-steady state diffusion.

At the start of the simulations all cytokines, MMP and fibronectin fragment concentrations are zero. For each simulation we run the model for 10000 MCS and simulate a trauma, a pulse of $p_s=10$, at $t = 1000$. In each case the biochemical variables reach a steady level by $t = 1000$ and then after the trauma either recovers to the original level or moves to a different steady level or oscillates. We measure the maximum and minimum and average value of p_s in the chondrocytes over the final 500 MCS in each simulation with and without a trauma and use this to construct a plot which we compare with a bifurcation plot from the ODE model, Figure 4.6.

Comparing the Cellular Potts model to the ODE model, we appear to have broadly the same behaviour. We have a steady state at a low concentration of p for low values of p_{pp} , which we lose as we increase this parameter. At higher values of p_{pp} we have oscillatory behaviour. In the Cellular Potts model the amplitude and average value of the oscillations is larger than for the ODE model. This is likely to

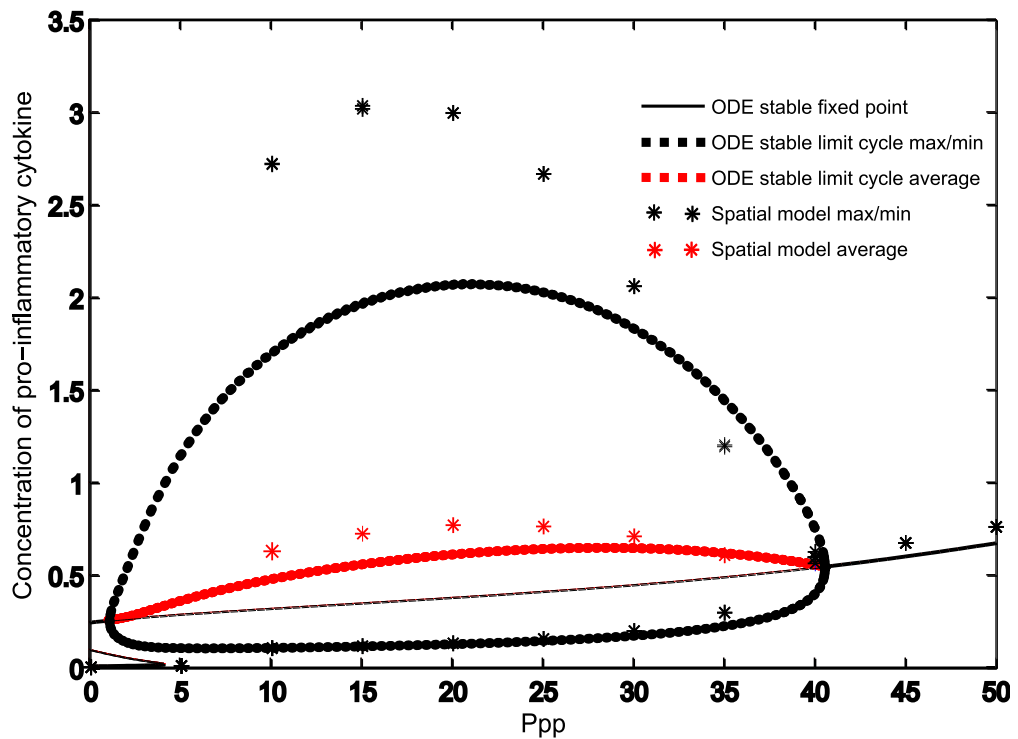


Figure 4.6: Comparison of bifurcation plot from the cartilage ODE model with the results from the spatial model with parameters approximating the ODE model. The solid lines are the stable and unstable branches of the ODE model bifurcations, The dashed black and red lines of the ODE limit cycle maximum, minimum and average values. The black and red stars are the maximum, minimum and average values from the spatial model at 10000 MCS.

be due to the slight differences in the two models, principally the effect of diffusion. At even larger values of the p_{pp} both models move to a stable steady state, at a similar level of p .

4.4.2 Number of cells

A major difference between the spatial model and the ODE model is the sparsity of chondrocytes, since the ODE model assumes spatial homogeneity which we can consider analogous to 100% chondrocytes in the spatial model. In cartilage tissue only 5% of the volume is chondrocytes. We now gradually reduce the number of chondrocytes in the Cellular Potts model, whilst still secreting fibronectin fragments from the chondrocytes. In these simulations the ECM plays no part in the cartilage dynamics, but instead acts as an inert connective tissue between cells. This allows us to consider the effect of reduced intercellular communication. Figure 4.7 shows a set of bifurcation plots as the proportion of chondrocytes is reduced from 100% to 10% and replaced by ECM.

As we reduce the number of chondrocytes in the tissue the bifurcation plot changes. The Hopf point appears to remain at a similar value of p_{pp} , but the amplitude of the oscillations reduces, possibly due to the limit cycle colliding with the unstable branch and the resulting homoclinic bifurcation moving up unstable branch of the fold. As the number of cells reduces further oscillatory behaviour is lost altogether. In addition, the disease branch rises, occurring at higher values of p as the number of chondrocytes reduces.

Reducing the number of cells has two effects on the model. Firstly the overall amount of all the variables secreted is reduced, due to the reduction in the number of cells. Secondly, communication between cells is reduced, due to being spaced further apart, and chemicals having to diffuse through the ECM, which can lead to cells behaving less uniformly. In the full model where tissue degradation further

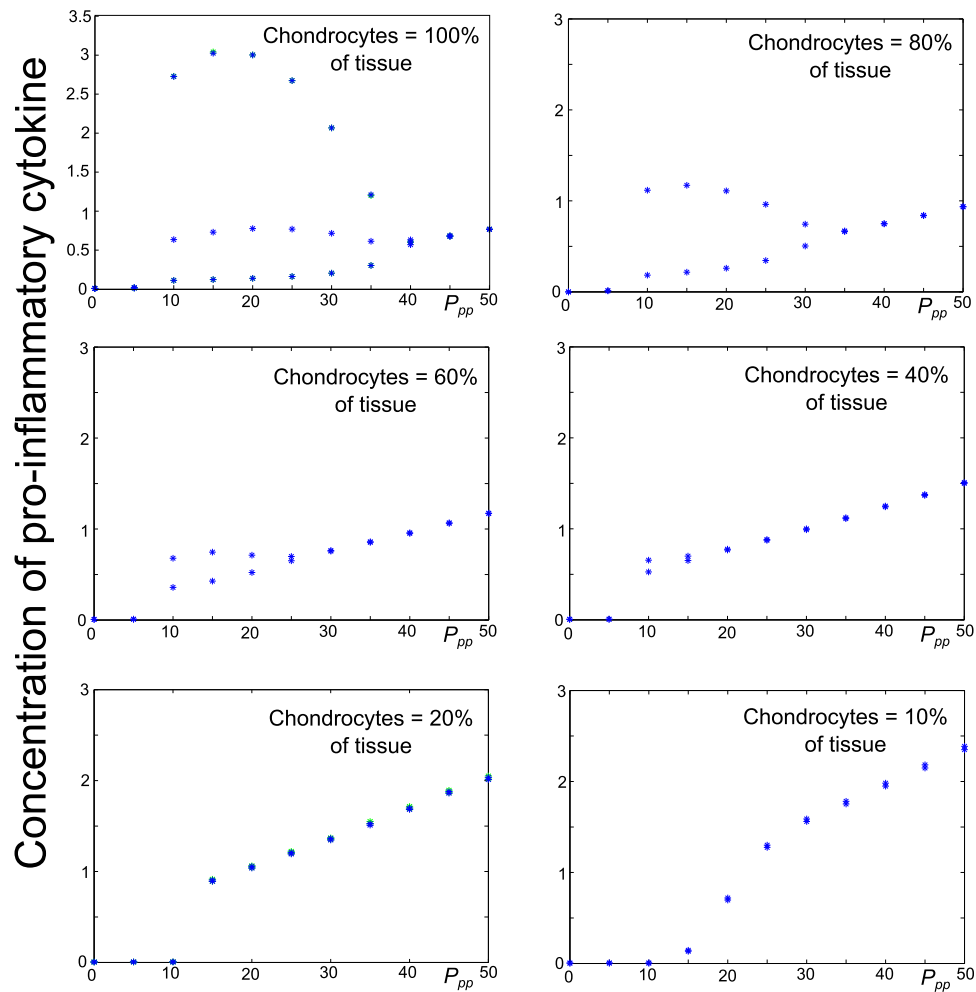


Figure 4.7: Bifurcation plots of p against p_{pp} showing the stable steady states. We reduce the proportion of chondrocytes, replacing them with ECM tissue. As the number of cells reduces we lose the oscillatory behaviour.

increases non-uniformity this effect could be more important.

In these simulations we have released fibronectin (f) from the chondrocytes. This is unrealistic so we next look at secretion of fibronectin from the ECM. We reduce the number of chondrocytes again, this time with f released from the ECM, Fig 4.8. Hence, when we have 100% chondrocytes we have no Fn-fs released. When f is released from the ECM we do not see any oscillatory states. As the number of cells reduces the disease state firstly lowers then rises again as the chondrocytes reduce to more realistic numbers. The range for which we have only a healthy state or both a healthy and disease state increases as we reduce the number of chondrocytes.

Overall, moving the system from 100% chondrocytes with f released from the cells to 5% chondrocytes with f released from the cells is more comparable to cartilage biology. This change introduces non-uniform behaviour in the tissue, which could not be modelled with ODE methods. The non-uniformity is dependent upon the diffusion rate, and is likely to reduce and disappear as we increase the rate of diffusion, which we show in Section 4.6.

4.4.3 Tissue boundaries

In the simulations so far we have considered only cartilage tissue. However in the joint the cartilage is anchored to bone and surrounded by synovial fluid. We now introduce these aspects back into the model. Figure 4.9c shows the initial configuration of the tissue with bone on the bottom boundary and synovial fluid on the top boundary. Since we now have different tissues on the boundary a periodic boundary condition is no longer appropriate for the y-axis so we instead change this to no flux. We leave the x-axis boundary periodic since we assume the cartilage is wider than it deep in line with normal cartilage histology in joint such as the knee or hip.

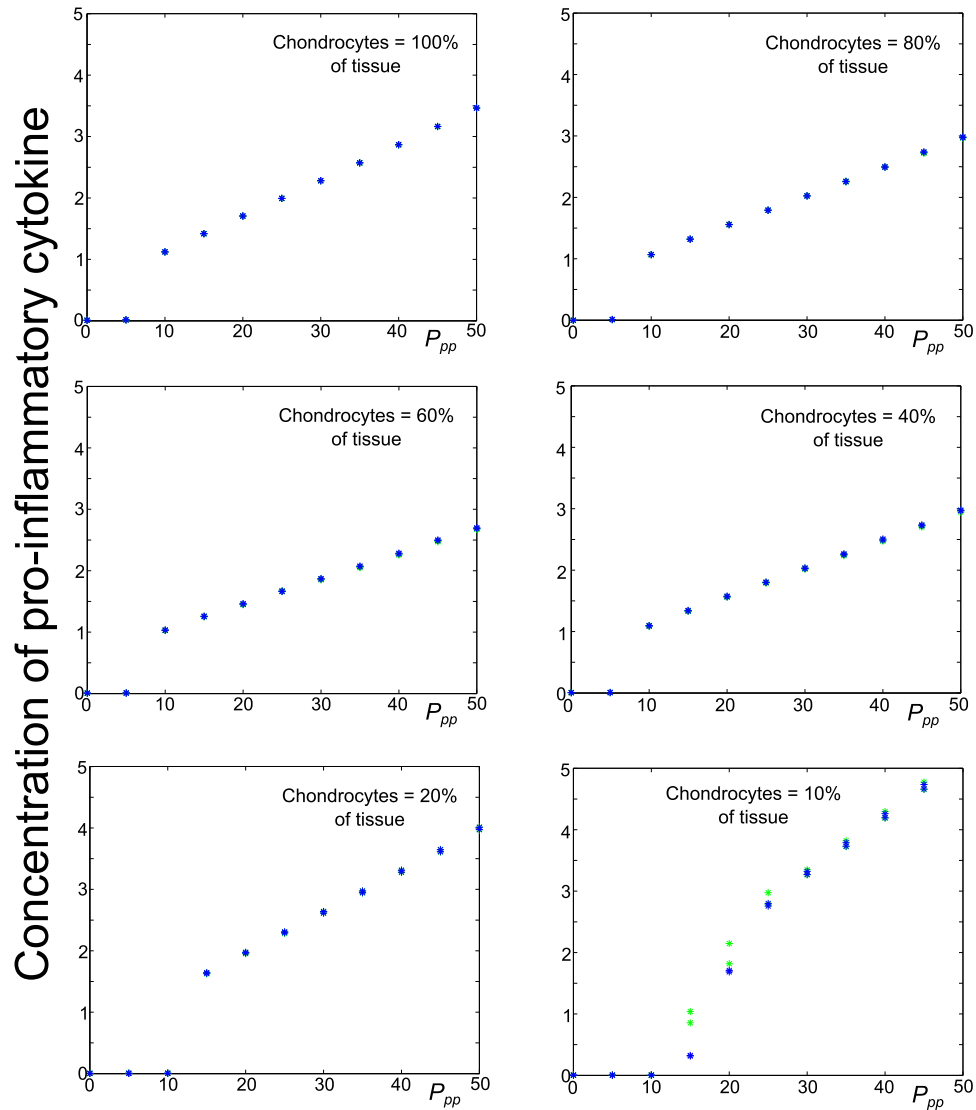


Figure 4.8: Bifurcation plots of p against p_{pp} showing the stable steady states for decreasing numbers of cells. Here, f is released from the ECM rather than from the chondrocytes.

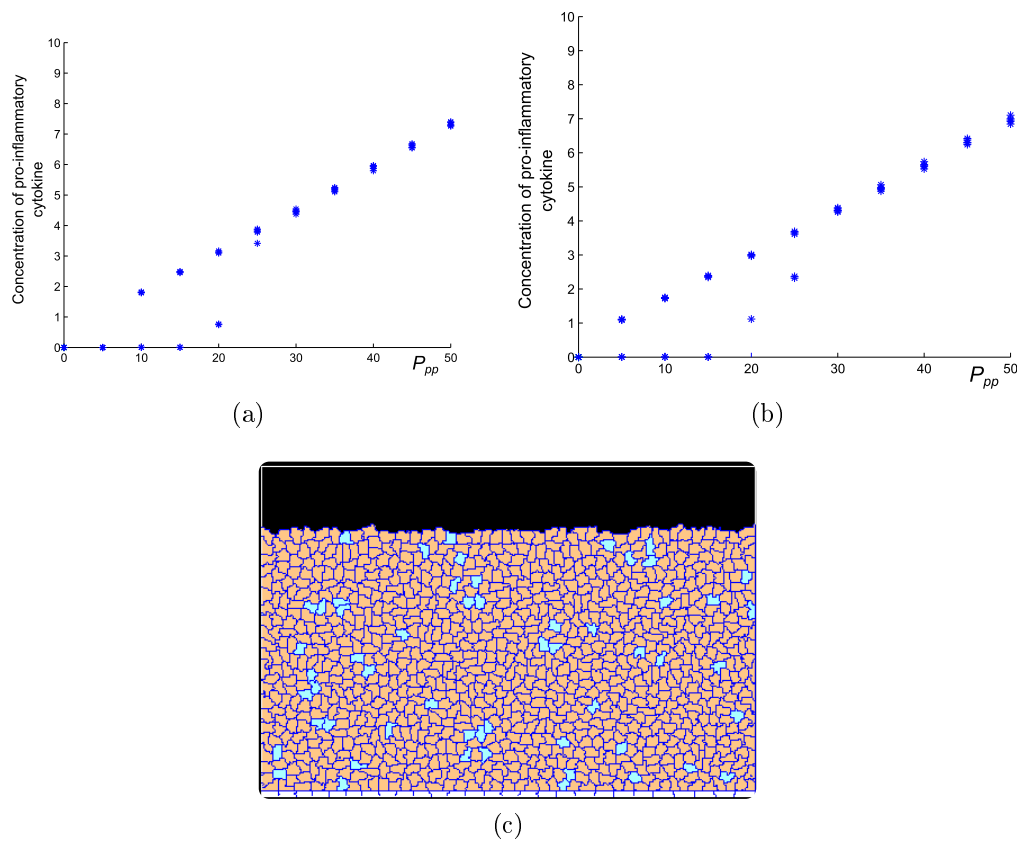


Figure 4.9: a) Bifurcation plot of spatial model with 5% chondrocytes in ECM with no other tissue types. b) Bifurcation plot of the spatial model with 5% chondrocytes in the ECM but realistic tissue boundaries of synovial fluid on the top boundary and bone on the bottom boundary. c) Initial spatial domain used in (b).

Figure 4.9a shows a bifurcation plot of p against p_{pp} where we have 5% chondrocytes. Comparing this to Figure 4.9b, in the first we have cartilage tissue only as in previous simulations, whereas in the second we have bone and synovial fluid. There is little difference between these two plots, so adding the bone and synovial fluid makes little difference for this configuration. When the percentage of chondrocytes is higher however, the effect of the change is greater. Since a higher percentage of chondrocytes is not biologically realistic we do not explore this further.

4.4.4 Tissue degradation and disease measures

The final feature that we need to add back into the model that is not present in the ODE model is the degradation of the cartilage. This is a significant change from the ODE model as it means that in disease we have a continually changing environment. At this point we also put anabolic cytokines back into the model, as even with low level of pro-inflammatory cytokines the background production would lead to tissue degradation without a balance to give homeostasis. Figure 4.10 shows a time course of the levels of p as the tissue is degraded. As the tissue is degraded the number of chondrocytes is reduced and cytokine feedback between cells is made more difficult by the tears that develop in the tissue, as this moves the cells further apart. This, coupled with the stochastic changes in the model means that to we can no longer consider the model in behaviour at a fixed time point, but instead need to consider the time course of the model. With these considerations in mind we will now move on to considering how this model behaves and how we define health and disease in the spatial model.

In the previous chapters we have used the concentration of pro-inflammatory cytokine as the main measure of disease, loosely defining health as very low concentrations of pro-inflammatory cytokine and disease as higher levels. This measure

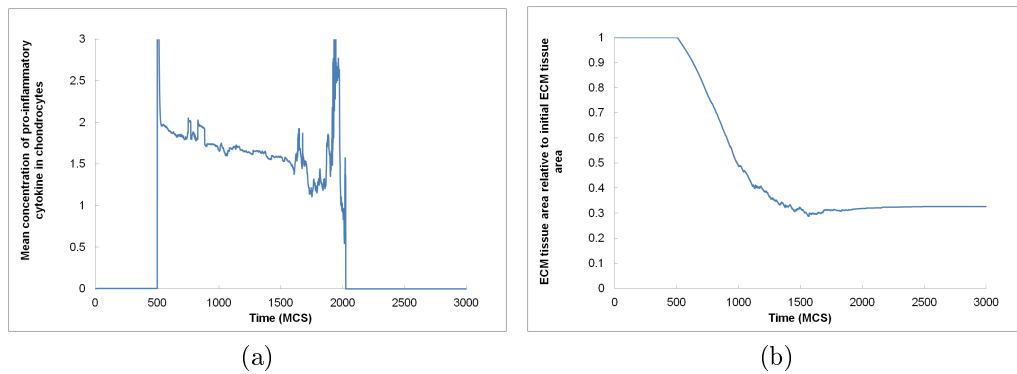


Figure 4.10: Time course plot of the model over 3000 MCS, an instantaneous increase in p is simulated at $t = 500$ to move the system to disease. a) The concentration of p initially remains at a low concentration suggesting a healthy state, but after the stimulus the level of p changes with time. b) The ECM volume continually degrades once disease is initiated. This may be a better measure of disease than pro-inflammatory cytokine concentration.

of disease has several limitations and with the spatial model we have the opportunity to consider other measures of disease. Specifically, a measure of the amount of tissue loss would seem intuitively to be a good disease measure. This measure of disease is more in line with clinical disease measures that often include joint space narrowing as seen on x-rays. In contrast, accurate measures of cytokine or MMP levels are not practical in a clinical environment due to the short half life of these biochemicals and the difficulty of extracting samples from patients. Since we know that tissue degradation is mediated by cytokines, we would expect strong correlation between high levels of cytokines in disease and tissue degradation. Figure 4.10 shows time courses for a simulation of the model showing the proportion of cartilage tissue remaining in addition to the pro-inflammatory cytokine levels. We see here that the level of p is very variable and drops to zero once all chondrocytes have died, which could be misinterpreted as a return to health. However the ECM plot clearly shows that the ECM volume is much reduced, and here the ECM volume is a better measure of disease stage and progression.

Overall in this section we have seen the effect of moving from an ODE to a Cellular Potts model. Whilst there are differences in model behaviour at certain parameter

values, generally comparable behaviour types seem to exist, which may mean that the treatment strategies seen in the ODE model are still applicable. In the next section we will further examine the behaviour groups that we see in this spatial model.

4.5 Classification of behaviours in the spatial model

In the ODE modelling we were able to classify behaviour based on the nature and stability of the steady states and limit cycles of the system. In the spatial model the domain is continually changing as the matrix remodels. Hence it is no longer possible to observe behaviour that is homogeneous either in time or space. For this reason we look at how the system behaves over time in the presence and absence of pro-inflammatory stimulus to classify different parameter sets into behavioural groups. This grouping is important as it determines the type of treatments that would be possible and the likelihood of slowing disease progression. Using the bifurcation analysis from the previous chapter to help identify different behaviour types we have found three behaviour groups: persistent health, inducible disease and persistent disease.

Persistent health is analogous to monostable health in the ODE model. With no stimulus we have low levels of all the variables, and if a stimulus is given we quickly move back down to a healthy state with little change to the ECM tissue (see Figure 4.11a). One point to note with this state is that if a pro-inflammatory stimulus is given it will damage the cartilage and degrade it slightly, and this damage is unlikely to recover, due to low levels of anabolic cytokines. For a short stimulus this is not a problem since the amount of damage is small relative to the healthy tissue (Figure 4.11c). However, if we stimulate repeated pro-inflammatory stimuli over a longer time period we see that the matrix can become significantly degraded, to the point where you may get loading problems in the joint (Figure 4.12). We expect

that the same result could be observed with a mechanical stimuli. This may be representative of a simple wear and tear process where the joint cartilage becomes degraded but the cartilage is not osteoarthritic. In these cases, removal of the pro-inflammatory stimulus is sufficient to halt the degradation process, however in a severely damaged joint the abnormal loading as a result of degradation may in itself act as an additional pro-inflammatory stimuli.

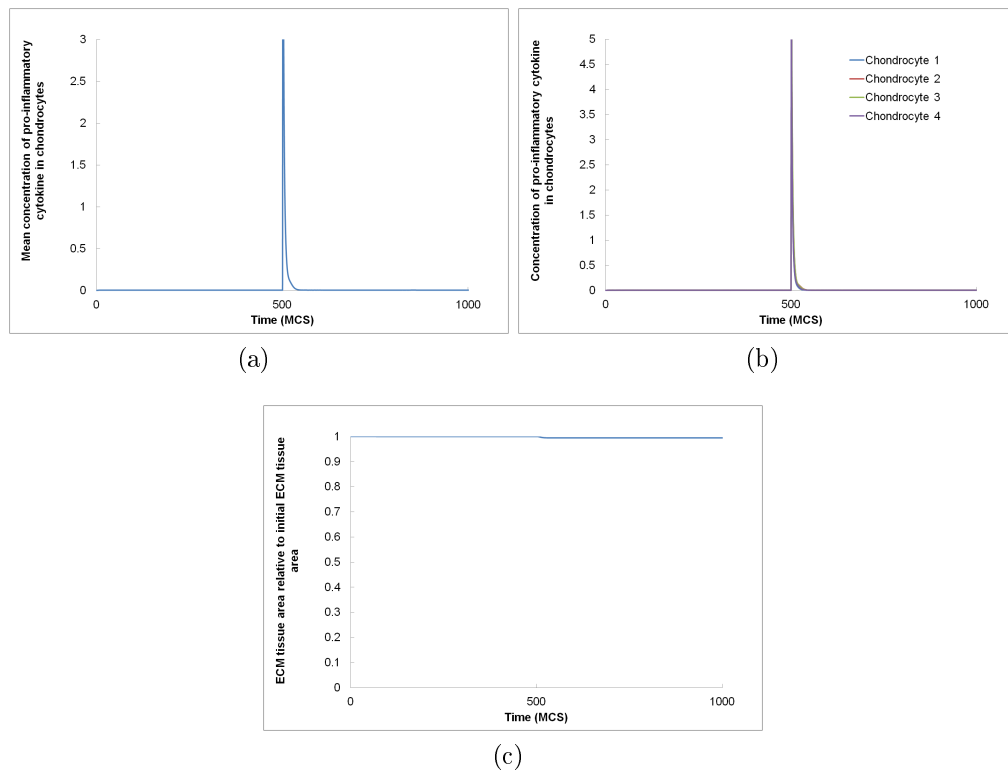


Figure 4.11: Plots showing behaviour of the persistent health type. a) Average concentration of p in the chondrocytes against time. A pro-inflammatory stimulus of $p = 10$ is given at $t = 500$. This quickly dies down without noticeable long term effects. b) Concentration of p in four individual chondrocytes plotted against time. These shows generally uniform cell behaviour c) Proportion of ECM tissue remaining relative to the initial level plotted against time. Only minor changes on the ECM tissue are seen. ($p_{pp} = 0$)

As we increase the value of p_{pp} we move out of the region of persistent health and into a region of inducible disease. Here for low initial conditions of all variables we have a state of health as before. However, if a pro-inflammatory stimulus is given the system will move to a disease state where the concentration of cytokines,

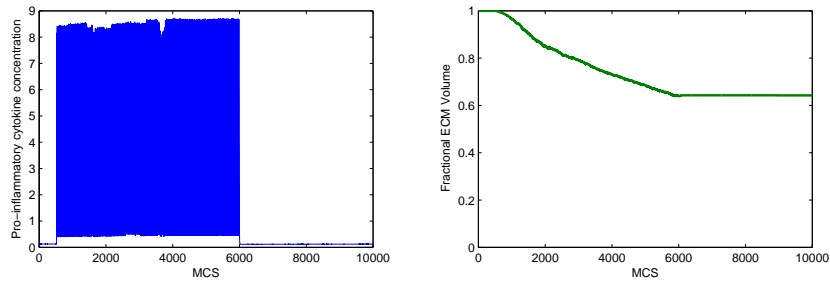


Figure 4.12: Time course plot of the spatial model over 10000 MCS, with a series of regular stimuli of p in all chondrocytes. Stimuli of 10 units of p are made at intervals of 20 MCS between $t = 500$ and $t = 6000$. These cause degradation of the ECM. However, once these secretions are halted at $t = 6000$ the degradation ceases. The parameters are as specified in Table 4.1 except that $p_{pp} = 2$.

MMPs and fibronectin are all comparatively high, and the ECM is being degraded. Figure 4.13a shows the average concentration of pro-inflammatory cytokine in the chondrocytes over time as the simulation progresses. A pro-inflammatory stimulus is given at $t = 1000$, at which point the level of p increases and then settles to a disease level and the ECM tissue starts to be degraded (Figure 4.13c). As the simulation progresses the number of chondrocytes is decreasing, hence the increasing variation in the concentration of p , until at approximately $t = 2500$ the level of p drops back down to zero as the last chondrocyte is degraded. Figure 4.13b shows time courses for four individual chondrocytes from the same simulation. This figure demonstrates that although broadly similar, the behaviour of each chondrocyte is individual and influenced by the concentration of biochemicals in its vicinity. Large spikes in the concentration of p are seen and the cells die at different times during the simulation.

Figure 4.14 shows spatial domain at four different time points through the simulation shown in Figure 4.13. We can see that as the tissue degrades the chondrocytes cluster together as the tissue between the chondrocytes degrades quicker than the rest of the tissue due to higher concentrations of cytokines. We also see that the pro-inflammatory cytokine concentration is higher in the locality of chondrocytes,

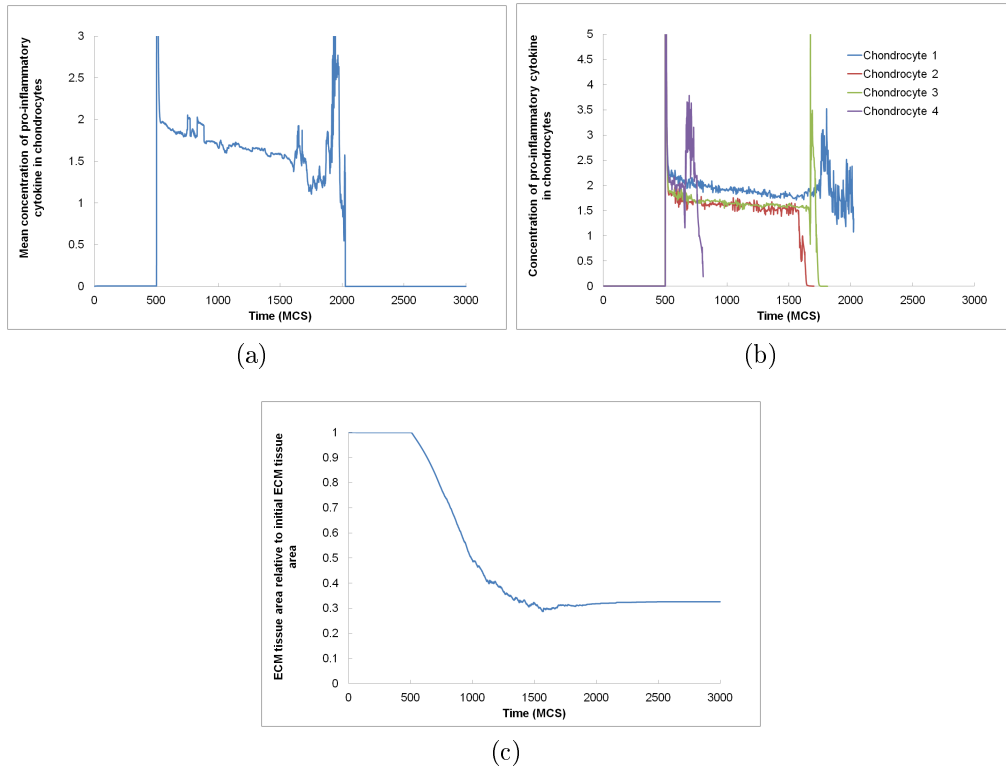


Figure 4.13: Plots showing behaviour of the inducible disease type. a) Average concentration of p in the chondrocytes against time. A pro-inflammatory stimulus of $p_s = 10$ is given at $t = 500$ which moves the model to a disease state. By $t = 2500$ all the chondrocytes have been degraded. b) Concentration of p in three individual chondrocytes plotted against time. c) Proportion of ECM tissue remaining relative to the initial level plotted against time. ($p_{pp} = 15$)

we will later contrast this with the case when we have faster diffusion.

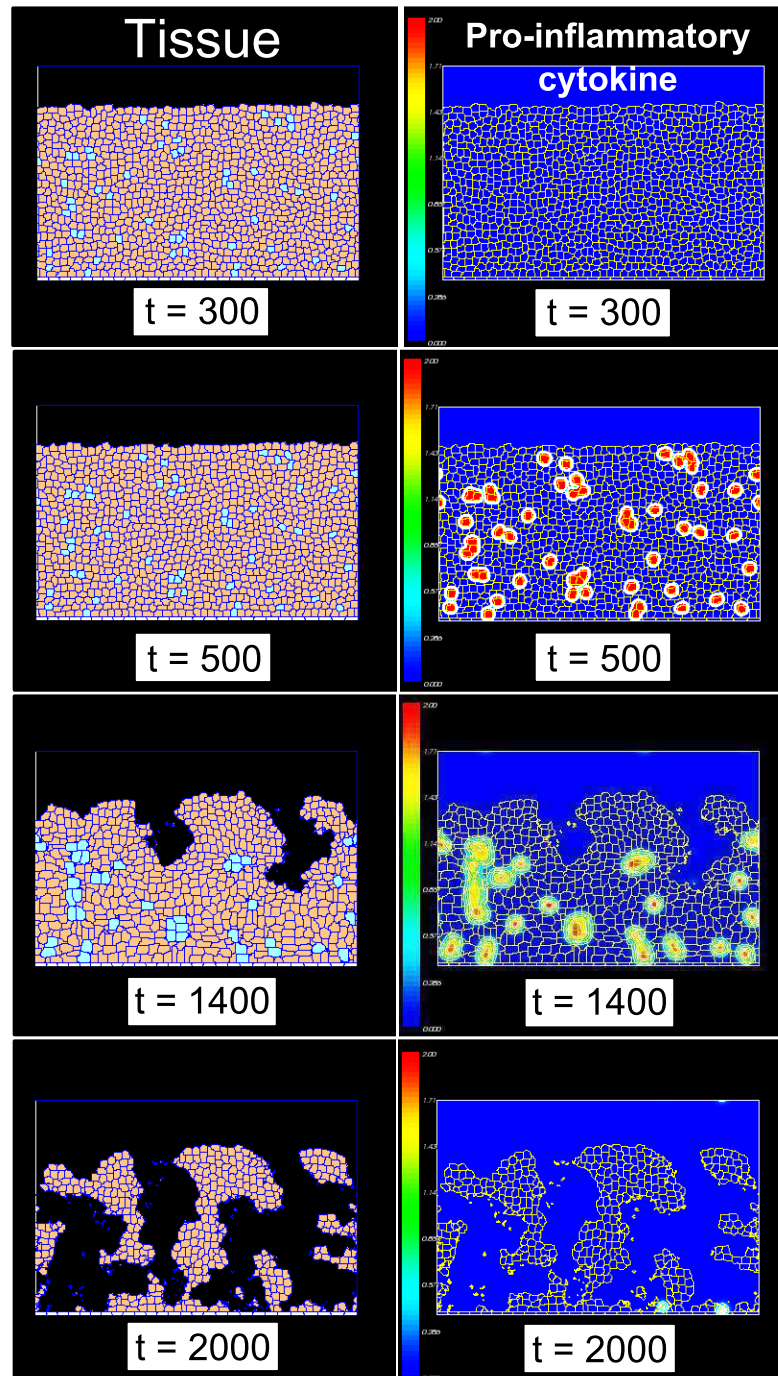


Figure 4.14: Plots showing behaviour of the inducible disease type at different time points. The first column shows the *cells* degrading whilst the second column shows the pro-inflammatory cytokine concentration through the domain at the same time points. The images show that the diffusion of the pro-inflammatory cytokine concentration in addition to the spatial configuration of the domain determine how the tissue degrades. ($p_{pp} = 15$)

Persistent disease is analogous to monostable disease in the ODE model, and we find this behaviour as we increase p_{pp} to 20 with the reference parameter set. Without any stimulus the system is in a disease state regardless of initial conditions. Figure 4.15a shows the average concentration of pro-inflammatory cytokine in the chondrocytes, and even though we start with initial conditions of zero for all variables in the model, the level of pro-inflammatory cytokines rise. The other variables rise in a similar fashion and the cartilage is degraded (Figure 4.15c). Interestingly, for some parameter ranges this does not occur uniformly in every chondrocyte. The majority of chondrocytes move quickly to be disease state (Chondrocytes 1 in Figure 4.15b) but some chondrocytes remain healthy for a short time before moving to disease (Chondrocytes 2 and 3), whilst others remain healthy throughout the simulation (Chondrocyte 4). This is likely to be dependent on the local positioning of the chondrocyte, and is suggestive that the structure of chondrocyte positioning through the tissue could be a factor in disease progression. This type of behaviour is seen close to the threshold where we switch between inducible and persistent disease.

Figure 4.16 shows the spatial domain during the simulation where $p_{pp} = 20$ and hence have non uniform cell behaviour. It is clear that cells that are in closest vicinity to other cells are the ones which reach disease levels soonest. Then as pro-inflammatory cytokine diffuses and as the ECM degrades the disease state spreads to cells further away. We can also see that the ECM degradation itself causes further clustering, presumably because the ECM tissue between two chondrocytes is subject to higher concentrations of pro-inflammatory cytokines and hence degrades quickest. Biologically, chondrocyte clustering is seen in OA, although it is theorised that this is due to cell division. It is possible that the movement of chondrocytes via ECM degradation may also be contributing to this observed phenomena.

At higher levels of p_{pp} ($p_{pp} = 50$), further away from this threshold, we get more

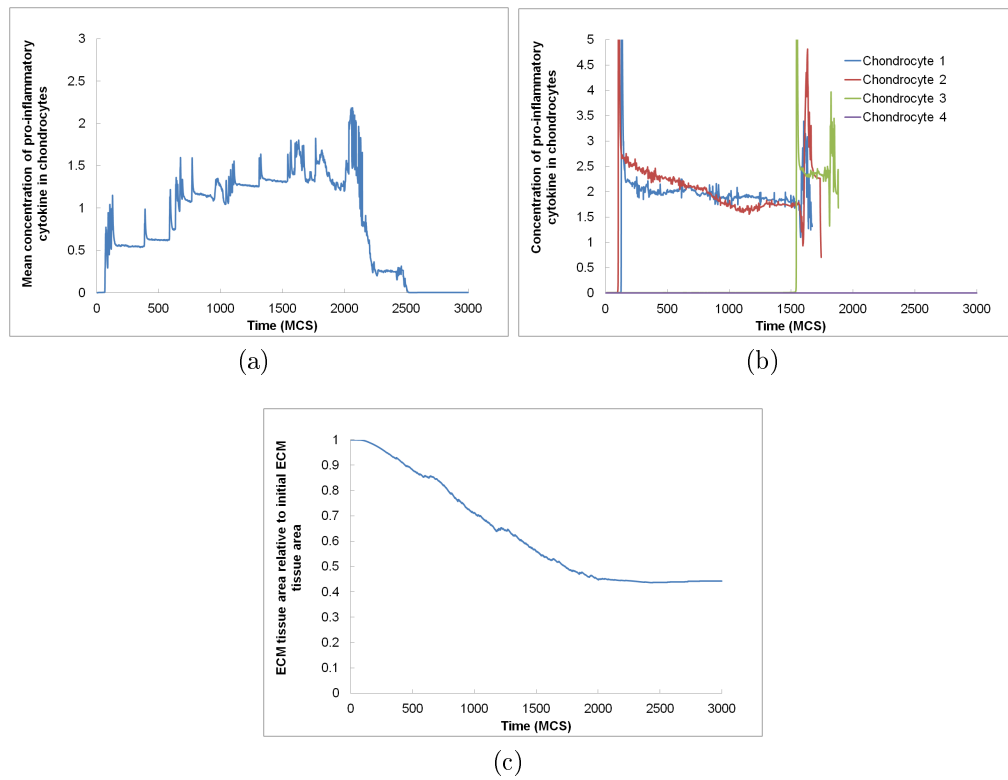


Figure 4.15: Plots showing behaviour of the persistent disease type. a) Average concentration of p in the chondrocytes against time. No stimulus is given in this simulation. By $t = 3000$ most of the chondrocytes have been degraded. b) Concentration of p in four individual chondrocytes plotted against time. c) Proportion of ECM tissue remaining relative to the initial level plotted against time ($p_{pp} = 20$).

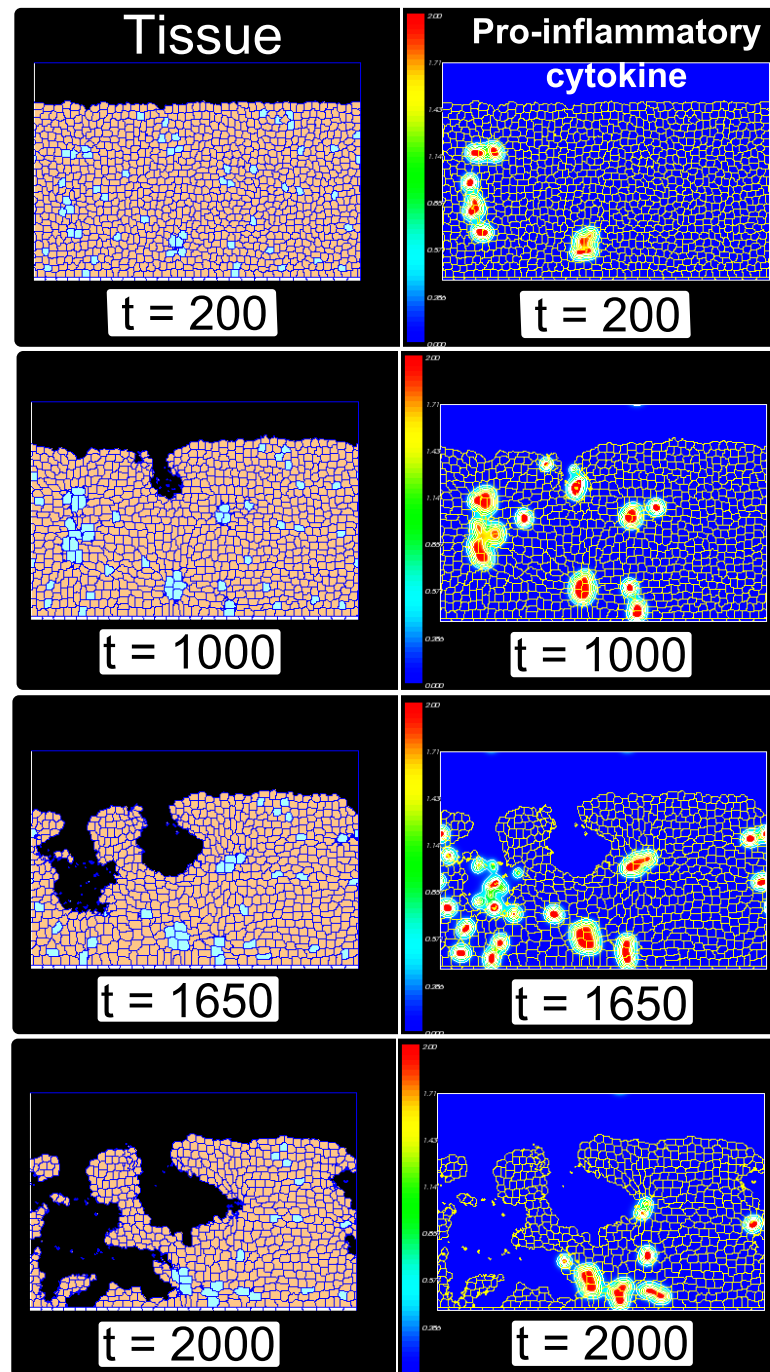


Figure 4.16: Plots showing behaviour of the persistent disease type at different time points. The first column shows the *cells* degrading whilst the second column shows the pro-inflammatory cytokine concentration through the domain at the same time points. The images show that cell clustering is occurring during the simulation as tissue between cells receives the highest concentration of pro-inflammatory cytokine. ($p_{pp} = 20$)

uniform cell behaviour, Figure 4.17b. As we might expect with a larger rate of pro-inflammatory production we also degrade the ECM much quicker. Here, we see that the additional disease measure of ECM tissue in the spatial model gives us a better link to the disease that an individual may experience. For example, where we see a drop to low cytokine levels in the ODE model, and assume health, we may find that the ECM is significantly damaged.

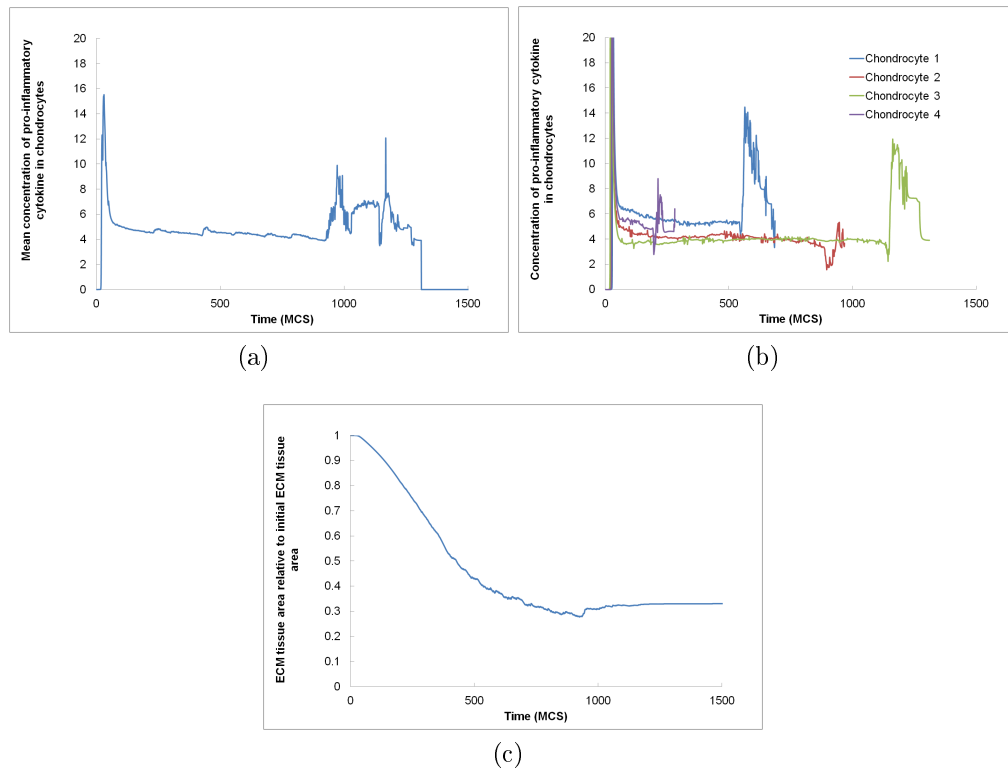


Figure 4.17: Plots showing behaviour of the persistent disease type for a high value of p_{pp} compared to Figure 4.15 a) Average concentration of p in the chondrocytes against time. No stimulus is given in this simulation. By $t = 1500$ most of the chondrocytes have been degraded. b) Concentration of p in four individual chondrocytes plotted against time. The chondrocyte behaviour is more uniform compared to persistent disease with lower p_{pp} (Figure 4.15) i.e. the chondrocytes all reach raised cytokine levels at the same time c) Proportion of ECM tissue remaining relative to the initial level plotted against time ($p_{pp} = 50$).

As Figures 4.14 and 4.16 show, the diffusion rate used in these simulations is such that the effective diffusion length is about 4-5 cell lengths. Since the diffusion coefficients for cytokines, MMPs and Fn-fs are poorly defined in cartilage, in the

next section we will consider how both slower and faster diffusion affect the tissue degradation.

4.6 Impact of diffusion rate variation

As discussed previously in this chapter the diffusion coefficients of cytokines, MMPs and fibronectin fragments in cartilage are poorly defined. The diffusion rates we have used so far for the simulations are slow compared to some estimates. We will now consider the effect of faster diffusion rates on the system. We will also consider how slower diffusion rates affect the simulations.

Large diffusion rates, present some practical problems in CompuCell3D, since the diffusion solver uses the forward Euler method, which is unstable for large diffusion coefficients. To avoid this CompuCell3D adjusts the diffusion time step, but this slows the simulations considerably. Hence, in order to consider faster diffusion without excessively long simulations we make the assumption that the concentration profile quickly settles to a steady state in time, allowing us to use steady state diffusion methods. A steady state diffusion solver is built in to CompuCell3D and is based on the Helmholtz equation,

$$\nabla^2 c - kc = F, \tag{4.6.1}$$

where c is the concentration, k is the decay and F is the source term. F can be input in the model through either an initial concentration, or through cellular secretion. However, the cellular secretion option is designed to take a constant, to be secreted at each MCS. To dynamically control the secretion amount at each MCS, such that the amount secreted is based on the concentration of the other

variables in the model we calculate this in a steppable written in Python then couple it to the diffusion through F . At each time step, on a pixel-by-pixel basis, we take the current concentration of all the chemical fields at the pixel. We then calculate the secretion amount based upon the equations in Section 4.2.3. The amount to be secreted is then fed back into the diffusion plugin as a constant concentration to be used at the next time step. This method solves the problem of non-constant secretion in CompuCell's steady state diffusion solver, however since the secretion is not fully integrated into the diffusion solver, there is an uncoupling effect that leads to unexpected results for some parameter regimes. For this reason we restrict the use of this solver to fast diffusion where the use of the non-steady state diffusion solver is impractical. For the parameters specified in Table 4.1 with changes only to p_{pp} we see sensible results in line with the non-steady state diffusion method.

In Section 4.5 where we had slower diffusion we found persistent health, persistent disease and inducible disease. We find that when we increase the diffusion (using the fast diffusion parameters from Table 4.1) that the regions of persistent health and inducible disease increase. The range of p_{pp} for which we see inducible disease increases significantly with the transition to persistent disease occurring at approximately $p_{pp} = 1000$ rather than 15. This finding is significant as it suggests that increasing the diffusion rate could transform the behaviour of the disease from incurable to potentially curable (i.e. does not require ongoing treatment to maintain low tissue degradation). It should be noted, however, that at the disease state the rate of degradation is higher than when we have slower diffusion. Figure 4.18 shows time course plots of pro-inflammatory cytokine concentration and ECM area for a simulation when $p_{pp} = 20$. If we compare this with Figure 4.15 we can see that not only is the degradation more complete but the degradation is approximately four times faster. This could have implications for the development of therapies based on altering diffusion rates.

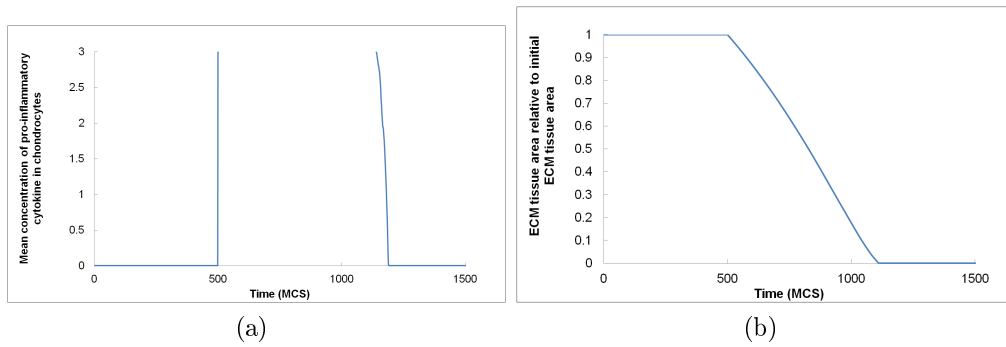


Figure 4.18: Plots showing behaviour when $p_{pp} = 20$ for a fast diffusion rate. Compared to Figures 4.15 and 4.17 the rate of tissue degradation is much faster, however, with a larger diffusion rate the behaviour is of the inducible disease type and hence potentially curable.

4.7 Discussion

In this chapter we have considered whether the spatial structure of cartilage tissue is of importance to the dynamics of the biochemical networks in OA. We have developed a spatial model in which we have two main tissue types, chondrocytes and ECM, along with bone and synovial fluid, within the CompuCell3D modelling environment. By modelling in CompuCell3D, which uses the Cellular Potts algorithm on a lattice, we have been able to use a complex and realistic spatial structure of chondrocytes spaced randomly through the ECM tissue. The modelling has shown that in the spatial model we lose the concepts of monostable health, monostable disease and multi-stability, which we saw in the ODE modelling (Chapter 3). This is due in part to the stochastic nature of the model, but mainly to the continually changing spatial domain. We do however have analogous behaviour types of persistent health, persistent disease and inducible disease. It is possible that inducible disease behaviour includes scenarios where there is more than one disease state, but we have not found this in the parameter regimes we have considered.

Persistent health, analogous to monostable health, maintains background levels of all biochemical species even after a stimulus. However, in the presence of a continual or regular stimulus damage to the ECM will occur. Clinically, radiographic

evidence (i.e. x-ray images) of OA is seen in almost all individuals over the age of 30, however not all of these go on to develop symptomatic and ongoing OA. It is possible then that this type of behaviour could explain those cases where evidence of OA is seen, i.e. wear and tear due to mechanical or biochemical stimuli over time, but OA does not develop. Persistent disease does not require any stimulus to enter a disease state, even when starting in the absence of any cytokines, MMPs or Fn-fs. Interestingly, our simulations suggest that for some parameter ranges, the disease state is not uniform through the tissue and some chondrocytes remain healthy. This behaviour depends of the diffusion rate with faster diffusion leading to more uniform behaviour. Since OA tends to develop with old age, it is likely that persistent disease only exists biologically if the parameters of the model, e.g. production rates, are able to change with either time or disease advancement. Given the changes that have been observed in OA, e.g. chondrocyte division and increased numbers of receptors, this is likely to be the case. However this would need to be studied in more detail.

Inducible disease requires a stimulus to move from a healthy state to disease. In our simulations we induced a pro-inflammatory stimulus in all the chondrocytes, leading to uniform disease behaviour. If the stimulus was confined to a specific area, the behaviour of the model would be less uniform. Inducible disease is analogous to the multi-stable behaviours seen in the ODE model and offers the possibility of treatment leading to remission since we could move the system back to health, as we discussed in detail in Chapter 3, in relation to the ODE model. With the spatial model we can also better consider how the method of treatment is likely to affect outcome, although a more accurate realisation of the synovial fluid may be required.

The most important finding of this modelling has been the importance of diffusion coefficients to disease initiation and progression. The structure of the cartilage tissue means that diffusion is key to intracellular communication. In the previous

chapter, we theorised that increased diffusion could increase clearance of Fn-fs, slowing disease progression. Here we also see that decreased diffusion halts intracellular communication, which also slows disease progression. The possibility of changing diffusion coefficients as a therapy for OA is not seen in the currently available literature, and it may not be possible to significantly change coefficients *in vivo*. However, it may be that changes to cyclic loading could offer a way of increasing the effective diffusion by increasing advection in the tissue. This could be investigated as a way of slowing disease progression.

This modelling has showed that a spatial model introduces important parameters that can not be considered in the ODE model, and gives a better disease measure that is more easily compared to clinical measures. There are many different directions which we would like to explore by extending this model in future. One important direction which would need significant expansion is the inclusion of the mechanical aspects of the joint in the model. This would allow us to consider both mechanical damage and whether cyclic loading of the tissue could affect transport of biochemicals through the tissue. We would also like to consider coupling the model with a model of cytokine dynamics in the synovial fluid, to be a better realisation of the cytokine dynamics through the whole joint. We have not fully considered the effect of stochasticity in this model, and this is something we could consider further in future.

Overall, the spatial model has demonstrated that whilst the ODE modelling is useful in considering the behaviour of the cartilage in osteoarthritis there are several advantages to using a spatial model. The additional complexity, while making interpretation more difficult, allows us to consider further possibilities for therapies.

Chapter 5

Binding interactions in cytokine mediated STAT signalling

5.1 Introduction

A group of proteins involved in signal transduction for some cytokine networks is a family of transcription factors called Signal Transducers and Activators of Transcription (STAT) [77]. STAT proteins are uniquely able to take signals directly from the cytokine receptors on the cell membrane to the DNA within the nucleus. An example of how this occurs is described below. There are seven different STATs identified; they share similar structure but properties can vary quite significantly, particularly in relation to binding affinities [78].

In this chapter we are particularly interested in STAT1 binding both alone and in the presence of STAT3 dimers. STAT1 is activated by Interferon- γ (IFN- γ) as part of the immune response. It is found in a wide range of mammalian cells and is responsible for the regulation of over 200 different genes. Activation of IFN- γ receptors leads to tyrosine phosphorylation of STAT1 which then dimerises with another STAT1 molecule and translocates to the nucleus. Tyrosine phosphorylation

is the binding of a phosphate group to the tyrosine residue of the STAT1 molecule, this process is described more fully in Chapter 1. Once in the nucleus the STAT1 dimers are able to bind to specific sequences of DNA and if the sequence is a IFN- γ activated (GAS) site, transcription will occur [78]. Once bound to DNA, STAT1 binds cooperatively with other STAT1 dimers at adjacent sites allowing it to remain on DNA. Experimental results suggest that this cooperativity is vital to STAT1 gene response. As well as binding to GAS sites the STAT protein may bind to non-GAS sites where there is partial conservation of STAT protein sequence. In this case the binding affinity is low and the STAT is more likely to disassociate than when it is bound to a GAS site [93]. The distribution of GAS sites in DNA is not known precisely and distinction between GAS and non GAS site is unclear.

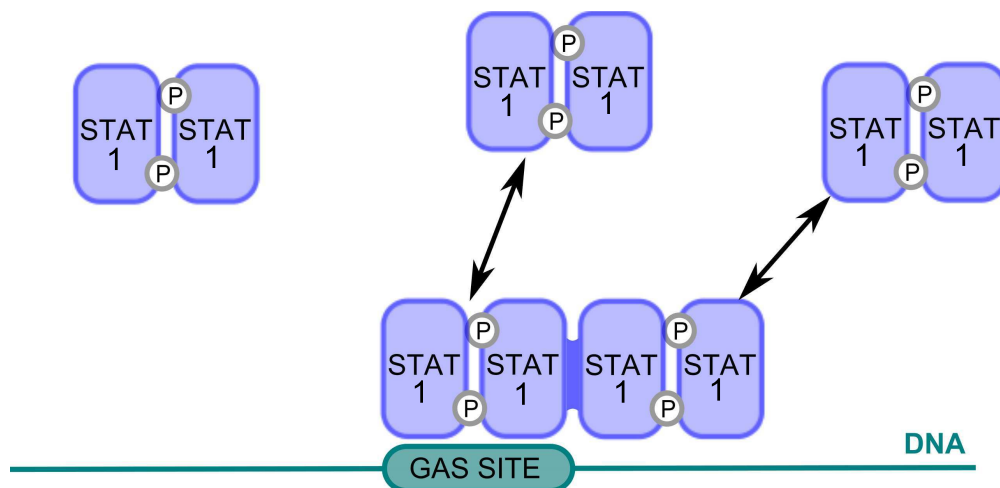


Figure 5.1: Schematic showing how STAT1 dimers bind to both GAS and non-GAS sites on the DNA then cooperatively form dimers to remain.

STAT3 is activated by Interleukin-6 (IL-6) and like STAT1 will dimerise and translocate to the nucleus. STAT3 is able to bind to the same sites as STAT1 since their conformations are very similar. However, STAT3 binding to GAS sites will not activate gene transcription. STAT3 is found mainly in dimer form but can rarely form polymers [77].

One of our aims in this chapter is to comment on the importance of GAS site position and binding strength to DNA binding and gene response. Early research

into STAT1 suggested that adjacent GAS sites were required to facilitate polymerisation and nuclear retention. More recent research has shown that single GAS sites are more abundant than these double sites, implying that having an adjacent GAS site is not a necessity for retention. We aim to show with modelling whether single GAS sites are sufficient for nuclear retention. We will also analyse how the two STAT proteins, STAT1 and STAT3, with different properties, co-exist whilst competing for binding at the same sites. We develop here two models of STAT binding, a cooperative binding model, and a competitive binding model.

5.2 Experimental Work

The importance of cooperativity to STAT1 gene expression has been demonstrated using a STAT1 mutant cell line, F77A [11]. In this mutant an amino acid residue, alanine, in the STAT1 N-domain is swapped for Phe77. Since cooperative binding occurs in the N-domain this inhibits cooperative binding. Figure 5.2a shows a competition electrophoretic mobility shift assay (EMSA) experiment for both F77A (KI) and wildtype STAT1 (ST). The plots show that for wildtype STAT1, STAT1 dimers are mostly bound as tetramers (GAFx2) suggesting cooperative binding is taking place. For F77A, STAT1 is bound mainly as dimers showing that cooperative binding is inhibited. STAT1 only remains in the nucleus when bound to DNA. Fluorescence recovery after photobleaching (FRAP) experiments measuring nuclear mobility can be used to measure STAT1-DNA binding. This involves making STAT1 molecules fluoresce by attaching a fluorescent tag, then using light to bleach an area of the nucleus. Fluorescence is then measured as the tagged STAT1 molecules move back into the bleached area giving a measure of the mobility of STAT1. Figure 5.2b shows FRAP recovery times for both wildtype and F77A STAT1. The mutant recovers quicker from bleaching than wildtype suggesting that it is more mobile and not bound as tightly to the DNA. This com-

bined with the results from Figure 5.2a show that inhibiting STAT1 cooperativity impedes its ability to effectively bind to DNA.

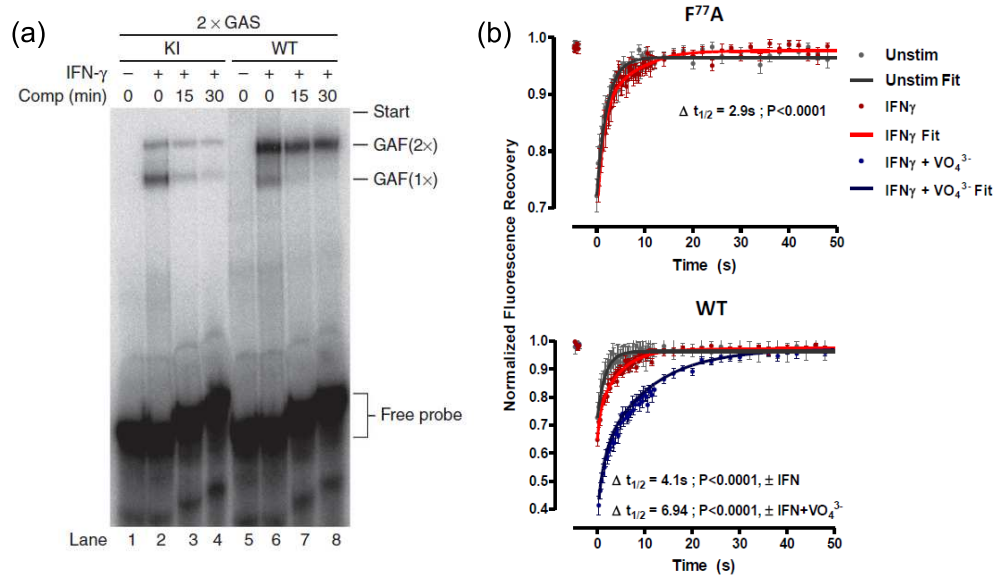


Figure 5.2: a) Adapted from Fig 1 in [11]. Competition EMSA with tandem GAS sites stimulated with IFN- γ for 60 mins. The wildtype is bound as tetramers to the DNA probe whilst the mutant is bound predominantly as dimers. b) Adapted from Fig 3.15 in [6]. FRAP recovery curves for the F77A mutant and wildtype STAT. The mutant recovers more quickly from photobleaching suggesting it is not bound as tightly to the DNA.

We are concerned in this modelling with STAT1-DNA binding to both single and tandem GAS sites. In [11] the authors discuss their experimental work with the F77A mutant, which has shown that cooperativity is beneficial at both single and tandem GAS sites. Figure 5.3 gives an example of two genes, one at a single GAS site and one at a tandem GAS site. In both cases gene expression is lost when cooperativity is inhibited. The authors found this with many of the genes they looked at. Additionally, they found that of the genes known to be activated by STAT1, 85% of these were single GAS sites rather than tandem GAS sites.

Finally, we considered how STAT3 interacts with STAT1 and affects gene expression. Figure 5.24 shows the gene expression of STAT1 after activation by IFN- γ . In these experiments cell lines were stimulated with low levels of IFN- γ to produce low concentrations of STAT1. The cells fell into three categories STAT3 KO, where

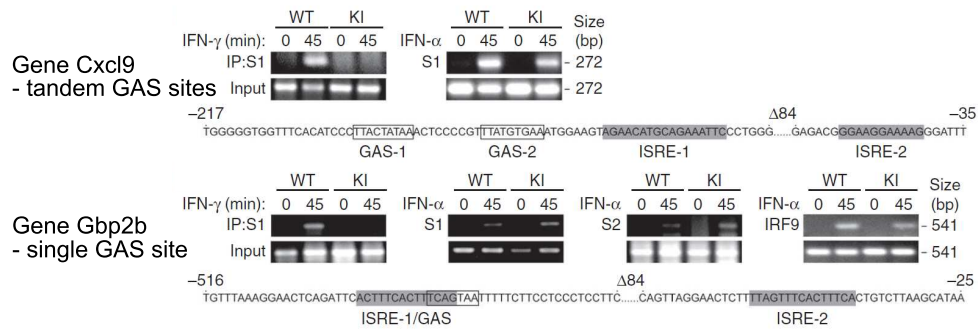


Figure 5.3: Example of STAT recruitment to a genes with (a) tandem GAS sites and (b) a single GAS site. These gels show that wildtype STAT1 binds to the gene cooperatively in both cases. Adapted from [11].

no STAT3 was activated, IFN- γ stimulation only, resulting in a very low concentration of STAT3 or IFN- γ and IL-6 stimulation, resulting in a high concentration of activated STAT3. The gene response was recorded in each case and found to be the same. All the cells were then boosted with high levels of IFN- γ , increasing the STAT1 concentration. STAT1 High refers to STAT1 after additional boosting with IFN- γ . When STAT1 is boosted to higher concentrations in the presence of STAT3, the gene expression is much reduced which we theorise is due to STAT3 competing for binding space with STAT1 [U. Vinkemeier, personal communication, 2013]. We will test this with modelling.

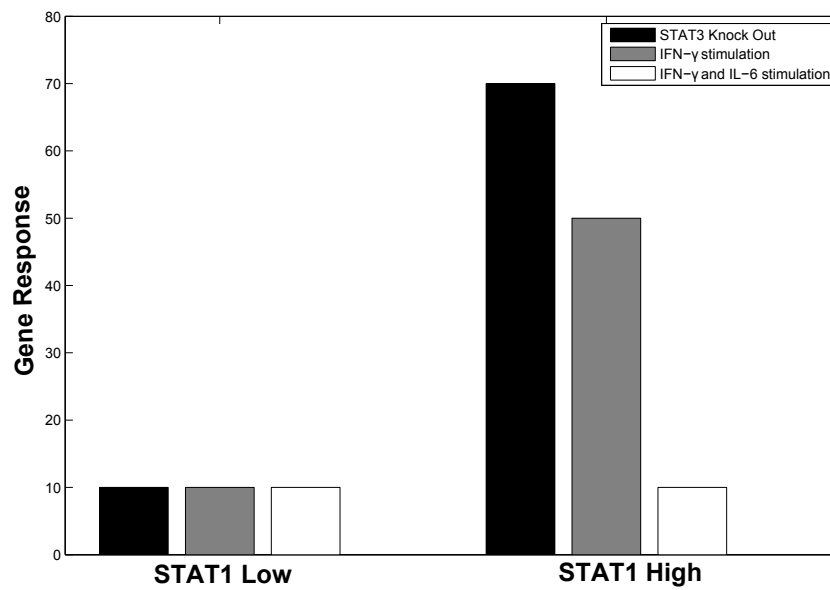


Figure 5.4: The gene expression of STAT1 with either no STAT3 (black) a low amount of STAT3 through cross stimulation (grey) or high STAT3 (white) after activation with IFN- γ and boosted with further IFN- γ to achieve higher STAT1 activation [U. Vinkemeier, personal communication 2013]. When we have low STAT1 the presence of STAT3 makes no difference to STAT1 binding. At higher concentrations of STAT1 the presence of STAT3 affects STAT1 binding.

5.3 Cooperative Binding Model

5.3.1 Model Rationale

In this model we consider free STAT1 dimers binding to promoter regions of DNA (Figure 5.5).

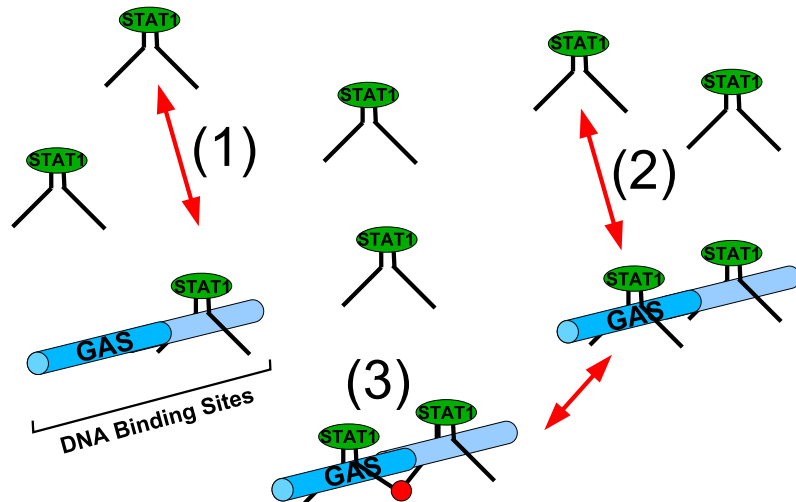
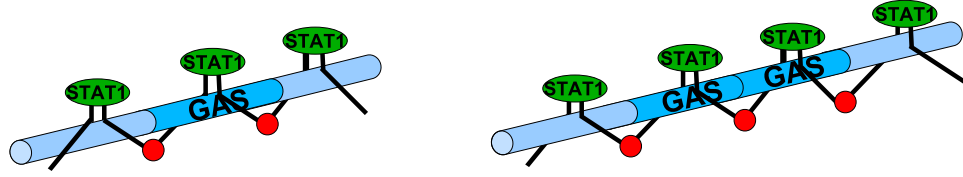


Figure 5.5: Diagram showing binding of STAT1 dimers to DNA in the cooperative binding model. Activated STAT1 dimers can bind to both the non-GAS DNA binding sites (1) and the GAS DNA binding sites (2). Adjacent bound STAT1 dimers can then polymerise (3). STAT1 dimers bind to the GAS and non-GAS sites with different affinities.

We produce three variations of the model with two, three and four binding sites. The two-site model replicates the typical *in vitro* situation where, generally, two binding sites are analysed. This may either be a double GAS site or a single GAS site adjacent to a non-GAS site. We also use a symmetric single GAS site and symmetric double GAS site model where we have either a single or double GAS site with a non-GAS site at either side (Figure 5.6). These models are closer to the *in vivo* situation where the GAS sites exist on the DNA strand.

Once bound to DNA, STAT1 dimers may form polymers with STAT1 dimers on adjacent sites leading to the formation of tetramers and longer polymers. We allow dimers to unbind from DNA and from each other. Polymer units cannot



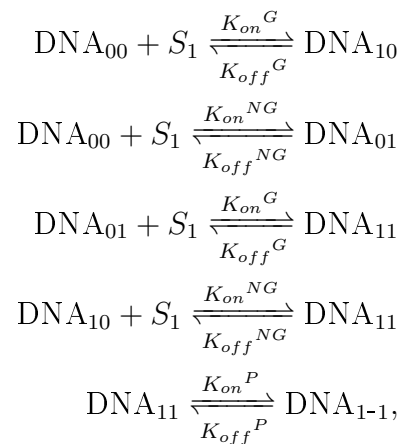
Single GAS site model

Double GAS site model

Figure 5.6: Diagram showing some of the binding possibilities in the symmetric single and double GAS site models. Activated STAT1 dimers can bind to either the central GAS binding sites or the non-GAS binding sites. This situation is more biologically feasible than the typical experimental two-site model.

unbind from DNA without first breaking down into dimers. The GAS sites have different binding rates to the non-GAS sites. We have three pairs of reaction rates, each containing an *on* and *off* rate. These are STAT-DNA binding rates at the GAS site, STAT-DNA binding rates at the non-GAS site and polymerisation rates (Figure 5.7). We neglect spatial dynamics, nuclear cycling and degradation in this model.

We model the system using mass action kinetics. The reactions for the two site model are,



where S_1 is the concentration of STAT1 dimers and the DNA sites are denoted

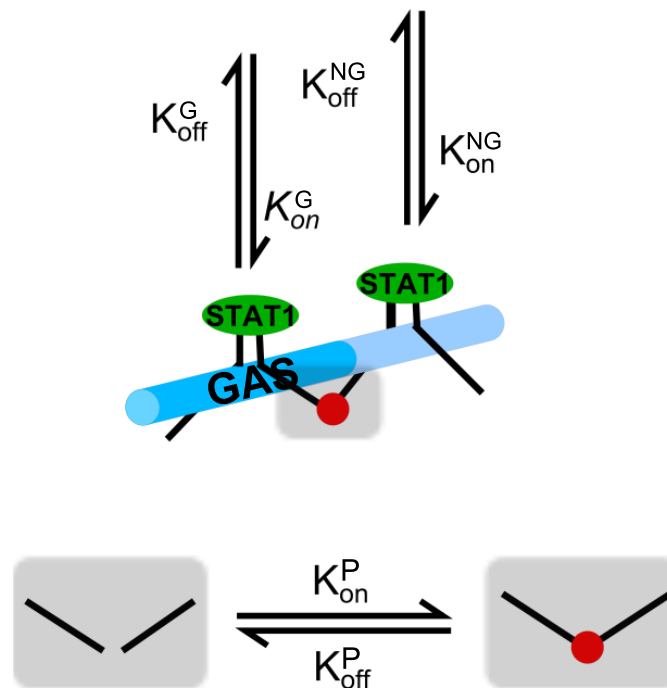
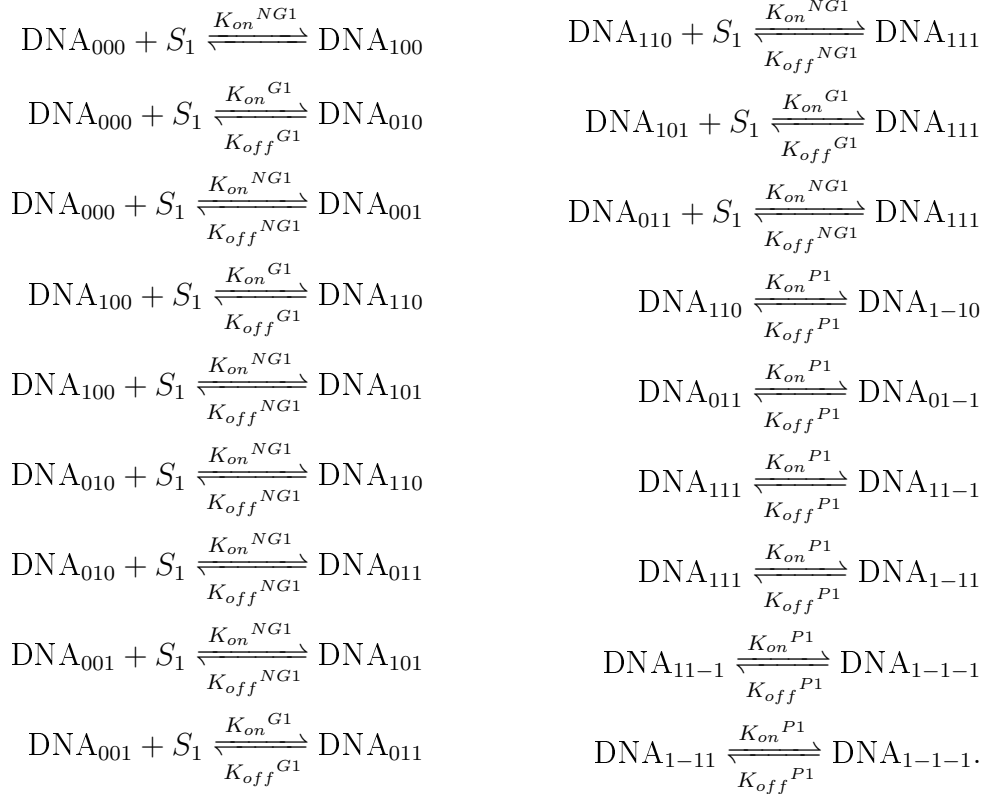


Figure 5.7: Diagram showing model parameters used in all the cooperative binding models. K_{on}^G and K_{on}^{NG} are the binding rates for STAT-DNA binding at GAS and non-GAS sites, respectively. Similarly, K_{off}^G and K_{off}^{NG} are the unbinding rates at the GAS and non-GAS sites. K_{on}^P and K_{off}^P are the binding and unbinding rates for bound STAT polymerisation reactions.

DNA_{XX} , where each subscript represents one of the sites of the DNA segment. The subscripts may take the value 0 or 1, representing an unbound site or a STAT1 bound site. For example, DNA_{01} is a length of DNA with a STAT1 dimer bound to site 2, the non-GAS site. Cooperative binding results in dimer-dimer bonds and these are denoted by a dash (-). Hence DNA_{1-1} , denotes a length of DNA with a STAT1 tetramer bound.

The symmetric single GAS site model has fourteen variables, and eighteen reversible reactions, composed of 12 STAT1-DNA binding reactions and 6 polymerisation reactions as follows:



The symmetric double GAS site model has 32 reversible STAT-DNA binding reactions and 25 polymerisation reaction, which are listed in Appendix B. We use Copasi [62] to generate ODEs from these reactions and to simulate the three systems. Algebraic analysis of these models is not practical due to the number of

Parameter or variable	Initial Conditions
DNA ₀₀ , DNA ₀₀₀ & DNA ₀₀₀₀	0.1nM
$S1$	varies
K_{on}^{G1}	$2 \times 10^{10} \text{M}^{-1} \text{s}^{-1}$
K_{off}^{G1}	100s^{-1}
K_{on}^{NG1}	$2 \times 10^{10} \text{M}^{-1} \text{s}^{-1}$
K_{off}^{NG1}	varies
K_{off}^P	100s^{-1}
K_{on}^P	$1000-60000 \text{s}^{-1}$
Resulting dissociation constants	
K_d^G	$5 \times 10^{-9} \text{M}$
K_d^{NG}	varies
K_d^P (high)	0.0017-0.1

Table 5.1: Parameter variations and initial conditions in cooperative binding models

variables.

In the simulations to follow we vary K_{on}^P , K_{off}^{NG} and the initial STAT1 concentration. The other parameters and initial conditions are fixed (summarised in Table 5.1). We start the simulations with only unbound DNA promoter fragments, at a concentration of 0.1nM , and free STAT1 dimers, whose concentration was varied in each simulation. The STAT-DNA binding rate used at the GAS sites is $2 \times 10^{10} \text{M}^{-1} \text{s}^{-1}$ and the unbinding rate is 100s^{-1} . This gives the dissociation constant a value of $5 \times 10^{-9} \text{M}$, in line with experimental results [1]. The STAT-DNA binding at the non-GAS sites retain the same on-rate as the GAS site, $2 \times 10^{10} \text{M}^{-1} \text{s}^{-1}$. The polymerisation rate parameters are set to either high or low cooperativity, with a 60-fold difference between the two groups in line with the difference between the polymerisation rates of wild-type STAT1 and mutant with a truncated N-domain [127]. The off-rate in both cases is 100s^{-1} and the on-rate is 1000s^{-1} in the low cooperativity case and 60000s^{-1} in the high cooperativity

case.

In order to make comparison with experimental results we use several results measures. The main measure we use is fractional GAS site occupancy, which we believe to be proportional to gene response. In the two site and single GAS site model this is the proportion of the DNA with the GAS site occupied by STAT1. Since the double GAS site model is symmetric, the fractional GAS site occupancy at each GAS site is identical. Hence, we can measure the results at either site. We also break this down by concentration of dimers and larger polymers, since some experimental methods are able to differentiate them by molecular weight.

5.3.2 Model Simulations

We know from experimental work that STAT1 binds well to DNA and is bound both as dimers and polymers [1]. When cooperative binding is inhibited, via mutation of the N-domain of the protein, DNA binding is much reduced [6]. We can replicate this mutant in the model by reducing the polymerisation on-rate. Experimental work suggests a 60-fold difference between wildtype and mutant binding rates [U Vinkemeier, personal communication 2013]. Figure 5.8 shows a time course simulation for the two site model with high cooperativity and low cooperativity, with a 60-fold difference in the polymerisation on rate. The STAT-DNA binding rates are the same on both sites, representing a double GAS site. Here we see that fractional GAS site occupancy is reduced from 1 to approximately 0.35 by the altered polymerisation rate. This is in line with experimental results that showed a reduction in nuclear mobility of STAT1 in the mutant compared to wildtype (see Figure 5.2b) [6].

For these simulations we assume a fixed initial STAT1 concentration and a double GAS site. It is likely that the STAT1 response, and therefore concentration, varies both between cells and with different stimuli. We also know that there are many

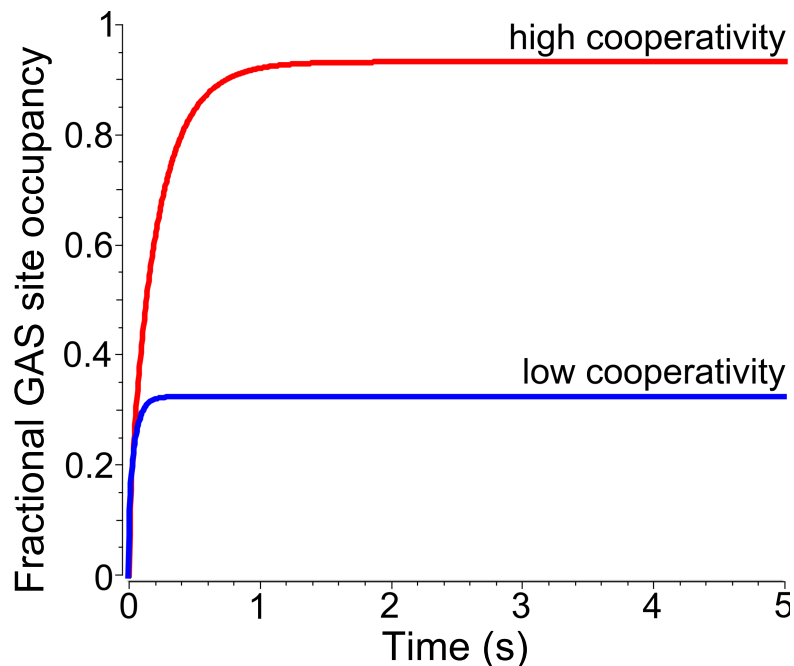


Figure 5.8: Time course simulation of free STAT1 binding to DNA in double GAS site (two site) cooperative model. When cooperativity is inhibited the fractional occupancy of the GAS site is much reduced. We set $K_{on}^P = 60000s^{-1}$ where we have cooperativity and $K_{on}^P = 1000s^{-1}$ to inhibit cooperativity. ($K_{on}^G = K_{on}^{NG} = 2 \times 10^{10} M^{-1} s^{-1}$, $K_{off}^G = K_{off}^{NG} = 100s^{-1}$, $K_{off}^P = 100s^{-1}$)

functional single GAS sites with a non-GAS site adjacent. A typical difference between the binding rate of a GAS and non-GAS site is 50-fold [11] so we simulated the model with this difference for a range of initial STAT1 concentrations. Figure 5.9 shows the single GAS site simulations compared to a double GAS site in the two site model. We can see that a single GAS site, as might be expected, will attain less GAS site occupancy than the double GAS site for a given STAT1 concentration. However, we can also see that for any particular level of GAS site occupancy for the double GAS site, the same level can be achieved at the single GAS site, with a higher STAT1 concentration.

The two site model artificially limits the length of polymers to tetramers or smaller there is no biological reason or evidence that longer polymers do not form. For this reason it is more useful to consider the single or double GAS sites as part of a longer chain, and for this we use the single GAS site model in a three-site chain and

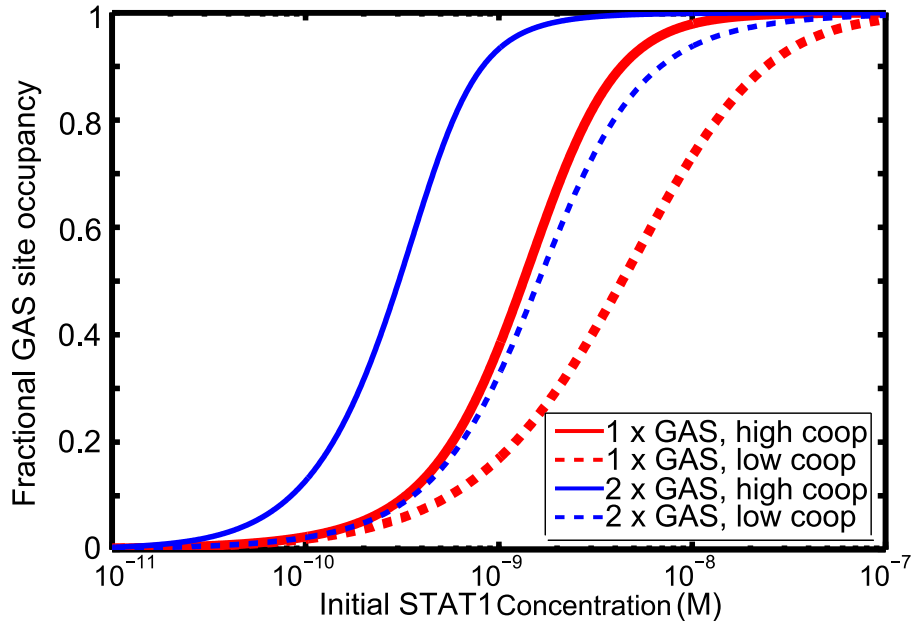


Figure 5.9: Plot of fractional GAS site occupancy against initial free STAT1 concentration for both single and double gas sites in the two site model. The plot shows that single GAS sites can attain the same occupancy as double GAS site but requires a greater STAT1 concentration. We set $K_{on}^P = 60000s^{-1}$ where we have cooperativity and $K_{on}^P = 1000s^{-1}$ to inhibit cooperativity. In the single GAS site simulations $K_{off}^{NG} = 5000s^{-1}$; in the double GAS site simulation $K_{off}^{NG} = 100s^{-1}$. ($K_{on}^G = K_{on}^{NG} = 2 \times 10^{10}M^{-1}s^{-1}$, $K_{off}^G = 100s^{-1}$, $K_{off}^P = 100s^{-1}$)

the double GAS site model in a four-site chain. Repeating the previous simulations in these models we see that the same behaviour is observed (Figure 5.10). Here for a GAS site occupancy of either 90% or 99% in the single site model we required roughly a three-fold increase in the initial STAT1 concentration compared to the double GAS site model, regardless of whether we have cooperativity (Figure 5.11a).

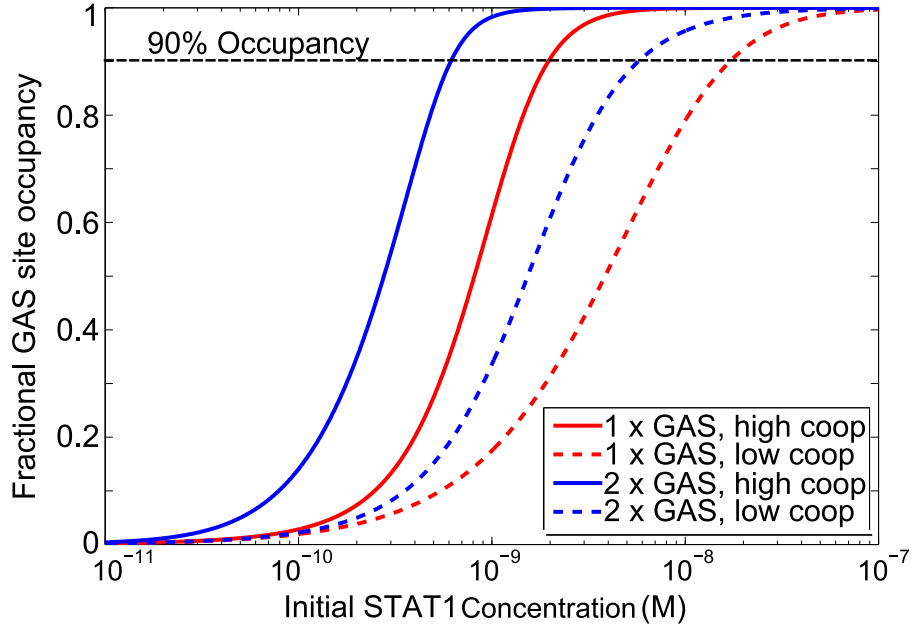


Figure 5.10: Plot of fractional GAS site occupancy against initial free STAT1 concentration for both the symmetric single and symmetric double gas site models. The plot shows that single GAS sites can attain the same occupancy as double GAS site but requires a greater STAT1 concentration. We set $K_{on}^P = 60000s^{-1}$ where we have cooperativity and $K_{on}^P = 1000s^{-1}$ to inhibit cooperativity. In the single GAS site simulations $K_{off}^{NG} = 5000s^{-1}$; in the double GAS site simulation $K_{off}^{NG} = 100s^{-1}$. ($K_{on}^G = K_{on}^{NG} = 2 \times 10^{10}M^{-1}s^{-1}$, $K_{off}^G = 100s^{-1}$, $K_{off}^P = 100s^{-1}$)

Figure 5.11b, based on the data in Figure 5.10, also shows that the loss of cooperativity would necessitate an 9-fold increase in STAT1 to reach the 90% occupancy level. If a 99% occupancy level is required then the reduction in cooperativity would require a 13-fold increase at the single gas site and a 22-fold increase at the double GAS site.

In experimental models, boosting of STAT1 concentration by increasing the stim-

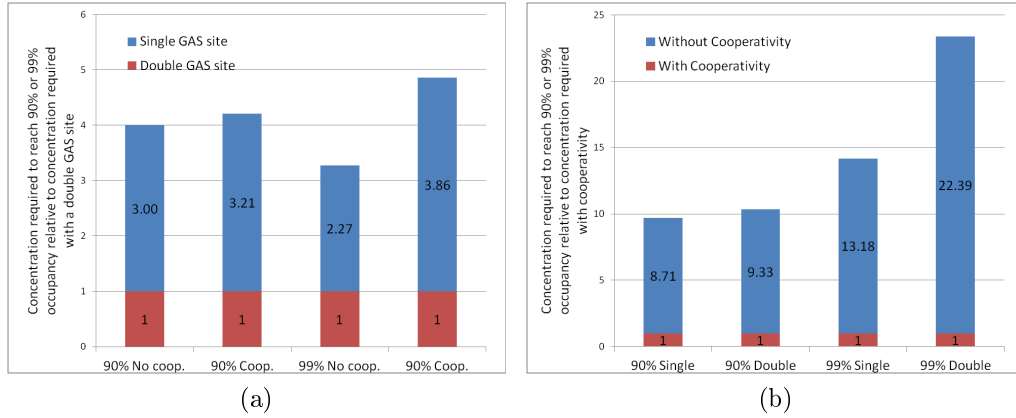


Figure 5.11: Plot of relative increasing in concentration required to compensate for: (a) the presence of only a single GAS site rather than a double GAS site with and without cooperativity at both 90% and 99% fractional GAS site occupancy; (b) the loss of cooperativity, at both 90% and 99% fractional GAS site occupancy for both the symmetric single and symmetric double gas site models. We set $K_{on}^P = 60000s^{-1}$ where we have cooperativity and $K_{on}^P = 1000s^{-1}$ to inhibit cooperativity. In the single GAS site simulations $K_{off}^{NG} = 5000s^{-1}$; in the double GAS site simulation $K_{off}^{NG} = 100s^{-1}$. ($K_{on}^G = K_{on}^{NG} = 2 \times 10^{10} M^{-1} s^{-1}$, $K_{off}^G = 100s^{-1}$, $K_{off}^P = 100s^{-1}$)

ulus can achieve up to approximately a three-fold increase. If this is indicative of the range of variation of STAT1 levels we may see *in vivo*, it implies two conclusions. Firstly, that double GAS sites are not required for effective gene response, since single GAS sites can achieve the same levels of occupancy, within the range of activated STAT1 concentrations we may achieve with boosting. Secondly, that cooperativity is essential to gene response, since to achieve the required levels of GAS site occupancy without cooperativity would require unrealistically high levels of activated STAT1.

The final source of natural variation that we consider is the strength of the non-GAS site compared to the GAS site. The non-GAS site *in vivo* will vary in the number of matching base pairs, and less matching base pairs leads to lower affinity. Hence, the affinity of this site will vary for different genes. The difference in K_{off}^{NG} between the GAS and non-GAS sites could be as much as 200-fold [U Vinkemeier, personal communication 2013]. Figure 5.12 shows the fractional GAS

site occupancy against initial STAT1 concentration for a range of different non-GAS site binding strengths relative to the GAS site binding strength in both the single and double GAS site models. As the non-GAS site binding rate gets weaker in the single GAS site model the fractional GAS site occupancy reduces quite significantly. In the double GAS site model, the reduction in binding strength of the non-GAS sites has much less effect; presumably the tetramerisation on the GAS sites is sufficient to retain the GAS site occupancy. In the single site case, the strength of the surrounding sites is much more important.

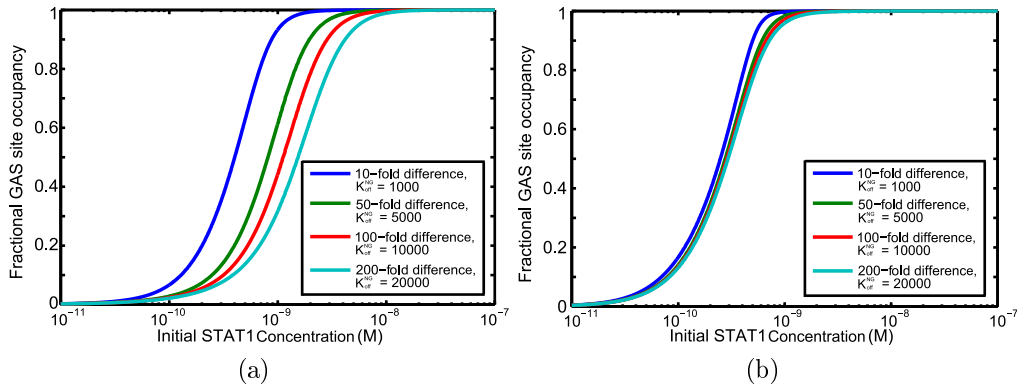


Figure 5.12: Plot of fractional GAS site occupancy against initial free STAT1 concentration for differing strengths of non-GAS site binding in the (a) single symmetric and (b) double symmetric GAS site models. The plots shows that in the single GAS site model GAS site occupancy reduces much more with increasing difference between GAS and non-GAS binding strength than in the double GAS site case. ($K_{on}^P = 60000 \text{ s}^{-1}$, $K_{off}^P = 100 \text{ s}^{-1}$, $K_{on}^G = K_{on}^{NG} = 2 \times 10^{10} \text{ M}^{-1} \text{ s}^{-1}$, $K_{off}^G = 100 \text{ s}^{-1}$)

5.4 Competitive Binding Model

5.4.1 Model Rationale

In the competitive binding model we extend the previous model to consider an additional species of STAT protein, STAT3. STAT1 behaves exactly as in the simpler model. STAT3, however, does not polymerise as readily. We therefore consider two scenarios (i) no cooperative binding of STAT3 (also comparable to a STAT mutant with cooperative binding inhibited) and (ii) a small amount of STAT3 cooperative binding compared to STAT1. We have STAT3-DNA binding on- and off- rates for both GAS and non-GAS sites and STAT3 polymerisation on- and off rates which are minimal. STAT1 and STAT3 may bind to adjacent DNA sites, but cannot bind with each other. We consider three different lengths of DNA segment: two, three and four (Figure 5.13). The reactions for each of these DNA lengths are listed in Appendix B.

We refer to STAT1 homodimers as S1 and STAT3 homodimers as S3. The DNA sites are denoted DNA_{XXX} , where each subscript represents one of the sites of the DNA segment. The subscripts may take the value 0, 1 or 3 representing an unbound site, a STAT1 bound site or a STAT3 bound site respectively. For example, DNA_{301} , is a length of DNA with a STAT3 dimer bound to site 1 (from left to right) and a STAT1 dimer bound to site 3. Cooperative binding results in dimer-dimer bonds and these are denoted by a dash (-) hence DNA_{1-10} , denotes a length of DNA with a STAT1 tetramer bound.

We have little data on binding rates for STAT3. We set the concentration of DNA, and the GAS and non-GAS on-rates to 1, and make all other concentrations and rates relative to these on-rates.

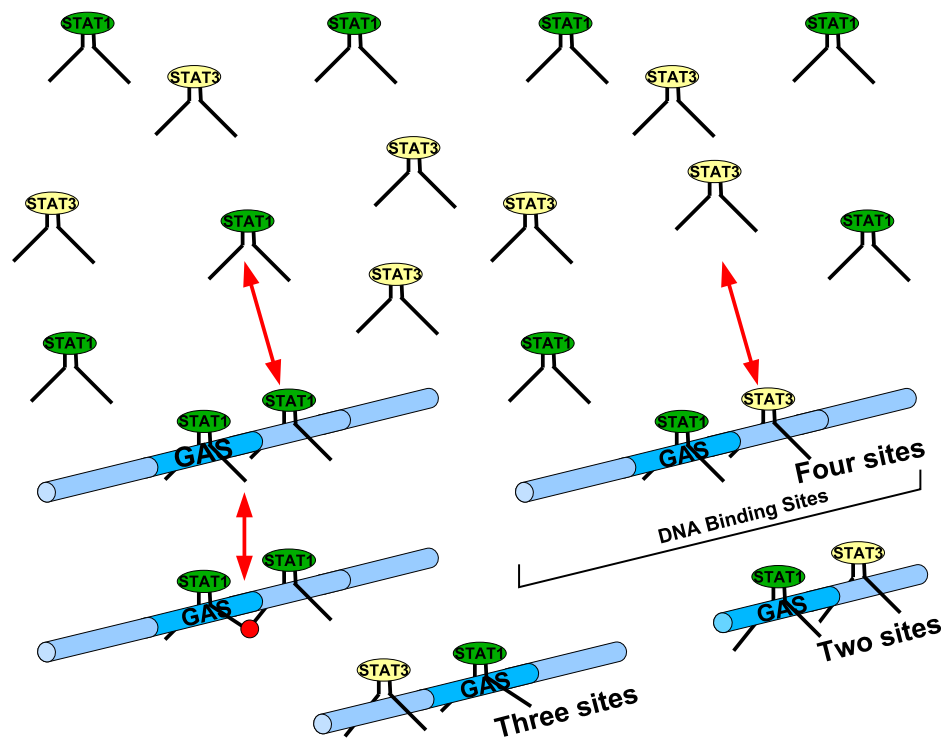


Figure 5.13: Diagram showing binding of STAT1 and STAT3 dimers to DNA in the competitive binding model. Activated STAT1 and STAT3 dimers can bind to the DNA binding sites and polymerise although STAT1 polymerises more readily than STAT3. Three variants of the model are considered, with 2, 3 or 4 binding sites. The GAS site position in each case is highlighted.

5.4.2 Model Simulations

The experimental data suggest that at high concentrations of STAT1 the presence of STAT3 dimers should reduce the amount of STAT1 that is bound to the GAS site, whilst at low concentrations of STAT1 we should not see this effect (Figure 5.24b). We believe this to be due to the STAT3 dimers competing with STAT1 at high concentrations to bind to DNA, hence interrupting the cooperative binding of STAT1. If this is the case we should be able to find parameters that demonstrate this behaviour.

No cooperative STAT3 binding

We ran several simulations for different initial concentrations of STAT1 and STAT3 using the two site model. In each simulation the fractional occupancy of the GAS site by STAT1 was recorded at steady state and plotted against STAT1 concentration (Figure 5.14).

We consider four different initial concentrations of STAT3. The simulation with a low STAT3 concentration represents a situation where only IFN- γ pathways are stimulated leading to activation of STAT1 and a small amount of STAT3 activation (STAT3 is known to be weakly activated by IFN- γ). As STAT1 concentration increases the occupation of the GAS site increases up to a limit close to one. Simulations with a higher STAT3 concentration (STAT3 mid and high) represent a situation where both the IFN- γ and the IL-6 pathways are stimulated leading to both STAT1 and STAT3 activation. In this situation, when the STAT1 concentration is low, the response is close to that seen for STAT3 low. As the STAT1 concentration increases the response seen deviates from the response at lower STAT3 concentrations, and the fractional occupation of the GAS site is lower. When the STAT3 concentration is zero (STAT3 KO) the response curve is very similar to STAT3 low. However at high STAT1 concentrations the response is slightly higher. When the

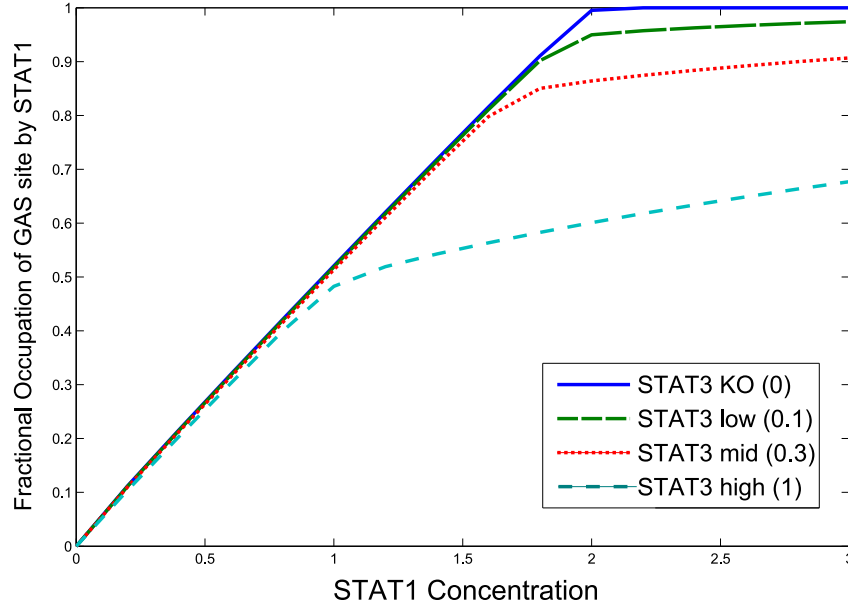


Figure 5.14: Plot of fractional occupation of the DNA GAS site against the initial concentration of free STAT1. The values are taken at steady state. The parameter values are: $K_{off}^{G1} = 0.01$; $K_{off}^{NG1} = 0.1$; $K_{off}^{G3} = 0.0001$; $K_{off}^{NG3} = 0.001$; $K_{off}^{P1} = 0.001$; $K_{on}^{G1} = K_{on}^{NG1} = K_{on}^{G3} = K_{on}^{NG3} = K_{on}^{P1} = 1$; $K_{on}^{P3} = K_{off}^{P3} = 0$

cooperative binding of STAT1 is turned off ($K_{on}^{P1} = 0$) but all other parameters kept the same the levels of GAS site occupation are similar to when cooperativity is on (Figure 5.15 compared to Figure 5.14), suggesting that if polymers cannot form, the GAS sites become occupied by STAT1 dimers. This is not the case *in vivo*, since without polymerisation gene response is much reduced [6]. Hence it is likely that the parameters we use here are not of similar magnitudes to those *in vivo*.

In order for the model display behaviour as seen *in vivo*, the disassociation rate of STAT1 binding to DNA needs to be increased further, and we do this by increasing the parameters K_{off}^{G1} and K_{off}^{NG1} . It is conventionally assumed that STAT3 and STAT1 dissociation constants are relatively similar, since their structure is so similar. However, if we make STAT3 *off* rates the same as STAT1 *off* rates then at steady state STAT1 dominates, since it is able to polymerise and we do not see the results observed experimentally (Figure 5.16). Hence, we keep the STAT3

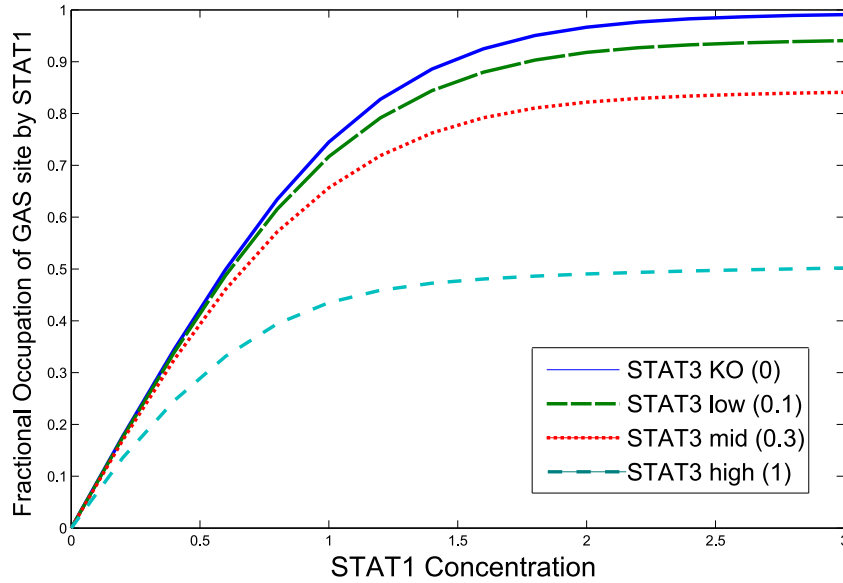


Figure 5.15: Plot of Fractional occupation of the DNA GAS site against the initial concentration of free STAT1. The values are taken at steady state. The parameter values are: $K_{off}^{G1} = 0.01$; $K_{off}^{NG1} = 0.1$; $K_{off}^{G3} = 0.0001$; $K_{off}^{NG3} = 0.001$; $K_{off}^{P1} = 0.001$; $K_{on}^{G1} = K_{on}^{NG1} = K_{on}^{G3} = K_{on}^{NG3} = 1$; $K_{on}^{P1} = K_{on}^{P3} = K_{off}^{P3} = 0$

dissociation rate small.

Figure 5.17 shows that increasing the STAT1 dissociation rate and maintaining the STAT3 rate lowers the GAS site occupation when there is no cooperativity as required (Figure 5.17a). An undesirable effect of this rate change is that the differences between different concentrations of STAT3 is greater even at low concentrations of STAT1 (Figure 5.17b).

We now look at increasing the number of DNA sites, and hence the maximum length of STAT1 polymers. Using the same rate parameters as in the two-site model and increasing the STAT1 and STAT3 concentrations proportionally to account for the additional DNA binding sites, the results (Figure 5.18) can be compared with Figure 5.17a and look quite similar.

However, with three sites we can consider higher concentrations of STAT3 (Figure 5.19), which will give a larger decrease in occupancy at higher STAT1 concentration. In the two site model, these larger concentrations resulted in large differences

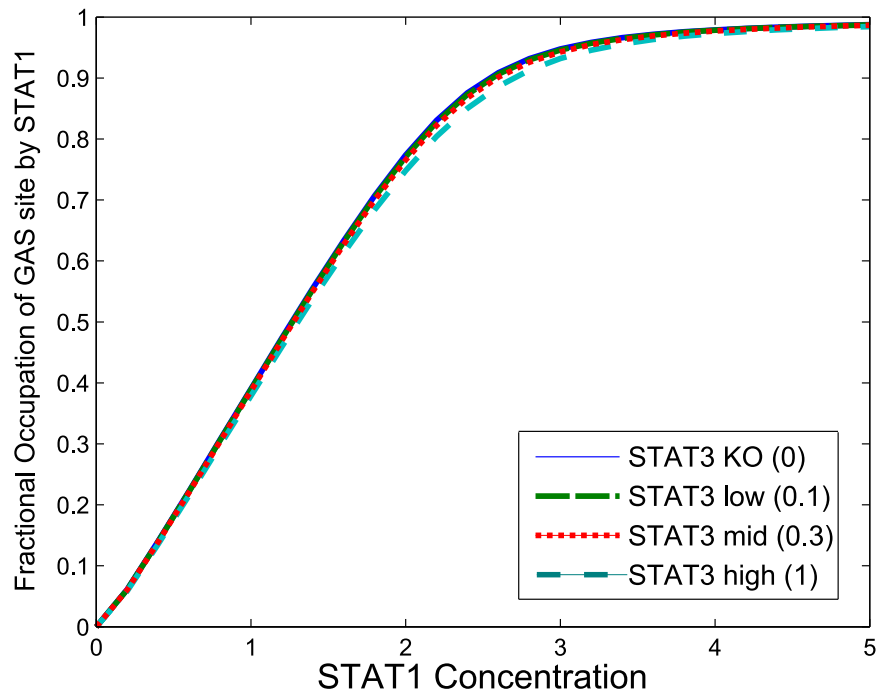


Figure 5.16: Plot of Fractional occupation of the DNA GAS site against the initial concentration of free STAT1, with no cooperative binding and larger STAT-DNA binding *off* rates compared to Figure 5.15. The values are taken at steady state. The parameter values are: $K_{off}^{G1} = 2$; $K_{off}^{NG1} = 20$; $K_{off}^{G3} = 2$; $K_{off}^{NG3} = 20$; $K_{off}^{P1} = 0.001$; $K_{on}^{G1} = K_{on}^{NG1} = K_{on}^{G3} = K_{on}^{NG3} = K_{on}^{P1} = 1$; $K_{on}^{P3} = K_{off}^{P3} = 0$

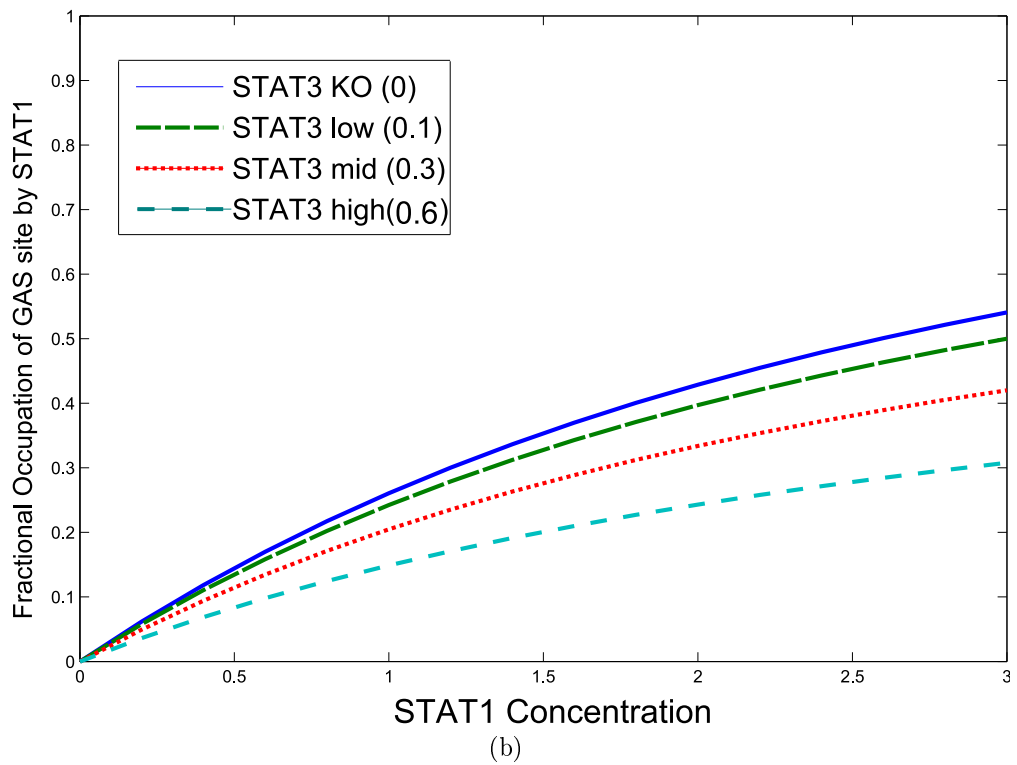
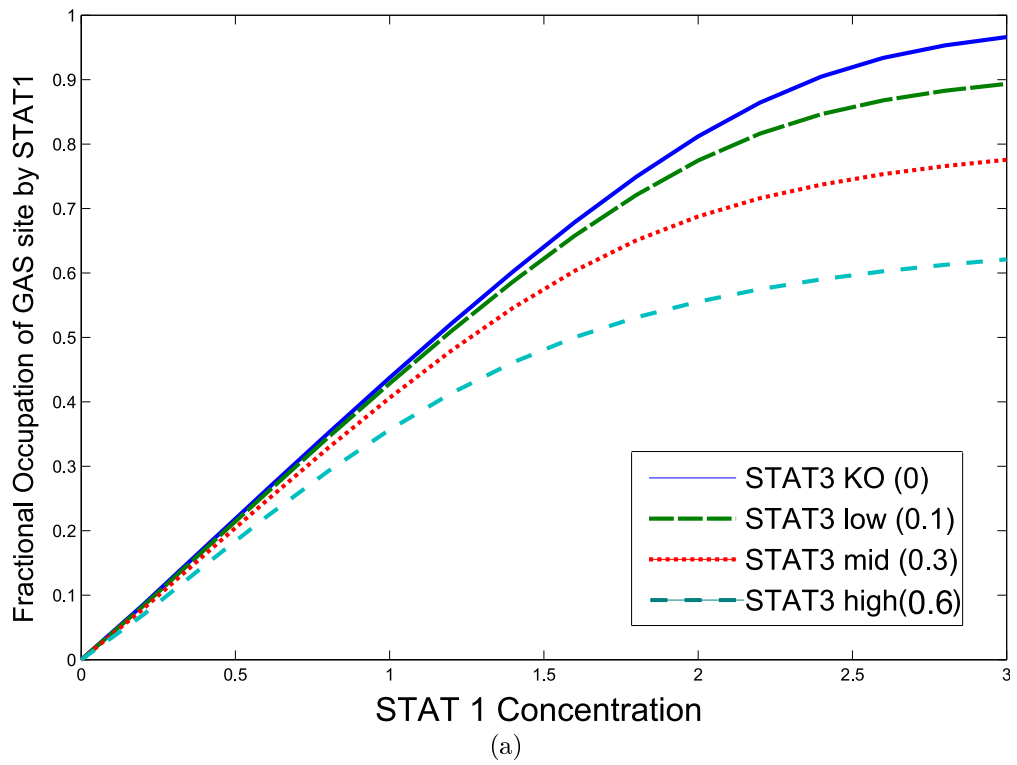


Figure 5.17: Plot of Fractional occupation of the DNA GAS site against the initial concentration of free STAT1, with and without cooperative binding. The values are taken at steady state. a) $K_{on}^{P1} = 1$ b) $K_{on}^{P1} = 0$. (The other parameter values are: $K_{off}^{G1} = 2$; $K_{off}^{NG1} = 20$; $K_{off}^{G3} = 0.0001$; $K_{off}^{NG3} = 0.001$; $K_{off}^{P1} = 0.001$; $K_{on}^{G1} = K_{on}^{NG1} = K_{on}^{G3} = K_{on}^{NG3} = 1$; $K_{on}^{P3} = K_{off}^{P3} = 0$)

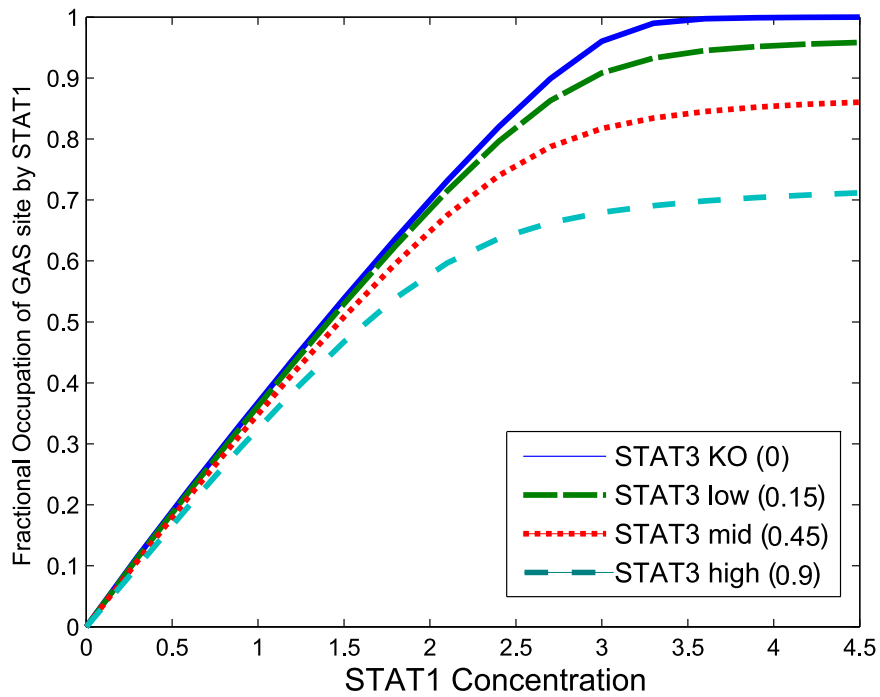


Figure 5.18: Plot of Fractional occupation of the DNA GAS site against the initial concentration of free STAT1 in the three site model. The values are taken at steady state. The parameter values are: $K_{off}^{G1} = 2$; $K_{off}^{NG1} = 20$; $K_{off}^{G3} = 0.0001$; $K_{off}^{NG3} = 0.001$; $K_{off}^{P1} = 0.001$; $K_{on}^{G1} = K_{on}^{NG1} = K_{on}^{G3} = K_{on}^{NG3} = 1$; $K_{on}^{P1} = 1$; $K_{on}^{P3} = K_{off}^{P3} = 0$

in occupancy at lower concentrations also. The difference in occupancy at lower concentrations in the three site model is still greater than the experimental results suggest (experimental results suggested the occupancy was unchanged), which may point to there being some level of STAT3 polymerisation, as discussed in the next section.

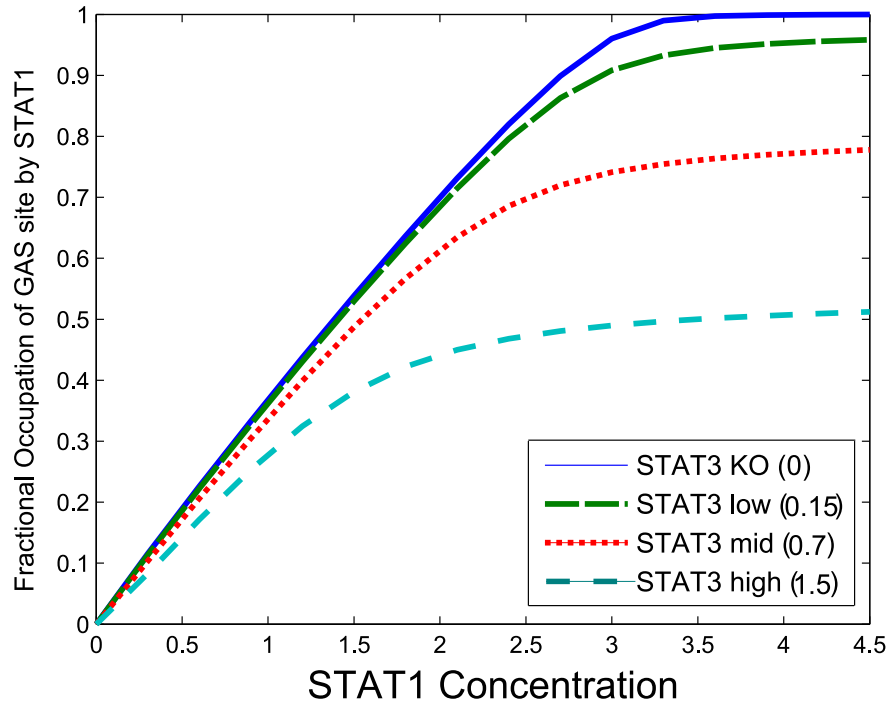


Figure 5.19: Plot of Fractional occupation of the DNA GAS site against the initial concentration of free STAT1 in the three site model. The values are taken at steady state. The parameter values are: $K_{off}^{G1} = 2$; $K_{off}^{NG1} = 20$; $K_{off}^{G3} = 0.0001$; $K_{off}^{NG3} = 0.001$; $K_{off}^{P1} = 0.001$; $K_{on}^{G1} = K_{on}^{NG1} = K_{on}^{G3} = K_{on}^{NG3} = 1$; $K_{on}^{P1} = 1$; $K_{on}^{P3} = K_{off}^{P3} = 0$

If we extend the model to four sites and again increase the STAT1 and STAT3 concentrations to account for the additional DNA binding site, the results (Figure 5.20) can be compared with Figure 5.18 and follow the same trend. With higher concentrations of STAT3, Figure 5.21 can be compared with Figure 5.19 in the three site model. These results show that the addition of another site increases the difference in GAS site occupancy at higher STAT1 concentrations, but also has a large effect on the difference at lower concentrations. Additionally at higher

STAT3 concentrations the shape of the curve as STAT1 is increased also starts to become sigmoidal, as the STAT3 concentration relative to STAT1 concentration increases.

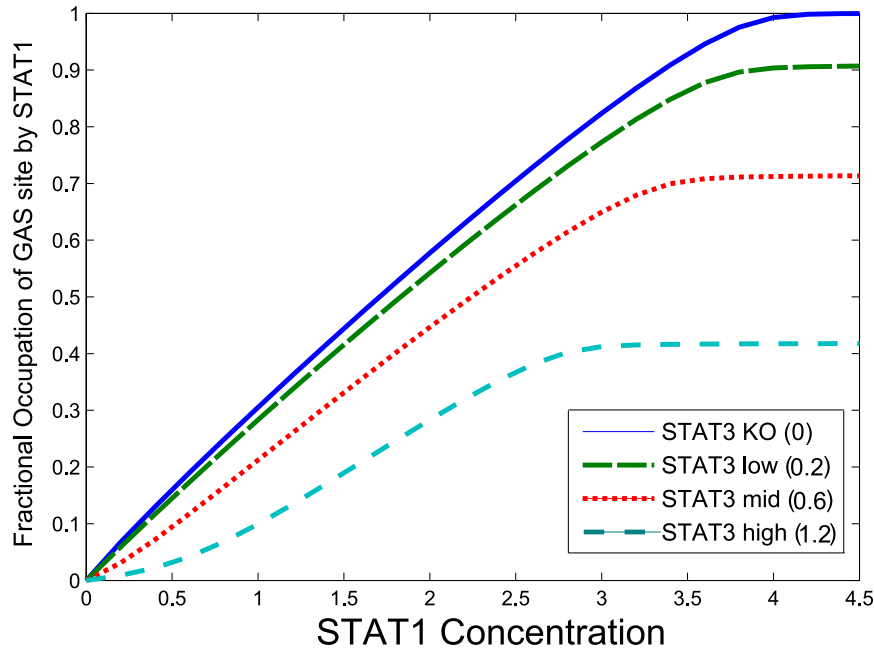


Figure 5.20: Plot of fractional occupation of the DNA GAS site against the initial concentration of free STAT1 in the four site model. The values are taken at steady state. The parameter values are: $K_{off}^{G1} = 2$; $K_{off}^{NG1} = 20$; $K_{off}^{G3} = 0.0001$; $K_{off}^{NG3} = 0.001$; $K_{off}^{P1} = 0.001$; $K_{on}^{G1} = K_{on}^{NG1} = K_{on}^{G3} = K_{on}^{NG3} = 1$; $K_{on}^{P1} = 1$; $K_{on}^{P3} = K_{off}^{P3} = 0$

So far the results have shown that introduction of STAT3 dimers does affect the fractional occupancy of GAS sites by STAT1, due to reducing the amount of STAT1 cooperative binding. We have also shown that this has a much greater effect at higher STAT1 concentrations than at lower concentrations where there is less competition for binding sites. However, the reduction in occupancy that we see at lower STAT1 concentrations is still of greater magnitude than experimental results. This may be due the assumption we have made that there is no cooperative binding of STAT3. Cooperative binding of STAT3 would increase the time that STAT3 remains on DNA and so could potentially account for this discrepancy. In the next section we assume a small amount of STAT3 cooperative binding.

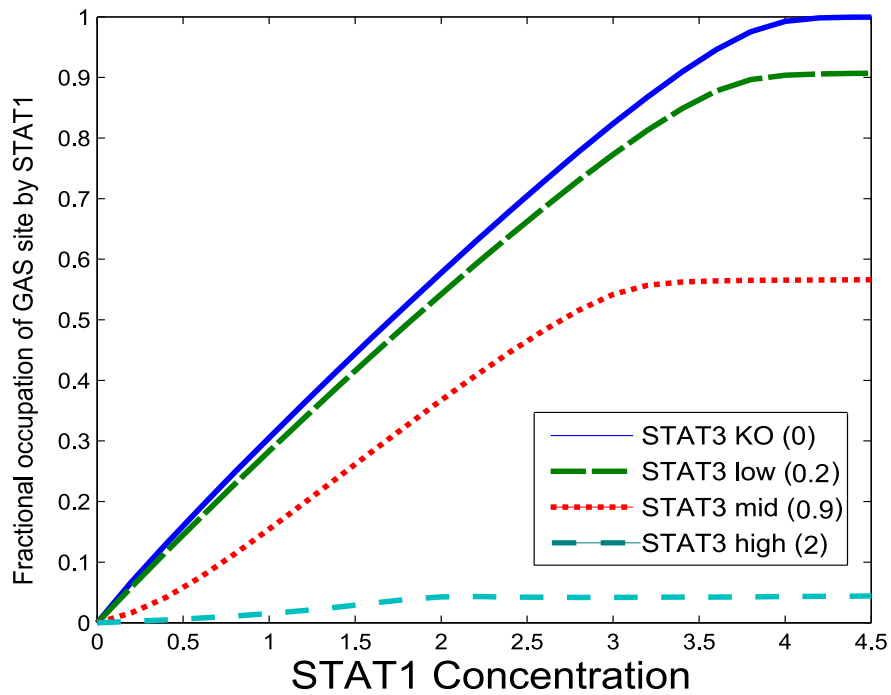


Figure 5.21: Plot of fractional occupation of the DNA GAS site against the initial concentration of free STAT1 in the four site model. The values are taken at steady state. The parameter values are: $K_{off}^{G1} = 2$; $K_{off}^{NG1} = 20$; $K_{off}^{G3} = 0.0001$; $K_{off}^{NG3} = 0.001$; $K_{off}^{P1} = 0.001$; $K_{on}^{G1} = K_{on}^{NG1} = K_{on}^{G3} = K_{on}^{NG3} = 1$; $K_{on}^{P1} = 1$; $K_{on}^{P3} = K_{off}^{P3} = 0$

Minimal cooperative STAT3 binding

The simulations from the previous section were repeated with the addition of a small amount of cooperative STAT3 binding. The results for the two site model (Figure 5.22) show that this increases the fractional occupation of the GAS site by STAT1 slightly, decreasing the effect seen in Figure 5.17a. Whilst this may seem counterintuitive, a close look at the differences in each variable provides the reason for this result. With no cooperative binding of STAT3, the STAT3 molecules are free to move on and off the DNA and spend a proportion of the time bound to DNA with an adjacent STAT1 molecule which restricts polymerisation of STAT1. With the addition of cooperative binding of STAT3, the free STAT3 molecules are more likely to become tightly bound to the DNA in the form of STAT3 tetramers. Hence there are less STAT1-STAT3 bound DNA sites, increasing the opportunities for STAT1 cooperative binding since there are more unbound double DNA sites.

Importantly, at lower STAT1 concentrations, the curves of Fig 5.22 are pulled closer together, and resemble more closely the response we see in the experimental results. This is quite subtle in the two site model but more obvious as the number of sites increases.

Adding cooperative binding of STAT3 into the three site model (Figure 5.23), we see these properties are displayed here as well. The curves are pulled together at low STAT1 concentrations and pulled up slightly at higher STAT1 concentrations compared to the situation when we have no cooperative STAT3 binding. However, since the reduction in fractional occupancy between low and high STAT3 is greater in the three site model, this increase less pronounced.

If we compare the results from this model to the experimental results (Figure 5.24) we now see that this model can explain the results gained from the experimental work.

Continuing to the four site model (Figure 5.25), again we get the same effect,

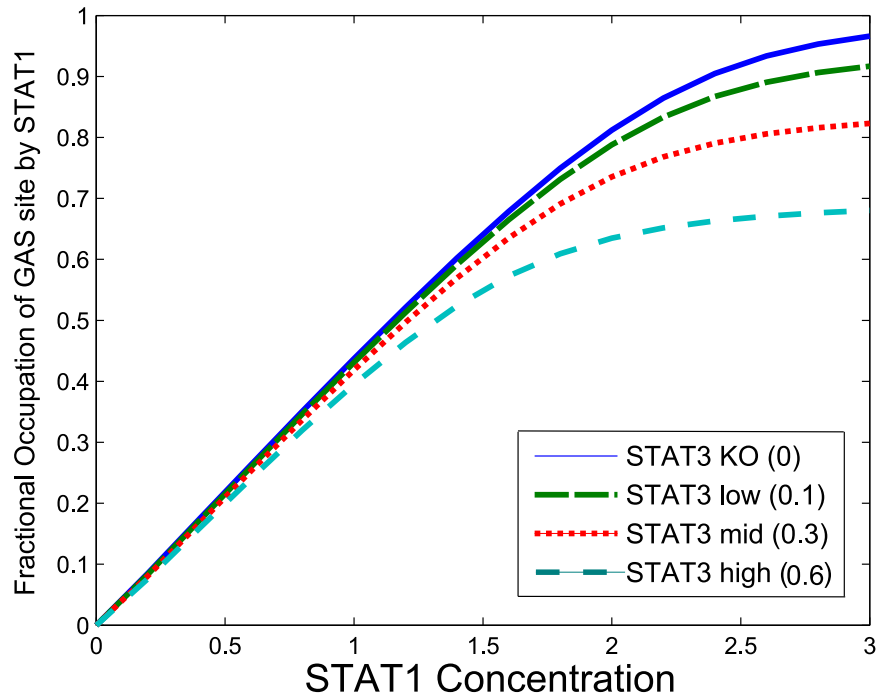


Figure 5.22: Plot of fractional occupation of the DNA GAS site against the initial concentration of free STAT1, with cooperative binding of both STAT1 and STAT3. The values are taken at steady state. The parameter values are: $K_{off}^{G1} = 2$; $K_{off}^{NG1} = 20$; $K_{off}^{G3} = 0.0001$; $K_{off}^{NG3} = 0.001$; $K_{off}^{P1} = 0.001$; $K_{off}^{P3} = 0.01$; $K_{on}^{G1} = K_{on}^{NG1} = K_{on}^{G3} = K_{on}^{NG3} = 1$; $K_{on}^{P1} = K_{on}^{P3} = 1$

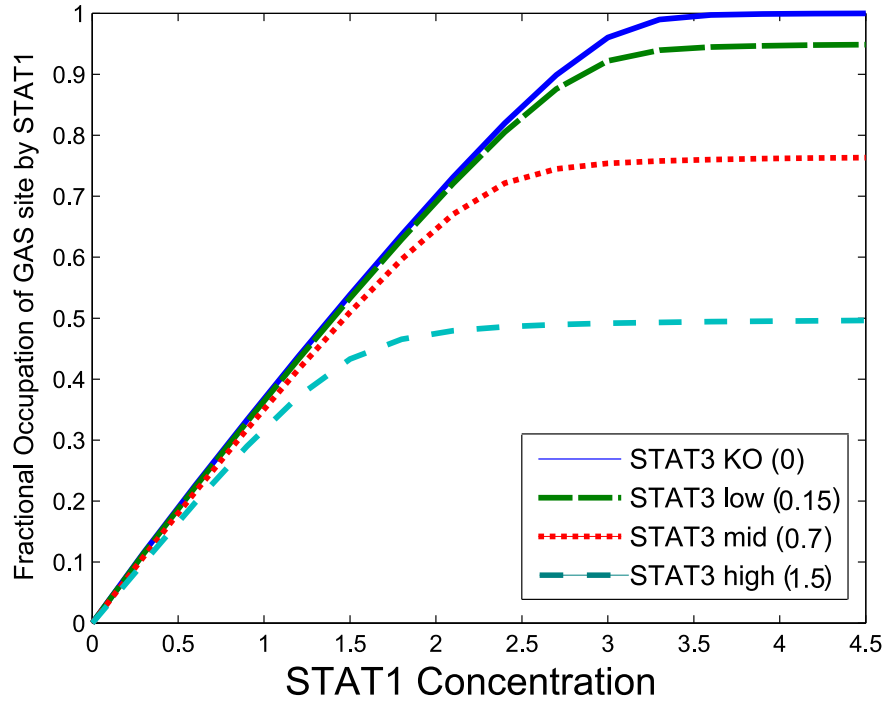


Figure 5.23: Plot of fractional occupation of the DNA GAS site against the initial concentration of free STAT1, with cooperative binding of both STAT1 and STAT3. The values are taken at steady state. The parameter values are: $K_{off}^{G1} = 2$; $K_{off}^{NG1} = 20$; $K_{off}^{G3} = 0.0001$; $K_{off}^{NG3} = 0.001$; $K_{off}^{P1} = 0.001$; $K_{off}^{P3} = 0.01$; $K_{on}^{G1} = K_{on}^{NG1} = K_{on}^{G3} = K_{on}^{NG3} = K_{on}^{P1} = K_{on}^{P3} = 1$

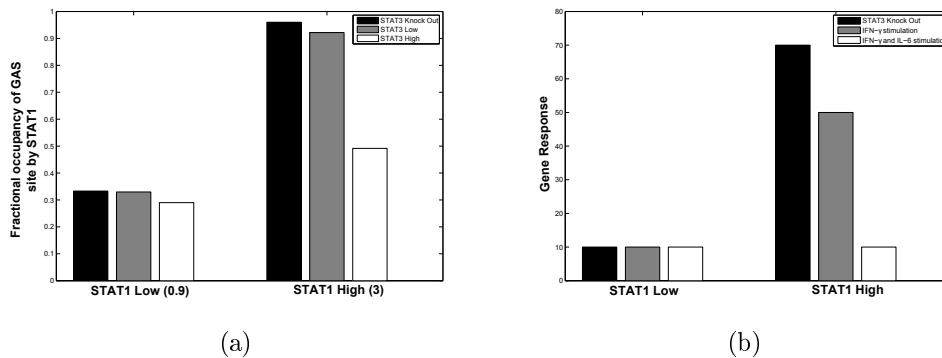


Figure 5.24: a) Plot of fractional occupation of the DNA GAS site against a low and high concentration of STAT1 for three different STAT3 concentration, with cooperative binding of both STAT types. (Parameters as in Figure 5.23). b) Plot of experimental results.

however this time the difference achieved in moving from three to four sites is minimal. This is likely to be due to the fact that the binding of polymers involving a GAS site is more important than binding to a non-GAS site, and the four-site model only allows additional non-GAS site bonds.

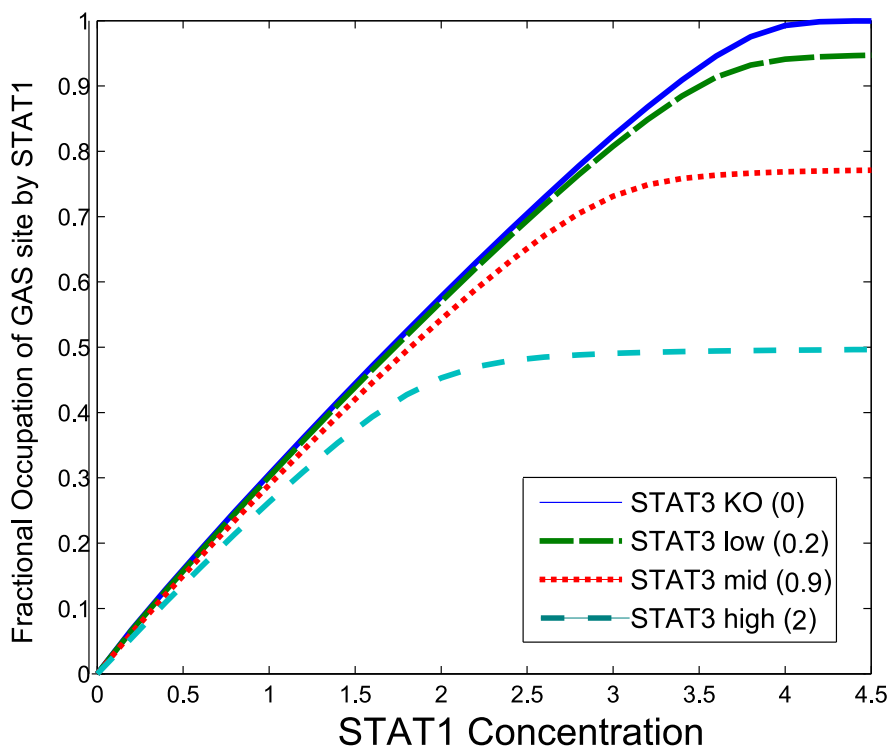


Figure 5.25: Plot of fractional occupation of the DNA GAS site against the initial concentration of free STAT1, with cooperative binding of both STAT1 and STAT3. The values are taken at steady state. The parameter values are: $K_{off}^{G1} = 2$; $K_{off}^{NG1} = 20$; $K_{off}^{G3} = 0.0001$; $K_{off}^{NG3} = 0.001$; $K_{off}^{P1} = 0.001$; $K_{off}^{P3} = 0.01$; $K_{on}^{G1} = K_{on}^{NG1} = K_{on}^{G3} = K_{on}^{NG3} = K_{on}^{P1} = K_{on}^{P3} = 1$

So far we have looked at a narrow range of parameters that display the behaviours similar to those seen *in vitro*. We have found that the STAT-DNA binding of STAT3 must be much stronger than the STAT-DNA binding of STAT1. Another possible explanation of the experimental results is that STAT1 will only initiate a gene response if a tetramer is bound to the binding sites. We will consider this scenario in the next section as we look at a wider parameter range.

Parameter Exploration

Since STAT1 and STAT3 both actively stimulate transcription of genes, we expect there must be conditions which allow STAT1 and STAT3 to both be bound on the DNA. The binding rates may vary from site to site. We will look at how changes in the parameters in the model affect the binding of both these proteins. We will first at the two-site model in which only STAT1 is able to bind cooperatively. We will initially set the GAS and non-GAS binding rates to be the same. In the case of STAT1 we will now consider the gene response to be proportional to the tetramer concentration. For STAT3 we will consider the gene response to be the concentration of STAT3 bound to the first DNA site regardless of what is bound to the second site.

We set the DNA binding rate parameters to be the same and start with equal concentrations of STAT1 and STAT3. Figure 5.26a shows that increasing the cooperativity of STAT1 is beneficial to the cooperative binder since it results in a greater gene response across all DNA binding rates. For the non-cooperative binder (STAT3), cooperativity of a competitor is detrimental to gene response, Figure 5.26b.

There are two ways in which the concentration can be increased, either increasing the total concentration whilst keeping the STAT1:STAT3 ratio the same or changing the relative concentrations. Figure 5.27 shows the effect of increasing the total initial concentration of free STAT dimers. At low binding strengths, increasing the concentration is marginally beneficial to both STAT1 and STAT3, since there is little competition for DNA sites. As the DNA binding strength increases the higher concentrations are still beneficial to the cooperative binder, but become detrimental to the non-cooperative binder.

We now keep the total concentration the same and change the STAT1:STAT3 ratio, Figure 5.28. As might be expected, STAT1 is at an advantage when its concentra-

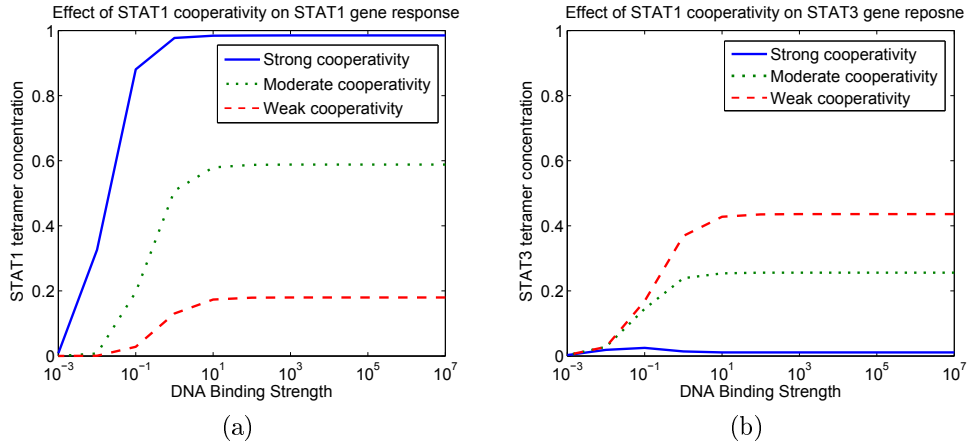


Figure 5.26: Plots of STAT1 and STAT3 gene response against the DNA binding strength (DNA *on* rate / DNA *off* rate) for three increasing levels of STAT1 cooperativity. The cooperativity binding strengths (K_{on}^{P1}/K_{off}^{P1}) are 1000 (Strong), 10 (Moderate) and 1 (Weak). The initial conditions are $S_1=3$, $S_3=3$, $DNA_{00}=1$. The values are taken at steady state.

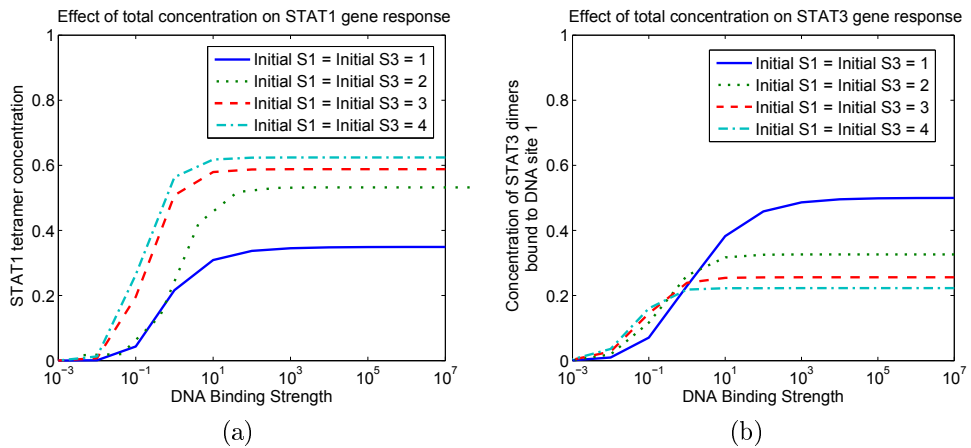


Figure 5.27: Plots of STAT1 and STAT3 gene response against the DNA binding strength (DNA *on* rate / DNA *off* rate) for increasing initial concentrations of STAT1 and STAT3. The cooperativity binding strength in all cases is 10. The values are taken at steady state.

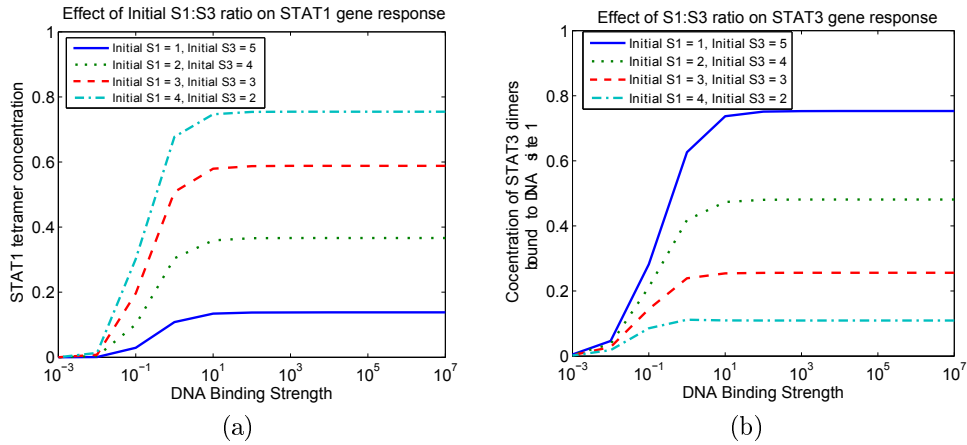


Figure 5.28: Plots of STAT1 and STAT3 gene response against the DNA binding strength (DNA *on* rate / DNA *off* rate) for different proportions of STAT1 and STAT3. The cooperativity binding strength in all cases is 10. The values are taken at steady state.

tion is dominant and similarly for STAT3.

The two types of STAT proteins elicit the greatest gene response in different environments. The cooperative STAT, works best in high concentrations, regardless of the concentration of non-cooperative STAT. However, if the concentration of the non-cooperative binder is low this increases the gene response further. The non-cooperative STAT gene response is more dependent on the concentration of the cooperative binder. The gene response is greatest where this is low. Where the DNA binding strength is low this relationship is slightly changed since increasing the concentration of both STATs is beneficial to STAT3, however increasing STAT3 concentration whilst keeping STAT1 low results in a greater gene response.

So far we have considered only situations where the DNA binding strength of the two STAT competitors is similar. Whilst we expect that generally the binding strength will be of similar order, natural variation does exist, particularly on sub-optimal sites where conservation of the genetic code is lower. We will now look at situations where either STAT1 or STAT3 have higher binding rates. Trends in the data show that the order of difference in the two binding rates is important in

determining the gene response. When the STAT3-DNA binding strength is larger than the STAT1 DNA binding strength the STAT1 gene response is much reduced (Figure 5.29).

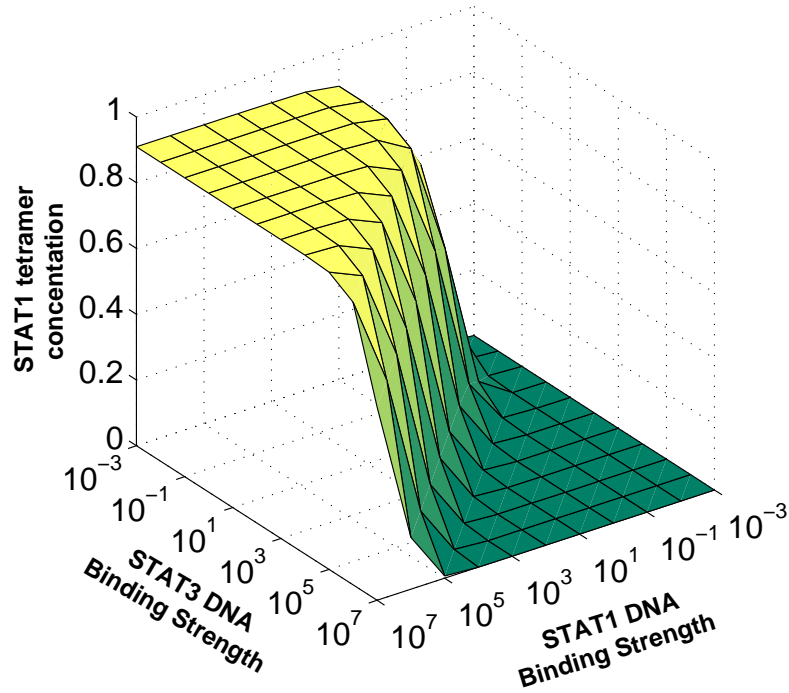


Figure 5.29: Plot of STAT1 gene response against the DNA binding strengths (DNA *on* rate / DNA *off* rate) of STAT1 and STAT3. The cooperativity binding strength in all cases is 10 and the initial conditions are $S_1=3$, $S_3=3$, $DNA_{00}=1$. The values are taken at steady state.

Similarly, if the STAT1 DNA binding strength is larger than the STAT3 DNA binding strength the STAT3 gene response is much reduced (Figure 5.30). This agrees with the results from Section 5.4.2 which shows that when the binding rates are different STAT1 gene response is reduced in the presence of STAT3.

So far in this section we have kept the DNA binding rates the same on both sites *i.e.* treating them as tandem GAS sites. As mentioned previously, affinity varies between sites and it is likely that the high affinity GAS site is next to a site of lower affinity, since double GAS sites are rare. Figure 5.31 shows the effect that differing site affinity has on STAT1 gene response.

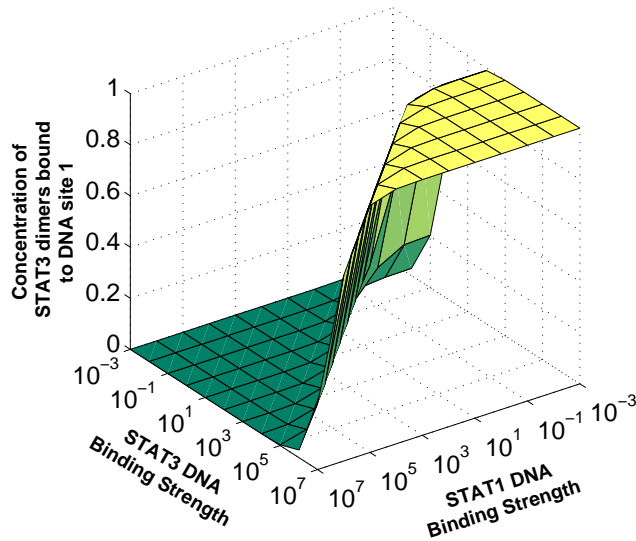


Figure 5.30: Plot of STAT3 gene response against the DNA binding strengths (DNA *on* rate / DNA *off* rate) of STAT1 and STAT3. The cooperativity binding strength in all cases is 10 and the initial conditions are $S_1=3$, $S_3=3$, $DNA_{00}=1$. The values are taken at steady state.

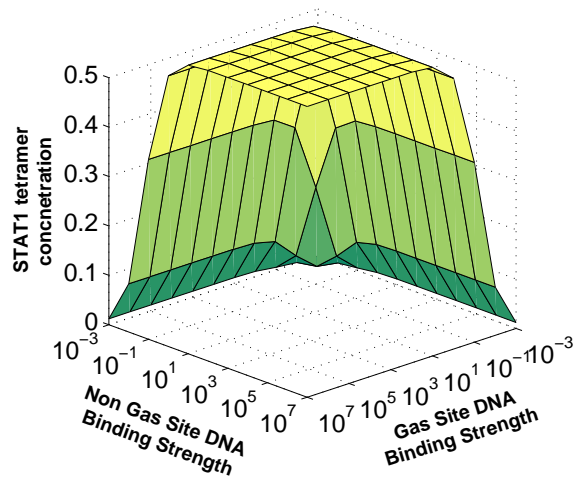


Figure 5.31: Plot of STAT1 gene response against the DNA binding strengths (DNA *on* rate / DNA *off* rate) of GAS and non-GAS sites. Here the DNA binding strength of STAT1 and STAT3 are equal. The cooperativity binding strength is 10 and the initial conditions are $S_1=3$, $S_3=3$, $DNA_{00}=1$. The values are taken at steady state.

The gene response is greatest when the DNA binding strength to either site is greater than the cooperativity strength. As the binding strength to either site decreases the gene response goes down. In the case of STAT3 gene response (Figure 5.32), if the non GAS site binding strength is greater than the cooperativity strength, then the gene response is at a maximum for strong GAS site binding and decreases as the binding strength decreases.

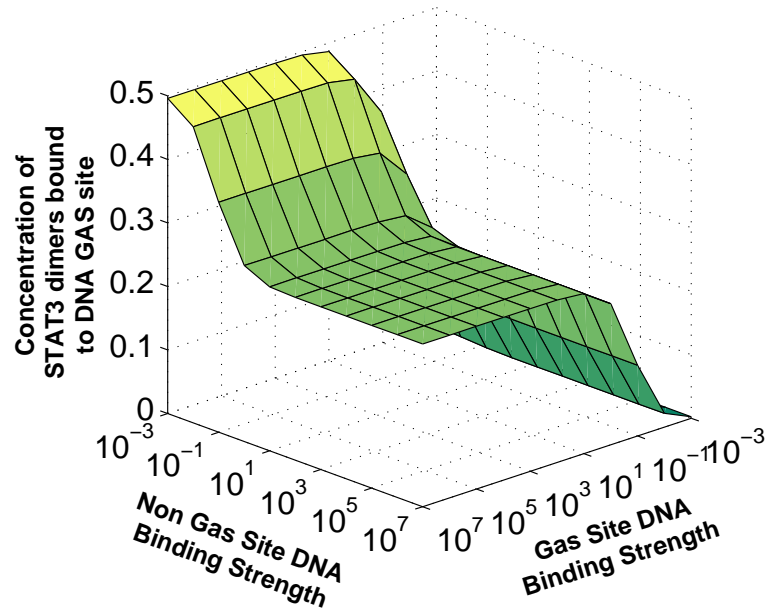


Figure 5.32: Plot of STAT3 gene response against the DNA binding strengths (DNA *on* rate / DNA *off* rate) of GAS and non-GAS sites. Here the DNA binding strength of STAT1 and STAT3 are equal. The cooperativity binding strength is 10 and the initial conditions are $S_1=3$, $S_3=3$, $DNA_{00}=1$. The values are taken at steady state.

However, unlike STAT1, when the non-GAS site binding strength is less than the cooperativity binding strength, the gene response increases. STAT3 gene response is less dependent on the non-GAS site than STAT1 so a low affinity site is advantageous as it reduces STAT1's ability to compete as well as increasing the concentration of free STAT3. This means that STAT1 is likely to be more effective where there are multiple high affinity sites, whereas STAT3 appears to be better

adapted to single high affinity sites.

5.5 Discussion

In this chapter we have developed models of the binding of STAT transcription factors to DNA. We have looked at STAT1 alone and in competition with STAT3. With appropriate parameters this model can be generalised to any STAT protein. We had four aims in this chapter. Firstly, we wanted to clarify the importance of tandem GAS sites to STAT1 gene response. Secondly, we wanted to confirm that cooperativity increased DNA binding and suggest rates that allow this. Thirdly, we wanted to show that STAT3 reduces the gene response of STAT1 by reducing cooperative binding. Finally, we wanted to suggest conditions which favour each of these species.

In Section 5.3 we showed that we could reproduce the results seen experimentally. Namely, high fractional occupancy of the GAS site with cooperativity, and little occupancy where cooperativity is blocked. We have shown that it is not necessary to have double GAS sites for STAT-DNA binding. The amount of binding, even to single GAS sites (those with poorly conserved neighbours), can be high given a large enough STAT1 concentration. This finding supports recent research suggesting that most of the STAT1 binding sites responsible for gene response are single GAS sites. We also showed that in the absence of cooperativity, STAT1 cannot effectively bind to DNA.

In Section 5.4 we produced three models of competitive binding of STAT proteins, each with a different number of binding sites. If we consider the difference in fractional occupancy of the GAS site by STAT1, between STAT3 at a high level and STAT3 at low level, this difference increases as the number of DNA sites increases. The change from three sites to four is less than that of two sites to three but

this is expected since it does not involve additional GAS site binding. We would expect this trend to continue up to a limit as the number of sites increases, since as the length of the chain increases so does the probability of a bond in the chain breaking resulting in two smaller polymers.

It has also emerged that with a small amount of STAT3 polymerisation the differences in occupancy at lower STAT1 concentration is reduced. This effect is most significant in the four site model, and is important in achieving results similar to experimental results. This may suggest that STAT3 does form polymers on DNA *in vivo*, albeit less frequently than STAT1. This also agrees with experimental work that shows that STAT3 tetramers can form on GAS sites [6].

The models used here require STAT3 to have a smaller dissociation rate than STAT1, and this is a restriction which has not been found experimentally. In the simple models we have used here there appears not to be a way to achieve competition between STAT1 and STAT3 where STAT1 is capable of cooperative binding, without STAT3 having a smaller dissociation rate. This suggests that either the dissociation rates *in vivo* are different, as we have used here, or there are more complex interactions involved than we have modelled here.

We propose here that although cooperativity may be necessary for STAT1 to bind remain bound to DNA, double or tandem GAS sites are not required for this cooperativity. However, under competitive conditions, such as the presence of STAT3, tandem GAS sites are extremely beneficial to STAT1. We believe that STAT3 interferes with the cooperative binding of STAT1 when the concentration of STAT1 creates competition for GAS sites. Although lack of cooperativity is disadvantageous to STAT3, there are situations where it can bind well and co-exist with STAT1. Namely, where we have only single high affinity GAS sites, and where STAT3 concentration greatly exceeds STAT1 concentration.

Chapter 6

Summary and Future Directions

Arthritic diseases affect millions of individuals worldwide and cause significant pain, disability and loss of independence. As well as the large effect this has on the individual's quality of life it also places a large burden on health and social services. Research into the pathobiology and treatment of these diseases is in the relatively early stages and whilst disease modifying treatments are available in some cases, most notably RA, there is not a full enough understanding of disease dynamics to approach treatment systematically.

A range of cytokines have been observed to be raised in arthritic disease. Experimental cell biology has shown that these cytokine pathways are important in the mediation and progression of disease. However, the nature of the dynamics between cytokines, particularly *in vivo*, is still largely unclear. One of the reasons for this is that the dynamics and the interactions of cytokines are difficult to capture experimentally, in part due to their short half-life. Therapies targeting cytokine pathways in arthritic disease have been partially successful for RA, but for OA have remained elusive. The purpose of this research has been to use mathematical modelling to clarify how different cytokine groups interact in arthritic disease. We have considered whether variations in cytokine production rate parameters

could lead to arthritic disease and progression and whether the dynamics of the cytokine interactions could identify treatment targets or strategies not previously considered.

We initially looked at a two variable model of cytokine dynamics where we grouped cytokines into pro- and anti-inflammatory groups (Chapter 2). We consider this to be a feasible model for cytokine dynamics in the synovium and hence an appropriate model for cytokine dynamics in RA. We found that the positive and negative feedback mechanisms in this model lead to complex dynamics, with monostable, bistable and oscillatory behaviours. We identified that where there is bistable behaviour there is the possibility of inducing remission with an appropriate treatment strategy. Effective treatment was shown to depend not only on dose size but also on dose timing and interval, and the optimum was not necessarily the highest dose over the shortest interval. We found that in some cases counter-intuitive treatment strategies worked well, such as increasing dose interval or increasing the concentration of pro-inflammatory cytokine. These types of treatment strategies may not have been considered clinically, and offer new opportunities for consideration.

To make the model of the synovium applicable to the cartilage we extended it to take into account two other major mediators of arthritic disease, MMPs and fibronectin fragments (Chapter 3). In this model we had two negative and two positive feedback networks, giving rise to both monostable and multi-stable behaviour. In contrast to the two variable synovium model, we found that most of the parameter space we explored contained disease states, which were either monostable or bistable. This is in line with the higher prevalence of OA than RA. We considered treatment targets for this extended model, and found that single target therapies aimed at reducing pro-inflammatory cytokine or MMP concentrations were ineffective, a result also observed in clinical trials. Simulations of therapies increasing anti-inflammatory cytokines were effective but required large

dose sizes. We found that combined target therapies were effective both at inducing remission in multi-stable cases, and slowing progression in monostable disease. We suggested that increasing cytokine clearance rates, for example through exercise, could be beneficial as a complimentary therapy alongside other treatments.

To consider how the spatial structure of cartilage affects the cytokine dynamics that we had observed in the ODE models we developed a spatial model of cartilage in the CompuCell3D modelling environment (Chapter 4). This allowed us to model the diffusion of cytokines between chondrocytes and through the tissue, and therefore investigate how chondrocyte spacing and diffusion rates affects the dynamics. We found that with slow diffusion the cells were less able to communicate (through cytokine signalling) and hence displayed less uniform behaviour. This resulted in some chondrocytes secreting only low levels of cytokines (and therefore considered healthy) whilst others secreted higher levels of cytokines (considered to be a pathological response). When the diffusion rate was faster the behaviour of the cells was more uniform. It is possible that this behaviour could be exploited to optimise treatments, for example increasing diffusion or advection so that treatments delivered to one area of cartilage would result in a tissue-wide response, or decreasing diffusion so that disease type behaviour is isolated in small areas of the tissue. This type of treatment strategy may be worthy of further modelling and consideration.

Whilst we have mainly focused on cytokine dynamics in this work, the pathway from signalling to cartilage degradation is much more complex with many downstream signalling factors. As with cytokines the dynamics of many of these factors are not yet fully understood. We have looked at one example of these downstream signalling factors, the STAT family of transcription factors (Chapter 5). In collaboration with experimentalists, we have considered a specific aspect of STAT proteins, the binding of STAT dimers to DNA. We were able to show that cooperativity between bound STAT1 dimers decreased the mobility of STAT1 even where

when there was a single high affinity site (GAS sites). We also showed that the presence of STAT3 interfered with the ability of STAT1 to bind cooperatively at high concentrations due to competition for binding sites. These findings helped to support the findings of the experimental work. This work also demonstrated that whilst we focus on cytokine dynamics in relation to OA initiation and progression, there are many other aspects of cartilage remodelling and degradation that could impact the condition.

Modelling of cytokines in terms of arthritic disease is a novel research area and the models in this thesis have shown conceptually that such models can replicate some of features of the behaviour seen *in vivo* and hence give insight into treatment strategies. However, this work is at a very early stage and refinement is needed for these models. The simplest two-variable model offers some insights into treatment of RA, but to be able to translate this into clinical practice we would need to be able to link the model parameters to measurable disease markers in individuals. Although in this work we have considered this model in the context of cytokine interactions in the synovium, cytokines are used throughout the body. It is entirely possible that this model could be applied to a range of conditions where cytokines play a role, with model extensions such as those used for OA applied where necessary. Conditions such as asthma, eczema, diabetes and lupus are all known to have some level of cytokine involvement.

The four-variable cartilage model concentrates on what we consider the four most important variables in cartilage degradation. However there are other important factors that could be considered such as nitric oxide and Prostaglandin E2, which have been shown to play a role in cartilage breakdown [5]. The spatial model of cartilage degradation should be expanded to consider the affects of the mechanical properties of the tissue. This needs to be considered at the tissue level, for example, the differing chondrocyte densities, material properties and proximity to bone in different cartilage zones may affect how the tissue responds to treatment.

Additionally, the mechanical properties of the tissue need, to be considered at joint level, by including joint morphology and loading. Finite element modelling would be an appropriate methodology to use to include these joint level extensions. The current model could also be extended to include a more accurate representation of synovial fluid and bone, which would enable the theoretical aspect of drug placement to be considered.

This work has demonstrated that mathematical models of arthritis disease could help to guide experimental research into treatment strategies and give a greater understanding of the disease dynamics. Future research with collaboration with both cell biologists and clinicians has the potential to make progress in our understanding of OA, leading to the development of disease modifying therapies, that could transform the experiences of individuals with this debilitating condition.

References

- [1]
- [2] S. B. Abramson and Y. Yazici. Biologics in development for rheumatoid arthritis: Relevance to osteoarthritis. *Advanced Drug Delivery Reviews*, 58: 212–225, 2006.
- [3] T. Aigner, A. Sachse, P. M. Gebhard, and H. I. Roach. Osteoarthritis: Pathobiology—targets and ways for therapeutic intervention. *Advanced Drug Delivery Reviews*, 58:128–149, 2006.
- [4] B. Alberts. *Molecular biology of the cell*. Garland Publishers, 1989.
- [5] A. R. Amin and S. B. Abramson. The role of nitric oxide in articular cartilage breakdown in osteoarthritis. *Current Opinion in Rheumatology*, 10(3):263–268, 1998.
- [6] F. Antunes. *Impact of STAT1 cooperative DNA binding on genomic binding site selection and subcellular dynamics*. PhD thesis, 2011.
- [7] N. Arden and C. Cooper. *Osteoarthritis Handbook*. Taylor & Francis, 2005.
- [8] O. J. Arntz, M. B. Bennink, P. M. van der Kraan, W. B. van den Berg, and F. A. J. van de Loo. Chondrocytes from arthritic cartilage in a subset of osteoarthritis patients express lower levels of NF κ B-P65: a survival factor against tumour necrosis factor α -induced cell death. *Annals of the Rheumatic Diseases*, 69:A18, 2010.

REFERENCES

- [9] A. Bailón-Plaza and M. C. H. Van Der Meulen. A mathematical framework to study the effects of growth factor influences on fracture healing. *Journal of Theoretical Biology*, 212(2):191–209, 2001.
- [10] M. Baker, S. Denman-Johnson, B. S. Brook, I. Gaywood, and M. R. Owen. Mathematical modelling of cytokine-mediated inflammation in rheumatoid arthritis. *Mathematical Medicine and Biology*, 30(4):311–337, 2013.
- [11] A. Begitt, M. Droescher, T. Meyer, C. D. Schmid, M. Baker, F. Antunes, K.-P. Knobloch, M. R. Owen, R. Naumann, T. Decker, and U. Vinkemeier. STAT1-cooperative DNA binding distinguishes type 1 from type 2 interferon signaling. *Nat Immunol*, 15(2):168–176, 2014.
- [12] F. Berenbaum. Targeted therapies in osteoarthritis: a systematic review of the trials on www.clinicaltrials.gov. *Best practice & research. Clinical rheumatology*, 24:107–119, 2010.
- [13] T. S. Blackwell and J. W. Christman. The role of nuclear factor-kappa b in cytokine gene regulation. *American journal of respiratory cell and molecular biology*, 17(1):3–9, 1997.
- [14] E. N. Blaney Davidson, P. M. van der Kraan, and W. B. van den Berg. TGF- β and osteoarthritis. *Osteoarthritis and Cartilage*, 15(6):597–604, 2007.
- [15] A. B. Blom and W. B. van den Berg. *The Synovium and Its Role in Osteoarthritis*, volume 4 of *Bone and osteoarthritis: Topics in Bone Biology*, pages 65–79. Springer London, 2008.
- [16] I. Blumenfeld and E. Livne. The role of transforming growth factor (TGF)- β , insulin-like growth factor (IGF)-1, and interleukin (IL)-1 in osteoarthritis and aging of joints. *Experimental Gerontology*, 34(7):821–829, 1999.

REFERENCES

- [17] J. Bondeson, S. Wainwright, S. Lauder, N. Amos, and C. Hughes. The role of synovial macrophages and macrophage-produced cytokines in driving aggrecanases, matrix metalloproteinases, and other destructive and inflammatory responses in osteoarthritis. *Arthritis Research & Therapy*, 8:R187, 2006.
- [18] T. Bongartz, C. Nannini, Y. F. Medina-Velasquez, S. J. Achenbach, C. S. Crowson, J. H. Ryu, R. Vassallo, S. E. Gabriel, and E. L. Matteson. Incidence and mortality of interstitial lung disease in rheumatoid arthritis: A population-based study. *Arthritis & Rheumatism*, 62(6):1583–1591, 2010.
- [19] C. S. Bonnet and D. A. Walsh. Osteoarthritis, angiogenesis and inflammation. *Rheumatology*, 44:7–16, 2005.
- [20] K. D. Brandt. Osteophytes in osteoarthritis. Clinical aspects. *Osteoarthritis and cartilage / OARS, Osteoarthritis Research Society*, 7:334–335, 1999.
- [21] F. M. Brennan, R. N. Maini, and M. Feldmann. TNF- α – a pivotal role in rheumatoid arthritis? *Rheumatology*, 31:293–298, 1992.
- [22] C. J. Catt, W. Schuurman, B. G. Sengers, P. R. van Weeren, W. J. Dhert, C. P. Please, and J. Malda. Mathematical modelling of tissue formation in chondrocyte filter cultures. *Eur Cell Mater*, 22:377–92, 2011.
- [23] R. M. Cawthon, K. R. Smith, E. O’Brien, A. Sivatchenko, and R. A. Kerber. Association between telomere length in blood and mortality in people aged 60 years or older. *The Lancet*, 361(9355):393–395, 2003.
- [24] S. R. W. L. Chan and E. H. Blackburn. Telomeres and telomerase. *Philosophical Transactions of the Royal Society of London. Series B: Biological Sciences*, 359(1441):109–122, 2004.
- [25] X. Chevalier, P. Goupille, A. D. Beaulieu, F. X. Burch, W. G. Bensen, T. Conrozier, D. Loeuille, A. J. Kivitz, D. Silver, and B. E. Appleton. In-

REFERENCES

- traarticular injection of Anakinra in osteoarthritis of the knee: A multicenter, randomized, double-blind, placebo-controlled study. *Arthritis Care & Research*, 61:344–352, 2009.
- [26] E. H. S. Choy and G. S. Panayi. Cytokine pathways and joint inflammation in rheumatoid arthritis. *New England Journal of Medicine*, 344:907–916, 2001.
- [27] N. P. Cohen, R. J. Foster, and V. C. Mow. Composition and dynamics of articular cartilage: structure, function, and maintaining healthy state. *The Journal of orthopaedic and sports physical therapy*, 28(4):203–215, 1998.
- [28] P. G. Conaghan. Osteoarthritis in 2012: Parallel evolution of OA phenotypes and therapies. *Nat Rev Rheumatol*, 9(2):68–70, 2013.
- [29] A. Csiszar, Z. Ungvari, A. Koller, J. G. Edwards, and G. Kaley. Aging-induced proinflammatory shift in cytokine expression profile in coronary arteries. *The FASEB Journal*, 17(9):1183–1185, 2003.
- [30] D. Cunningham. Textbook of anatomy, 1937. *London*.
- [31] J. E. Darnell Jr, I. M. Kerr, and G. R. Stark. JAK-STAT pathways and transcriptional activation in response to IFNs and other extracellular signaling proteins. *Science-AAAS-Weekly Paper Edition-including Guide to Scientific Information*, 264(5164):1415–1420, 1994.
- [32] S. K. Das and A. Farooqi. Osteoarthritis. *Best Practice & Research Clinical Rheumatology*, 22:657–675, 2008.
- [33] I. M. de Kleer, L. R. Wedderburn, L. S. Taams, A. Patel, H. Varsani, M. Klein, W. de Jager, G. Pugayung, F. Giannoni, G. Rijkers, S. Albani, W. Kuis, and B. Prakken. CD4+CD25 bright regulatory T cells actively regulate inflammation in the joints of patients with the remitting form of

REFERENCES

- juvenile idiopathic arthritis. *The Journal of Immunology*, 172:6435–6443, 2004.
- [34] S. Dhawan and A. Quyyumi. Rheumatoid arthritis and cardiovascular disease. *Current Atherosclerosis Reports*, 10:128–133, 2008.
- [35] A. Dhooge, W. Govaerts, and Y. A. Kuznetsov. Matcont: A matlab package for numerical bifurcation analysis of odes. *ACM Trans. Math. Softw.*, 29(2): 141–164, June 2003. ISSN 0098-3500.
- [36] C. A. Dinarello and L. L. Moldawer. *Pro-inflammatory and anti-inflammatory cytokines in rheumatoid arthritis*. Amgen Inc., USA, 2nd edition, 2002.
- [37] J. H. W. Distler, A. Jungel, L. C. Huber, C. A. Seemayer, C. F. Reich, R. E. Gay, B. A. Michel, A. Fontana, S. Gay, D. S. Pisetsky, and O. Distler. The induction of matrix metalloproteinase and cytokine expression in synovial fibroblasts stimulated with immune cell microparticles. *Proceedings of the National Academy of Sciences of the United States of America*, 102:2892–2897, 2005.
- [38] M. Domaille, R. Mascarenhas, N. Dayal, and J. Kirwan. Evaluation of the Bristol Royal Infirmary physiotherapy programme for the management of patients with osteoarthritis of the knee. *Musculoskeletal Care*, 4(2):78–87, 2006.
- [39] B. Ermentrout. *Simulating, Analyzing, and Animating Dynamical Systems: A Guide to Xppaut for Researchers and Students*. Society for Industrial and Applied Mathematics, 2002.
- [40] W. H. Ettinger, Jr, R. Burns, S. P. Messier, and et al. A randomized trial comparing aerobic exercise and resistance exercise with a health education

REFERENCES

- program in older adults with knee osteoarthritis: The fitness arthritis and seniors trial (fast). *JAMA*, 277(1):25–31, 1997.
- [41] C. H. Evans, J. N. Gouze, E. Gouze, P. D. Robbins, and S. C. Ghivizzani. Osteoarthritis gene therapy. *Gene Ther*, 11:379–389, 2004.
- [42] R. C. Evans and T. M. Quinn. Dynamic compression augments interstitial transport of a glucose-like solute in articular cartilage. *Biophysical Journal*, 91(4):1541–1547, 2006.
- [43] M. Feldmann. Development of anti-TNF therapy for rheumatoid arthritis. *Nat Rev Immunol*, 2(5):364–371, 2002.
- [44] M. Feldmann and R. N. Maini. Anti-TNF α therapy of rheumatoid arthritis: What have we learned? *Annual Review of Immunology*, 19(1):163–196, 2001.
- [45] D. T. Felson, R. C. Lawrence, P. A. Dieppe, R. Hirsch, C. G. Helmick, J. M. Jordan, R. S. Kington, N. E. Lane, M. C. Nevitt, Y. Zhang, M. Sowers, T. McAlindon, T. D. Spector, A. R. Poole, S. Z. Yanovski, G. Ateshian, L. Sharma, J. A. Buckwalter, K. D. Brandt, and J. F. Fries. Osteoarthritis: New insights. Part 1: The disease and its risk factors. *Annals of Internal Medicine*, 133(8):635–646, 2000.
- [46] T. Funck-Brentano and M. Cohen-Solal. Crosstalk between cartilage and bone: When bone cytokines matter. *Cytokine & Growth Factor Reviews*, 22(2):91–97, 2011.
- [47] K. Gelse, K. von der Mark, T. Aigner, J. Park, and H. Schneider. Articular cartilage repair by gene therapy using growth factor - producing mesenchymal cells. *Arthritis & Rheumatism*, 48:430–441, 2003.
- [48] R. J. Goekoop, M. Kloppenburg, H. M. Kroon, M. Fr  lich, T. W. J. Huizinga, R. G. J. Westendorp, and J. Gussekloo. Low innate production of

REFERENCES

- interleukin-1 β and interleukin-6 is associated with the absence of osteoarthritis in old age. *Osteoarthritis and cartilage / OARS, Osteoarthritis Research Society*, 18:942–947, 2010.
- [49] R. Goldbach-Mansky and P. E. Lipsky. New concepts in the treatment of rheumatoid arthritis. *Annual Review of Medicine*, 54(1):197–216, 2003.
- [50] M. Goldring. Osteoarthritis and cartilage: The role of cytokines. *Current Rheumatology Reports*, 2:459–465, 2000.
- [51] R. S. Goomer, L. J. Deftos, R. Terkeltaub, T. Maris, M. C. Lee, F. L. Harwood, and D. Amiel. High-efficiency non-viral transfection of primary chondrocytes and perichondrial cells for ex-vivo gene therapy to repair articular cartilage defects. *Osteoarthritis and Cartilage*, 9:248–256, 2001.
- [52] J. Goronzy and C. Weyand. Developments in the scientific understanding of rheumatoid arthritis. *Arthritis Research & Therapy*, 11:1–14, 2009.
- [53] H. Gray. *Anatomy of the human body*. philadelphia: Lea & febiger, 1918; bartleby. com, 2000. 2001.
- [54] G. Gridley, J. K. McLaughlin, A. Ekbom, L. Klareskog, H.-O. Adami, D. G. Hacker, R. Hoover, and J. F. Fraumeni. Incidence of cancer among patients with rheumatoid arthritis. *Journal of the National Cancer Institute*, 85(4): 307–311, 1993.
- [55] A. J. Grodzinsky, M. E. Levenston, M. Jin, and E. H. Frank. Cartilage tissue remodeling in response to mechanical forces. *Annual Review of Biomedical Engineering*, 2(1):691–713, 2000.
- [56] C. Han, D. W. Robinson, M. V. Hackett, L. C. Paramore, K. H. Fraeman, and M. V. Bala. Cardiovascular disease and risk factors in patients with

REFERENCES

- rheumatoid arthritis, psoriatic arthritis, and ankylosing spondylitis. *The Journal of Rheumatology*, 33(11):2167–2172, 2006.
- [57] C. B. Harley, A. B. Futcher, and C. W. Greider. Telomeres shorten during ageing of human fibroblasts. *Nature*, 345(6274):458–460, 1990.
- [58] G. A. Hawker, L. Stewart, M. R. French, J. Cibere, J. M. Jordan, L. March, M. Suarez-Almazor, and R. Gooberman-Hill. Understanding the pain experience in hip and knee osteoarthritis: an OARSI/OMERACT initiative. *Osteoarthritis and Cartilage*, 16(4):415–422, 2008.
- [59] E. Hedbom and H. J. Häuselmann. Molecular aspects of pathogenesis in osteoarthritis: the role of inflammation. *Cellular and Molecular Life Sciences CMLS*, 59(1):45–53, 2002.
- [60] M. Herald. General model of inflammation. *Bulletin of Mathematical Biology*, 72:765–779, 2010.
- [61] M. Hochberg, A. Silman, J. Smolen, M. Weinblatt, and M. Weisman. *Rheumatoid Arthritis*. Elsevier Health Sciences, 2008.
- [62] S. Hoops, S. Sahle, R. Gauges, C. Lee, J. Pahle, N. Simus, M. Singhal, L. Xu, P. Mendes, and U. Kummer. Copasi—a complex pathway simulator. *Bioinformatics*, 22(24):3067–74, 2006.
- [63] J. N. Ihle. The STAT family in cytokine signaling. *Current Opinion in Cell Biology*, 13(2):211–217, 2001.
- [64] J. B. Imboden, J. H. Stone, and D. B. Hellmann. *Current rheumatology diagnosis & treatment*. Lange Medical Books/McGraw-Hill, Medical Pub. Division, New York, N.Y., 2007.

REFERENCES

- [65] T. Iwanaga, M. Shikichi, H. Kitamura, H. Yanase, and K. Nozawa-Inoue. Morphology and functional roles of synoviocytes in the joint. *Arch Histol Cytol*, 63:17–31, 2000.
- [66] E. Izhikevich. *Dynamical Systems in Neuroscience: The Geometry of Excitability and Bursting*. MIT Press, 2006.
- [67] C. A. Janeway, P. Travers, M. Walport, and M. J. Shlomchik. *Immunobiology*. Garland Science, 5th editio edition, 2001.
- [68] M. Jit, B. Henderson, M. Stevens, and R. M. Seymour. TNF- α neutralization in cytokine-driven diseases: a mathematical model to account for therapeutic success in rheumatoid arthritis but therapeutic failure in systemic inflammatory response syndrome. *Rheumatology*, 44:323–331, 2005.
- [69] P. Jones and B. Sleeman. Angiogenesis - understanding the mathematical challenge. *Angiogenesis*, 9:127–138, 2006.
- [70] B. Kidd, R. Langford, and T. Wodehouse. Arthritis and pain. Current approaches in the treatment of arthritic pain. *Arthritis Research & Therapy*, 9:214, 2007.
- [71] R. U. Kleemann, D. Krockner, A. Cedraro, J. Tuischer, and G. N. Duda. Altered cartilage mechanics and histology in knee osteoarthritis: relation to clinical assessment (ICRS grade). *Osteoarthritis and Cartilage*, 13(11): 958–963, 2005.
- [72] K. Koetz, E. Bryl, K. Spickschen, W. M. O’Fallon, J. J. Goronzy, and C. M. Weyand. T cell homeostasis in patients with rheumatoid arthritis. *Proceedings of the National Academy of Sciences*, 97(16):9203–9208, 2000.
- [73] R. Kumar, G. Clermont, Y. Vodovotz, and C. C. Chow. The dynamics of acute inflammation. *Journal of Theoretical Biology*, 230:145–155, 2004.

REFERENCES

- [74] S. Kwan Tat, D. Lajeunesse, J.-P. Pelletier, and J. Martel-Pelletier. Targeting subchondral bone for treating osteoarthritis: what is the evidence? *Best Practice & Research Clinical Rheumatology*, 24(1):51–70, 2010.
- [75] D. Lajeunesse and P. Reboul. Subchondral bone in osteoarthritis: a biologic link with articular cartilage leading to abnormal remodeling. *Current Opinion in Rheumatology*, 15(5):628–633, 2003.
- [76] H. Leddy and F. Guilak. Site-specific molecular diffusion in articular cartilage measured using fluorescence recovery after photobleaching. *Annals of Biomedical Engineering*, 31(7):753–760, 2003.
- [77] D. E. Levy and J. E. Darnell. STATs: transcriptional control and biological impact. *Nat Rev Mol Cell Biol*, 3(9):651–662, 2002.
- [78] C. P. Lim and X. Cao. Structure, function, and regulation of STAT proteins. *Molecular BioSystems*, 2(11):536–550, 2006.
- [79] E. Lindqvist, T. Saxne, P. Geborek, and K. Eberhardt. Ten year outcome in a cohort of patients with early rheumatoid arthritis: health status, disease process, and damage. *Annals of the rheumatic diseases*, 61(12):1055–1059, 2002.
- [80] P. E. Lipsky, D. M. van der Heijde, E. W. St. Clair, D. E. Furst, F. C. Breedveld, J. R. Kalden, J. S. Smolen, M. Weisman, P. Emery, M. Feldmann, G. R. Harriman, and R. N. Maini. Infliximab and methotrexate in the treatment of rheumatoid arthritis. *New England Journal of Medicine*, 343(22):1594–1602, 2000.
- [81] R. F. Loeser. Aging and osteoarthritis: the role of chondrocyte senescence and aging changes in the cartilage matrix. *Osteoarthritis and Cartilage*, 17(8):971–979.

REFERENCES

- [82] H. Lorenz and W. Richter. Osteoarthritis: Cellular and molecular changes in degenerating cartilage. *Progress in Histochemistry and Cytochemistry*, 40: 135–163, 2006.
- [83] M. Lutianov, S. Naire, S. Roberts, and J.-H. Kuiper. A mathematical model of cartilage regeneration after cell therapy. *Journal of Theoretical Biology*, 289(0):136–150, 2011.
- [84] A. Malviya and A. McCaskie. Surgery for osteoarthritis. 34:369–372, 2006.
- [85] J. Martel-Pelletier. Pathophysiology of osteoarthritis. *Osteoarthritis and cartilage / OARS, Osteoarthritis Research Society*, 12:31–33, 2004.
- [86] J. Martel-Pelletier, C. Boileau, J.-P. Pelletier, and P. J. Roughley. Cartilage in normal and osteoarthritis conditions. *Best Practice & Research Clinical Rheumatology*, 22:351–384, 2008.
- [87] P. Martens and J. Goronzy. Expansion of unusual CD4+ T cells in severe rheumatoid arthritis. *Arthritis & Rheumatism*, 40(6):1106–1114, 1997.
- [88] S. McDougall. Mathematical modelling of flow through vascular networks: implications for tumour-induced angiogenesis and chemotherapy strategies. *Bulletin of mathematical \hat{A} e*, 64(4):673–702, 2002.
- [89] I. B. McInnes and G. Schett. Cytokines in the pathogenesis of rheumatoid arthritis. *Nat Rev Immunol*, 7(6):429–442, 2007.
- [90] I. B. McInnes and G. Schett. The pathogenesis of rheumatoid arthritis. *New England Journal of Medicine*, 365(23):2205–2219, 2011.
- [91] H. J. McQuay, R. A. Moore, C. Eccleston, S. Morley, and A. C. Williams. Systematic review of outpatient services for chronic pain control. *Health technology assessment (Winchester, England)*, 1(6):i–iv, 1–135, 1997.

REFERENCES

- [92] L. Mellekjær, M. S. Linet, G. Gridley, M. Frisch, H. Møller, and J. H. Olsen. Rheumatoid arthritis and cancer risk. *European Journal of Cancer*, 32(10):1753–1757, 1996.
- [93] T. Meyer and U. Vinkemeier. Nucleocytoplasmic shuttling of stat transcription factors. *European Journal of Biochemistry*, 271(23-24):4606–4612, 2004.
- [94] V. Moos, S. Fickert, and B. Müller. Immunohistological analysis of cytokine expression in human osteoarthritic and healthy cartilage. *Journal of rheumatology*, 26(4):870–9, 1999.
- [95] T. I. Morales. Chondrocyte moves: clever strategies? *Osteoarthritis and Cartilage*, 15(8):861–871, 2007.
- [96] T. Mottonen, P. Hannonen, M. Korpela, M. Nissila, H. Kautiainen, J. Ilonen, L. Laasonen, O. Kaipiainen-Seppänen, P. Franzen, T. Helve, J. Koski, M. Gripenberg-Gahmberg, R. Myllykangas-Luosujärvi, and M. Leirisalo-Repo. Delay to institution of therapy and induction of remission using single-drug or combination disease-modifying antirheumatic drug therapy in early rheumatoid arthritis. *Arthritis & Rheumatism*, 46(4):894–898, 2002.
- [97] H. Muir. The chondrocyte, architect of cartilage. biomechanics, structure, function and molecular biology of cartilage matrix macromolecules. *Bioessays*, 17(12):1039–1048, 1995.
- [98] H. Nakamura, S. Yoshino, and T. Kato. T-cell mediated inflammatory pathway in osteoarthritis. *Osteoarthritis and Cartilage*, 7(4):401–402, 1999.
- [99] V. P. K. Nell, K. P. Machold, G. Eberl, T. A. Stamm, M. Uffmann, and J. S. Smolen. Benefit of very early referral and very early therapy with disease-modifying anti-rheumatic drugs in patients with early rheumatoid arthritis. *Rheumatology*, 43(7):906–914, 2004.

REFERENCES

- [100] NICE. Osteoarthritis: national clinical guideline for care and management in adults, 2008.
- [101] NICE. Rheumatoid arthritis: The management of rheumatoid arthritis in adults, 2009.
- [102] L. A. J. O'Neill and C. Kaltschmidt. Nf-kb: a crucial transcription factor for glial and neuronal cell function. *Trends in Neurosciences*, 20(6):252–258, 1997.
- [103] S. M. Opal and V. A. DePalo. Anti-inflammatory cytokines. *Chest*, 117: 1162–1172, 2000.
- [104] J. J. O'Shea, M. Gadina, and R. D. Schreiber. Cytokine signaling in 2002: New surprises in the Jak/Stat pathway. *Cell*, 109(2, Supplement 1):S121–S131, 2002.
- [105] M. B. Pepys, G. M. Hirschfield, G. A. Tennent, J. Ruth Gallimore, M. C. Kahan, V. Bellotti, P. N. Hawkins, R. M. Myers, M. D. Smith, A. Polara, A. J. A. Cobb, S. V. Ley, J. Andrew Aquilina, C. V. Robinson, I. Sharif, G. A. Gray, C. A. Sabin, M. C. Jenvey, S. E. Kolstoe, D. Thompson, and S. P. Wood. Targeting c-reactive protein for the treatment of cardiovascular disease. *Nature*, 440(7088):1217–1221, 2006.
- [106] G. Pettet and H. Byrne. A model of wound-healing angiogenesis in soft tissue. *Mathematical biosciences*, 136(1):35–63, 1996.
- [107] M. A. Pollatschek and A. M. Nahir. A mathematical model of osteoarthrosis. *Journal of theoretical biology*, 143(6):497–505, 1990.
- [108] A. R. Poole. Cartilage in health and disease. *Arthritis and allied conditions: a textbook of rheumatology*, 14:226–284, 1993.

REFERENCES

- [109] C. Poole. Review. Articular cartilage chondrons: form, function and failure. *Journal of anatomy*, 191:1–13, 1997.
- [110] P. Qvist, A.-C. Bay-Jensen, C. Christiansen, E. B. Dam, P. Pastoureau, and M. A. Karsdal. The disease modifying osteoarthritis drug (DMOAD): Is it in the horizon? *Pharmacological Research*, 58(1):1–7, 2008.
- [111] P. Revell and V. Mayston. The synovial membrane in osteoarthritis: a histological study including the characterisation of the cellular infiltrate present in inflammatory osteoarthritis. *Annals of the rheumatic diseases*, 47(4):300–307, 1988.
- [112] H. Rgind, B. Bibow-Nielsen, B. Jensen, H. C. MÃyller, H. Frimodt-MÃyller, and H. Bliddal. The effects of a physical training program on patients with osteoarthritis of the knees. *Archives of Physical Medicine and Rehabilitation*, 79(11):1421–1427, 1998.
- [113] J. A. Roman-Blas, D. G. Stokes, and S. A. Jimenez. Modulation of TGF- β signaling by proinflammatory cytokines in articular chondrocytes. *Osteoarthritis and Cartilage*, 15(12):1367–1377, 2007.
- [114] R. Roubenoff, T. B. Harris, L. W. Abad, P. W. F. Wilson, G. E. Dallal, and C. A. Dinarello. Monocyte cytokine production in an elderly population: Effect of age and inflammation. *The Journals of Gerontology Series A: Biological Sciences and Medical Sciences*, 53A(1):M20–M26, 1998.
- [115] L. J. Sandell and T. Aigner. Articular cartilage and changes in arthritis. An introduction: cell biology of osteoarthritis. *Arthritis Res*, 3(2):107–113, 2001.
- [116] C. R. Scanzello and S. R. Goldring. The role of synovitis in osteoarthritis pathogenesis. *Bone*, 51(2):249–257, 2012.

REFERENCES

- [117] A. Serafini-Fracassini and J. W. Smith. *The structure and biochemistry of cartilage*. Churchill Livingstone, Edinburgh, 1974.
- [118] R. M. Seymour and B. Henderson. Pro-inflammatory - anti-inflammatory cytokine dynamics mediated by cytokine receptor dynamics in monocytes. *Mathematical Medicine and Biology*, 18(2):159–192, 2001.
- [119] M. M. Smith and P. Ghosh. The synthesis of hyaluronic acid by human synovial fibroblasts is influenced by the nature of the hyaluronate in the extracellular environment. *Rheumatology International*, 7(3):113–122, 1987.
- [120] T. D. Spector and D. J. Hart. How serious is knee osteoarthritis? *Annals of the rheumatic diseases*, 51(10):1105–1106, 1992.
- [121] M. Stefanovic-Racic, J. Stadler, and C. H. Evans. Nitric oxide and arthritis. *Arthritis & Rheumatism*, 36:1036–1044, 1993.
- [122] M. H. Swat, G. L. Thomas, J. M. Belmonte, A. Shirinifard, D. Hmeljak, and J. A. Glazier. *Chapter 13 - Multi-Scale Modeling of Tissues Using CompuCell3D*, volume Volume 110, pages 325–366. Academic Press, 2012.
- [123] Z. Tabor. Simulated aging—a novel method for estimating the risk of fracture of trabecular bone. *Bone*, 3(2):229–236, 2003.
- [124] P. W. Thavasu, S. Longhurst, S. P. Joel, M. L. Slevin, and F. R. Balkwill. Measuring cytokine levels in blood: Importance of anticoagulants, processing, and storage conditions. *Journal of Immunological Methods*, 153(1&A2):115–124, 1992.
- [125] A. Trewenack. A continuum model for the development of tissue-engineered cartilage around a chondrocyte. *Mathematical Medicine and Biology*, 26(3):241–262, 2009.

REFERENCES

- [126] M. Vincenti and C. Brinckerhoff. Transcriptional regulation of collagenase (MMP-1, MMP-13) genes in arthritis: integration of complex signaling pathways for the recruitment of gene-specific. *Arthritis research*, 4(3):157–164, 2002.
- [127] N. Wenta, H. Strauss, S. Meyer, and U. Vinkemeier. Tyrosine phosphorylation regulates the partitioning of STAT1 between different dimer conformations. *Proceedings of the National Academy of Sciences*, 105(27):9238–9243, 2008.
- [128] T. Witten. Modeling the progression of articular erosion in rheumatoid arthritis (RA): Initial mathematical models. *Mathematical and computer modelling*, 31(2-3):31–38, 2000.
- [129] A. D. Woolf and B. Pfleger. Burden of major musculoskeletal conditions. *Bull World Health Organ*, 81(9):646–56, 2003.
- [130] J. Wu. Modelling of location-and time-dependent deformation of chondrocytes during cartilage loading. *Journal of biomechanics*, 32(6):563–572, 1999.

Appendices

Appendix A

Hill Coefficients in the Pro- and anti-inflammatory cytokine model

So far we have taken all the Hill coefficients (m_1 , m_2 and m_3) to be 2. In this section we will justify this choice by examining the some other possibilities and considering the effect these would have on the model.

$$\frac{dp}{dt} = -\gamma_p p + \frac{1}{1 + a^{m_2}} \left(P_{bp} + P_{pp} \frac{p^{m_1}}{1 + p^{m_1}} \right) \quad (\text{A.0.1})$$

$$\frac{da}{dt} = -a + A_{pp} \frac{p^{m_3}}{A_{ph} + p^{m_3}} \quad (\text{A.0.2})$$

The Hill coefficients from the functions $\phi(p)$, $\psi(p)$ and $\theta(a)$ also appear in the nondimensionalised equations in the form of equations (A.0.1)-(A.0.2). There are three main alternatives to the assumption we have made, firstly that all the coefficients are the same but are some value greater than 2, secondly that all the coefficients are 1 or finally that we have some combination of different coefficients for the different terms in the model.

Hill Coefficients $m_1, m_2, m_3 > 2$

For coefficients greater than two the qualitative shape of the Hill function does not change, only its steepness. This means that for $m_1, m_2, m_3 > 2$ the nullclines of the system will cross in a similar manner, and we expect qualitatively similar behaviour, with the stability of the steady states and the types of bifurcations unchanged. The only change we would expect is alterations in the parameters values at which the various bifurcations occur.

Hill Coefficient $m_1 = m_2 = m_3 = 1$

Since the shape of the Hill function when the coefficient is 1 is different from when it is greater than 1, the behaviour of the model is also likely to change. In this situation, the model equations become,

$$\frac{dp}{dt} = -\gamma_p p + \frac{1}{1+a} \left(P_{bp} + P_{pp} \frac{p}{1+p} \right), \quad (\text{A.0.3})$$

$$\frac{da}{dt} = -a + A_{pp} \frac{p}{A_{ph} + p}, \quad (\text{A.0.4})$$

which gives the nullclines,

$$a = N_1(p) = \frac{A_{pp} p}{A_{ph} + p}$$

$$a = N_2(p) = \frac{p(P_{bp} + P_{pp}) + P_{bp}}{\gamma_p p(1+p)} - 1.$$

As in the original model, N_1 is monotonically increasing. However, now N_2 is monotonically decreasing in p and hence there can be no more than a single steady state.

Mixed Hill Coefficients

So far we have only considered situations where all three Hill coefficients are ≥ 2 or equal to 1, but the coefficients are independent and could have different values. Since values greater than 2 behave the same as a value of 2, we only need to consider combinations of 1 and 2. Also, if we look at the nullcline N_1 it is a monotonically increasing function regardless of the value of m_3 , so, we need only look at two situations: $m_1 = 2, m_2 = m_3 = 1$ and $m_1 = 1, m_2 = 2, m_3 = 1$.

In the first case, when $m_1 = 2, m_2 = m_3 = 1$, N_2 becomes

$$a = N_2(p) = \frac{p^2(P_{bp} + P_{pp}) + P_{bp}}{\gamma_p p(1 + p^2)} - 1.$$

This two real, positive turning points, meaning that we can have either one or three steady states. This exhibits similar behaviour to the original model except that the steady states tend to occur at larger values of both p and a .

In the second case, when $m_1 = 1, m_2 = 2$ and $m_3 = 1$, N_2 becomes,

$$a = N_2(p) = \sqrt{f(p)}$$

where

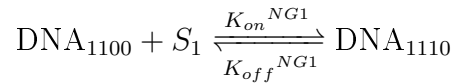
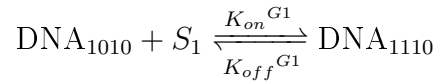
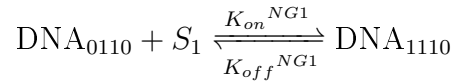
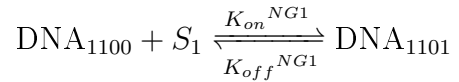
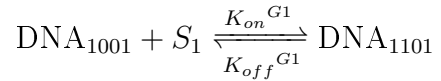
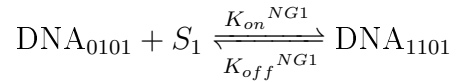
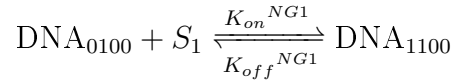
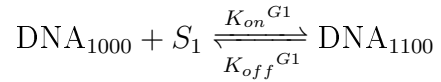
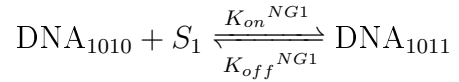
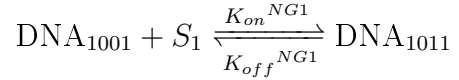
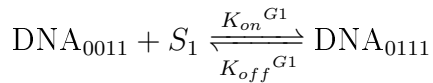
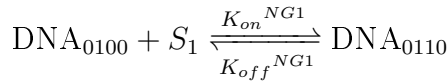
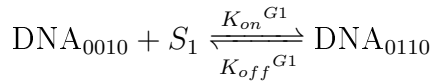
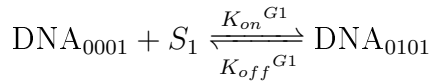
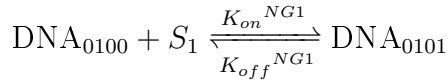
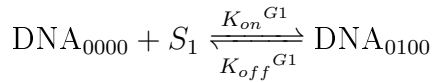
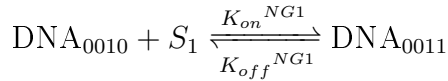
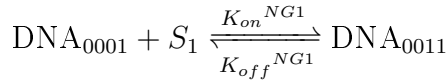
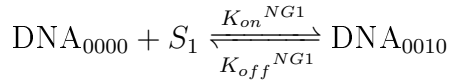
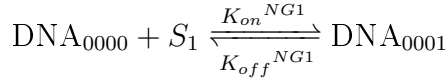
$$f(p) = \frac{p(P_{bp} + P_{pp}) + P_{bp}}{\gamma_p p(1 + p)} - 1.$$

$f(p)$ is monotonically decreasing, so that N_2 must also be monotonically decreasing in the positive quadrant, and can cross N_1 only once giving, exactly one steady state. This situation is similar to the case when all the coefficients are 1 and exhibits similar behaviour. Essentially, m_1 must be greater than 1 to give bifurcations and bistability in the model, i.e. strong feedback in p is required.

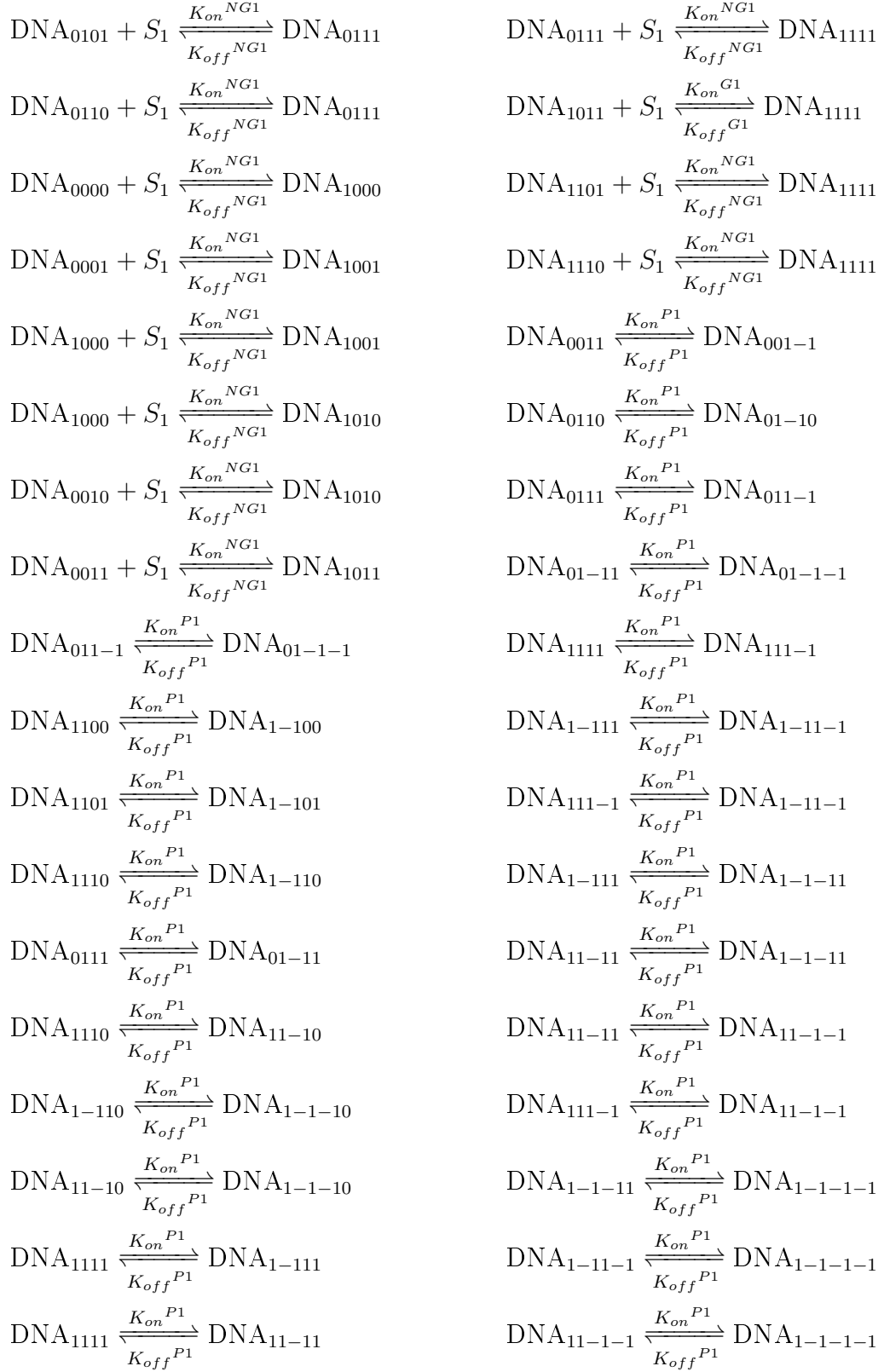
Appendix B

STAT signalling model reactions

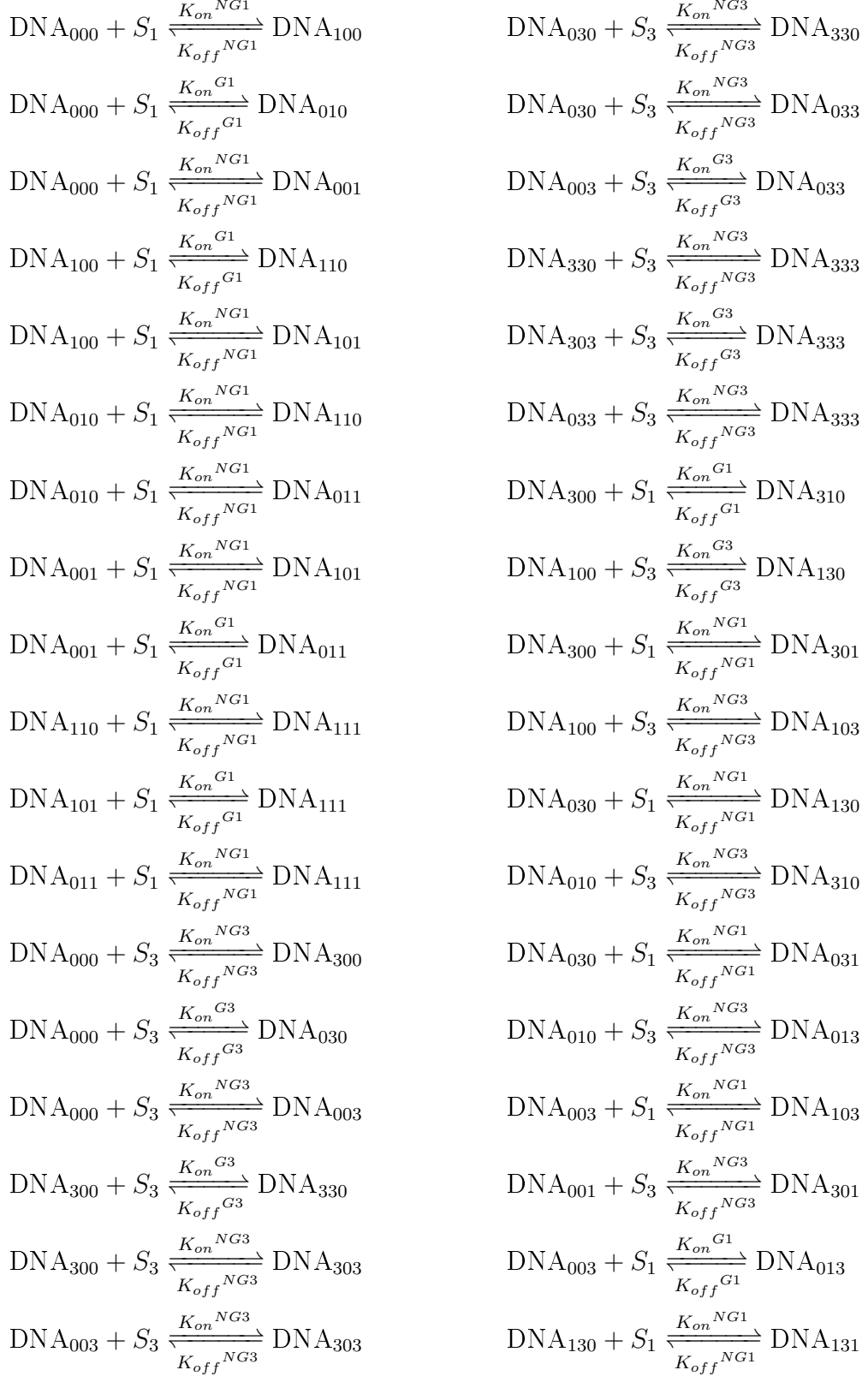
B.0.1 Cooperative Four Site Model



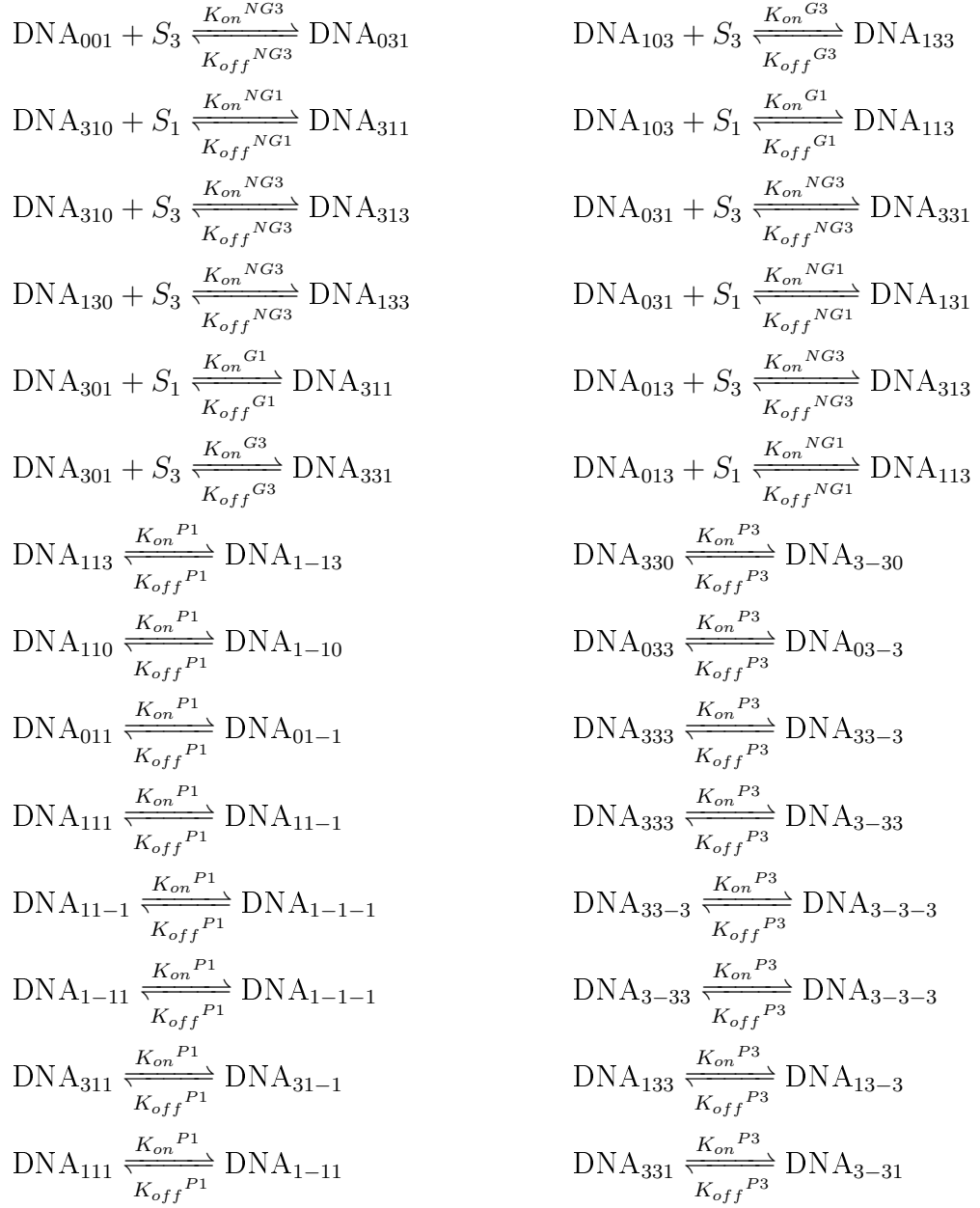
APPENDIX B: STAT SIGNALLING MODEL REACTIONS



B.0.2 Competitive Three Site Model



APPENDIX B: STAT SIGNALLING MODEL REACTIONS



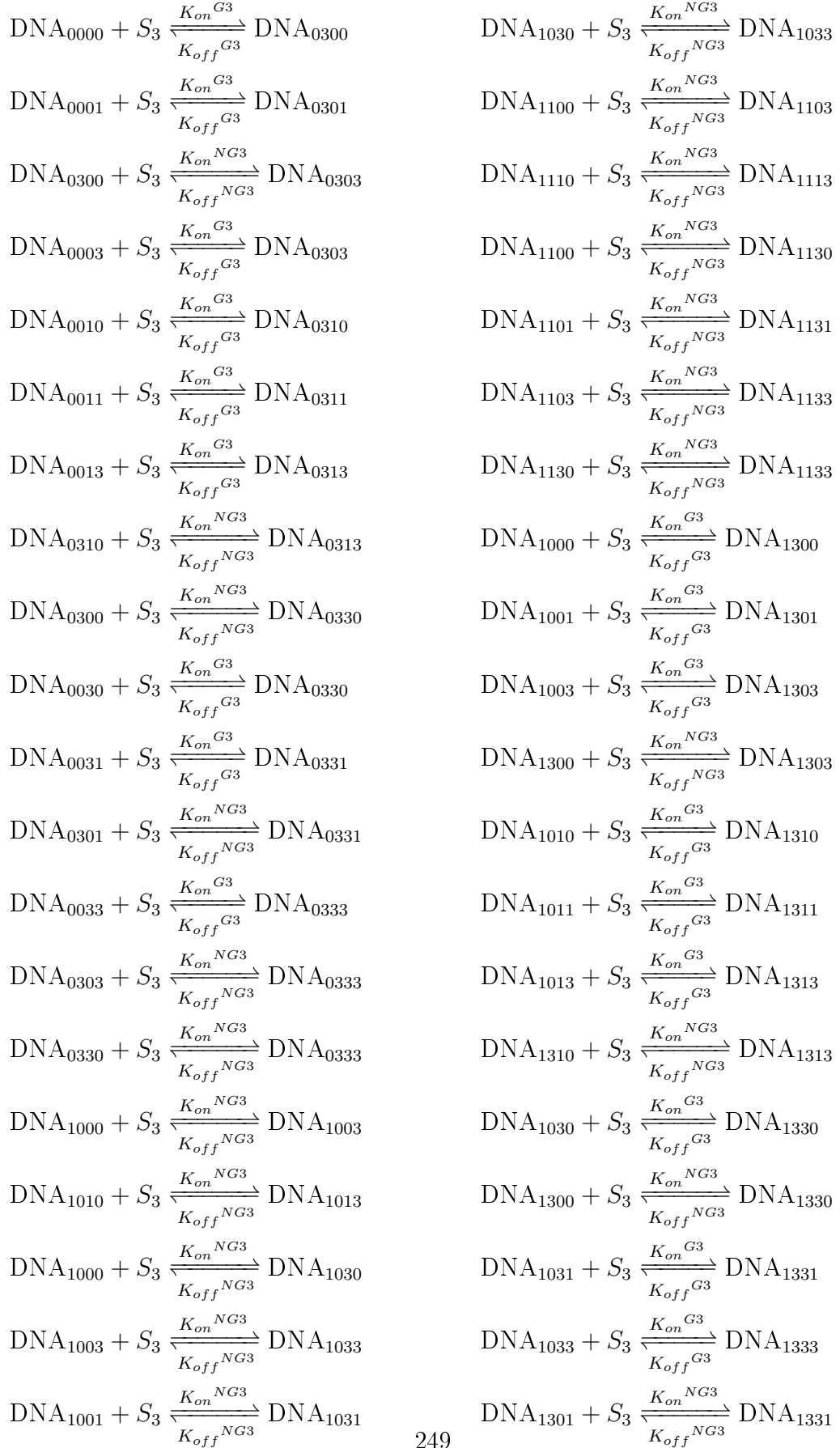
B.0.3 Competitive Four Site Model



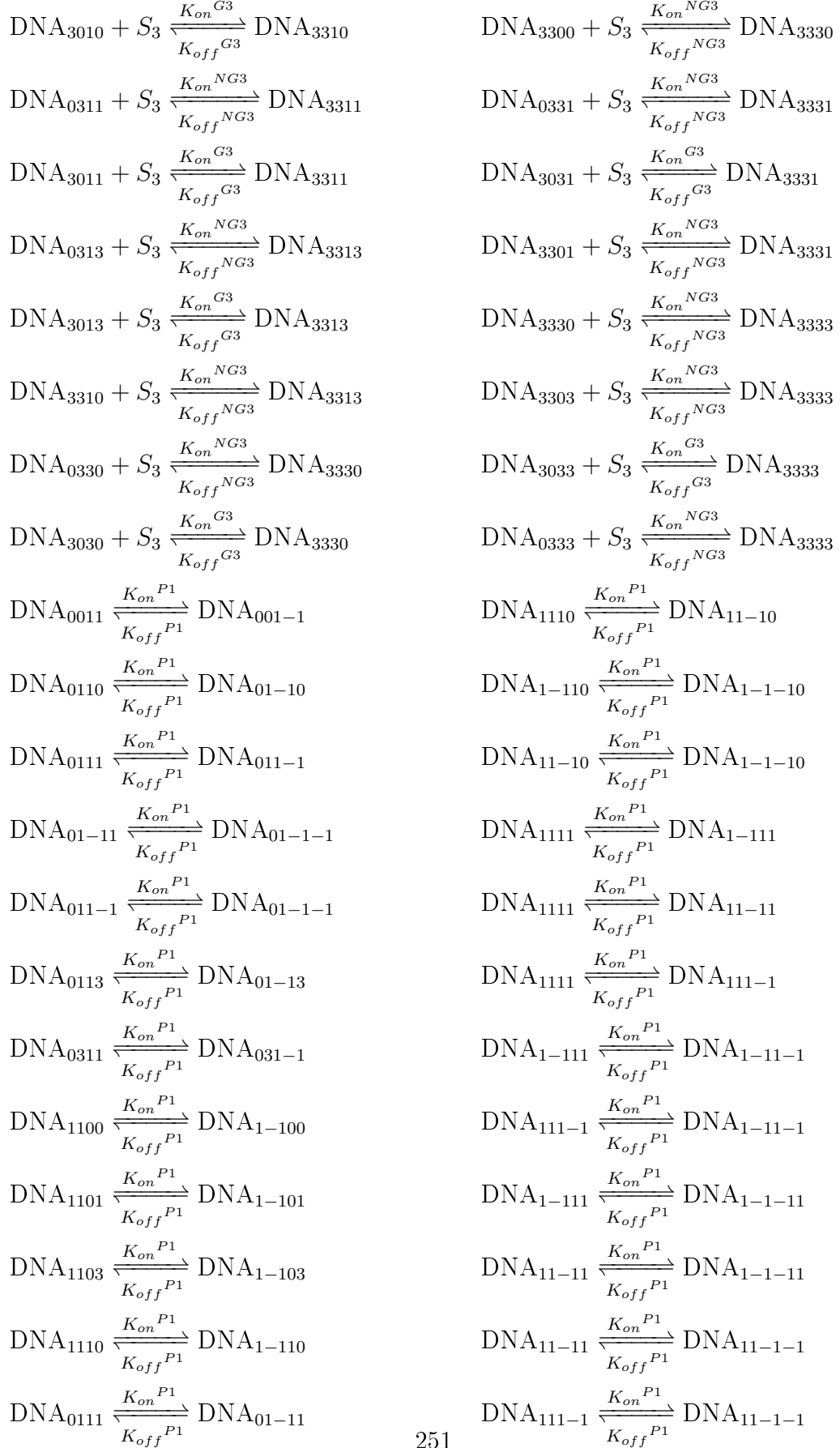
APPENDIX B: STAT SIGNALLING MODEL REACTIONS



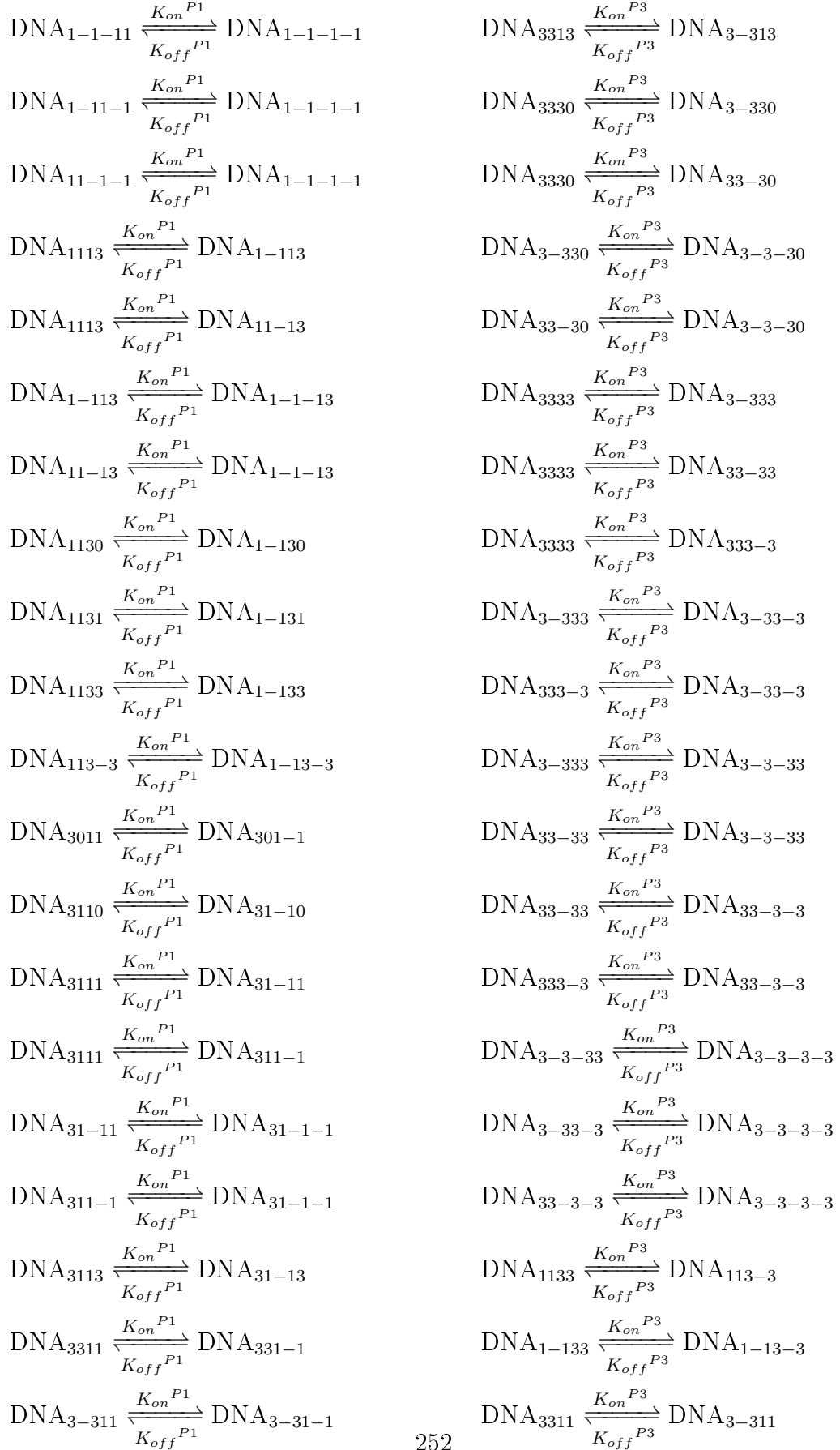
APPENDIX B: STAT SIGNALLING MODEL REACTIONS



APPENDIX B: STAT SIGNALLING MODEL REACTIONS



APPENDIX B: STAT SIGNALLING MODEL REACTIONS



APPENDIX B: STAT SIGNALLING MODEL REACTIONS

